Appendix F

Modeling Attainment Demonstration and Modeling Protocol

This page intentionally blank.

Appendix F: Modeling Protocol and Attainment Demonstration

[This Appendix provided by the California Air Resources Board]

Modeling Protocol & Attainment Demonstration for the 2022 San Joaquin Valley Ozone SIP

Prepared by

California Air Resources Board

San Joaquin Valley Air Pollution Control District

Prepared for

United States Environmental Protection Agency Region IX

July 2022

Table of Contents

List of Figures

List of Tables

Acronyms

AQMIS – Air Quality and Meteorological Information System

BCs – Boundary Conditions

CalNex – Research at the Nexus of Air Quality and Climate Change conducted in 2010

CARB – California Air Resources Board

CARES – Carbonaceous Aerosols and Radiative Effects Study in 2010

CEPAM – California Emissions Projection Analysis Model

CMAQ Model – Community Multi-scale Air Quality Model

CSJV – Central San Joaquin Valley

CTM – Chemical Transport Model

DV – Design Value

HD I/M – Heavy-Duty Vehicle Inspection and Maintenance

ICs – Initial Conditions

IOA – Index Of Agreement

LAI – Leaf Area Index

MB – Mean Bias

MDA8 – Maximum Daily Average 8-hour

ME – Mean Error

MEGAN – Model of Emissions of Gases and Aerosols from Nature

MFB – Mean Fractional Bias

MFE – Mean Fractional Error

MM5 – Mesoscale Meteorological Model Version 5

MOZART – Model for Ozone and Related chemical Tracers

NAAQS – National Ambient Air Quality Standard

NARR – North American Regional Reanalysis

NCAR – National Center for Atmospheric Research

NMB – Normalized Mean Bias

NME – Normalized Mean Error

NO_x – Oxides of nitrogen

NSJV – Northern San Joaquin Valley

$PM_{2.5}$ – Particulate Matter with aerodynamic diameter less than 2.5 micrometers

PM_{10} – Particulate Matter with aerodynamic diameter less than 10 micrometers

R – Correlation coefficient

R^2 – R-squared/Coefficient of determination

RFP – Reasonable Further Progress

RH – Relative Humidity

RMSE – Root Mean Square Error

ROG – Reactive Organic Gases

RRF – Relative Response Factor

SAPRC – Statewide Air Pollution Research Center

SIP – State Implementation Plan

SJV – San Joaquin Valley

SJVAPCD – San Joaquin Valley Air Pollution Control District

SSJV – Southern San Joaquin Valley

U.S. EPA – United States Environmental Protection Agency

VOC – Volatile Organic Compounds

WRF Model – Weather and Research Forecast Model

1. Introduction

The San Joaquin Valley (SJV or the Valley) covers an area of 23,490 square miles and is home to approximately 4 million residents. The Valley is bordered on the west by the coastal mountain ranges and on the east by the Sierra Nevada range (Figure 1). Most of the population is centered in the large urban areas of Bakersfield, Fresno, Modesto, and Stockton. The Valley is one of the most severely polluted air basins in the U.S. and it is designated as an extreme ozone nonattainment area for the U.S. EPA 2015 National Ambient Air Quality Standard (NAAQS) for 8-hour ozone. The nonattainment area includes seven full counties (San Joaquin, Stanislaus, Merced, Madera, Fresno, Kings, and Tulare) and one partial county Kern, including only the western portion of Kern County, which lies in the jurisdiction of the San Joaquin Valley Air Pollution Control District (SJVAPCD). Weather conditions and summer ozone levels during much of the summer ozone season are dominated by an area of high pressure, known as the East Pacific Ridge, which creates a broad region of warm, descending air over Central California. Studies have revealed that the position and strength of the Pacific High has a dominant influence on ozone levels throughout the Central Valley, along with the height of the marine inversion and strength of the low-level onshore flow (Lehrman et al., 2001, 2004; Pun et al., 2008, Blanchard et al., 2008; Beaver and Palazoglu, 2009, Fujita et al., 1999; Jin et al., 2008, 2010).

The Valley can be divided into three regions that are characterized by distinct geography, meteorology, and air quality: 1) Northern SJV (NSJV) which includes San Joaquin, Stanislaus, and Merced counties), 2) Central SJV (CSJV) which includes Madera, Fresno, and King counties, and 3) Southern SJV (SSJV) which includes Tulare and Western Kern counties. A third of the Valley population lives in the northern SJV. This lowland area is bordered by the Sacramento Valley and Delta lowland to the north, the central portion of the SJV to the south, and mountain ranges to the east and west. Because of the marine influence, which extends into this area through gaps in the coastal mountains to the west, the northern SJV experiences a more temperate climate than the rest of the Basin. These cooler temperatures and the predominant air flow patterns generally favor better air quality. Similar to the northern SJV, the central and southern SJV are also low-lying areas, flanked by mountains on their west and east sides. The worst air quality within the Valley occurs in these two regions, where the population is primarily clustered around the Fresno and Bakersfield urban areas. In these regions the interaction between geography, climate, and a mix of natural (biogenic) and anthropogenic emissions pose significant challenges to air quality progress. The southern SJV represents the terminus of the Valley and is flanked by mountains on the south, as well. The surrounding mountains in both areas act as barriers to air flow and combined with recirculation patterns and stable air to trap emissions and pollutants near the valley floor. The higher temperatures and more stagnant conditions in these two regions lead to a build-up of ozone and overall poorer air quality.

Figure 1. Map of California (left) along with the location of San Joaquin Valley (SJV) in magenta. The shaded and gray line contours denote the gradients in topography (km). The outer box of the left panel is the California statewide 12 km modeling domain, while the inner box shows the 4 km modeling domain covering Central California. The insert on the right shows the zoomed-in view of the spatial extent (magenta line) and approximate regional boundary along with the location of sites in the Northern (red triangle markers), Central (red circle makers) and Southern (red square markers) sub regions in the Valley. (Figure adapted from Kulkarni et al., 2014)

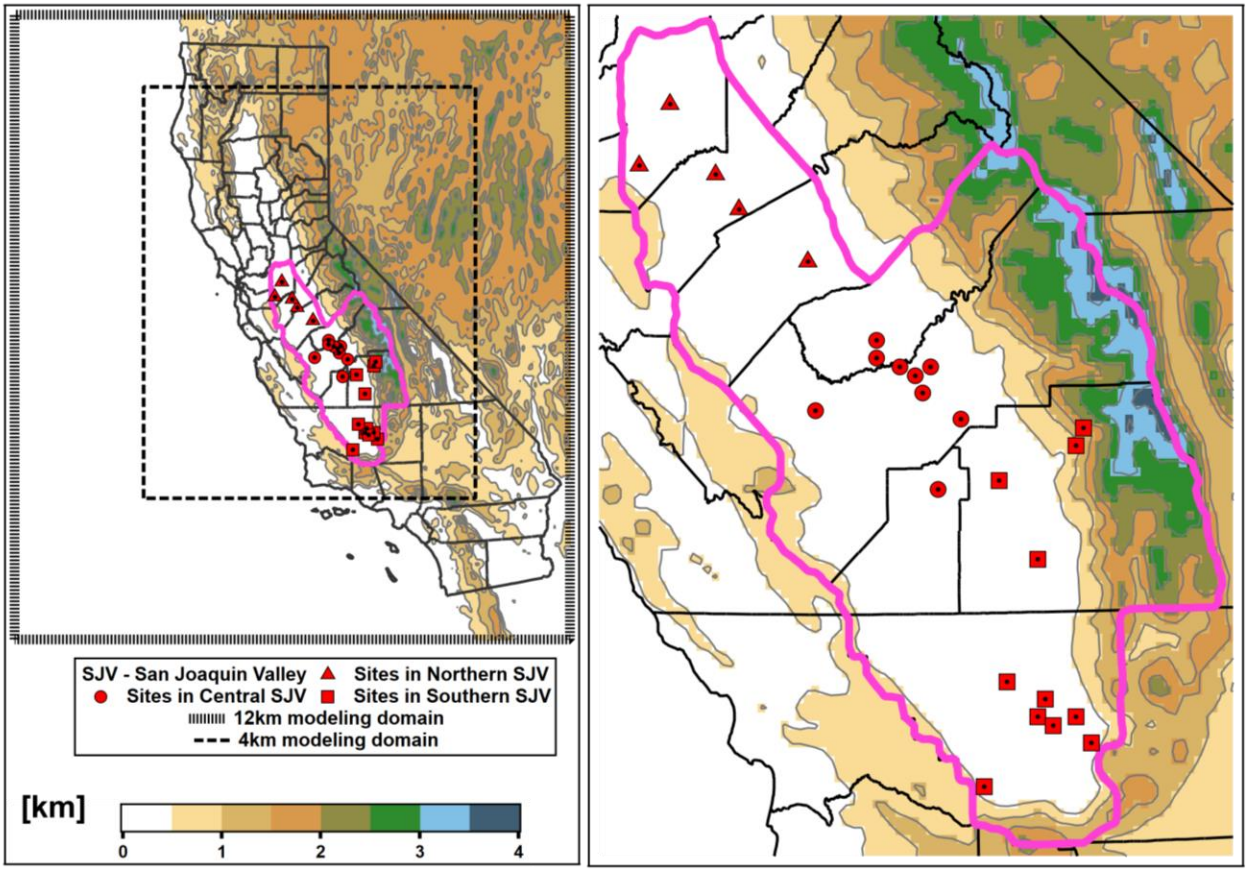

Anthropogenic sources of the oxides of nitrogen (NO_x) and reactive organic gases (ROG) are the major precursors that lead to ozone formation in the valley. Biogenic hydrocarbons are also important contributors to ozone precursors in the region and are projected to play an even more important role in the future as emission controls reduce anthropogenic ROG. Since the 1980's, the Valley's emission control programs have substantially reduced the amounts of both anthropogenic NO_x and ROG throughout the Valley. As these control programs have led to changes in the relative levels of NO_x and ROG in the Valley over time, the control programs have also adapted to reduce ozone levels as rapidly as possible. This adaptation within the control programs is necessary because ozone formation responds differently to NO_x and ROG controls as the relative levels of NO_x and ROG in the atmosphere change.

Figure 2. Trend in summer emissions of NOx and ROG (tons per day), Maximum Daily Average 8-hour Ozone Design Value (ppb) and 70 ppb 8-hour Ozone NAAQS exceedance days between 2000 and 2020 in the SJV. Anthropogenic Emissions estimates are from the California Emission Projection Model (CEPAM) 2019 Ozone SIP Baseline Projection Version 1.04 with 2017 base year. 2018 biogenic ROG emissions are from MEGAN 3.0 biogenic model calculations.

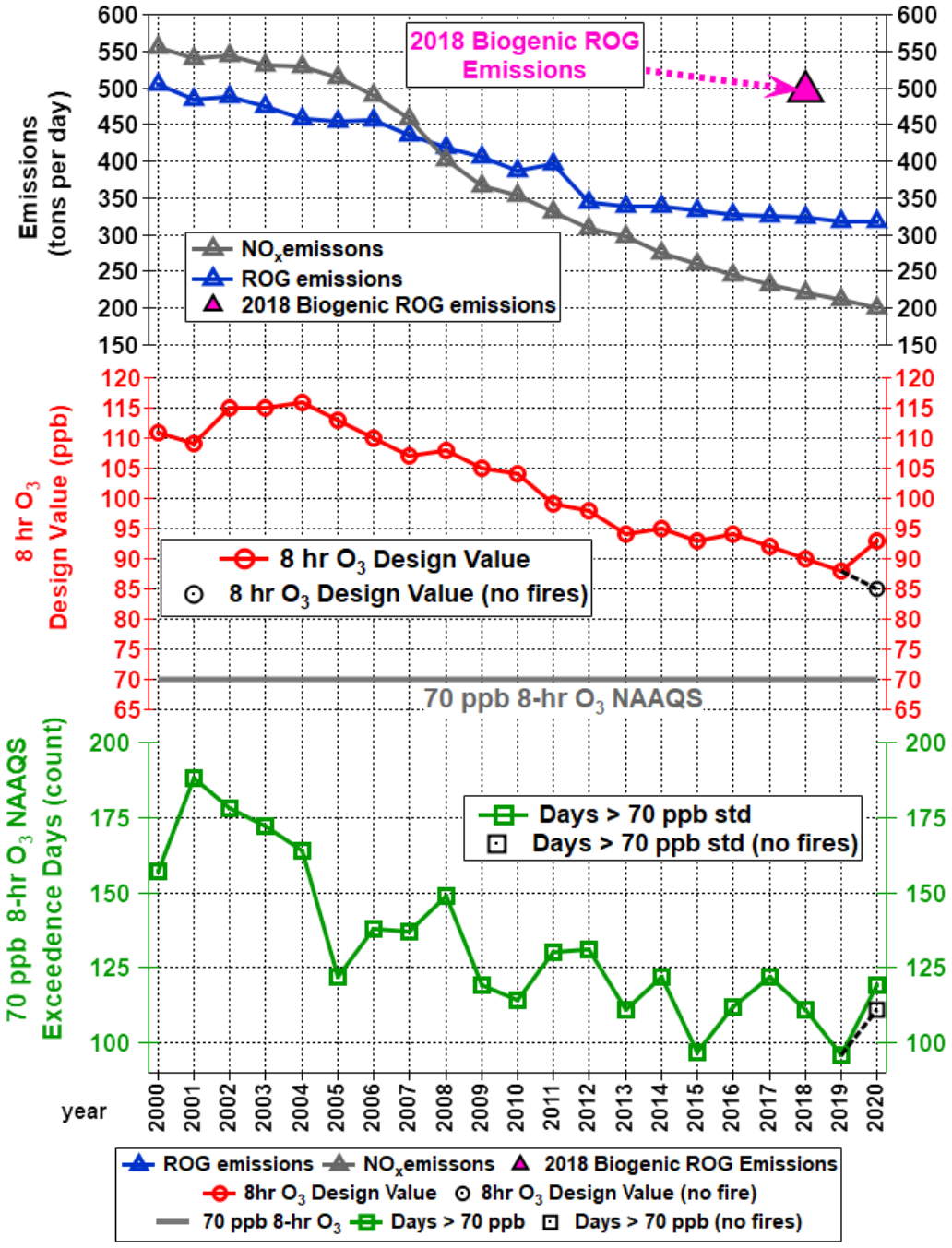

Basin-wide summer emission trends from 2000 to 2020 for the SJV are shown in Figure 2 (top panel) for anthropogenic NO_x and ROG along with summer biogenic ROG emissions in the SJV averaged from May to October 2018 (magenta triangle marker). Figure 2 clearly shows large decrease in both anthropogenic NO_x (from 555 tpd to 200 tpd) and ROG (from 504 tpd to 317 tpd) emissions from 2000 to 2020. In 2018, biogenic ROG (495 tpd) is estimated to be ~1.5 times higher than the corresponding anthropogenic emissions (324 tpd) in the SJV.

Over the same 2000 to 2020 time period, the ozone design value within the SJV declined steadily (Figure 2, middle panel), but did also exhibit a fair amount of variability due to year-to-year variability in meteorology and the associated changes in biogenic emissions. Overall, the basin-wide design values (DVs) have declined from 111 ppb in 2000 to 93 ppb in 2020. However, these DVs are still substantially higher than the current 70 ppb standard. Exceedance days in the Valley (Figure 2 bottom panel) have substantially decreased over time from 157 in 2000 to 119 in 2020 indicating significant improvements in ozone air quality across the entire valley. In recent years, the prevalence of forest fires during the summer ozone season significantly impacted the air quality in the Valley. High ozone concentrations were observed at several SJV sites on days impacted by forest fire (see Weight of Evidence section of the SIP document) and likely caused the upward trend in the DVs seen between 2019 and 2020. To remove the impact of forest fires in 2020, ozone DVs were calculated by excluding high ozone days that were impacted by forest fires. Details about fire impact days can be found in the Weight of Evidence analysis. Excluding the fire impacts, ozone DVs would be 85 ppb in 2020 (8 ppb lower than observed 93 ppb DV) denoted by black circle markers in middle panel of Figure 2. The number of exceedance days also dropped to 111 (from 119) in 2020 when the forest fire impacted days were excluded (black square markers in bottom panel of Figure 2).

The SJV classification of extreme nonattainment for the 2015 70 ppb O_3 standard means it has an attainment year of 2037. The remainder of this document serves as the modeling protocol and attainment demonstration for the Valley's 2022 Plan for the 2015 8-hour ozone standard, which utilizes a base and reference year of 2018 and demonstrates attainment of the standard in 2037.

2. Methodology

U.S. EPA modeling guidance (U.S. EPA, 2018) outlines the approach for utilizing regional chemical transport models (CTMs) to predict future attainment of the 2015 (70 ppb) 8-hour ozone standard. This model attainment demonstration requires that CTMs be used in a relative sense, where the relative change in ozone to a given set of emission reductions (i.e., predicted change in future anthropogenic emissions) is modeled, and then used to predict how current/present-day ozone levels would change under the future emissions scenario.

The starting point for the attainment demonstration is the observational based design value (DV), which is used to determine the compliance with the ozone standards. The DV for a specific monitor and year represents the three-year average of the annual 4th highest 8-hour

ozone mixing ratio observed at the monitor. For example, the 8-hour O_3 DV for 2018 is the average of the observed 4th highest 8-hour O_3 mixing ratio from 2016, 2017, and 2018 (Table 1). The U.S. EPA recommends using an average of three DVs to better account for the year-to-year variability in ozone levels due to meteorology. This average DV is called a weighted DV (in the context of this SIP document, the weighted DV will also be referred to as the reference year DV or DV_R). Since 2018 represents the reference year for projecting DVs to the future, site-specific DVs should be calculated for the three-year periods ending in 2018, 2019, and 2020, and then these three DVs are averaged. However, 2020 was an atypical year with large societal changes in response to the COVID19 pandemic and is not suitable for use in the DV_R calculation. To remove the impact from 2020 observations, we utilize an alternative methodology for calculating the average DVs by excluding year 2020. In this method, the 8-hour O_3 DV for 2020 was replaced by the two-year average of the 4th highest 8-hour O_3 concentrations from 2018 and 2019. Table 1 illustrates the observational data from each year that goes into the average DV_R and Equation 1 shows how the DV_R is calculated.

Table 1. Data from each year that are utilized in the Design Value calculation for a specific year (DV Year), and the yearly weighting of data for the average Design Value calculation (or DV_R).

DV Year	Years Averaged for the Design Value (4th highest observed 8-hr O_3)			
2018	2016	2017	2018	
2019		2017	2018	2019
2020			2018	2019

$$DV_R = \frac{DV_{2018} + DV_{2019} + \frac{4th\ highest\ MDA8\ O_3\ (2018+2019)}{2}}{3} \quad (1)$$

Table 2 lists the design values for the sites within the three major sub-regions of the Valley that were used in the model attainment demonstration. Note that the DVs are listed in descending order for sites within each sub-region. The Edison monitoring site, located in the Southern SJV, has the highest average DV in the SJV non-attainment area with an average DV of 89.0 ppb. All remaining sites, excluding the Stockton-Hazelton monitor in the northern SJV, have average DVs that exceed the 70 ppb standard.

Table 2. Year-specific 8-hour ozone design values for 2018, 2019 and 2020, and the average baseline design value (represented as the average of three design values) for 2018 at the monitoring sites in SJV. 2020 DVs are the two-year averages of the 4th highest 8-hour O_3 concentrations from 2018 and 2019.

Sub-region	Site	2018 DV (ppb)	2019 DV (ppb)	2020 DV (ppb)	2018-2020 Average DV (ppb)
Northern SJV	Turlock-S Minaret St.	84	82	81	82.3
Northern SJV	Modesto-14th St.	80	80	78	79.3
Northern SJV	Merced-S Coffee Av.	79	76	75	76.7
Northern SJV	Tracy-Airport	76	73	72	73.7
Northern SJV	Stockton-Hazelton St.	66	66	66	66.0
Central SJV	Fresno-Garland	90	86	81	85.7
Central SJV	Clovis	89	84	83	85.3
Central SJV	Parlier	88	84	81	84.3
Central SJV	Fresno-Drummond St.	86	82	78	82.0
Central SJV	Fresno- Sierra Skypark #2	83	80	77	80.0
Central SJV	Hanford-S. Irwin St.	82	80	78	80.0
Central SJV	Madera-28261 Avenue 14	81	78	74	77.7
Central SJV	Madera-Pump Yard	78	76	73	75.7
Central SJV	Tranquility	75	72	71	72.7
Southern SJV	Edison	89	88	90	89.0
Southern SJV	Arvin-Di Giorgio	89	87	88	88.0
Southern SJV	Bakersfield-5558 California Avenue	88	87	87	87.3

Sub-region	Site	2018 DV (ppb)	2019 DV (ppb)	2020 DV (ppb)	2018-2020 Average DV (ppb)
Southern SJV	Sequoia and Kings Canyon Natl Park	89	86	85	86.7
Southern SJV	Bakersfield-Municipal Airport	88	84	84	85.3
Southern SJV	Visalia-N Church Street	85	84	83	84.0
Southern SJV	Maricopa-Stanislaus Street	85	83	83	83.7
Southern SJV	Sequoia Natl Park-Lower Kaweah	86	82	82	83.3
Southern SJV	Oildale-3311 Manor Street	82	84	83	83.0
Southern SJV	Shafter-Walker Street	81	79	79	79.7
Southern SJV	Porterville-1839 Newcomb Street	83	77	74	78.0

Projecting the reference DVs to the future requires three photochemical model simulations, described below:

1. Base Year Simulation

The base year simulation for 2018 is used to assess model performance (i.e., to ensure that the model is reasonably able to reproduce the observed ozone mixing ratios). Since this simulation will be used to assess model performance, it is essential to include as much day-specific detail as possible in the emissions inventory, including, but not limited to hourly adjustments to the motor vehicle and biogenic inventories based on local meteorological conditions, known wildfire and agricultural burning events, and any exceptional events such as refinery fires.

2. Reference Year Simulation

The reference year simulation was identical to the base year simulation, except that certain emissions events which are either random and/or cannot be projected to the future are removed from the emissions inventory. For 2018, the only difference

between the base and reference year simulations was that wildfires were excluded from the reference year simulation.

3. Future Year Simulation

The future year simulation (2037) was identical to the reference year simulation, except that the projected future year anthropogenic emission levels were used rather than the reference year emission levels. All other model inputs (e.g., meteorology, chemical boundary conditions, biogenic emissions, and calendar for day-of-week specifications in the inventory) are the same as those used in the reference year simulation.

Projecting the reference DVs to the future is done by first calculating the fractional change in ozone between the modeled future and reference years for each monitor location. These ratios, called "relative response factors" or RRFs, are calculated based on the ratio of modeled future year ozone to the corresponding modeled reference year ozone (Equation 2).

$$\text{RRF} = \frac{\frac{1}{N}\sum_{d=1}^{N}(MDA8\ O_3)_{future}^{d}}{\frac{1}{N}\sum_{d=1}^{N}(MDA8\ O_3)_{reference}^{d}} \quad (2)$$

Where, MDA8 O_3 refers to the maximum daily average 8-hour ozone, d refers to the day (chosen from the reference year), and N is the total number of days used in the RRF calculation. These MDA8 ozone values are based on the maximum simulated ozone within a 3x3 array of cells surrounding the monitor (Figure 3). Not all modeled days are used to calculate the average MDA8 ozone from the reference and future year simulations. The form of the 8-hour ozone NAAQS is such that it is focused on the days with the highest mixing rations in any ozone season (i.e., the 4th highest MDA8 ozone). Therefore, the modeled days used in the RRF calculation also reflect days with the highest ozone levels. As a result, the current U.S. EPA modeling guidance (U.S. EPA, 2018) recommends using the 10 days with the highest modeled MDA8 ozone at each monitor location, where the 10 days are chosen from the reference year simulation and then the same corresponding days are selected from the future year simulation. Since the relative sensitivity to emissions changes (in both the model and real world) can vary from day-to-day due to meteorology and emissions (e.g., temperature dependent emissions or day-of-week variability) using the top 10 days ensures that the calculated RRF is not overly sensitive to any single day. Note that the MDA8 ozone from the reference and future year simulations are paired in both time (the same days are selected from each simulation) and space (the location of the peak MDA8 ozone within the 3x3 array of grid cells surrounding the monitor is selected from the reference year simulation and the same location is used when selecting the corresponding data from the future year simulation).

Figure 3. Example showing how the location of the MDA8 ozone for the top ten days in the reference and future years are chosen.

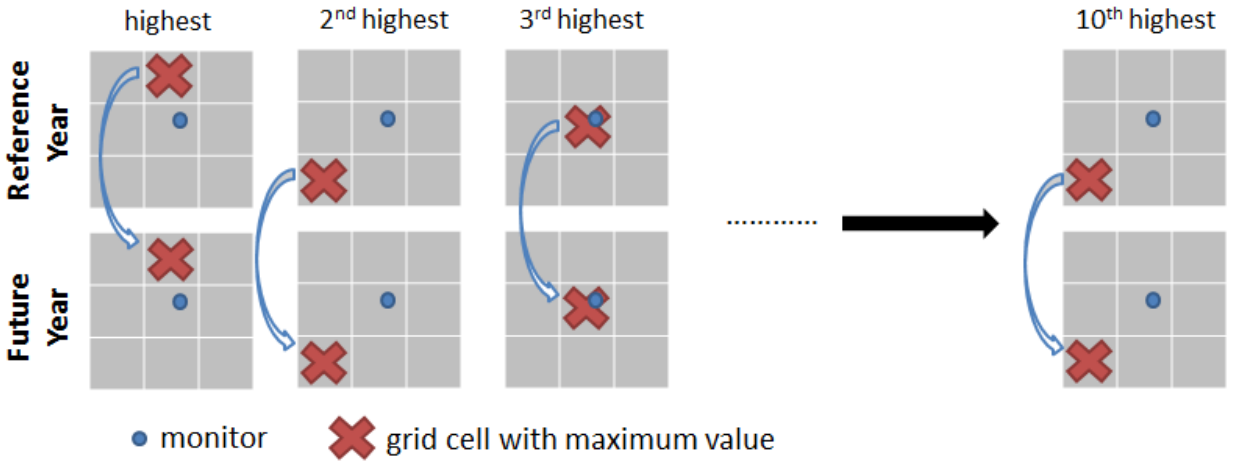

When choosing the top 10 days, the U.S. EPA recommends beginning with all days in which the simulated reference year MDA8 ozone is >= 60 ppb and then calculating RRFs based on the 10 days with the highest ozone in the reference simulation. If there are fewer than 10 days with MDA8 ozone >= 60 ppb then all days >= 60 ppb are used in the RRF calculation, as long as there are at least 5 days used in the calculation. If there are fewer than 5 days >= 60 ppb, an RRF cannot be calculated for that monitor. To ensure that only modeled days which are consistent with the observed ozone levels are used in the RRF calculation, the modeled days are further restricted to days in which the reference MDA8 ozone is within ± 20% of the observed value at the monitor location.

Future year DVs at each monitor are then calculated by multiplying the corresponding reference year DV by the site-specific RRF.

$$DV_F = DV_R \times RRF \quad (3)$$

where, DV_F is the future year design value, DV_R is the reference year design value, and RRF is the site-specific RRF from Equation 2. The resulting future year DVs are then compared to the 8-hour ozone NAAQS to demonstrate whether attainment will be reached under the emissions scenario utilized in the future year modeling. A monitor is considered to be in attainment of the 8-hour ozone standard if the estimated future year DV does not exceed the level of the standard.

2.1. Meteorological Modeling

California's proximity to the ocean, complex terrain, and diverse climate represents a unique challenge for reproducing meteorological fields that adequately represent the synoptic and mesoscale features of the regional meteorology. In summertime, the majority of the storm

tracks are far to the north of the state and a semi-permanent Pacific high pressure system typically sits off the California coast. Interactions between this eastern Pacific subtropical high pressure system and the thermal low pressure further inland over the Central Valley or South Coast lead to conditions conducive to pollution buildup over large portions of the state (Bao et al., 2008; Fosberg et al., 1966).

The state-of-the-science Weather Research and Forecasting (WRF) prognostic model (Skamarock, et al. 2008) 4.2.1 was employed in the modeling. Its domain consisted of three nested Lambert projection grids of 36 km (D01), 12 km (D02), and 4 km (D03) uniform horizontal grid spacing as shown in Figure 4. The 4 km innermost domain has 427x427 grid points and spans 1748 km in the east-west and the north-south directions. All three domains utilized 30 vertical sigma layers with the lowest layer extending to 30 m above the surface (Table **3**). The North America Regional Reanalysis (NARR) fields, enhanced with surface and upper-air observations, were used for initial and boundary conditions as well as Four Dimension Data Assimilation (FDDA) on the outermost (36 km) domain. The horizontal spatial resolution of the NARR data is 32 km. The major physics options for each domain are listed in Table 4, which include the Yon-Sei University (YSU) planetary boundary layer (PBL) scheme, Kain-Fritsch cumulus parameterization for the outer two domains, and 5-layer thermal diffusion land-surface option.

Figure 4. WRF modeling domains (D01 36 km; D02 12 km; and D03 4 km).

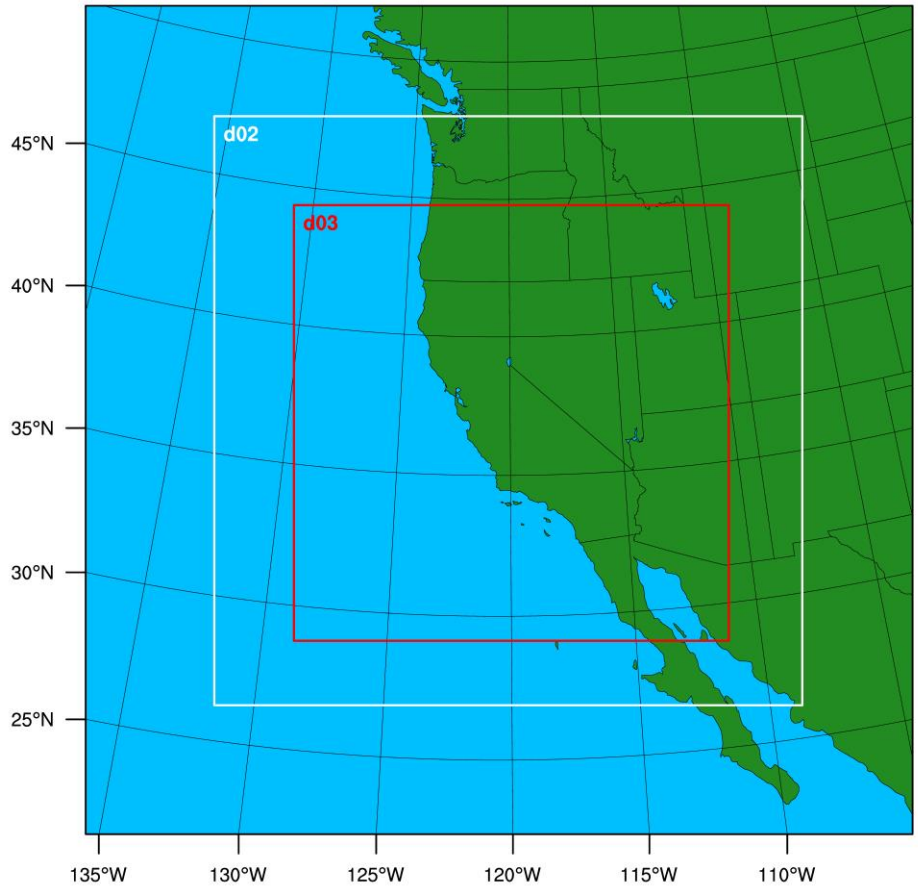

Table 3. WRF vertical layer structure.

Layer Number	Height (m)	Layer Thickness (m)	Layer Number	Height (m)	Layer Thickness (m)
30	16082	1192	15	2262	403
29	14890	1134	14	1859	334
28	13756	1081	13	1525	279
27	12675	1032	12	1246	233
26	11643	996	11	1013	194
25	10647	970	10	819	162
24	9677	959	9	657	135
23	8719	961	8	522	113
22	7757	978	7	409	94
21	6779	993	6	315	79
20	5786	967	5	236	66
19	4819	815	4	170	55
18	4004	685	3	115	46
17	3319	575	2	69	38
16	2744	482	1	31	31

To prevent any large deviations from the reanalysis data, analysis nudging was applied to the outermost domain (D01) above the planetary boundary layer (PBL) for moisture and above 2 km for wind and temperature. No nudging was used on the two inner domains to allow the model physics to work fully without externally imposed forcing. Boundary conditions on the outermost domain were updated every 6 hours, while WRF was reinitialized every 6 days with one day overlap, where the first day after being reinitialized was discarded as model spin-up.

The Meteorology-Chemistry Interface Processor (MCIP) version 5.1 was used to process the 4 km (D03) WRF output for use in the CTM simulations.

Table 4. WRF Physics options.

Physics Option	D01 (36 km)	D02 (12 km)	D03 (4 km)
Microphysics	WSM 6-class	WSM 6-class	WSM 6-class
Longwave Radiation	RRTM	RRTM	RRTM
Shortwave Radiation	Dudhia	Dudhia	Dudhia
Surface Layer	Revised MM5 Monin-Obukhov	Revised MM5 Monin-Obukhov	Revised MM5 Monin-Obukhov
Land Surface	5-layer Thermal Diffusion	5-layer Thermal Diffusion	5-layer Thermal Diffusion
Planetary Boundary Layer	YSU	YSU	YSU
Cumulus Parameterization	Kain-Fritsch Scheme	Kain-Fritsch Scheme	No

2.2. Emissions

The anthropogenic emissions inventory used in this modeling was based on the California Emissions Projection Analysis Model (CEPAM) v1.03 augmented with updates consistent with CEPAM v1.04 for select source categories. These sources are described in *http://outapp.arb.ca.gov/cefs/2019ozsip/CEPAM2019_key_updates_chron.pdf* under version "March 29, 2022 Release of Version 1.04 Planning Projections", with the exception of emissions from Ocean Going Vessels (OGV). For a detailed description of the anthropogenic emissions inventory, updates to the inventory, and how it was processed from the planning totals to a gridded inventory for modeling, see the Modeling Emissions Inventory Appendix.

Table 5. SJV Summer Planning Emissions for 2018, 2032, and 2037 (tons/day).

	CEPAM v1.04						With CARB Commitments			
Source Category	2018 NOx (tpd)	2018 ROG (tpd)	2032 NOx (tpd)	2032 ROG (tpd)	2037 NOx (tpd)	2037 ROG (tpd)	2032 NOx (tpd)	2032 ROG (tpd)	2037 NOx (tpd)	2037 ROG (tpd)
Stationary	24.1	84.0	16.5	87.7	16.2	92.9	16.5	87.7	16.2	92.9
Area	7.7	157.1	3.8	156.8	3.6	159.2	3.8	156.8	3.6	159.2
On-road Mobile	93.4	31.2	24.4	15.5	20.9	13.4	21.0	14.5	13.2	11.2
Other Mobile	96.6	51.6	55.5	30.2	46.6	25.5	41.2	28.9	29.0	23.5
Total	221.8	323.9	100.2	290.1	87.3	291.0	82.5	287.8	62.0	286.8

* Note that emissions for 2032 are shown because they will be utilized in Section 3 to estimate final design values. Rounding errors may result in emissions totals that do not exactly match the sum of the individual categories.

Table 5 summarizes the 2018 and 2037 SJV anthropogenic emissions. Overall, anthropogenic NOx emissions in CEPAMv1.04 were projected to decrease by ~61% between 2018 and 2037 from 221.8 tpd to 87.3 tpd with bulk of the reductions coming from on-road mobile sources. In contrast, anthropogenic ROG was projected to decrease by ~10% from 323.9 tpd to 290.9 tpd with the bulk of those reductions coming from all mobile sources including on-road and other mobile sources. CEPAMv1.04 emissions for 2037 reflect emission reductions from CARB's Heavy-Duty Vehicle Inspection and Maintenance (HD I/M) Program and the District's (i.e., SJVAPCD) recent rules pertaining to open burning, boilers, glass melting furnaces and internal combustion engines. The right two columns in Table 5 show the 2037 emissions after further incorporating CARB commitments from the State SIP Strategy. In addition, the emission inventory for 2037 includes an additional 2.43 tpd of NOx emissions from Emission Reduction Credits (ERCs) and 4.35 fewer tpd of NOx emissions from the Federal Clean Truck Plan (CTP) and Federal Tier 5 Off-Road measure. For 2032, the emission inventory includes 2.62 fewer tpd of NOx emissions from the Federal CTP and Tier 5 Off-Road measure. Details on these rules/adjustments can be found in the Modeling Emissions Inventory Appendix. Note that the change in ozone from the Federal CTP and Tier 5 Off-Road NOx emission reductions were estimated and excluded from the final future DV calculations (see Section 3.5).

Biogenic emissions were generated using the Model of Emissions of Gases and Aerosols from Nature (MEGAN3.0) biogenics emissions model (*https://bai.ess.uci.edu/megan*). MEGAN3.0 incorporates a new pre-processor (MEGAN-EFP) for estimating biogenic emission factors based on available landcover and emissions data. The MEGAN3.0 default datasets for plant

growth form, ecotype, and emissions were utilized. Leaf Area Index (LAI) for non-urban grid cells was based on the 8-day 500 m resolution MODIS Terra/AQUA combined product (MCD15A2H) for 2018 (*https://earthdata.nasa.gov/*). The LAI data was converted to LAIv, which represents the LAI for the vegetated fraction within each grid cell, by dividing the gridded MODIS LAI values by the Maximum Green Vegetation Fraction for each grid cell (*https://archive.usgs.gov/archive/sites/landcover.usgs.gov/green_veg.html*). The MODIS LAI product does not provide information on LAI in urban regions, so urban LAIv was estimated from the US Forest Service's Forest Inventory and Analysis urban tree plot data, processed through the i-Tree v6 software (*https://www.itreetools.org/tools/i-tree-eco*). Peak summertime urban LAIv for SJV was estimated to be 5.0, and this peak value was adjusted for each 8-day MODIS period based on the relative change in non-urban MODIS LAI across the state. Hourly meteorology was provided by the 4 km WRF simulation described above, and all stress factor adjustments were turned off.

Monthly biogenic ROG totals for 2018 within the Valley are shown in Figure 5 (note that the same biogenic emissions were used in 2018 and 2037 modeling). Throughout the summer, biogenic ROG emission ranged from 572 tpd in June to 935 tpd in July and 663 tpd in August, with the difference in emissions primarily due to differences in temperature and leaf area from month-to-month. In addition to biogenic ROG emissions, the MEGAN model also estimates NOx emissions from soils using the Yienger and Levy scheme (Yienger and Levy, 1995), which accounts for natural emissions from soils as well as enhanced emissions from managed crop lands. Figure 6 shows the monthly average soil NOx emissions for 2018 from MEGAN. Soil NOx emissions are highest during summer months, where the emissions peaked at 34 tpd in July.

Figure 5. Monthly average biogenic ROG emissions for 2018.

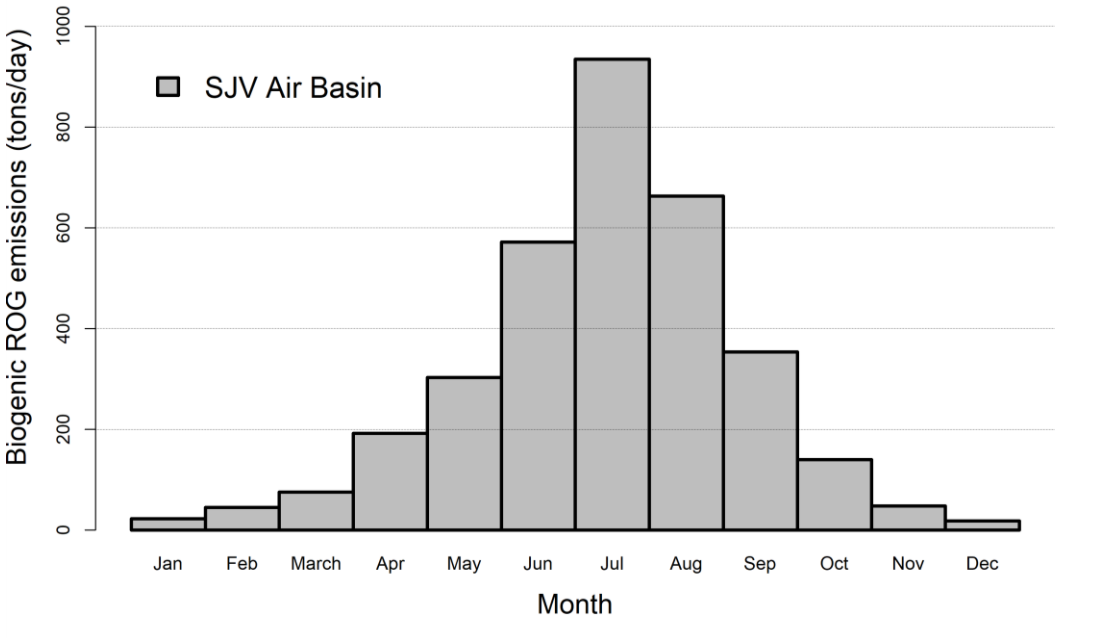

Figure 6. Monthly average soil NOx emissions for 2018.

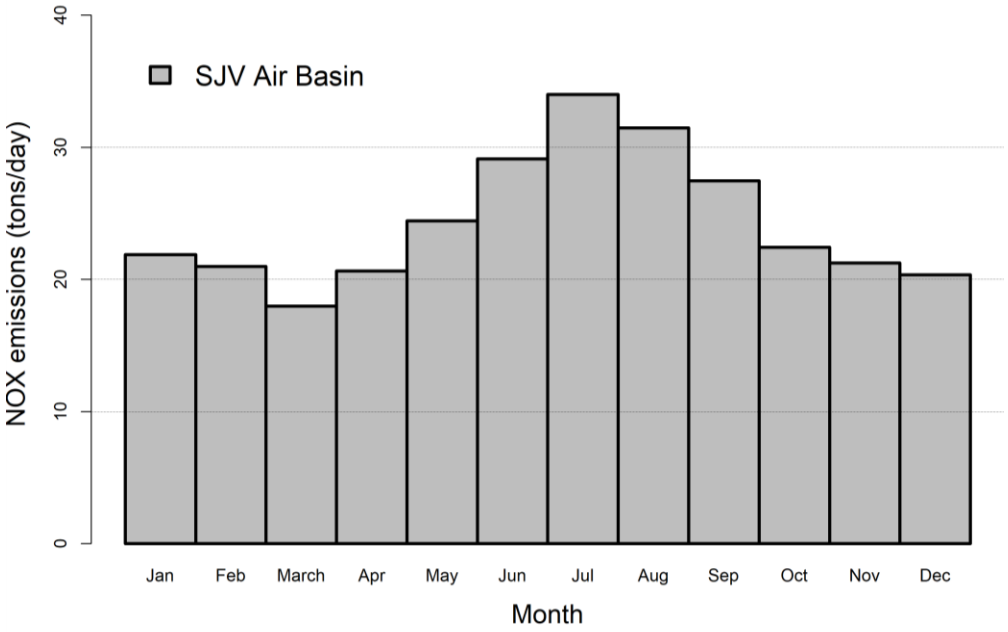

2.3. Air Quality Modeling

Figure 1 shows the CMAQ modeling domains used in this work. The larger domain covering all of California has a horizontal grid size resolution of 12 km with 107x97 lateral grid cells for each vertical layer and extends from the Pacific Ocean in the west to Eastern Nevada in the east and runs from the U.S.-Mexico border in the south to the California-Oregon border in the north. The smaller nested domain covering the SJV region has a finer scale 4 km grid resolution and includes 192x192 lateral grid cells. The 12 km and 4 km domains are based on a Lambert Conformal Conic projection with reference longitude at -120.5°W, reference latitude at 37°N, and two standard parallels at 30°N and 60°N, which is consistent with WRF domain settings. The CMAQ vertical layer structure is based on the WRF sigma-pressure coordinates and the exact layer structure used can be found in Table 3. The original 30 vertical layers from WRF were used for the CMAQ simulations, extending from the surface to 100 mb such that the majority of the vertical layers fall within the planetary boundary layer.

The CTM utilized in the modeling is the Community Multiscale Air Quality (CMAQ) model version 5.2.1 (U.S. EPA, 2018). CMAQ is the U.S. EPA's open-source regional air quality model, which is widely used in the regulatory and scientific communities, and represents the current state-of-the-science. CMAQ has been utilized for studying ozone and $PM_{2.5}$ formation in California for over a decade (e.g., Cai et al., 2016, 2019; Jin et al., 2008, 2010; Kelly et al., 2010, 2014; Livingstone et al., 2009; Pun et al., 2009; Tonse et al., 2008; Vijayaraghavan et al., 2006; Zhang et al., 2010), and has been the primary CTM used in California SIPs since

2008 (SJV, 2008), having been used in over a dozen ozone and $PM_{2.5}$ SIPs (Eastern Kern, 2017; Imperial, 2017, 2018; Sacramento, 2017; SJV, 2012, 2013, 2016a,b, 2018; South Coast, 2012, 2016; Ventura, 2016; Western Mojave, 2016; Western Nevada, 2018).

The SAPRC07tic chemical mechanism (Carter, 2010a,b) was chosen to represent the gas-phase photochemistry in the atmosphere, along with the aero6 aerosol module for simulating aerosol dynamics and chemistry. Photolysis rates were calculated in-line to better represent changes in photolysis rates due to meteorological conditions and gaseous and particulate pollutant levels in the atmosphere.

Global chemical transport Community Atmosphere Model with Chemistry (CAM-Chem) coupled to the Community Earth System Model (CESM2) (Emmons, 2020; Lamarque et al., 2012) was developed by NCAR (National Center for Atmospheric Research) and used for simulations of global tropospheric and stratospheric atmospheric compositions. CAM-Chem modeling outputs have been widely used to provide chemical boundary conditions for various regional air quality models (Feifan Yan, 2021; Hao He, 2018; Nasimeh Shahrokhishahraki, 2022; Pengfei Wang, 2022). In this work, chemical boundary conditions for the outer 12-km domain were extracted from the CAM-Chem output based on vertical and horizontal setups of CMAQ meteorological inputs, and processed into CMAQ model ready format as well as mapped to CMAQ chemical species. The CAM-chem data for 2018 was obtained from the National Center for Atmospheric Research (*https://www.acom.ucar.edu/cam-chem/cam-chem.shtml*) (Buchholz, 2019) and processed using the mozart2camx preprocessor version 3.2.3 (https://www.camx.com/download/support-software/). The same CAM-chem derived BCs for the 12 km outer domain were used for both base year, reference year and future year simulations. The inner 4 km domain simulations utilized BCs that were based on the output from the corresponding12 km domain simulations.

The extended ozone season (April – October) was simulated through parallel individual monthly simulations for the base year, reference year and future year. For each month, the CMAQ simulations included a seven-day spin-up period (i.e., the last seven days of the previous month) for the outer 12 km domain where initial conditions for the beginning day were set to the default initial conditions included with the CMAQ release. The 4 km inner domain simulations utilized a three-day spin-up period, where the initial conditions for the starting day were based on output from the corresponding day of the 12 km domain simulation. These spin-up periods were chosen based on previous testing, which showed that influence from the initial conditions was negligible after the seven- and three-day spin-up periods for the 12 km and 4 km simulations, respectively. Table 6 lists the CMAQ configuration and settings used in the modeling.

Table 6. CMAQ configuration and settings.

Process	Scheme
Advection	Yamo module for horizontal and WRF module for vertical
Horizontal diffusion	Multi-scale

Process	Scheme
Vertical diffusion	ACM2 (Asymmetric Convective Model version 2)
Gas-phase chemical mechanism	SAPRC version 07tc gas-phase mechanism with extended isoprene chemistry
Chemical solver	EBI (Euler Backward Iterative solver)
Aerosol module	Aero6 (the sixth generation CMAQ aerosol mechanism)
Cloud module	ACM_AE6 (ACM cloud processor that uses the ACM methodology to compute convective mixing with heterogeneous chemistry for AERO6)
Photolysis rate	Phot/inline (calculating photolysis rates inline)

3. Results

3.1. Meteorological Model Evaluation

Simulated surface wind speed, temperature, and relative humidity from the 4 km domain were validated against hourly observations at 66 surface stations in the SJV. Observational data for the surface stations were obtained from the CARB archived meteorological database (*http://www.arb.ca.gov/aqmis2/aqmis2.php*). Table 7 lists the monitoring stations and which parameters are measured at each station, including wind speed, wind direction wind, temperature at 2 meters (T2) above ground level (AGL) and relative humidity at 2 meters (RH2) AGL. The location of each of these sites is shown in Figure 7. Several quantitative performance metrics were used to compare hourly surface observations and modeled estimates: mean bias (MB), mean error (ME) and index of agreement (IOA) based on recommendations from Simon et al. (2012). A summary of these statistics by performance region is shown in Table 8. The distribution of hourly mean bias and mean error are shown in Figure 8. The spatial distributions of the mean bias and mean error of modeled surface wind, temperature and relatively humidity are shown in Figure 9, while observed vs. modeled scatter plots are shown in Figure 10.

Figure 7. Meteorological monitoring sites in the San Joaquin Valley: red markers represent sites in the northern SJV; green markers represent sites in the central SJV, while blue markers represent sites in the southern SJV.

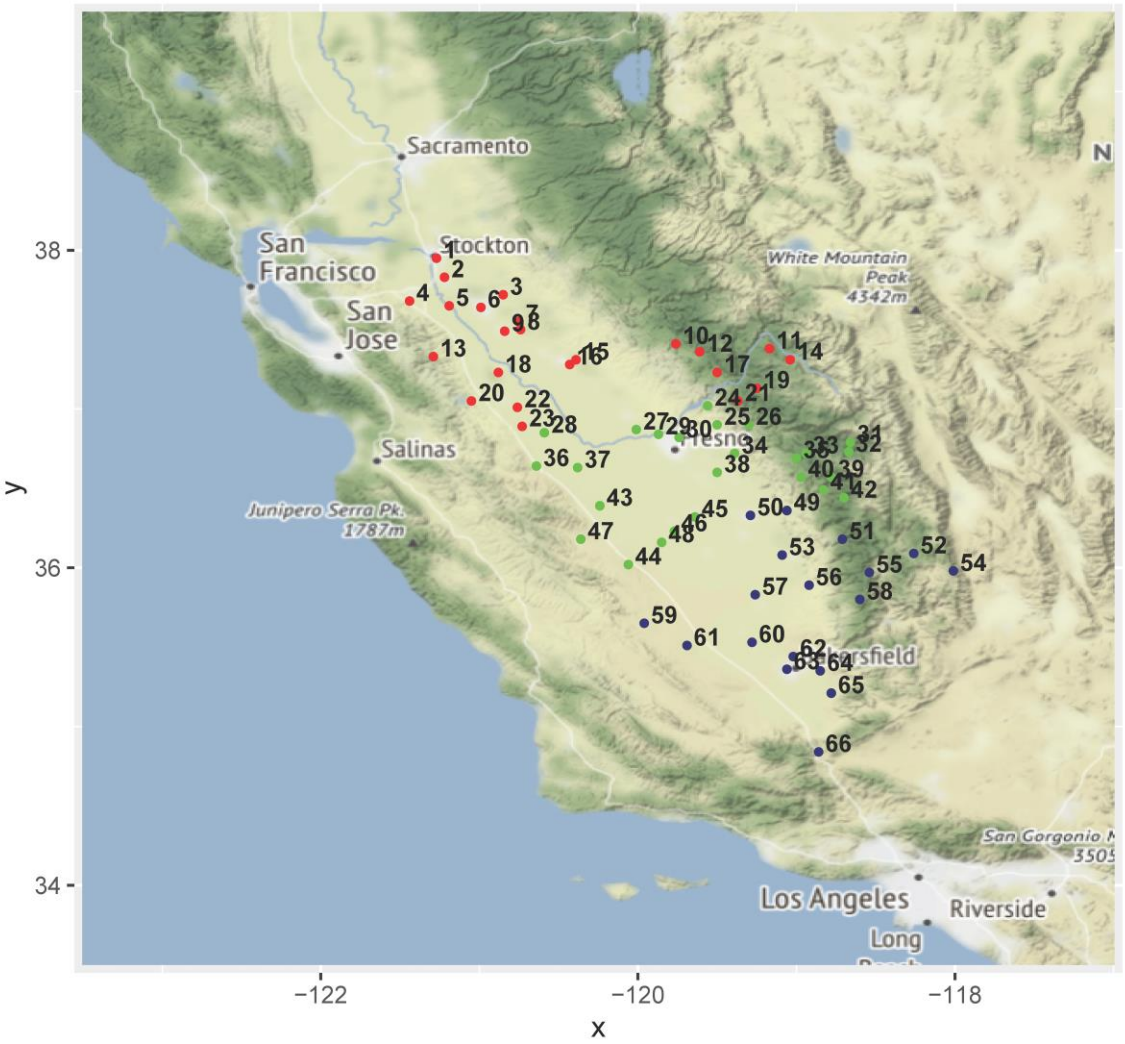

Table 7. Meteorological site location and parameter measured.

Site Number (Figure 7)	Site ID	Site Name	Region	Parameter(s) Measured
1	2094	Stockton-Hazelton Street	NSJV	Wind
2	5736	Manteca	NSJV	Wind, T2, RH2
3	5831	Oakdale #2	NSJV	Wind, T2, RH2
4	3696	Tracy-Airport	NSJV	Wind
5	5737	Modesto #3	NSJV	Wind, T2, RH2
6	2833	Modesto-14th Street	NSJV	Wind
7	7233	Denair II	NSJV	Wind, T2, RH2
8	3303	Rose Peak	NSJV	Wind
9	2996	Turlock-S Minaret Street	NSJV	Wind
10	3344	Metcalf Gap	NSJV	Wind
11	3570	Mount Tom (FTS)	NSJV	Wind
12	3582	Batterson	NSJV	Wind
13	3526	Diablo Grande	NSJV	Wind
14	3510	High Sierra	NSJV	Wind
15	5793	Merced	NSJV	Wind, T2, RH2
16	3022	Merced-S Coffee Avenue	NSJV	Wind
17	3455	North Fork	NSJV	Wind
18	5752	Kesterson	NSJV	Wind, T2, RH2
19	3649	Shaver #2	NSJV	Wind
20	3307	Los Banos	NSJV	Wind

Site Number (Figure 7)	Site ID	Site Name	Region	Parameter(s) Measured
21	3638	Mountain Rest (FTS)	NSJV	Wind
22	5730	Los Banos #2	NSJV	Wind, T2, RH2
23	5770	Panoche	NSJV	Wind, T2, RH2
24	3522	Hurley 1	CSJV	Wind
25	3346	Fancher Creek	CSJV	Wind
26	3535	Trimmer (FTS)	CSJV	Wind
27	3211	Madera-Pump Yard	CSJV	Wind
28	5711	Firebaugh - Telles	CSJV	Wind, T2, RH2
29	2844	Fresno-Sierra Skypark #2	CSJV	Wind
30	5741	Fresno State #2	CSJV	Wind, T2, RH2
31	3550	Cedar Grove	CSJV	Wind
32	3348	Sugarloaf	CSJV	Wind
33	3534	Park Ridge	CSJV	Wind
34	5787	Orange Cove	CSJV	Wind, T2, RH2
35	3523	Pinehurst	CSJV	Wind
36	3309	Panoche Road	CSJV	Wind
37	5757	Westlands	CSJV	Wind, T2, RH2
38	5723	Parlier #2	CSJV	Wind, T2, RH2
39	3036	Sequoia Natl Park-Lower Kaweah	CSJV	Wind
40	3349	Shadequarter	CSJV	Wind
41	3484	Sequoia and Kings Canyon Natl Park	CSJV	Wind

Site Number (Figure 7)	Site ID	Site Name	Region	Parameter(s) Measured
42	3533	Wolverton	CSJV	Wind
43	5828	Five Points SW	CSJV	Wind, T2, RH2
44	3330	Kettleman Hills	CSJV	Wind
45	3129	Hanford-S Irwin Street	CSJV	Wind
46	3712	Santa Rosa Rancheria-17225 Jersey	CSJV	Wind
47	6028	Coalinga-CIMIS	CSJV	Wind, T2, RH2
48	5715	Stratford #2	CSJV	Wind, T2, RH2
49	5746	Lindcove	SSJV	Wind, T2, RH2
50	2032	Visalia-N Church Street	SSJV	Wind
51	3457	Oak Opening	SSJV	Wind
52	3519	Blackrock	SSJV	Wind
53	5812	Porterville #3	SSJV	Wind, T2, RH2
54	3543	Whittier Hills	SSJV	Wind
55	3554	Johnsondale	SSJV	Wind
56	3350	Fountain Springs	SSJV	Wind
57	5823	Delano #2	SSJV	Wind, T2, RH2
58	3476	UHL	SSJV	Wind
69	5729	Blackwells Corner	SSJV	Wind, T2, RH2
60	5709	Shafter - USDA	SSJV	Wind, T2, RH2
61	5791	Belridge	SSJV	Wind, T2, RH2
62	2772	Oildale-3311 Manor Street	SSJV	Wind

Site Number (Figure 7)	Site ID	Site Name	Region	Parameter(s) Measured
63	3146	Bakersfield-5558 California Avenue	SSJV	Wind
64	2312	Edison	SSJV	Wind
65	5771	Arvin-Edison	SSJV	Wind, T2, RH2
66	5414	Lebec	SSJV	Wind

Wind Speed biases are positive in each of the three regions, with the smallest bias occurring in CSJV (0.33 m/s) and the largest bias occurring in the NSJV (0.62 m/s). Temperature bias is relatively small in the NSJV (-0.16 ˚K), and higher in the SSJV and CSJV, -1.1 ˚K and -1.47 ˚K, respectively. Temperature generally shows very good agreement between the observations and simulation in all regions with IOA values above 0.90. Relative humidity biases range from 9.42 % to 21.51%, with the largest bias occurring in the CSJV. These results are comparable to other WRF modeling efforts in California investigating ozone formation in Central California (e.g. Hu et al., 2012) and modeling analysis for the CalNex, CARES and Discover-AQ field studies (e.g. Fast et al., 2012; Baker et al., 2013; Kelly et al., 2014; Angevine et al., 2012; Chen et al., 2020). Detailed hourly time-series of surface temperature, relative humidity, wind speed, and wind direction for each sub-region can be found in the supplemental materials. Wind Roses from observations and WRF model results at the sites with the highest average DV for each region (Table 2) are also included in the supplemental materials.

Table 8. Hourly surface wind speed, temperature and relative humidity statistics by region for April-October 2018.

Variable	Region	Observed Mean	Modeled Mean	Mean Bias	Mean Error	IOA
Wind Speed (m/s)	SSJV	1.82	2.34	0.52	0.56	0.81
Wind Speed (m/s)	CSJV	1.93	2.26	0.33	0.46	0.83
Wind Speed (m/s)	NSJV	2.01	2.64	0.62	0.68	0.77
Temperature (˚K)	SSJV	295.94	294.83	-1.10	2.72	0.94
Temperature (˚K)	CSJV	295.82	294.35	-1.47	2.73	0.94
Temperature (˚K)	NSJV	293.37	293.22	-0.16	2.48	0.95
Relative Humidity (%)	SSJV	47.51	66.56	19.05	19.41	0.68
Relative Humidity (%)	CSJV	45.60	67.11	21.51	21.73	0.67
Relative Humidity (%)	NSJV	56.95	66.38	9.42	11.32	0.86

Figure 8. Distribution of hourly mean bias (left) and mean error (right) for April-October 2018. Results are shown for wind speed (top), temperature (middle), and RH (bottom).

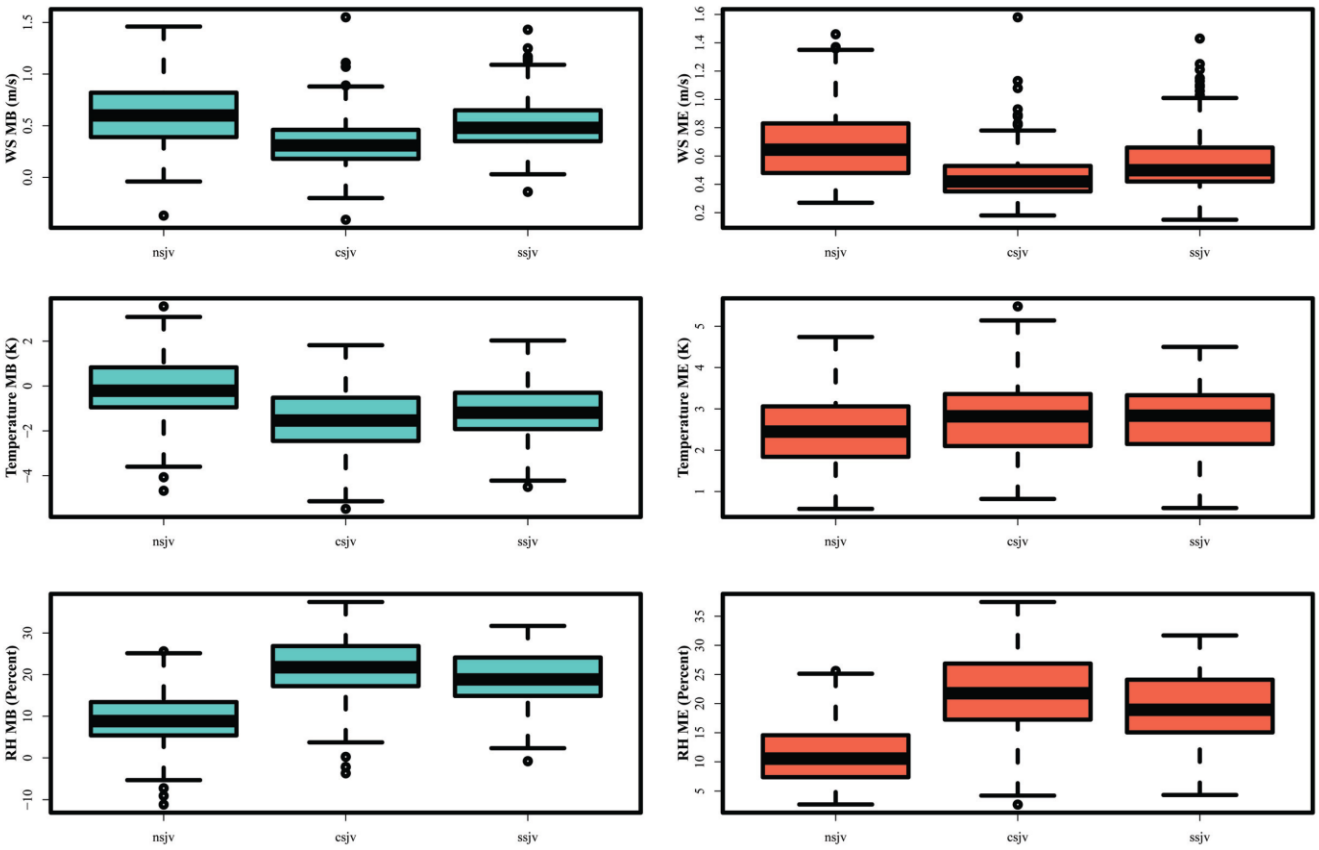

Figure 9. Spatial distribution of mean bias (left) and mean error (right) for April-October 2018. Results are shown for wind speed (top), temperature (middle), and RH (bottom).

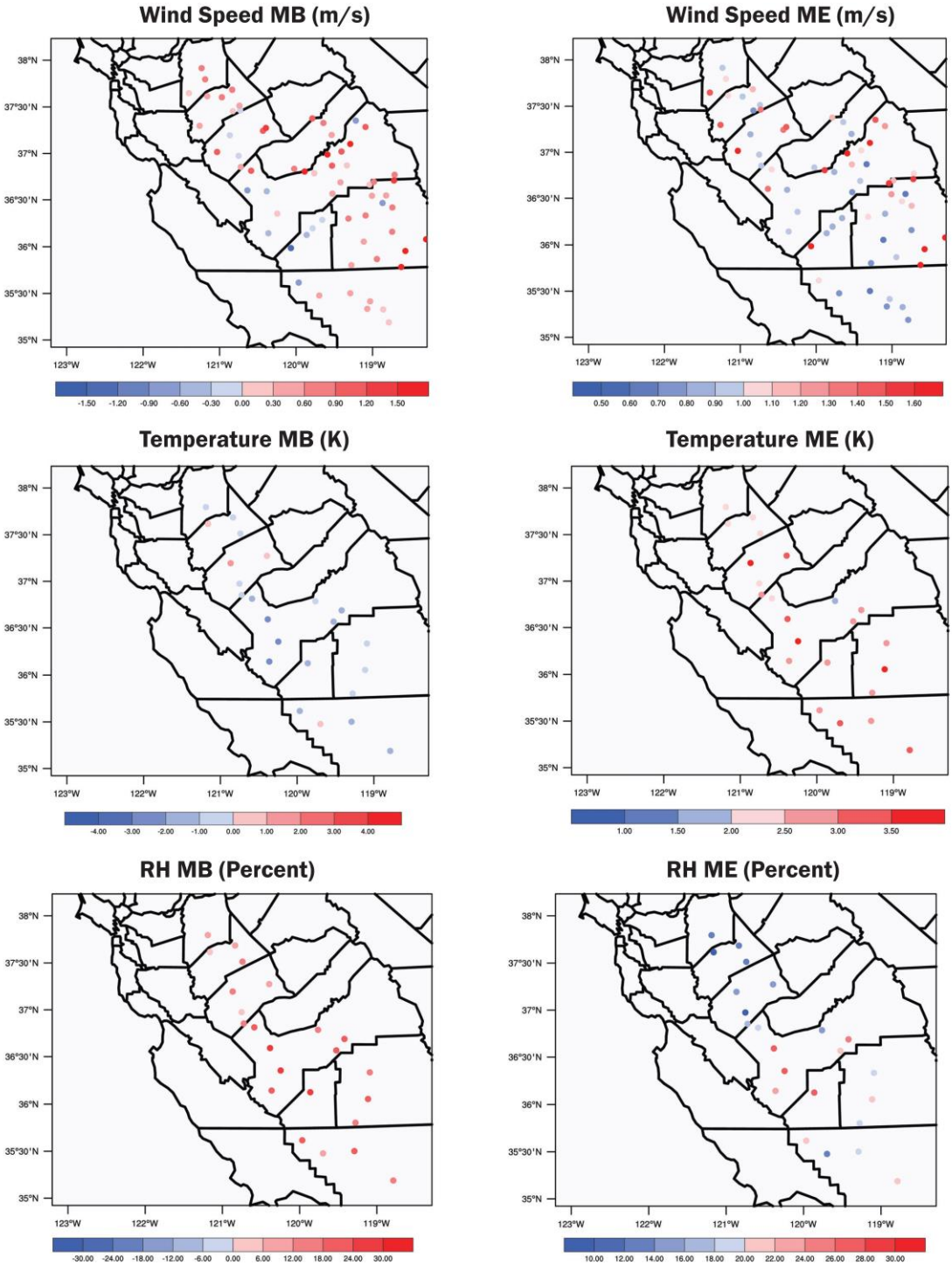

Figure 10. Comparison of modeled and observed hourly wind speed (left column), 2-meter temperature (middle column), and relative humidity (right column). Results for the Northern SJV are shown in the top row, Central SJV in the middle row, and Southern SJV in the bottom row.

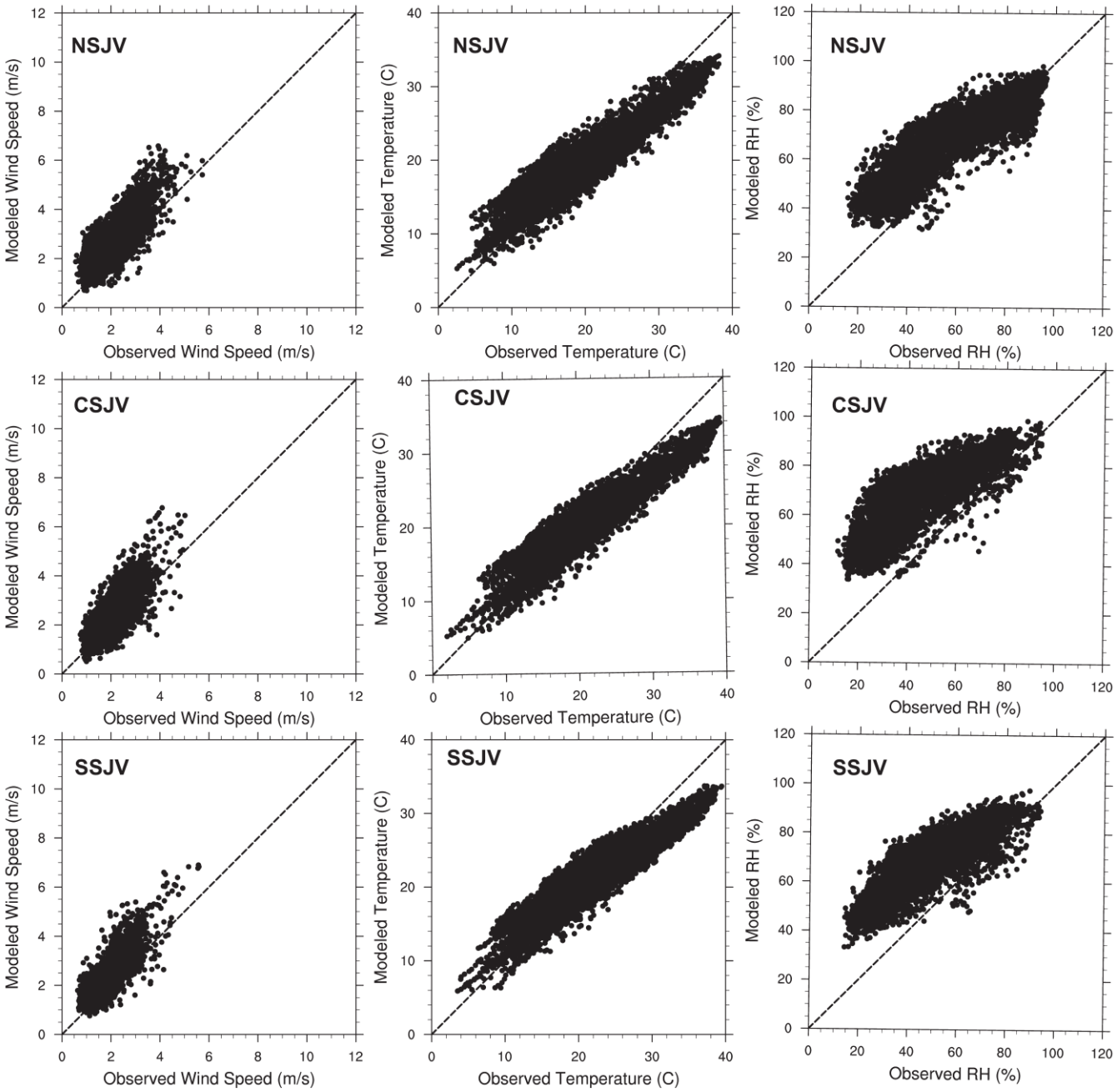

3.2. Phenomenological Evaluation

Conducting a detailed phenomenological evaluation for all modeled days can be resource intensive given that the entire ozone season (April – October) was modeled for the attainment demonstration. However, some insight and confidence that the model is able to reproduce the meteorological conditions leading to elevated ozone can be gained by investigating the meteorological conditions during a period of peak ozone within the Valley in more detail.

As described in Section 2, the Edison monitoring site located in the SSJV has the highest average DV in the SJV non-attainment area (Table 2). Since RRF calculations in the model attainment test described previously are based on the top 10 peak ozone days, the modeled and measured winds in the region were examined in further detail for the top 10 ozone days observed at the Edison site in 2018. The ten highest maximum daily average 8-hour ozone mixing ratios observed at the Edison site in 2018 occurred on July 31, August 8, August 9, August 1, August 7, August 4, September 22, September 26, September 28, July 29, respectively. Figure 11 shows the surface wind fields in the early afternoon (13:00 PST) and the evening (20:00 PST) on the highest ozone day (July 31, 2018) at the Edison site with the observed and modeled values denoted by red and black arrows, respectively. Overall, modeled winds compare relatively well with the observed values. The model was able to capture many of the important features of the wind fields in the SJV. The winds in the area of the Sacramento–San Joaquin River Delta split into flows going up towards the Sacramento Valley and down towards SJV. The westerly winds also penetrated into SJV via Pacheco pass. The changes of the up-slope wind in the early afternoon and down-slope wind in the evening are well reproduced in the model, both over the eastern slope of the Coastal Ranges and western slope of the Sierras.

Figure 12 shows the mean wind field (vector average) for the top 10 ozone days at 14:00 PST and 21:00 PST, respectively. Overall, the surface wind distribution indicates that the model is in general agreement with the observations and is able to capture many of the important features of the observed meteorological fields on those days when elevated ozone levels occurred.

Figure 11. Surface wind field at 13:00 PST (top) and 20:00 PST (bottom) on July 31, 2018. Modeled wind field is shown with black wind vectors, while observations are shown in red.

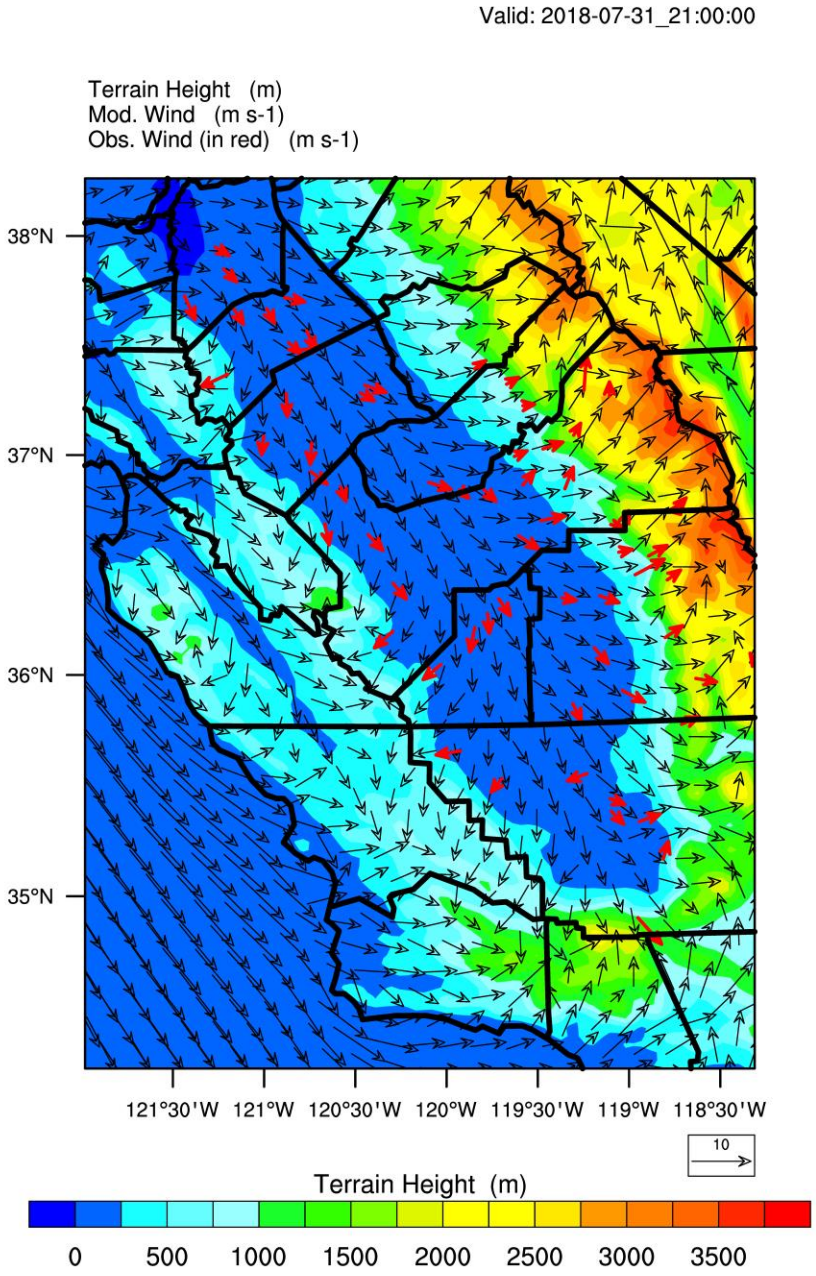

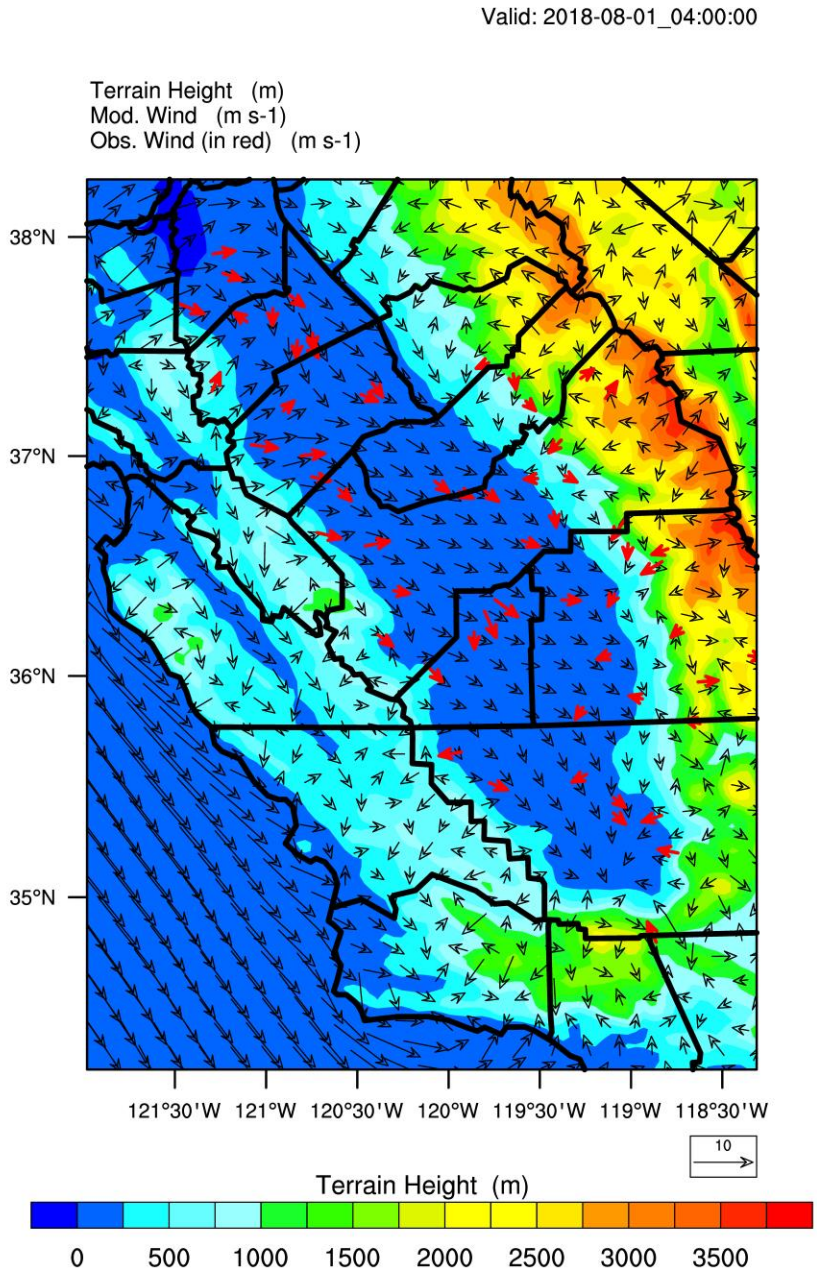
Valid: 2018-08-01_04:00:00
Terrain Height (m)
Mod. Wind (m s-1)
Obs. Wind (in red) (m s-1)
38°N
37°N
36°N
35°N
121°30'W
121°W
120°30'W
120°W
119°30'W
119°W
118°30'W
10
Terrain Height (m)
0
500
1000
1500
2000
2500
3000
3500

Figure 12. Average wind field at 14:00 PST (top) and 21:00 PST (bottom) for the top 10 observed ozone days at Edison monitoring site in 2018. Modeled wind field is shown with black wind vectors, while observations are shown in red.

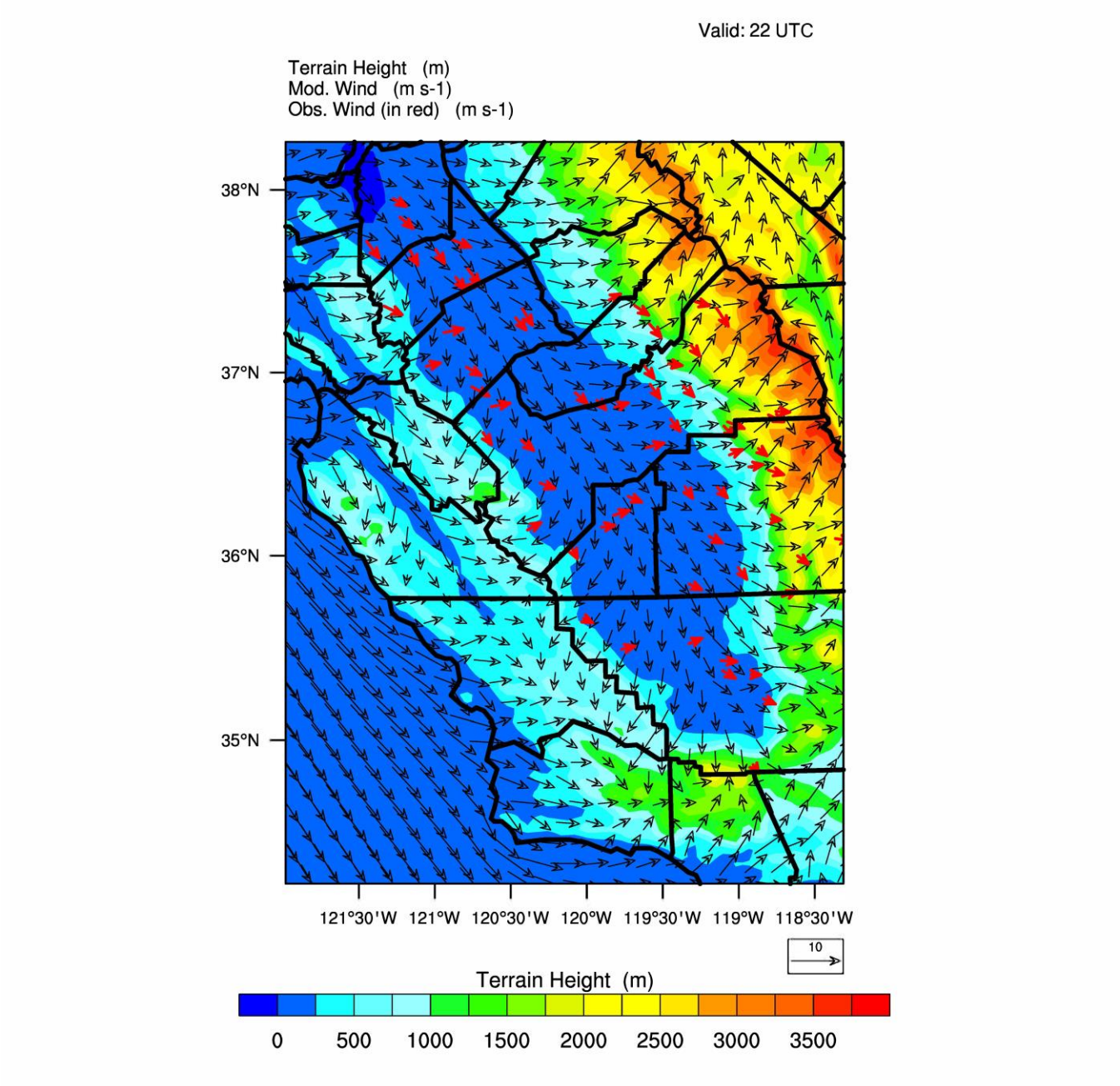

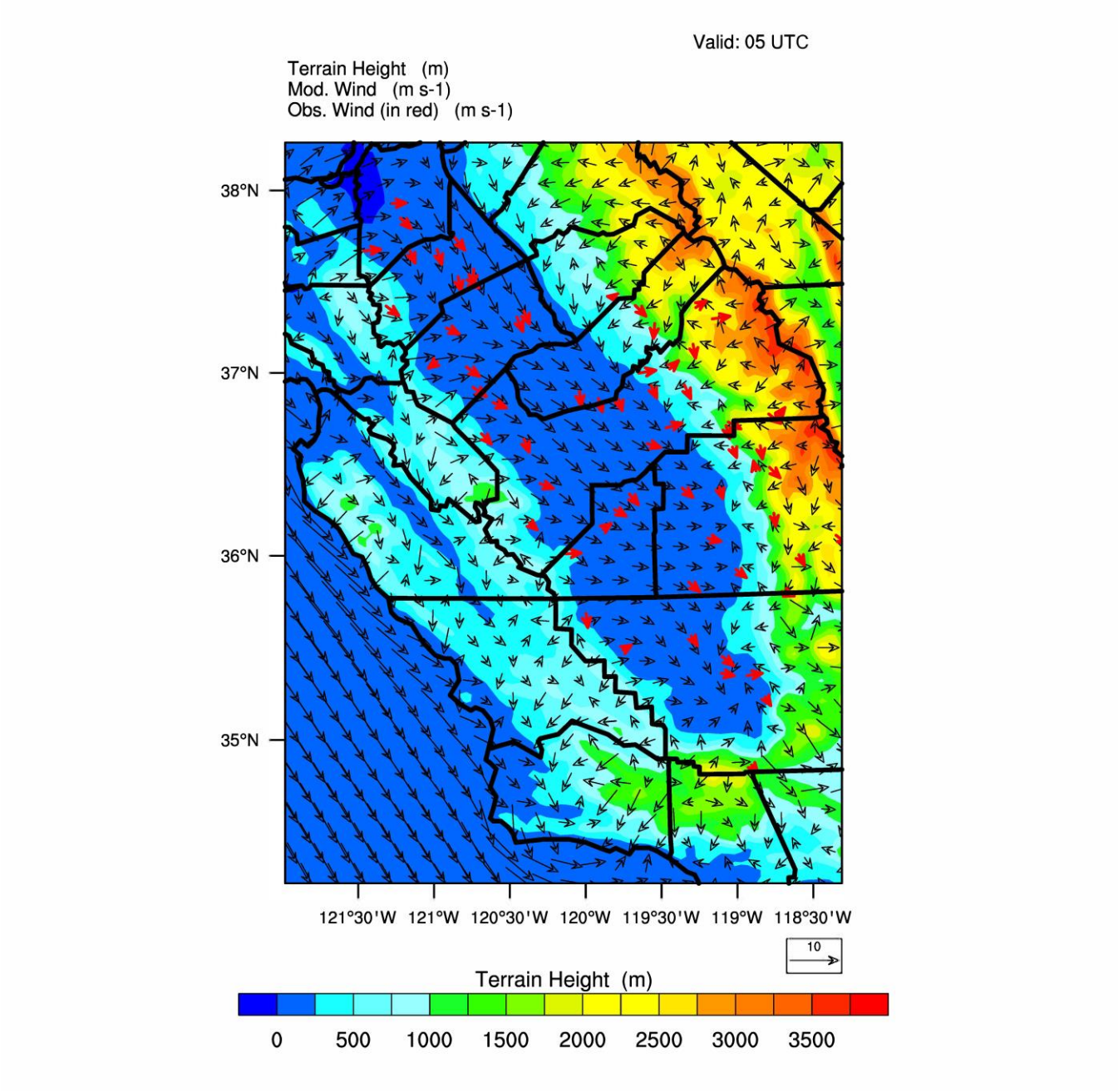

Figure 13 shows the 500 hPa geopotential height at 00:00 UTC and 12:00 UTC for the top 10 ozone days in 2018 at the Edison site. These times were chosen to coincide with timing of the upper-air observations in the region. In this figure, the North American Regional Reanalysis (NARR) data is used to represent the observations. The NARR dataset is a product of observational data assimilated (including upper-air observations) into some of the NOAA model products for the purpose of producing a snapshot of the weather over North America at any given time. The 500 hPa geopotential height is a useful metric to evaluate, because it is one of the major parameters related to regional synoptic patterns. It can be seen from Figure 13 that on average the 500 hPa geopotential height is ~5800 m above sea level on these peak

ozone days, and the modeled 500 hPa geopotential height closely matches the observed values.

Figure 13. Modeled and observed 500 hPa geopotential height at 00:00 UTC (top) and 12:00 UTC (bottom) for the top 10 observed ozone days at the Edison monitoring site in 2018.

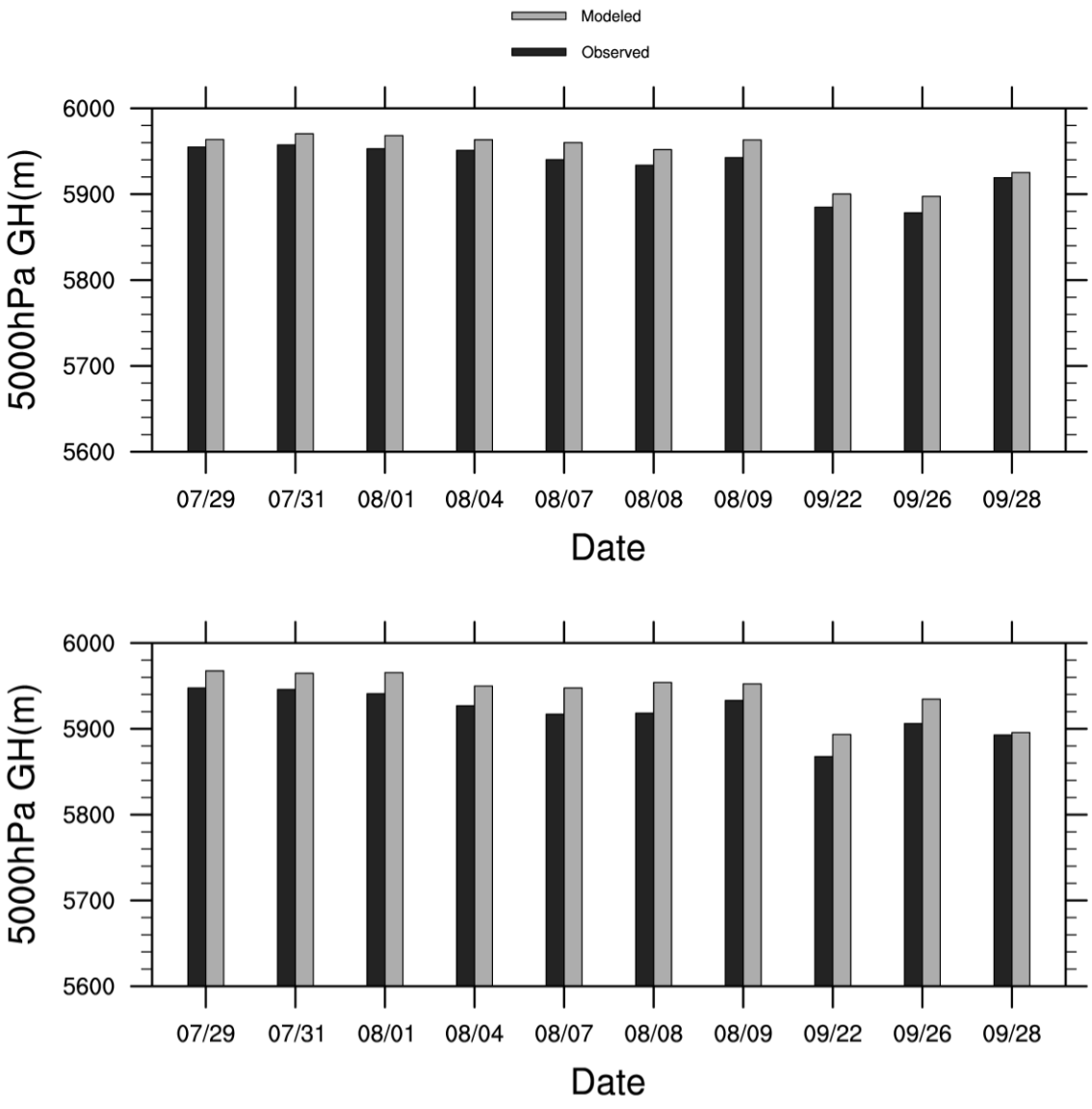

3.3. Air Quality Model Evaluation

Observed ozone data from CARB's Air Quality and Meteorological Information System (AQMIS) database (*www.arb.ca.gov/airqualitytoday/*) and Aerometric Data Analysis and Management (ADAM) database (*www.arb.ca.gov/adam/*) were used to evaluate the accuracy of the 4 km CMAQ modeling for all ozone monitors listed in Table 2. The U.S. EPA modeling guidance (U.S. EPA, 2018) recommends using the grid cell value where the monitor is located, to pair observations with simulated values in operational evaluation of model predictions. Since the future year design value calculations are based on simulated values near the monitor (i.e., the maximum simulated ozone within a 3x3 array of grid cells with the grid cell containing the monitor located at the center of the array), model performance was evaluated by comparing observations against the simulated values at the monitored grid cell as well as the peak grid cell within the 3x3 grid array centered on the monitor (i.e., the 3x3 maximum). While different cutoff criteria have be used in different model evaluation studies (Emery et al., 2017), U.S. EPA suggests the days with simulated values > 60 ppb should receive higher priority in evaluation to give more attention to the model outputs that could potentially impact the outcome of the attainment test. Model performance is further summarized separately for the three sub-regions in the Valley due to their distinct geographical, meteorological and air quality patterns.

As recommended by U.S. EPA modeling guidance, a number of statistical metrics have been used to evaluate the model performance for ozone. These metrics include mean bias (MB), mean error (ME), mean fractional bias (MFB), mean fractional error (MFE), normalized mean bias (NMB), normalized mean error (NME), root mean square error (RMSE), and correlation coefficient (R^2). In addition, the following plots were used in evaluating the modeling with all available data: time-series plots comparing the predictions and observations, scatter plots for comparing the magnitude of the simulated and observed concentrations, as well as frequency distributions.

The model performance evaluation is presented for the entire SJV region and also disaggregated for the three sub regions. Performance statistics for modeling scenarios with data above 60 ppb are reported separately for different ozone metrics including maximum daily average 8-hour ozone, maximum daily average 1-hour ozone, and hourly ozone (all hours of the day) for the monitored grid cell as well as the 3x3 maximum. Performance statistics for MDA8 O_3 are shown in Table 9 and Table 10. Overall, when simulated data extracted at the grid cell is used for comparison with observations (as shown in Table 9), the model shows a slight negative bias in MDA8 O_3 greater than 60 ppb in all regions, with the smallest bias occurring in the northern SJV (-0.34 ppb) and the largest bias occurring in the southern SJV (-3.69 ppb). However, when the 3x3 maximum is used instead, model shows a positive bias of 1.58 ppb at northern SJV and the bias at southern SJV reduces to -1.57 ppb. Mean error shows a consistent trend with the error getting smaller from 6.97 ppb to 6.63 ppb for the entire SJV when the 3x3 maximum is considered. Similar statistics for maximum daily average 1-hour ozone (monitor grid cell and 3x3 maximum) and hourly ozone can be found in Table 11, Table 12 and Table 13, respectively.

The model performance statistics shown in Table 9 through Table 13 are consistent with previous studies in California and elsewhere in the U.S. Hu et al. (2012), simulated an ozone episode in Central California (July 27 – August 2, 2000) using the SAPRC07 chemical mechanism and found that a model bias of -10.8 ppb for MDA8 O_3 with 60 ppb cutoff (compared to -3.34 ppb and -1.35 ppb for the entire SJV of this work). Hu et al. also shows a model bias of -12.7 ppb for maximum daily average 1-hour ozone in Central California with 60 ppb cutoff (compared to -4.50 ppb and -1.88 ppb in this work). Similarly, Shearer et al. (2012) compared model performance in Central California during two episodes in 2000 (July 24 – 26 and July 31 – August 2) for two different chemical mechanisms and found that normalized bias for MDA8 O_3 ranged from -7% to -14% with hourly peak ozone showing a range of -7% to -18%. These values are greater than the statistics found in this work, which were calculated as -5.28% for MDA8 O_3 and -6.47% for maximum daily average 1-hour O_3. Jin et al. (2010) conducted a longer-term simulation over Central California (summer 2000) and found a RMSE for MDA8 O_3 of 14 ppb, which is greater than the 9.25 ppb found in this work. Jin et al. (2010) also showed an overall negative bias of -2 ppb, which is in the similar range of -3.34 ppb (-1.35 ppb with 3x3 maximum values) found in this work. Zhu et al. (2019) shows hourly O_3 NMB of 8.2% and NME of 11.3% for July and August 2012 with 20 ppb cutoff, both are consistent with the NMB and NME we show in Table 13.

Table 9. Maximum daily average 8-hour ozone performance statistics by modeling subregions and entire SJV region for the 2018 ozone season (April - October). Maximum daily average 8-hour ozone (>60ppb) with simulated data extracted at grid cell where the monitor is located.

Parameter	NSJV	CSJV	SSJV	Entire SJV
Number of data points	238	796	1303	2337
Mean obs (ppb)	67.77	68.12	70.64	69.49
Mean Bias (ppb)	-0.34	-3.66	-3.69	-3.34
Mean Error (ppb)	7.14	6.68	7.11	6.97
RMSE (ppb)	9.44	9.05	9.33	9.25
Mean Fractional Bias (%)	-0.98	-5.80	-5.75	-5.28
Mean Fractional Error (%)	10.66	10.23	10.56	10.46
Normalized Mean Bias (%)	-0.51	-5.37	-5.23	-4.81
Normalized Mean Error (%)	10.53	9.81	10.06	10.03
R-squared	0.10	0.11	0.28	0.22

Table 10. Maximum daily average 8-hour ozone performance statistics by modeling subregions and entire SJV region for the 2018 ozone season (April - October). Maximum daily average 8-hour ozone (>60ppb) with simulated data extracted from the 3x3 grid cell array maximum centered at the monitor.

Parameter	NSJV	CSJV	SSJV	Entire SJV
Number of data points	238	796	1303	2337
Mean obs (ppb)	67.77	68.12	70.64	69.49
Mean Bias (ppb)	1.58	-1.87	-1.57	-1.35
Mean Error (ppb)	7.22	6.39	6.66	6.63

Parameter	NSJV	CSJV	SSJV	Entire SJV
RMSE (ppb)	9.34	8.53	8.73	8.72
Mean Fractional Bias (%)	1.90	-3.12	-2.64	-2.34
Mean Fractional Error (%)	10.55	9.63	9.70	9.76
Normalized Mean Bias (%)	2.34	-2.75	-2.22	-1.95
Normalized Mean Error (%)	10.66	9.38	9.43	9.54
R-squared	0.11	0.14	0.30	0.24

Table 11. Maximum daily average 1-hour ozone performance statistics by modeling subregions and entire SJV region for the 2018 ozone season (April - October). Maximum daily average 1-hour ozone (>60ppb) with simulated data extracted at grid cell where the monitor is located.

Parameter	NSJV	CSJV	SSJV	Entire SJV
Number of data points	436	1140	1649	3225
Mean obs (ppb)	71.33	72.93	75.19	73.87
Mean Bias (ppb)	0.08	-5.70	-4.88	-4.50
Mean Error (ppb)	8.62	8.97	8.24	8.55
RMSE (ppb)	11.37	12.17	10.75	11.35
Mean Fractional Bias (%)	-0.42	-8.13	-6.91	-6.47
Mean Fractional Error (%)	12.10	12.70	11.46	11.98
Normalized Mean Bias (%)	0.11	-7.82	-6.48	-6.09
Normalized Mean Error (%)	12.09	12.30	10.97	11.58
R-squared	0.17	0.17	0.40	0.28

Table 12. Maximum daily average 1-hour ozone performance statistics by modeling subregions and entire SJV region for the 2018 ozone season (April - October). Maximum daily average 1-hour ozone (>60ppb) with simulated data extracted from the 3x3 grid cell array maximum centered at the monitor.

Parameter	NSJV	CSJV	SSJV	Entire SJV
Number of data points	436	1140	1649	3225
Mean obs (ppb)	71.33	72.93	75.19	73.87
Mean Bias (ppb)	2.80	-3.40	-2.07	-1.88
Mean Error (ppb)	9.12	8.44	7.64	8.12
RMSE (ppb)	11.79	11.33	9.97	10.72
Mean Fractional Bias (%)	3.29	-4.90	-3.05	-2.84
Mean Fractional Error (%)	12.47	11.79	10.41	11.17
Normalized Mean Bias (%)	3.92	-4.66	-2.75	-2.55
Normalized Mean Error (%)	12.78	11.57	10.16	11.00
R-squared	0.20	0.21	0.41	0.30

Table 13. Hourly ozone performance statistics by modeling subregions and entire SJV region for the 2018 ozone season (April - October). Hourly ozone (>60ppb) with simulated data extracted at grid cell where the monitor is located. Note that only statistics for the grid cell in which the monitor is located were calculated for hourly ozone.

Parameter	NSJV	CSJV	SSJV	Entire SJV
Number of data points	2228	7084	13172	22484
Mean obs (ppb)	68.91	68.86	70.51	69.83
Mean Bias (ppb)	-2.38	-5.47	-5.33	-5.08
Mean Error (ppb)	9.21	8.73	8.91	8.89

Parameter	NSJV	CSJV	SSJV	Entire SJV
RMSE (ppb)	12.10	11.66	11.86	11.82
Mean Fractional Bias (%)	-4.46	-8.70	-8.62	-8.23
Mean Fractional Error (%)	13.92	13.41	13.65	13.60
Normalized Mean Bias (%)	-3.46	-7.95	-7.56	-7.28
Normalized Mean Error (%)	13.37	12.68	12.64	12.72
R-squared	0.10	0.09	0.21	0.16

Simon et al. (2012) conducted a review of photochemical model performance statistics published between 2006 and 2012 for North America (from 69 peer-reviewed articles). In Figure 13, the statistical evaluation of this model attainment demonstration is compared to the model performance summary presented in Simon et al. (2012) by overlaying various summary statistics onto the Simon et al. (2012) model performance summary. Note that the box-and-whisker plot (colored in black) shown in Figure 14 is reproduced using data from Figure 4 of Simon et al. (2012). The red dot and blue triangle in each of the panels in Figure 14Figure denote the model performance statistics from the current modeling work, calculated using the simulated monitor grid cell and the 3x3 maximum, respectively. Figure 14 clearly shows that the model performance statistical metrics for hourly, maximum daily average 8-hour and maximum daily average 1-hour ozone from this work are consistent with previous modeling studies reported in the scientific literature, and in most cases are better than those statistics. In particular, the Simon et. al. (2012) study found that mean bias for maximum daily average 8-hour ozone ranged from approximately -7 ppb to 13 ppb, while mean error ranged from around 4 ppb to 22 ppb, and RMSE varied from approximately 8 ppb to 23 ppb; all of which are similar in magnitude to the statistics presented in Table 9 and Table 10.

Spatial distributions of modeled and observed average MDA8 ozone for the top 10 O_3 days at the Edison site are displayed in Figure 15. The model is able to capture the observed spatial distribution of ozone showing relatively lower values in NSJV and high values in CSJV and SSJV. Time series of the hourly, maximum daily average 1-hr and maximum daily average 8-hour ozone data used to generate Table 9 to Table 13 can be found in the supplemental materials.

Figure 14. Comparison of various statistical metrics from the attainment demonstration modeling to the range of statistics from the 69 peer-reviewed studies summarized in Simon et al (2012). (MDA denotes Maximum Daily Average). Red circular markers show statistics calculated from modeled ozone at the monitor location, while blue triangular markers show statistics calculate from the maximum ozone in the 3x3 array of grid cells surrounding the monitor. Statistics for hourly ozone were only calculated from data over 60 ppb.

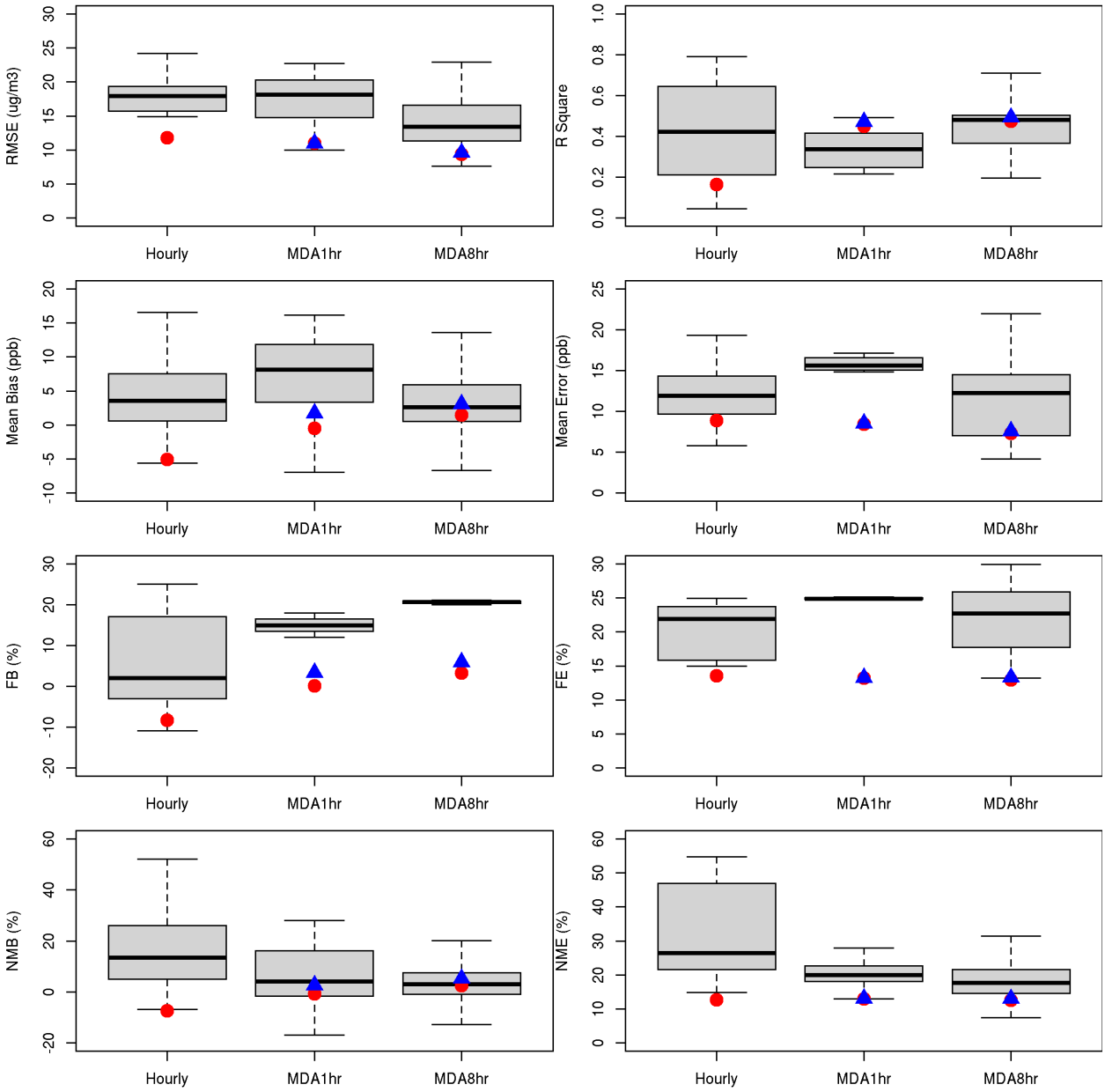

Figure 15. Average MDA8 ozone for the top 10 ozone days from the model simulations overlaid with observation data (marked as circle), where the top 10 days from the observations were chosen based on the Edison monitor.

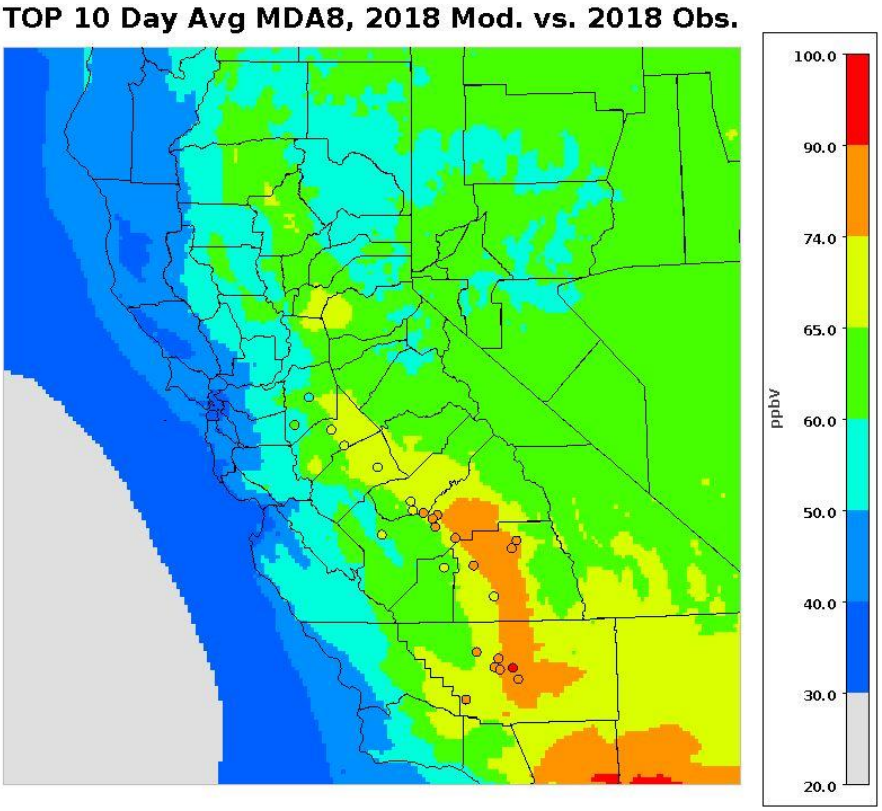

3.4. Air Quality Model Diagnostic Evaluation

In addition to the statistical evaluation presented above it is also useful to consider whether the model is able to reproduce observable relationships between changes in emissions and ozone. One approach to this would be to conduct a retrospective analysis where additional years are modeled (e.g., 2000 or 2005) so that the ability of the modeling system to reproduce the observed change in ozone over time can be investigated. However, this approach is extremely time consuming because it requires the development of additional meteorological fields and emission inventories, as well as multi-year air quality modeling. Another approach to investigating the ozone response to changes in emissions is through the so called “weekend effect”.

The weekend effect is a well-known phenomenon in some major urbanized areas where emissions of NOx are substantially lower on weekends than on weekdays, but measured levels of ozone are higher on weekends than on weekdays. This is due to the complex and

non-linear relationship between NOx and ROG precursors and ozone. Ozone formation exhibits a nonlinear dependence to NO_x and ROG precursors in the atmosphere. In general terms, under ambient conditions of high-NOx and low-ROG (NOx-disbenefit region in Figure 16), ozone formation tends to exhibit a disbenefit to reductions in NOx emissions (i.e., ozone increases with decreases in NOx) and a benefit to reductions in ROG emissions (i.e., ozone decreases with decreases in ROG). In contrast, under ambient conditions of low-NOx and high-ROG (NOx-limited region in Figure 16), ozone formation shows a benefit to reductions in NOx emissions, while changes in ROG emissions result in only minor decreases in ozone. These two distinct "ozone chemical regimes" are illustrated in Figure 16 along with a transitional regime that can exhibit characteristics of both the NOx-disbenefit and NOx-limited regimes. Note that Figure 16 is shown for illustrative purposes only and does not represent the actual ozone sensitivity within the SJV for a given combination of NOx and VOC (ROG) emissions.

In this context, the prevalence of the weekend effect in a region suggests that the region is in a NO_x-disbenefit regime (Heuss et al., 2003). A lack of a weekend effect (i.e., no pronounced high O_3 occurrences during weekends) would suggest that the region is in a transition regime and moving between exhibiting a NOx-disbenefit and being NOx-limited. A reversed weekend effect (i.e., lower O_3 during weekends) would suggest that the region is NO_x-limited.

Figure 16. Illustration of a typical ozone isopleth plot, where each line represents ozone mixing ratio, in 10 ppb increments, as a function of initial NOx and VOC (or ROG) mixing ratio (adapted from (Seinfeld and Pandis 1998), Figure 5.15). General chemical regimes for ozone formation are shown as NOx-disbenefit (red circle), transitional (blue circle), and NOx-limited (green circle).

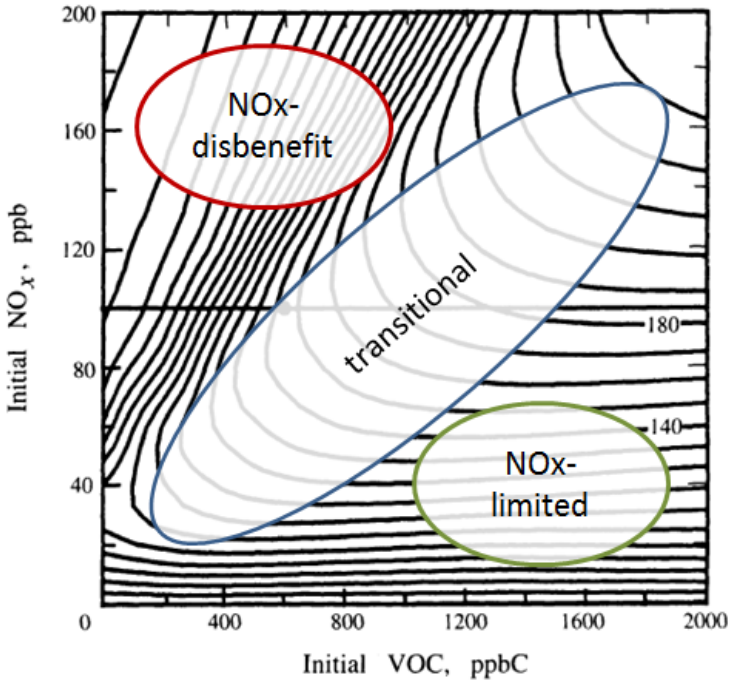

Investigating the “weekend effect” and how it has changed over time is a useful real-world metric for evaluating the ozone chemistry regime in the SJV and how well it is represented in the modeling. The trend in day-of-week dependence of the Valley’s sub-regional observed ozone levels between 2000 and 2020 is shown in Figure 17. The six-panel scatter plot compares the average site-specific weekday (Wednesday and Thursday) and weekend (Sunday) observed summertime (June through September) maximum daily average 8-hr ozone value by year (2000 to 2020) and separated into three sub-regions: northern SJV (top), central SJV (middle), and southern SJV (bottom). The dark gray square and light gray triangle markers denote the predicted baseline (2018) and future (2037) average site-specific weekday and weekend ozone values from the attainment demonstration modeling. Different definitions of weekday and weekend days were also investigated and did not show appreciable differences from the Wednesday/Thursday and Sunday definitions.

Figure 17. Site-specific average weekday and weekend maximum daily average 8-hour ozone for each year from 2000 to 2020 for the Northern SJV (top), Central SJV (middle), and Southern SJV (bottom). The colored circle markers denote observed values while the dark gray square and light gray triangle markers denote the simulated baseline 2018 and future 2037 values. Points falling below the 1:1 dashed line represent a NOx-disbenefit regime, those on the 1:1 dashed line represent a transitional regime, and those above the 1:1 dashed line represent a NOx-limited regime.

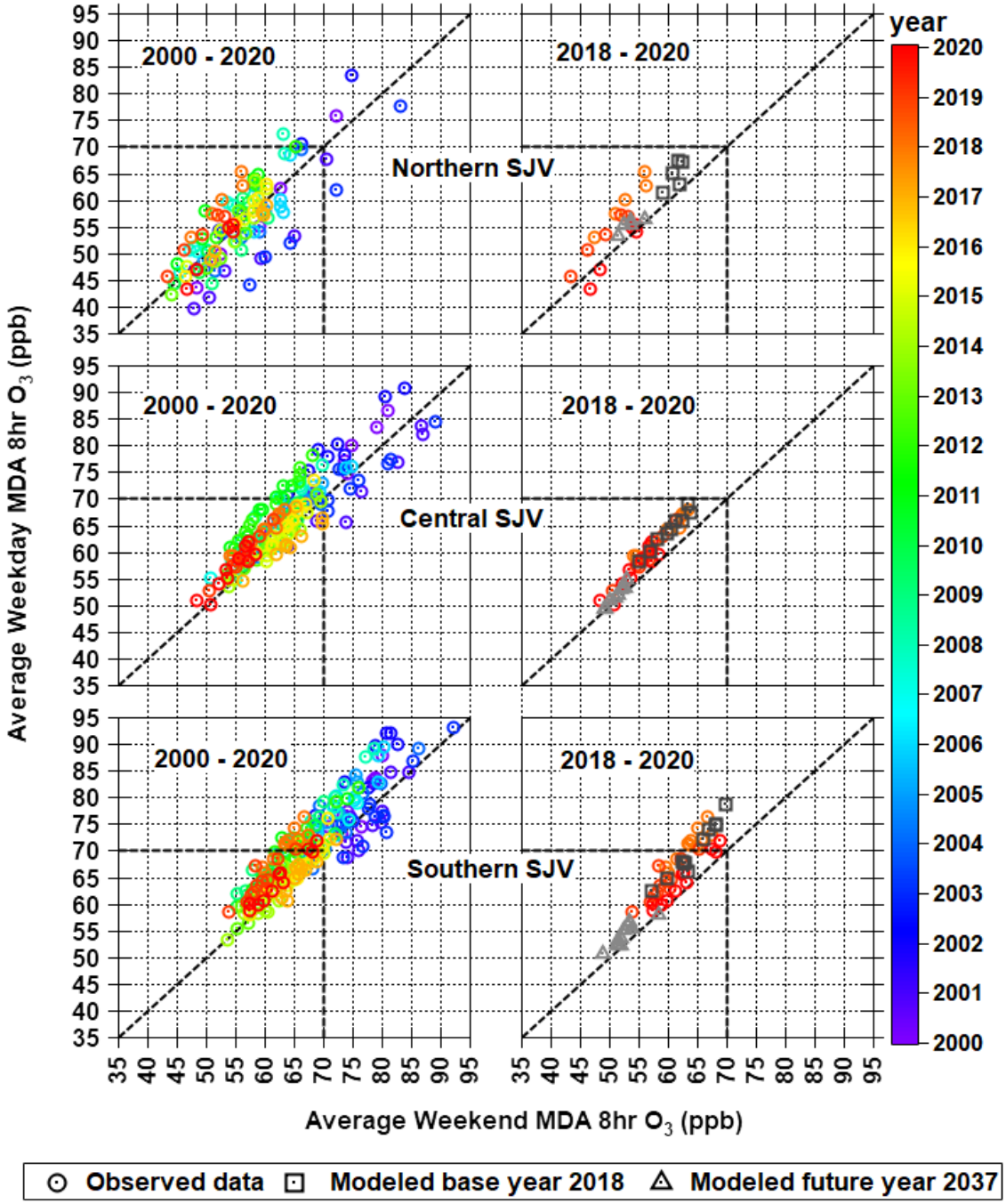

Figure 17 shows that ozone levels are highest in the southern (i.e., Bakersfield area) and central (i.e., Fresno area) SJV regions, with the lowest levels seen in the northern SJV region. A key observation in Figure 17 is that the summertime average weekday and weekend ozone levels have steadily declined between 2000 and 2020.

Along with the declining ozone, there is a pattern shift in the weekday and weekend ozone between 2000 and 2020. In the early 2000's, the central and southern regions of the SJV exhibited roughly an equal number of sites with weekend ozone greater and less than weekday ozone, which suggests that the regions may have been in the transitional chemical regime for ozone formation. By the mid-2000's, majority of the sites were showing weekday ozone greater than weekend ozone, which is consistent with a shift into complete NOx-limited chemistry. However, some of the sites had shifted back towards a more equal distribution between weekday and weekend ozone, likely due to interannual variability in the biogenic emissions and meteorology. In contrast to the central and southern portions of the SJV, the northern region clearly experienced a greater NOx-disbenefit in the early 2000's and then moved into a transitional chemical regime in the mid-2000's. These findings are also consistent with an independent analysis by UC Berkeley researchers on the observed response of ozone in the SJV to emission reductions in NOx and VOC reactivity from 1995 to 2010 (Pusede et al., 2012). The Pusede et al. study concluded that NOx emission reductions have been effective at reducing ozone levels and have successfully transitioned the southern and central portions of the SJV into a NOx-limited chemistry regime, while the northern portion of the SJV was in the process of transitioning to the same chemical regime during 1995-2010 timeframe.

The right panels of Figure 17 show that all the three sub-regions have almost fully transitioned to the NOx-limited regime in recent years (2018-2020) except for some sites in the northern region, which continue to oscillate (top right panel) falling above, close to or below the 1:1 dashed line depending on the year and likely due to the year-to-year variability in meteorology and associated changes in biogenic ROG emissions. The simulated baseline 2018 weekday/weekend values (dark gray square markers in the right panels of Figure 17) fall above the 1:1 dashed line for Northern, Central and Southern SJV with values in the Northern region falling relatively closer to the 1:1 dashed line. These predicted values are generally consistent with observed findings that show a shift into NOx-limited chemistry first in the central and southern regions, followed by northern region in the Valley.

The predicted future 2037 values (light gray triangle markers in the right panels) clearly show that weekday and weekend ozone decline significantly (all values are below 60 ppb) and all three sub-regions show a shift to a NOx-limited regime with all values falling above the 1:1 dashed line. This shift in chemistry by 2037 is corroborated by a study from UC Berkeley researchers that analyzed the impacts of future emissions controls using an analytical model constrained by CalNex 2010 measurements in the Valley (Pusede et. al., 2014) and concluded that the NO_x controls will be immediately and incrementally more effective than corresponding ROG controls in lowering the Valley's ozone levels.

3.5. Future Design Values

The RRFs and the future 2037 ozone design values for monitoring sites in the northern, central, and southern regions of the Valley were calculated using the procedures outlined in the Methodology section of this document and are summarized in Table 14. Note that the results shown in the table are ordered by each sub-region in descending order of the average reference year 2018 DVs. The 2037 future year design values in this table account for all the emissions controls described in Section 3.5, including federal clean truck and Tier 5 off-road commitments. To estimate future 2037 DVs without the effects of the federal clean truck and Tier 5 off-road commitments, the change in model generated DVs from 2032 to 2037 can be combined with the emissions for 2032 and 2037 to estimate the change in DV per ton of NOx emissions. Note that between 2032 and 2037 NOx emissions within the Valley decrease by 19.85 tpd, while ROG emissions are reduced by 1.08 tpd in the modeling, so the change in DV between 2032 and 2037 is almost entirely driven by the change in NOx emissions. If the federal clean truck and Tier 5 off-road commitments (a total of 4.35 tpd of NOx emissions in SJV) are excluded, the 2037 future year design values will increase by up to 1.2 ppb (Table 15). The new 2037 DVs in Table 15 are the actual future design values because the Federal Clean Truck and Tier 5 Off-Road measures are not part of the final SIP commitments.

The three sub regions show varied response to emission controls as evident from the RRF values shown in Table 14. Southern SJV has the greatest response, as seen from the low values of the site-specific RRF, followed by Central SJV and Northern SJV.

The results in Table 15 show that all monitoring sites in the Valley have a future DV less than 70 ppb based on the 2037 emissions inventory, with the Clovis monitor in Central SJV having the highest predicted future design value of 68.8 ppb and truncated value of 68 ppb in 2037. Therefore, the attainment demonstration modeling predicts that the entire Valley will attain the 70 ppb 8-hour O_3 standard by 2037 with the commitments outlined in the SIP.

Table 14. Summary of key parameters related to the future year 2037 ozone design value (DV) calculation, where the 2037 DVs include federal clean truck and Tier 5 off-road commitments.

Sub-region	Site	RRF	2018 Average DV (ppb)	2037 DV (ppb)	2037 Truncated DV (ppb)
Northern SJV	Turlock-S Minaret St.	0.7924	82.3	65.2	65
Northern SJV	Modesto-14th St.	0.8300	79.3	65.8	65
Northern SJV	Merced-S Coffee Av.	0.7771	76.7	59.6	59
Northern SJV	Tracy-Airport	0.8682	73.7	64.0	64
Northern SJV	Stockton-Hazelton St.	0.8795	66.0	58.0	58
Central SJV	Fresno-Garland	0.7889	85.7	67.6	67
Central SJV	Clovis	0.7943	85.3	67.8	67
Central SJV	Parlier	0.7483	84.3	63.1	63
Central SJV	Fresno-Drummond St.	0.7930	82.0	65.0	65
Central SJV	Fresno- Sierra Skypark #2	0.7845	80.0	62.8	62
Central SJV	Hanford-S. Irwin St.	0.8075	80.0	64.6	64
Central SJV	Madera-28261 Avenue 14	0.7681	77.7	59.7	59
Central SJV	Madera-Pump Yard	0.8045	75.7	60.9	60
Central SJV	Tranquility	0.8322	72.7	60.5	60

Sub-region	Site	RRF	2018 Average DV (ppb)	2037 DV (ppb)	2037 Truncated DV (ppb)
Southern SJV	Edison	0.6918	89.0	61.6	61
Southern SJV	Arvin-Di Giorgio	0.6887	88.0	60.6	60
Southern SJV	Bakersfield-5558 California Avenue	0.7521	87.3	65.7	65
Southern SJV	Sequoia and Kings Canyon Natl Park	0.7002	86.7	60.7	60
Southern SJV	Bakersfield-Municipal Airport	0.7047	85.3	60.1	60
Southern SJV	Visalia-N Church Street	0.7518	84.0	63.2	63
Southern SJV	Maricopa-Stanislaus Street	0.7843	83.7	65.6	65
Southern SJV	Sequoia Natl Park-Lower Kaweah	0.6984	83.3	58.2	58
Southern SJV	Oildale-3311 Manor Street	0.7562	83.0	62.8	62
Southern SJV	Shafter-Walker Street	0.7786	79.7	62.1	62
Southern SJV	Porterville-1839 Newcomb Street	0.7396	78.0	57.7	57

Table 15. Summary of key parameters related to the future year 2037 ozone design value (DV) calculation excluding federal clean truck and Tier 5 off-road commitments.

Sub-region	Site	2032 DV (ppb)	2037 DV (ppb)	$\Delta O_3/\Delta NOx$ (ppb/tpd)	New 2037 DV (ppb)	New 2037 Truncated DV (ppb)
Northern SJV	Turlock-S Minaret St.	68.6	65.2	0.1713	65.9	65
Northern SJV	Modesto-14th St.	68.7	65.8	0.1461	66.4	66
Northern SJV	Merced-S Coffee Av.	62.9	59.6	0.1662	60.3	60
Northern SJV	Tracy-Airport	65.9	64.0	0.0957	64.4	64
Northern SJV	Stockton-Hazelton St.	59.7	58.0	0.0856	58.4	58
Central SJV	Fresno-Garland	71.4	67.6	0.1914	68.4	68
Central SJV	Clovis	72.2	67.8	0.2217	68.8	68
Central SJV	Parlier	67.9	63.1	0.2418	64.2	64
Central SJV	Fresno-Drummond St.	68.9	65.0	0.1965	65.9	65
Central SJV	Fresno-Sierra Skypark #2	66.0	62.8	0.1612	63.5	63
Central SJV	Hanford-S. Irwin St.	67.7	64.6	0.1562	65.3	65
Central SJV	Madera-28261 Avenue 14	63.1	59.7	0.1713	60.4	60
Central SJV	Madera-Pump Yard	63.6	60.9	0.1360	61.5	61
Central SJV	Tranquility	62.8	60.5	0.1159	61.0	61

Sub-region	Site	2032 DV (ppb)	2037 DV (ppb)	$\Delta O_3/\Delta NOx$ (ppb/tpd)	New 2037 DV (ppb)	New 2037 Truncated DV (ppb)
Southern SJV	Edison	67.3	61.6	0.2872	62.8	62
Southern SJV	Arvin-Di Giorgio	66.0	60.6	0.2720	61.8	61
Southern SJV	Bakersfield-5558 California Avenue	70.3	65.7	0.2317	66.7	66
Southern SJV	Sequoia and Kings Canyon Natl Park	66.1	60.7	0.2720	61.9	61
Southern SJV	Bakersfield-Municipal Airport	65.3	60.1	0.2620	61.2	61
Southern SJV	Visalia-N Church Street	67.7	63.2	0.2267	64.2	64
Southern SJV	Maricopa-Stanislaus Street	68.9	65.6	0.1662	66.3	66
Southern SJV	Sequoia Natl Park-Lower Kaweah	63.5	58.2	0.2670	59.4	59
Southern SJV	Oildale-3311 Manor Street	67.2	62.8	0.2217	63.8	63
Southern SJV	Shafter-Walker Street	65.6	62.1	0.1763	62.9	62
Southern SJV	Porterville-1839 Newcomb Street	61.7	57.7	0.2015	58.6	58

3.6. NOx/VOC Sensitivity Analysis for Reasonable Further Progress (RFP)

For the Clean Air Act 182(c)(2)(B) RFP requirement for areas classified as Serious nonattainment and above, U.S. EPA guidance allows for NOx substitution to demonstrate the annual 3 percent reduction of ozone precursors if it can be demonstrated that substitution of NOx emission reductions (for ROG reductions) yield equivalent decreases in ozone. Additional U.S. EPA guidance states that certain conditions are needed to use NOx substitution in an RFP demonstration (U.S.EPA 1993). First, an equivalency demonstration must show that cumulative RFP emission reductions are consistent with the NOx and ROG emission reductions determined in the ozone attainment demonstration. Second, the reductions in NOx and ROG emissions should be consistent with the continuous RFP emission reduction requirement.

For the equivalency demonstration, ROG and NOx emissions within the nonattainment area boundary were reduced by 60% (3% for each of the 20 years between the designation year of 2017 and attainment year of 2037) independently from the baseline modeling year of 2018. These sensitivity simulations were used to develop RRFs and design values following the same methodology utilized in the attainment demonstration, where the sensitivity simulation was treated analogous to the future year. Table 16 summarizes the design values calculated for the 60% NOx and ROG sensitivity simulations. At all sites in the SJV, the ratios of the ozone design value change to the NOx emissions change ($\Delta O_3/\Delta NOx$) are greater than those of the ROG emissions change ($\Delta O_3/\Delta ROG$). For sites with the highest 2018 ozone design values, $\Delta O_3/\Delta NOx$ can be an order of magnitude larger than $\Delta O_3/\Delta ROG$. Since the ozone improvement from NOx reductions is greater than that for ROG reductions, the use of NOx substitution will result in improved ozone air quality.

Table 16. Summary of the ozone improvement from the 60% emissions reductions at the monitoring sites in SJV.

Sub-region	Site	2018 Average DV (ppb)	DV After 60% NOx Reductions (ppb)	$\Delta O_3/\Delta NOx$ (ppb/tpd)	DV After 60% ROG Reductions (ppb)	$\Delta O_3/\Delta ROG$ (ppb/tpd)
Northern SJV	Turlock-S Minaret St.	82.3	74.7	0.0567	80.9	0.0072
Northern SJV	Modesto-14th St.	79.3	74.8	0.0336	77.9	0.0072
Northern SJV	Merced-S Coffee Av.	76.7	68.5	0.0612	75.6	0.0057
Northern SJV	Tracy-Airport	73.7	73.2	0.0037	73.4	0.0015

Sub-region	Site	2018 Average DV (ppb)	DV After 60% NOx Reductions (ppb)	$\Delta O_3/\Delta NOx$ (ppb/tpd)	DV After 60% ROG Reductions (ppb)	$\Delta O_3/\Delta ROG$ (ppb/tpd)
Northern SJV	Stockton-Hazelton St.	66.0	64.9	0.0082	65.6	0.0021
Central SJV	Fresno-Garland	85.7	77.6	0.0604	83.8	0.0098
Central SJV	Clovis	85.3	77.2	0.0604	81.0	0.0221
Central SJV	Parlier	84.3	73.2	0.0828	82.0	0.0118
Central SJV	Fresno-Drummond St.	82.0	74.8	0.0537	79.6	0.0123
Central SJV	Fresno-Sierra Skypark #2	80.0	71.5	0.0634	78.9	0.0057
Central SJV	Hanford-S. Irwin St.	80.0	72.5	0.0560	78.9	0.0057
Central SJV	Madera-28261 Avenue 14	77.7	68.5	0.0687	76.4	0.0067
Central SJV	Madera-Pump Yard	75.7	68.3	0.0552	74.7	0.0051
Central SJV	Tranquility	72.7	68.3	0.0328	72.3	0.0021
Southern SJV	Edison	89.0	72.9	0.1201	85.8	0.0165
Southern SJV	Arvin-Di Giorgio	88.0	71.4	0.1239	85.8	0.0113
Southern SJV	Bakersfield-5558 California Avenue	87.3	75.6	0.0873	85.9	0.0072

Sub-region	Site	2018 Average DV (ppb)	DV After 60% NOx Reductions (ppb)	$\Delta O_3/\Delta NOx$ (ppb/tpd)	DV After 60% ROG Reductions (ppb)	$\Delta O_3/\Delta ROG$ (ppb/tpd)
Southern SJV	Sequoia and Kings Canyon Natl Park	86.7	70.6	0.1201	85.3	0.0072
Southern SJV	Bakersfield-Municipal Airport	85.3	70.7	0.1089	83.4	0.0098
Southern SJV	Visalia-N Church Street	84.0	72.6	0.0851	81.8	0.0113
Southern SJV	Maricopa-Stanislaus Street	83.7	73.9	0.0731	82.7	0.0051
Southern SJV	Sequoia Natl Park-Lower Kaweah	83.3	68.0	0.1142	81.9	0.0072
Southern SJV	Oildale-3311 Manor Street	83.0	72.3	0.0798	81.4	0.0082
Southern SJV	Shafter-Walker Street	79.7	69.7	0.0746	78.6	0.0057
Southern SJV	Porterville-1839 Newcomb Street	78.0	66.4	0.0866	76.5	0.0077

3.7. Unmonitored Area Analysis

The unmonitored area analysis is used to ensure that there are no regions outside of the existing monitoring network that would exceed the NAAQS if a monitor was present (U.S. EPA, 2018). U.S. EPA recommends combining spatially interpolated design value fields with modeled ozone gradients and grid-specific RRFs in order to generate gridded future year gradient adjusted design values.

This analysis can be done using SMAT-CE (Software for the Modeled Attainment Test – Community Edition, *https://www.epa.gov/scram/photochemical-modeling-tools*). However, this software is not open source and comes as a precompiled software package. To maintain transparency and flexibility in the analysis, in-house R codes developed at CARB, were utilized in this analysis.

The unmonitored area analysis was conducted using the 8-hr O_3 weighted DVs from available sites that fall within the 4 km inner modeling domain along with the reference year 2018 and future year 2037 4 km CMAQ model output. The steps followed in the unmonitored area analysis are as follows:

Step 1: At each grid cell, the top 10 modeled maximum daily average 8-hour ozone mixing ratios from the reference year simulation were averaged, and a gradient in this top 10-day average between each grid cell and grid cells which contain a monitor was calculated.

Step 2: A single set of spatially interpolated 8-hour ozone DV fields was generated based on the observed 5-year weighted base year 8-hour ozone DVs from the available monitors. The interpolation is done using normalized inverse distance squared weightings from each monitor within the Voronoi regions that boarder that of the grid cell (calculated with the R tripack library), and adjusted based on the gradients between the grid cell and the corresponding monitor from Step 1.

Step 3: At each grid cell, the RRFs are calculated based on the reference- and future-year modeling following the same approach outlined in Section 2, except that the +/- 20% limitation on the simulated and observed maximum daily average 8-hour ozone was not applied because observed data do not exist for grid cells in unmonitored areas.

Step 4: The future year gridded 8-hour ozone DVs were calculated by multiplying the gradient-adjusted interpolated 8-hour ozone DVs from Step 2 with the gridded RRFs from Step 3

Step 5: The future-year gridded 8-hour ozone DVs (from Step 4) were examined to determine if there are any peak values higher than those at the monitors, which could potentially cause violations of the applicable 8-hour ozone NAAQS.

Under Voronoi diagram method, each monitoring site was assigned to a Voronoi region based on location and the distance to each grid cell (Sen 2016), and the interpolations were done between each grid cell and all the monitors in surrounding Voronoi regions. Voronoi diagram with inverse distance weighting method has been used in various 2-D data analysis areas, including air quality measurements interpolations (Atsuyuki, et al. 2009) (Deligiorgi and Philippopoulos 2011).

Figure 18 shows the spatial distribution of gridded 2037 DVs for the SJV non-attainment area based on the unmonitored area analysis (left panel), and the population distribution in the SJV

based on 2020 census data (right panel). The black star markers denote the monitoring sites, which have valid reference year 2018 DVs and were used in the analysis. Gridded DVs are below the 70ppb standard in all areas within the nonattainment region, except at sparsely populated elevated locations over the Sierra Nevada Mountains.

Figure 18. Spatial distribution of the future 2037 DVs based on the unmonitored area analysis in the Valley (left), and the population distribution in the Valley (right) based on 2020 US census data.

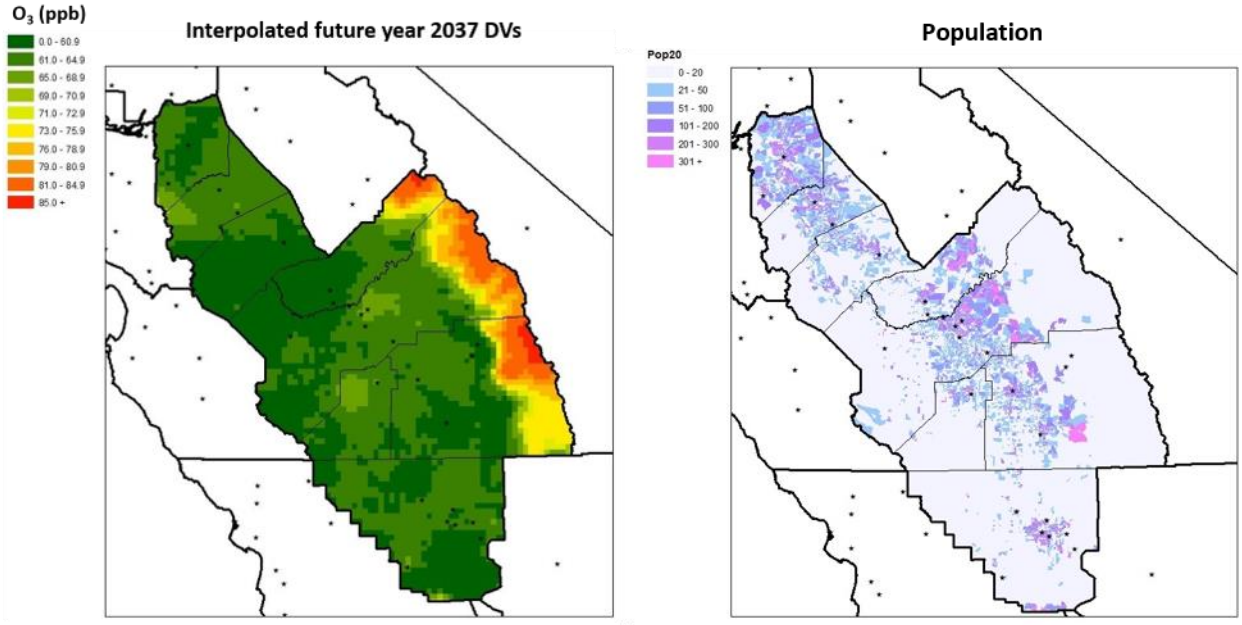

Figure 19 shows the spatially interpolated base year DV from Step 2 above (left panel), and the RRF value at each model grid from Step 3 above (right panel). The RRF calculation is based on the top 10 days from the 2018 reference year model simulations for each grid cell. In 2018, the interpolated DVs exhibit high levels of ozone within the valley floor and foothills as well as at higher elevations over the mountain regions. In contrast, RRF values over the mountain regions are generally close to 1.0 while the RRF values within the valley floor and foothills are mostly below 0.8, which indicates that the remote mountain regions are not responsive to the emission reductions within the Valley.

Further analysis of the modeling results shows there is a disconnect between when peak ozone occurs in the valley floor and foothills compared to the elevated mountain regions. Within the mountain regions, the simulated high O_3 concentrations occur in the springtime from April to June, while the high O_3 concentrations at the valley floor and foothills occurs during the peak summer ozone season from July to September. Figure S 105 shows an east-west cross sectional curtain plot of monthly average of O_3 in May 2018 and 2037 at row 64 of the model domain, which crosses through the Sequoia and Kings Canyon National Park monitor. From

the figure, it is clearly seen that O_3 concentrations over the top of the mountains are significantly impacted by transport from aloft, including the impact of stratospheric intrusion of O_3, which is strongest during the spring season. Figure S 106 shows a similar curtain plot, but for August, which clearly shows that even during the peak ozone summer season, ozone pollution within the valley does not strongly affect ozone levels at elevations above 2500 m.

When spring months are excluded from the unmonitored area analysis (only data from July to October is used), the interpolated O_3 DVs in the mountain regions for both 2018 and 2037 are reduced significantly and the unmonitored peaks disappear, while the DVs within the valley floor and foothill regions only exhibit very minor changes (see Figure 19 and Figure 20 for 2018, and Figure 18 and Figure 20 for 2037).

Our analysis shows that the high ozone levels within the Sierra Nevada Mountains predicted by the unmonitored area analysis are likely due to impacts from higher ozone aloft and stratospheric influences in springtime, and are not influenced by pollution emitted and formed within the valley during the peak ozone season summer months. This means that reducing anthropogenic emissions in the SJV is not likely to affect ozone levels within elevated regions of the Sierra Nevada Mountains. It is important to note that while these unmonitored peaks are consistent with our understanding of the physical processes in the atmosphere and the role of stratospheric ozone influences in the spring (e.g., Lin et al., 2012), additional investigation and possibly measurements will be needed to corroborate the modeling analysis. Some of that information may be available from previous field campaigns, such as the California Baseline Ozone Transport Study (CABOTS) in 2016 (https://csl.noaa.gov/projects/cabots/scienceintro.html), and the regular ozonesonde measurements at Trinidad Head, CA (https://gml.noaa.gov/dv/site/THD.html). Those data sets will be investigated to determine if they are sufficient or if additional measurements are needed to determine if the unmonitored peaks within the Sierra Nevada Mountains are real or an artifact of the unmonitored area modeling analysis.

Figure 19. Spatially interpolated 2018 base year DVs with gradient adjustment based on the unmonitored area analysis (left), and the RRF calculated for each grid (right)

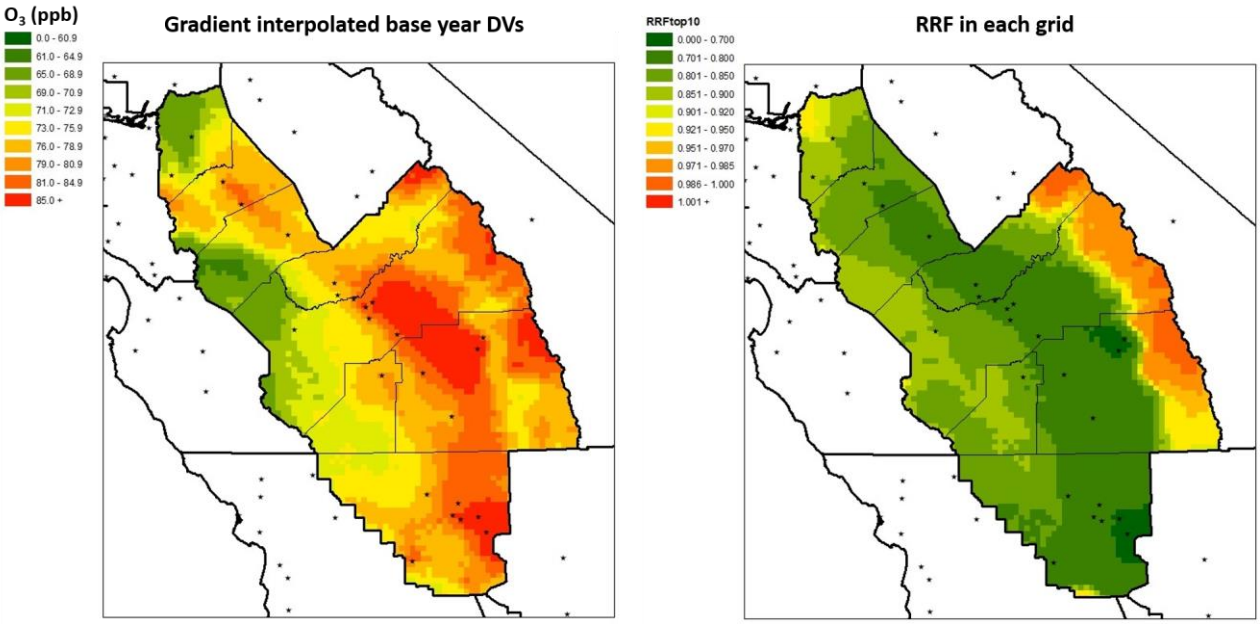

Figure 20. Spatially interpolated 2018 base year DVs with gradient adjustment based on the unmonitored area analysis (left), and the spatial distribution of the future year 2037 DVs using modeling data of July – October (right).

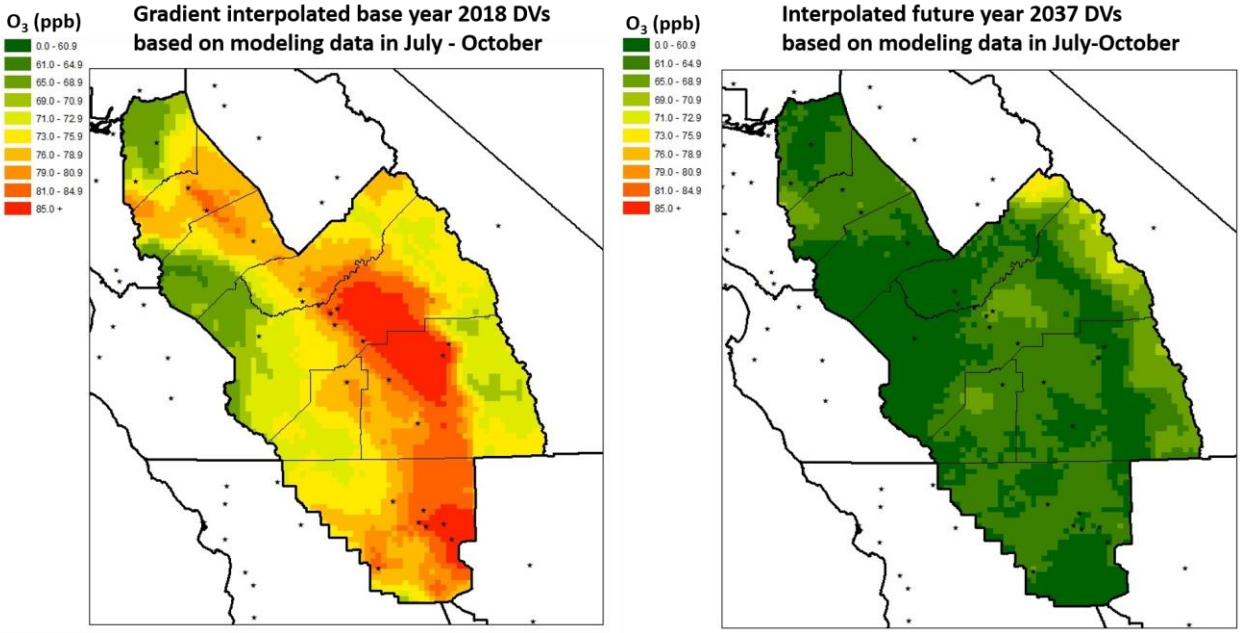

4. References

Angevine, W. M., L. Eddington, K. Durkee, C. Fairall, L. Bianco, and J. Brioude. 2012. "Meteorological model evaluation for CalNex 2010." *Monthly Weather Review* (140): 3885-3906.

Atsuyuki, O., B. Boots, K. Sugihara, and S. N. Chiu. 2009. *Spatial tessellations: concepts and applications of Voronoi diagrams.* Second. John Wiley & Sons.

Baker, K. R., C. Misenis, M. D. Obland, R. A. Ferrare, A. J. Scarino, and J. T. Kelly. 2013. "Evaluation of surface and upper air fine scale WRF meteorological modeling of the May and June 2010 CalNex period in California." *Atmospheric Environment* (80): 299-309.

Bao, J.W., S.A. Michelson, P.O.G. Persson, I.V. Djalalova, and J.M. Wilczak. 2008. "Observed and WRF-simulated low-level winds in a high-ozone episode during the Central California ozone study." *Journal of Applied Meteorology and Climatology* 47: 2372-2394.

Beaver, S., and A. Palazoglu. 2009. "Influence of synoptic and mesoscale meteorology on ozone pollution potential for San Joaquin Valley of California." *Atmospheric Environment* 43 (10).

Blanchard, C.L., S. Tanenbaum, E.M. Fujita, D. Campbell, and J. Wilkinson. 2008. *Understanding Relationships between Changes in Ambient Ozone and Precursor Concentrations and Changes in VOC and NOx Emissions from 1990 to 2004 in Central California.* Report prepared for the California Air Resources Board, Envair, DRI and Alpine Geophysics.

Buchholz, R. R., Emmons, L. K., Tilmes, S., & The CESM2 Development Team. 2019. "CESM2.1/CAM-chem Instantaneous Output for Boundary Conditions." UCAR/NCAR - Atmospheric Chemistry Observations and Modeling Laboratory. https://doi.org/10.5065/NMP7-EP60.

Cai, C., J. C. Avise, A. Kaduwela, J. DaMassa, C. Warneke, J. B. Gilman, W. Kuster, et al. 2019. "Simulating the Weekly Cycle of NOx-VOC-HOx-O3Photochemical System in the South Coast ofCalifornia During CalNex-2010 Campaign." *Journal of Geophysical Research: Atmospheres* 3532–3555.

Cai, C., S. Kulkarni, Z. Zhao, A. Kaduwela, J. C. Avise, and J. A. DaMassa. 2016. "Simulating Reactive Nitrogen, Carbon Monoxide, and Ozone in California During ARCTAS-CARB 2008 with High Wildfire Activity." *Atmospheric Environment* 28-44.

Carter, W.P.L. 2010b. "Development of a condensed SAPRC-07 chemical mechanism." *Atmospheric Environment* 5336-5345.

Carter, W.P.L. 2010a. "Development of the SAPRC-07 chemical mechanism." *Atmospheric Environment* 5324-5335.

Chen, J., D. Yin, Z. Zhao, A. P. Kaduwela, J. C. Avise, J. A. DaMassa, A. Beyersdorf, and S. Burton et al. 2020. "Modeling air quality in the San Joaquin Valley of California during the 2013 DISCOVER-AQ field campaign." *Atmospheric Environment* (5): 100067.

Deligiorgi, D., and K. Philippopoulos. 2011. "Spatial Interpolation Methodologies in Urban Air Pollution Modeling: Application for the Greater Area of Metropolitan Athens, Greece." In *Advanced Air Pollution*. doi:10.5772/17734.

EasternKern. 2017. "2017 Ozone Attainment Plan, available at: http://www.kernair.org/Documents/Announcements/Attainment/2017%20Ozone%20Plan_EKAPCD_Adopted_7-27-17.pdf."

Emmons, L. K., R. H. Schwantes, J. J. Orlando, G. Tyndall, D. Kinnison, and J.-F. Lamarque et al. 2020. "The Chemistry Mechanism in the Community Earth System Model version 2 (CESM2)." *Journal of Advances in Modeling Earth Systems.* https://doi.org/10.1029/2019MS001882.

Fast, J. D., W. I. Gustafson Jr, L. K. Berg, W. J. Shaw, M. Pekour, and M. Shrivastava et al. 2012. "Transport and mixing patterns over Central California during the carbonaceous aerosol and radiative effects study (CARES)." *Atmospheric Chemistry and Physics* (12): 1759-1783.

Fosberg, M.A., and M.J. Schroeder. 1966. "Marine air penetration in Central California." *Journal of Applied Meteorology* (5): 573-589.

Fujita, E. M., R. E. Keislar, D. L. Freeman, J. Watson, A. J. Ranzieri, S. Tanrikulu, and K. Magliano. 1999. *Field study plan for the Central California Ozone Study.*

He, H., X-Z. Liang, and D. J. Wuebbles. 2018. "Effects of emissions change, climate change and long-range transport on regional modeling of future U.S. particulate matter pollution and speciation." *Atmospheric Environment*, 166-176. doi:https://doi.org/10.1016/j.atmosenv.2018.02.020.

Heuss, J. M., D. F. Kahlbaum, and G. T. Wolff. 2003. "Weekday/Weekend Ozone Differences: What Can We Learn from Them?" *Journal of the Air & Waste Management Association* 53 (7): 772-788.

Hu, J., C. J. Howard, F. Mitloehner, P. G. Green, and M. J. Kleeman. 2012. "Mobile Source and Livestock Feed Contributions to Regional Ozone Formation in Central California." *Environmental Science and Technology* (46): 2781-2789.

Imperial. 2017. " Imperial County 2017 State Implementation Plan for the 2008 8-Hour Ozone Standard, available at: https://ww3.arb.ca.gov/planning/sip/planarea/imperial/2017o3sip_final.pdf ."

Imperial. 2018. " Imperial County 2018 Annual Particulate Matter Less than 2.5 Microns in Diameter State Implementation Plan, available at: https://ww3.arb.ca.gov/planning/sip/planarea/imperial/final_2018_ic_pm25_sip.pdf ."

Jin, L., N. J. Brown, R. A. Harley, J-W. Bao, S. A. Michelson, and J. M. Wilczak. 2010. "Seasonal versus episodic performance evaluation for an Eulerian photochemical air quality model." *Journal of Geophysical Research: Atmospheres* 115, D09302.

Jin, L., S. Tonse, D. S. Cohan, X Mao, R. A. Harley, and N. J. Brown. 2008. "Sensitivity analysis of ozone formation and transport for a central California air pollution episode." *Environmental Science and Technology* 3683-3689.

Kelly, J. T., K. R. Baker, J. B. Nowak, J. G. Murphy, Z. M. Milos, T. C. VandenBoer, R. A. Ellis, et al. 2014. "Fine-scale simulation of ammonium and nitrate over the South Coast Air Basin and San Joaquin Valley of California during CalNex-2010." *Journal of Geophysical Research* (119): 3600-3614. doi:doi:10.1002/2013JD021290.

Kelly, J.T., J. Avise, C. Cai, and A. Kaduwela. 2010. "Simulating particle size distributions over California and impact on lung deposition fraction." *Aerosol Science and Technology* 148-162.

Kelly, J.T., K.R Baker, J.B. Nowak, and J.G Murphy et al. 2014. "Fine-scale simulation of ammonium and nitrate over the South Coast Air Basin and San Joaquin Valley of California during CalNex-2010." *Journal of Geophysical Research: Atmosphere* 3600–3614.

Kulkarni, S., A. P. Kaduwela, J. C. Avise, J. A. DaMassa, and D. Chau. 2014. "An extended approach to calculate the ozone relative response factors used in the attainment demonstration for the National Ambient Air Quality Standards." *Journal of the Air and Waste Management Association* 1204-1213.

Lamarque, J.-F., L. K. Emmons, P. G. Hess, D. E. Kinnison, S. Tilmes, F. Vitt, C. L. Heald, et al. 2012. "CAM-chem: description and evaluation of interactive atmospheric chemistry in the Community Earth System Model." *Geoscientific Model Development* 369-411.

Lehrman, D. 2001. *Characterization of the 2000 Measurement Period.* Interim Report prepared for California Air Resources Board, Technical and Business Systems, Inc.,.

Lehrman, D., D. Bush, B. Knuth, D. Fairley, and C. Blanchard. 2004. *Characterization of the CCOS 2000 measurement period.* Final Report prepared for California Air Resources Board, Technical and Business Systems, Inc.

Lin, M., A. M. Fiore, O. R. Cooper, L. W. Horowitz, A. O. Langford, H. Levy II, B. J. Johnson, V. Naik, and S. J. Oltmans. 2012. "Springtime high surface ozone events over the western United States: Quantifying the role of stratospheric." *Journal of Geophysical Research* D00V22, doi:10.1029/2012JD018151.

Livingstone, P.L., K. Magliano, K. Gurer, P.D. Allen, K.M. Zhang, Q. Ying, and , B.S. Jackson et al. 2009. "Simulating PM concentration during a winter episode in a subtropical valley: Sensitivity simulations and evaluation methods." *Atmospheric Environment* 5971-5977.

Pun, B. K., J. F. Loius, and C. Seigneur. 2008. *A conceptual model of ozone formation in the San Joaquin Valley.* CP049-1-98, Atmospheric and Environmental Research Inc., San Ramon, CA.

Pun, B.K., R.T.F. Balmori, and C. Seigneur. 2009. "Modeling wintertime particulate matter formation in central California." *Atmospheric Environment* 402-409.

Pusede, S. E., and R. C. Cohen. 2012. "On the observed response of ozone to NOx and VOC reactivity reductions in San Joaquin Valley California 1995–present." *Atmospheric Chemistry and Physics* 8323-8339.

Pusede, S. E., D. R. Gentner, P. J. Wooldridge, E. C. Browne, A. W. Rollins, K. E. Min, A. R. Russell, et al. 2014. "On the temperature dependence of organic reactivity, nitrogen oxides, ozone production, and the impact of emission controls in San Joaquin Valley, California." *Atmospheric Chemistry and Physics* 3373-3395.

Sacramento. 2017. "Sacramento Regional 2008 NAAQS 8-Hour Ozone Attainment And Reasonalbe Further Progress Plan, available at http://www.airquality.org/ProgramCoordination/Documents/Sac%20Regional%202008%20NAAQS%20Attainment%20and%20RFP%20Plan.pdf."

Seinfeld, J. H., and S. N. Pandis. 1998. *Atmospheric Chemistry and Physics: From Air Pollution to Climate Change.* Edited by 1. New York: J. Wiley.

Sen, Zekai. 2016. "2.8.1 Delaney, Varoni, and Thiessen Polygons." In *Spatial Modeling Principles in Earth Sciences*, 57. Springer.

Shahrokhishahraki, N., P. J. Rayner, J. D. Silver, S. Thomas, and R. Schofield. 2022. "High-resolution modeling of gaseous air pollutants over Tehran and validation with surface and satellite data." *Atmospheric Environment.* doi:https://doi.org/10.1016/j.atmosenv.2021.118881.

Sillman, S. 1999. "The relation between ozone, NOx and hydrocarbons in urban and polluted rural environments." *Atmospheric Environment* 33 (12): 1821-1845.

Simon, H., K. R. Baker, and S. Phillips. 2012. "Compilation and interpretation of photochemical model performance statistics published between 2006 and 2012." *Atmospheric Environment* (61): 124-139.

SJV. 2018. " 2018 PM2.5 Plan for the San Joaquin Valley, available at: http://valleyair.org/pmplans/ ."

SJV. 2008. "2008 PM2.5 Plan, available at: http://www.valleyair.org/Air_Quality_Plans/AQ_Proposed_PM25_2008.htm."

SJV. 2012. "2012 PM2.5 Plan, available at: http://www.valleyair.org/Air_Quality_Plans/PM25Plans2012.htm ."

SJV. 2013. "2013 Plan for the Revoked 1-Hour Ozone Standard, available at: http://valleyair.org/Air_Quality_Plans/Ozone-OneHourPlan-2013.htm ."

SJV. 2016a. "2016 Moderate Area Plan for the 2012 PM2.5 Standard, available at: http://www.valleyair.org/Air_Quality_Plans/docs/PM25-2016/2016-Plan.pdf ."

SJV. 2016b. "2016 Plan for the 2008 8-Hour Ozone Standard, available at: http://valleyair.org/Air_Quality_Plans/Ozone-Plan-2016.htm ."

Skamarock, W. C., J. B. Klemp, J. Dudhia, D. O. Gill, D. M. Barker, M. G. Duda, X.-Y. Huang, W. Wang, and J. G. Powers. 2008. ""Description ofthe Advanced Research WRF version 4,Rep. NCAR/TN-475++STR,Natl. Cent. for Atmos. Res., ."." Boulder, Colo.

SouthCoast. 2012. "Final 2012 Air Quality Management Plan, available at: http://www.aqmd.gov/home/air-quality/clean-air-plans/air-quality-mgt-plan/final-2012-air-quality-management-plan ."

SouthCoast. 2016. "Final 2016 Air Quality Management Plan, available at: http://www.aqmd.gov/docs/default-source/clean-air-plans/air-quality-management-plans/2016-air-quality-management-plan/final-2016-aqmp/cover-and-opening.pdf?sfvrsn=6."

Tonse, S. R., N. J. Brown, R. A. Harley, and L. Jin. 2008. "A process-analysis based study of the ozone weekend effect." *Atmospheric Environment* 7728-7736.

U.S. EPA. 2018. *Modeling Guidance for Demonstrating Attainment of Air Quality Goals for Ozone, PM2.5, and Regional Haze.* 11 29. https://www.epa.gov/scram/sip-modeling-guidance-documents.

U.S.EPA. 1993. "NOx Substitution Guidance, available at https://www3.epa.gov/ttn/naaqs/aqmguide/collection/cp2/19931201_oaqps_nox_substitution_guidance.pdf."

Ventura. 2016. "Final 2016 Ventura County Air Quality Management Plan, available at: http://www.vcapcd.org/pubs/Planning/AQMP/2016/Final/Final-2016-Ventura-County-AQMP.pdf ."

Vijayaraghavan, K., P. Karamchadania, and C. Seigneur. 2006. "Plume-in-grid modeling of summer air pollution in Central California." *Atmospheric Environment* 5097-5109.

Wang, P., P. Wang, K. Chen, J. Du, and H Zhang. 2022. "Ground-level ozone simulation using ensemble WRF/Chem predictions over the Southeast United States." *Chemosphere.* doi:https://doi.org/10.1016/j.chemosphere.2021.132428.

WesternMojave. 2016. "2016 8-Hour Ozone SIP: Western Mojave Desert Nonattainment Area, available at: https://ww3.arb.ca.gov/planning/sip/planarea/mojavesedsip.htm#2016."

WesternNevada. 2018. "Western Nevada County 8-hour Ozone Attainment Plan, available at: https://ww3.arb.ca.gov/planning/sip/planarea/wncsip.htm."

Yan, F., Y. Gao, M. Ma, C. Liu, X. Ji, F. Zhao, X. Yao, and H. Gao. 2021. "Revealing the modulation of boundary conditions and governing processes on ozone formation over northern China in June 2017." *Environmental Pollution* 272. doi:https://doi.org/10.1016/j.envpol.2020.115999.

Yienger, J. J., and H. Levy II. 1995. "Empirical model of global soil-biogenic NOχ emissions." *Journal of Geophysical Research: Atmospheres* 11447-11464.

Zhang, Y., P. Liu, X. Liu, B. Pun, C. Seigneur, M.Z. Jacobson, and W. Wang. 2010. "Fine scale modeling of wintertime aerosol mass, number, and size distributions in Central California." *Journal of Geophysical Research* D15207, doi:10.1029/2009JD012950.

5. Supplemental Materials

Supplemental Materials List of Figures

Figure S 1. Time series of temperature, relative humidity, wind speed, and direction for the Northern San Joaquin Valley in April 2018.

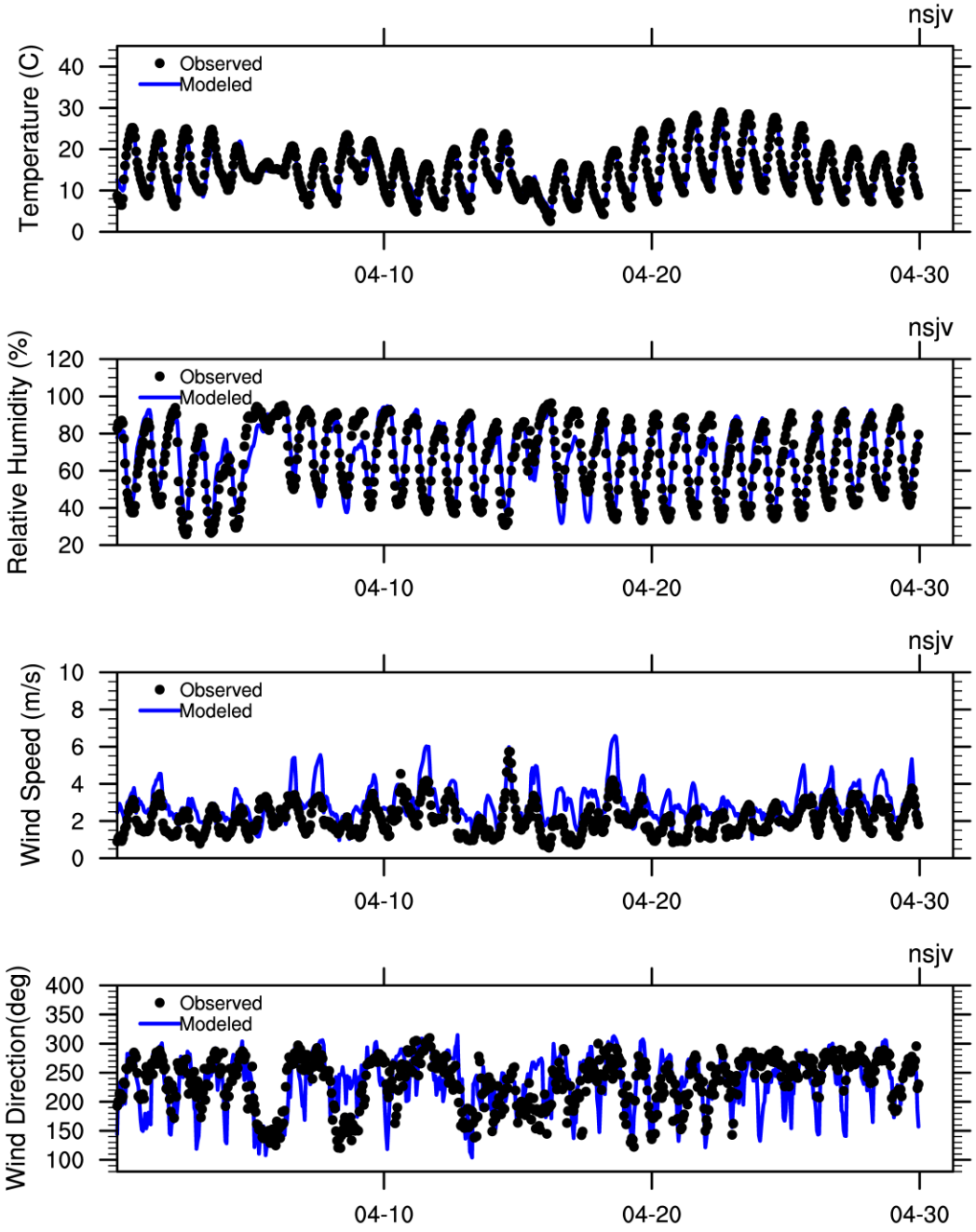

Figure S 2. Time series of temperature, relative humidity, wind speed, and direction for the Central San Joaquin Valley in April 2018.

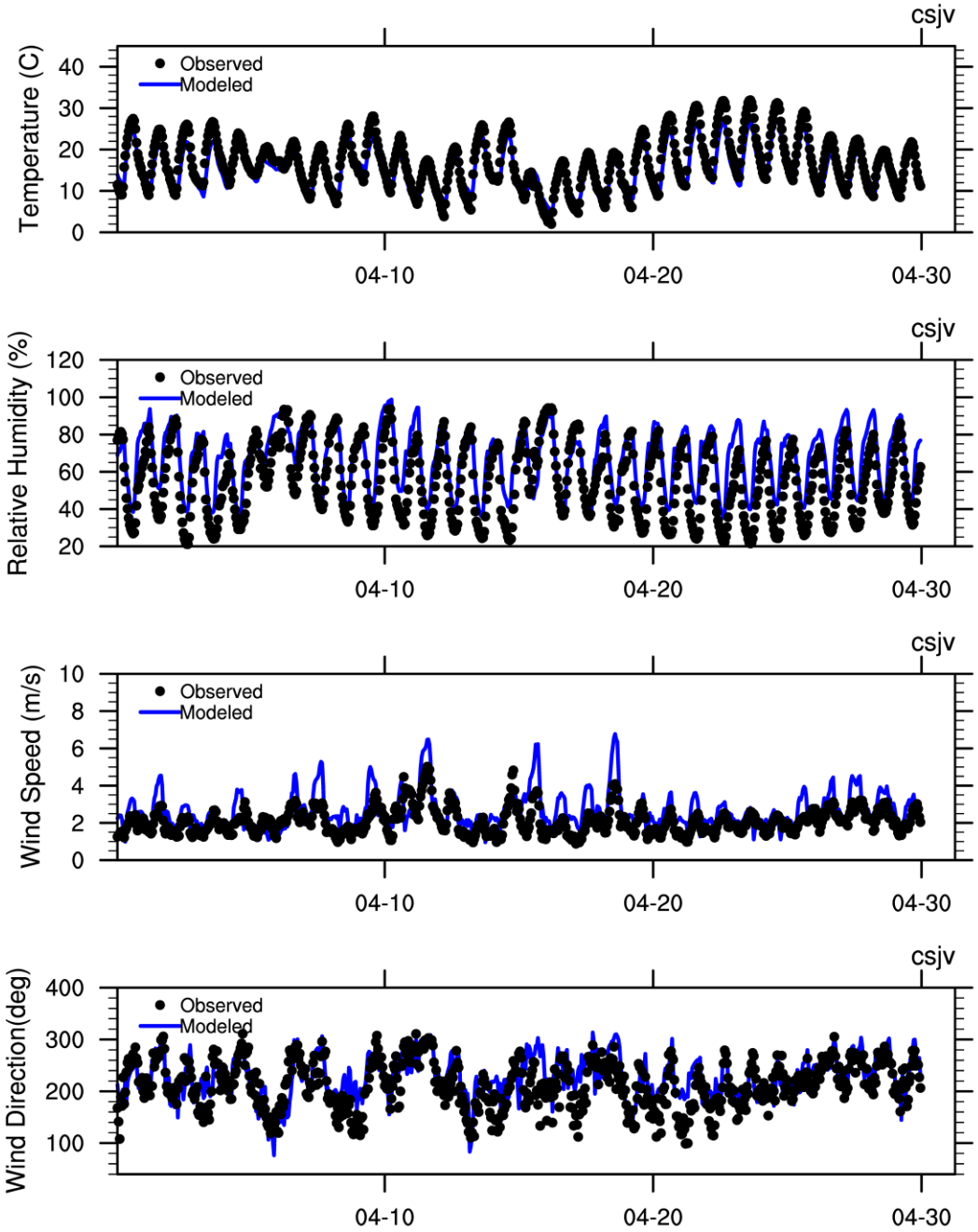

Figure S 3. Time series of temperature, relative humidity, wind speed, and direction for the Southern San Joaquin Valley in April 2018.

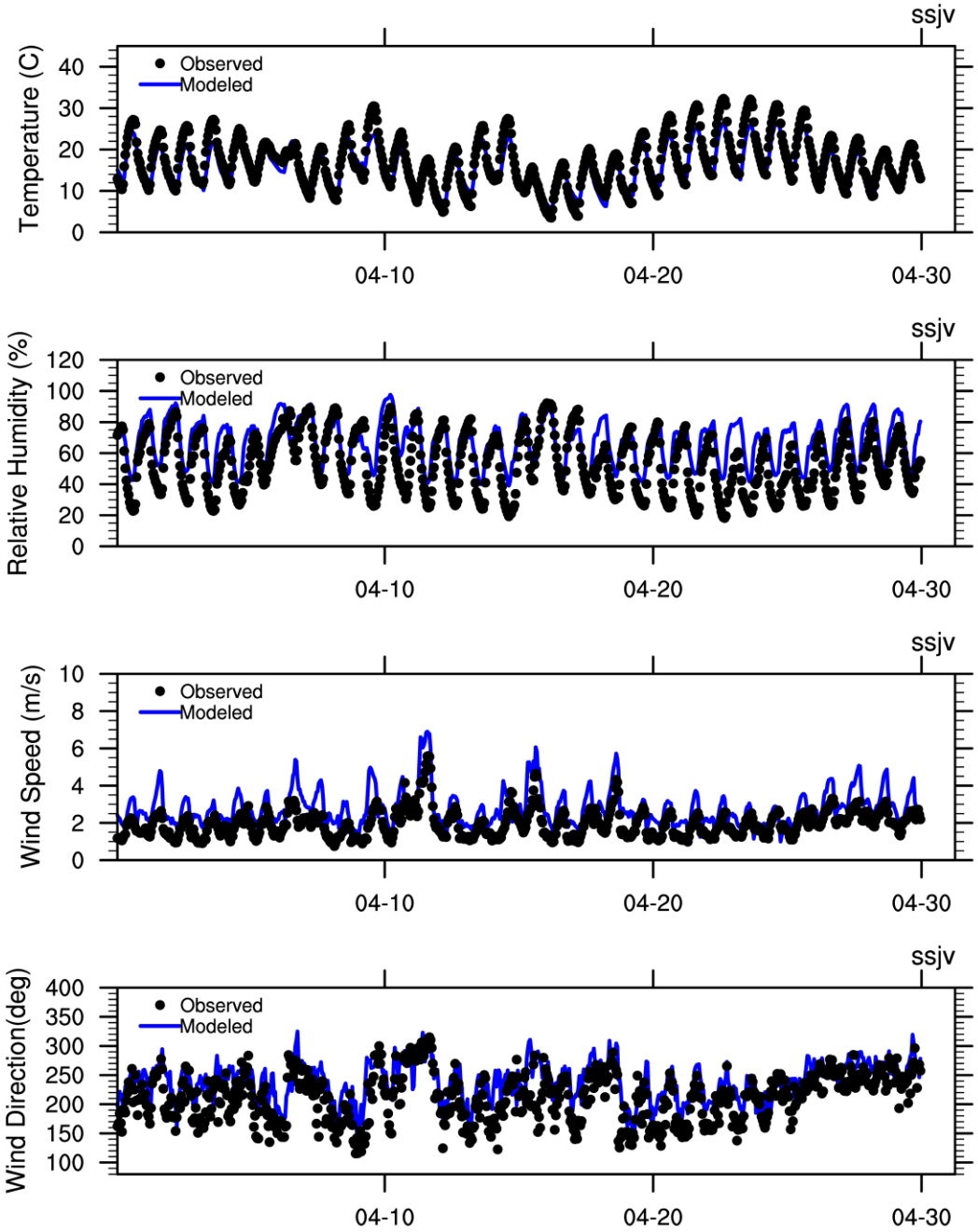

Figure S 4. Time series of temperature, relative humidity, wind speed, and direction for the Northern San Joaquin Valley in May 2018.

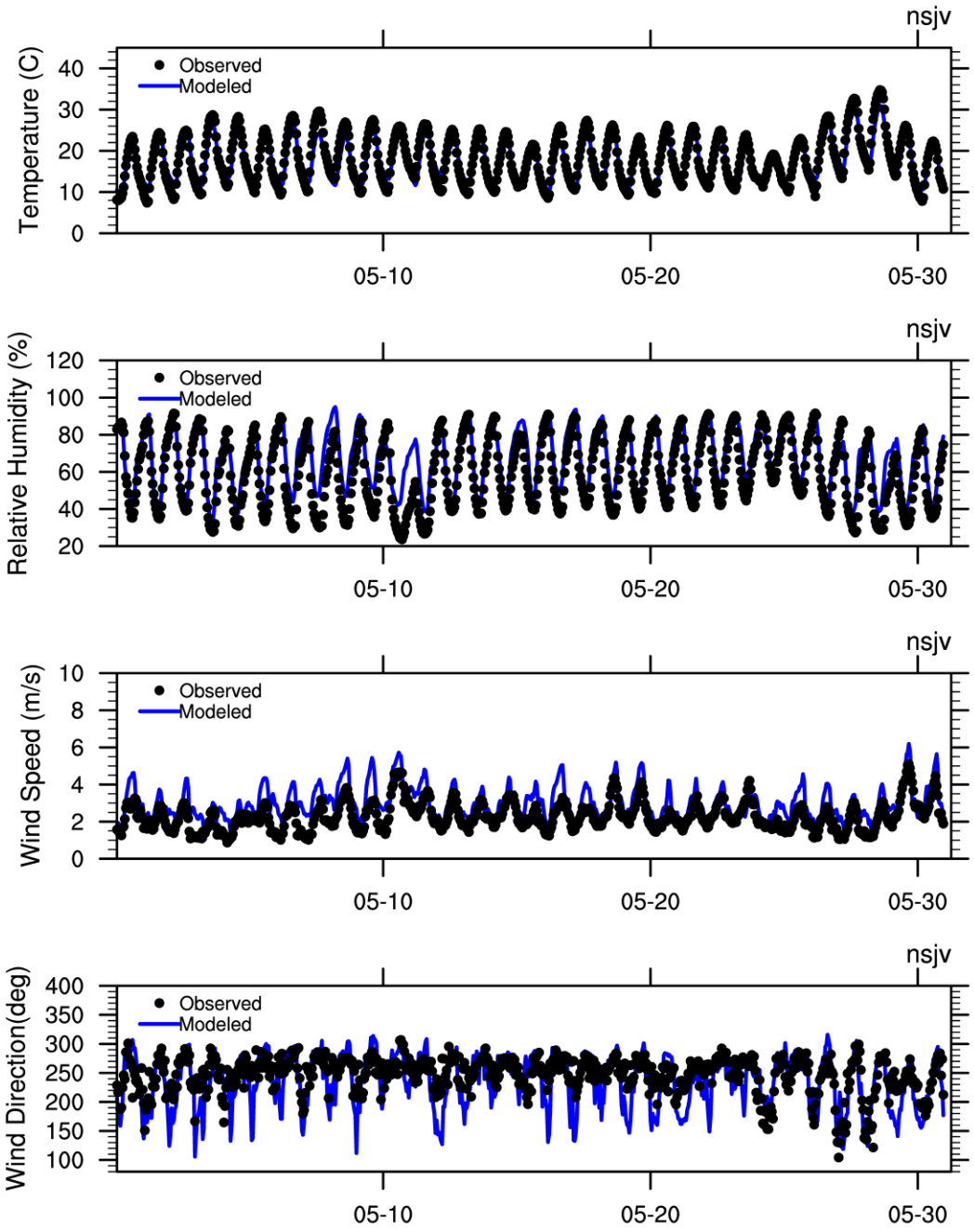

Figure S 5. Time series of temperature, relative humidity, wind speed, and direction for the Central San Joaquin Valley in May 2018.

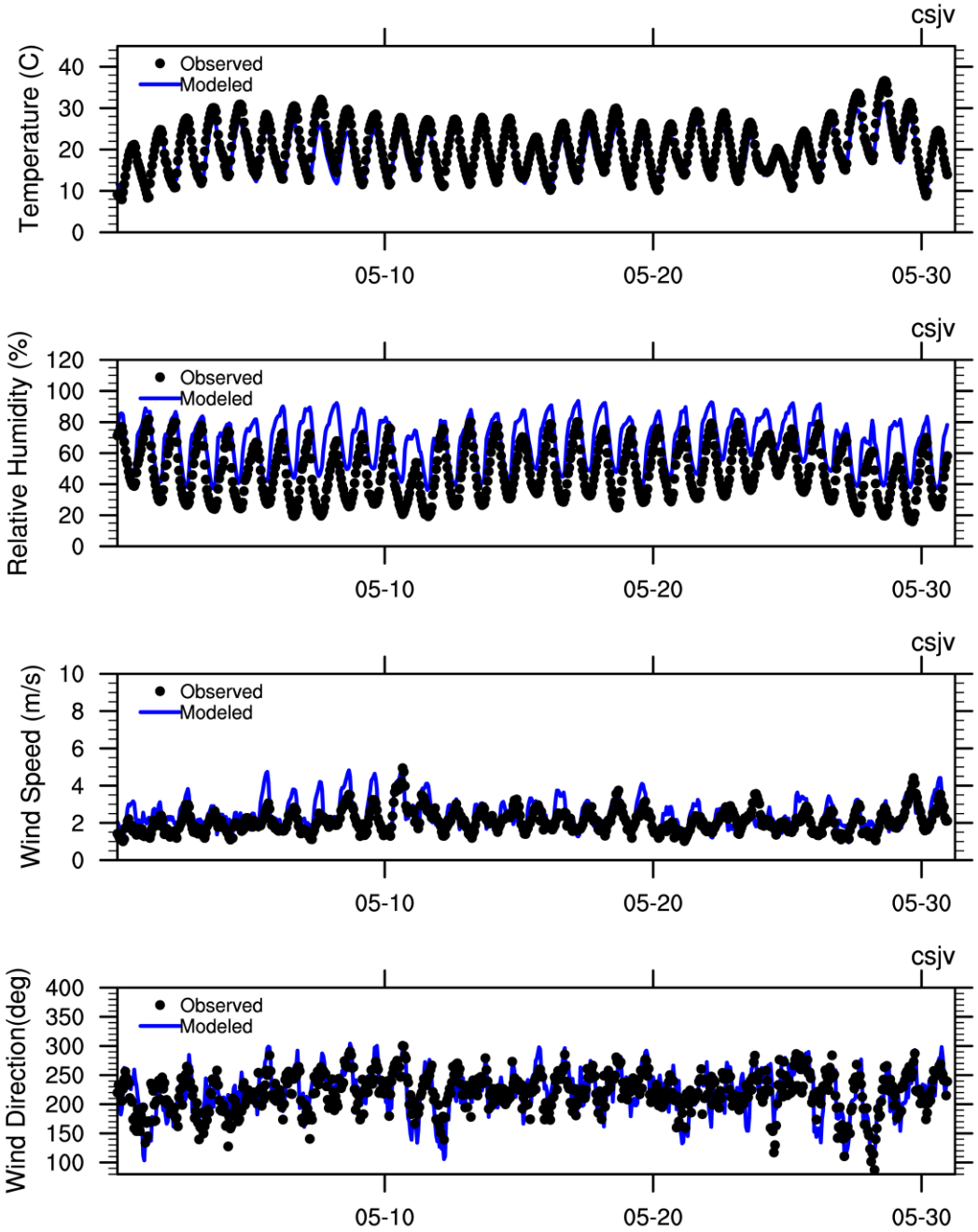

Figure S 6. Time series of temperature, relative humidity, wind speed, and direction for the Southern San Joaquin Valley in May 2018.

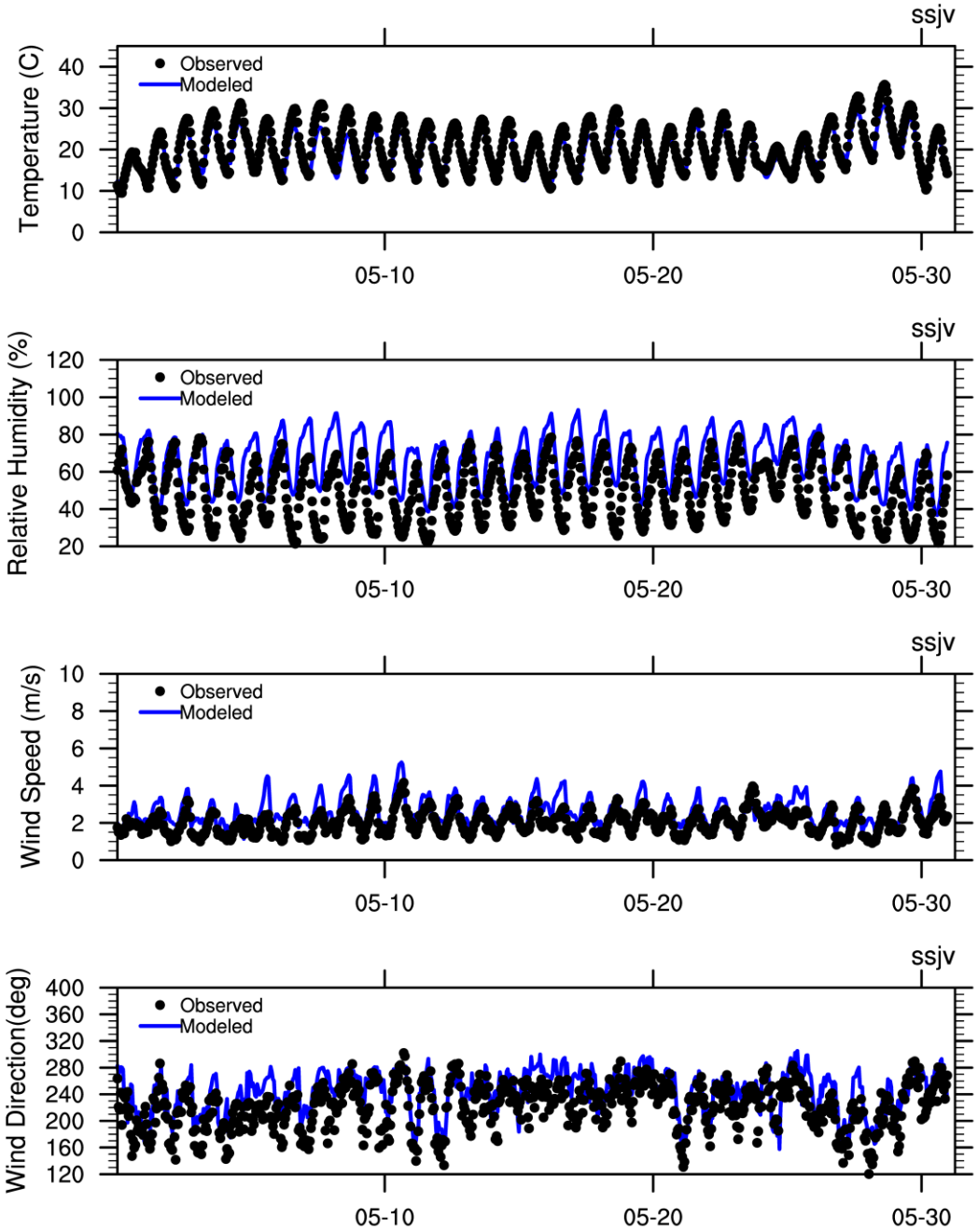

Figure S 7. Time series of temperature, relative humidity, wind speed, and direction for the Northern San Joaquin Valley in June 2018.

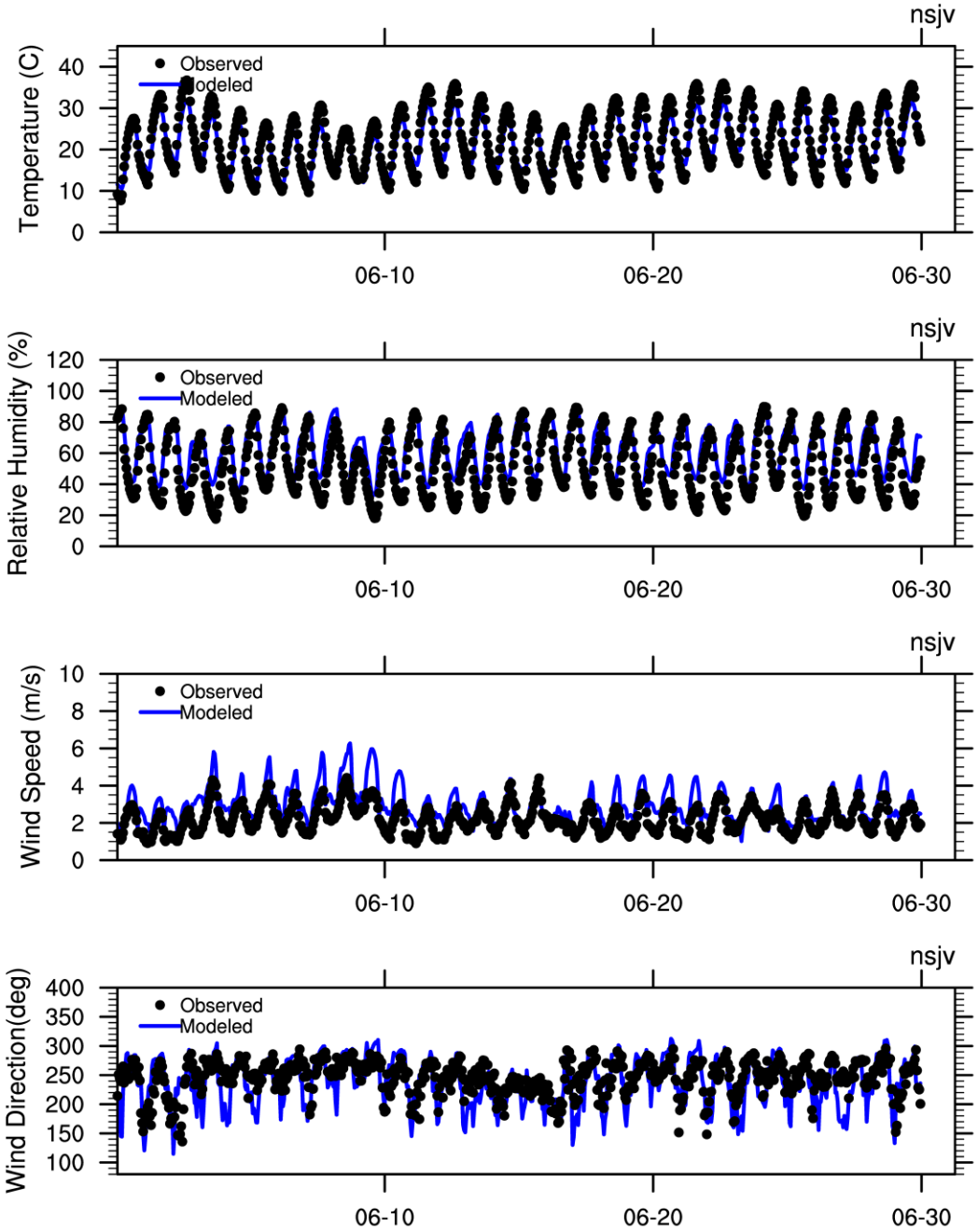

Figure S 8. Time series of temperature, relative humidity, wind speed, and direction for the Southern San Joaquin Valley in June 2018.

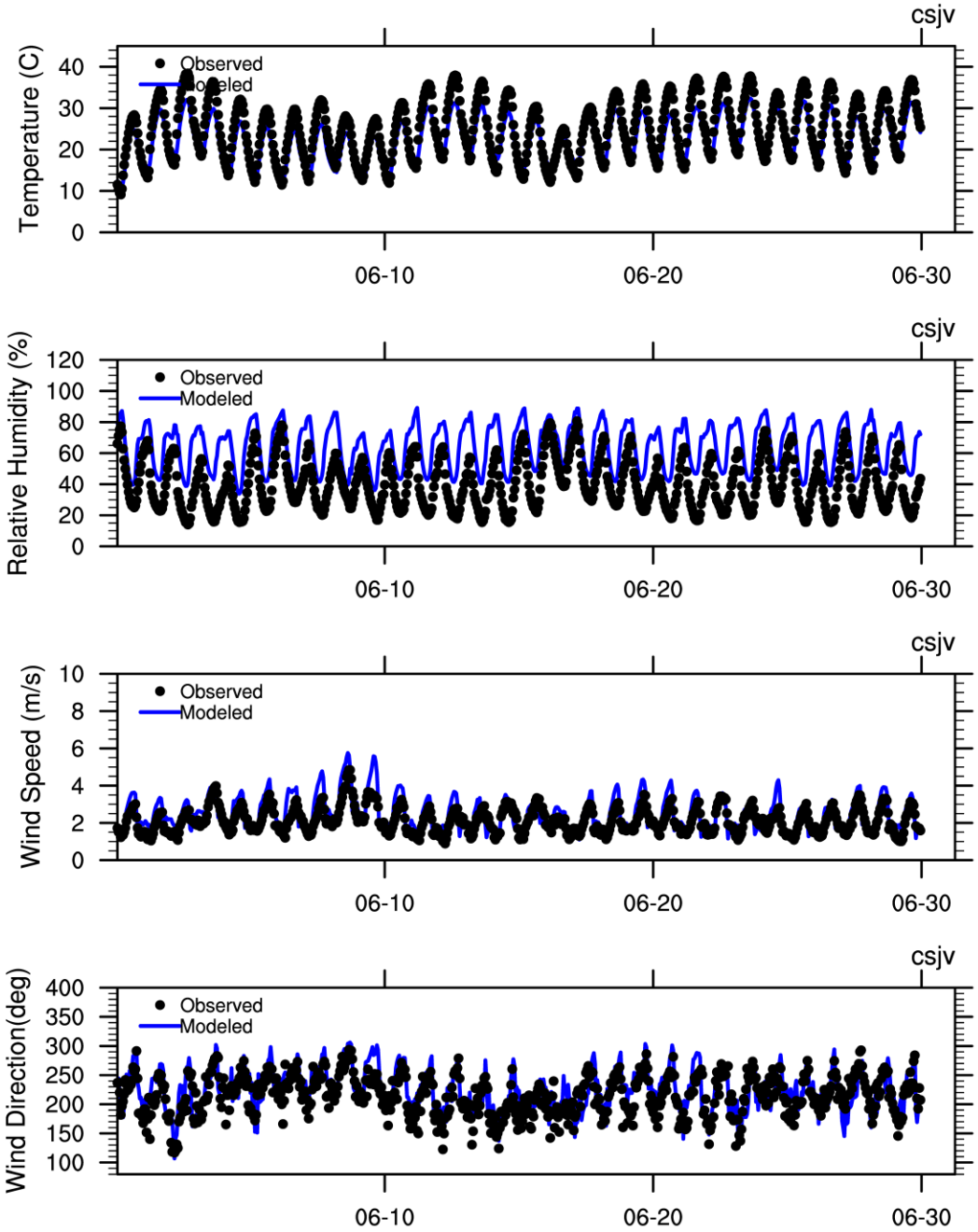

Figure S 9. Time series of temperature, relative humidity, wind speed, and direction for the Southern San Joaquin Valley in June 2018.

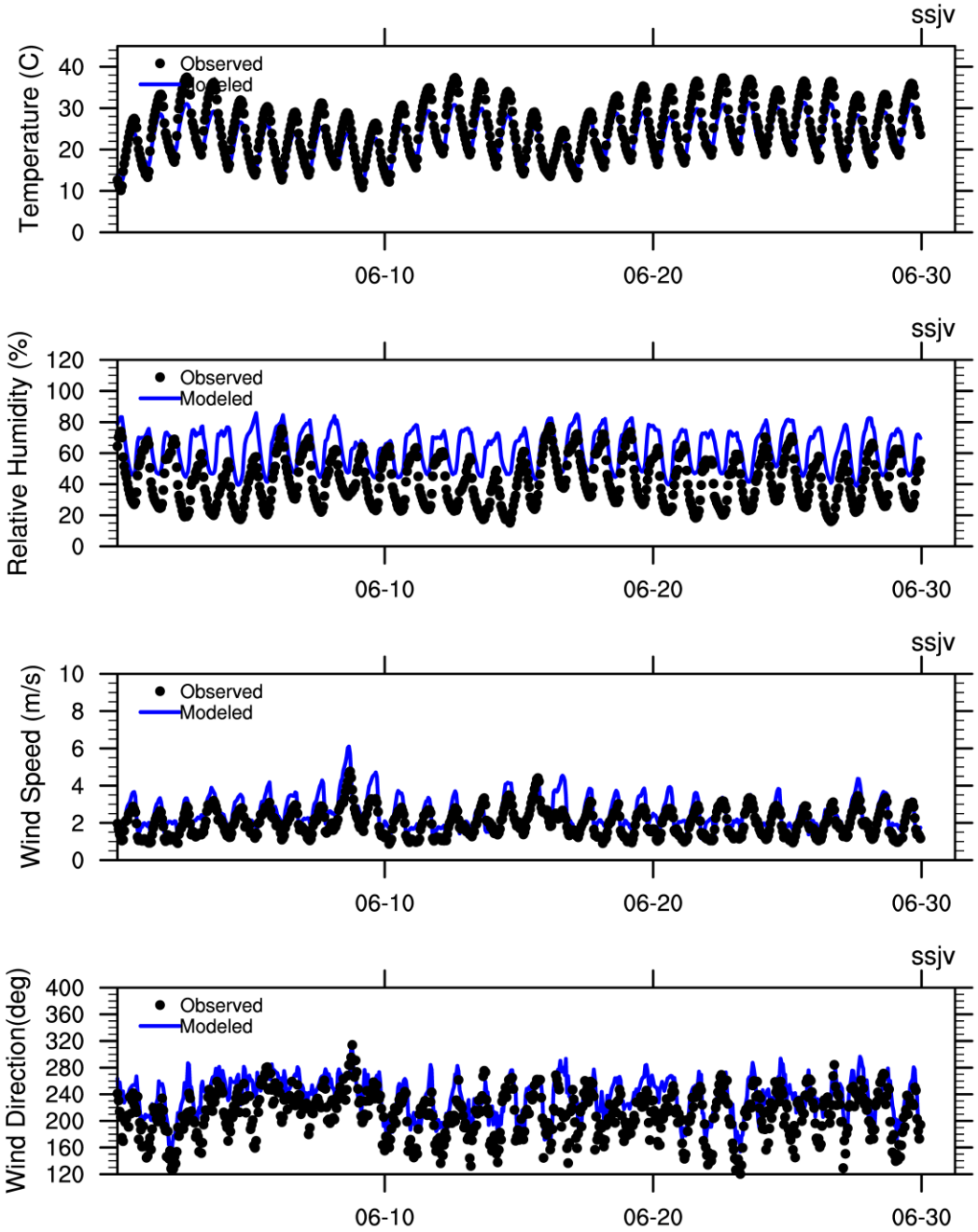

Figure S 10. Time series of temperature, relative humidity, wind speed, and direction for the Northern San Joaquin Valley in July 2018.

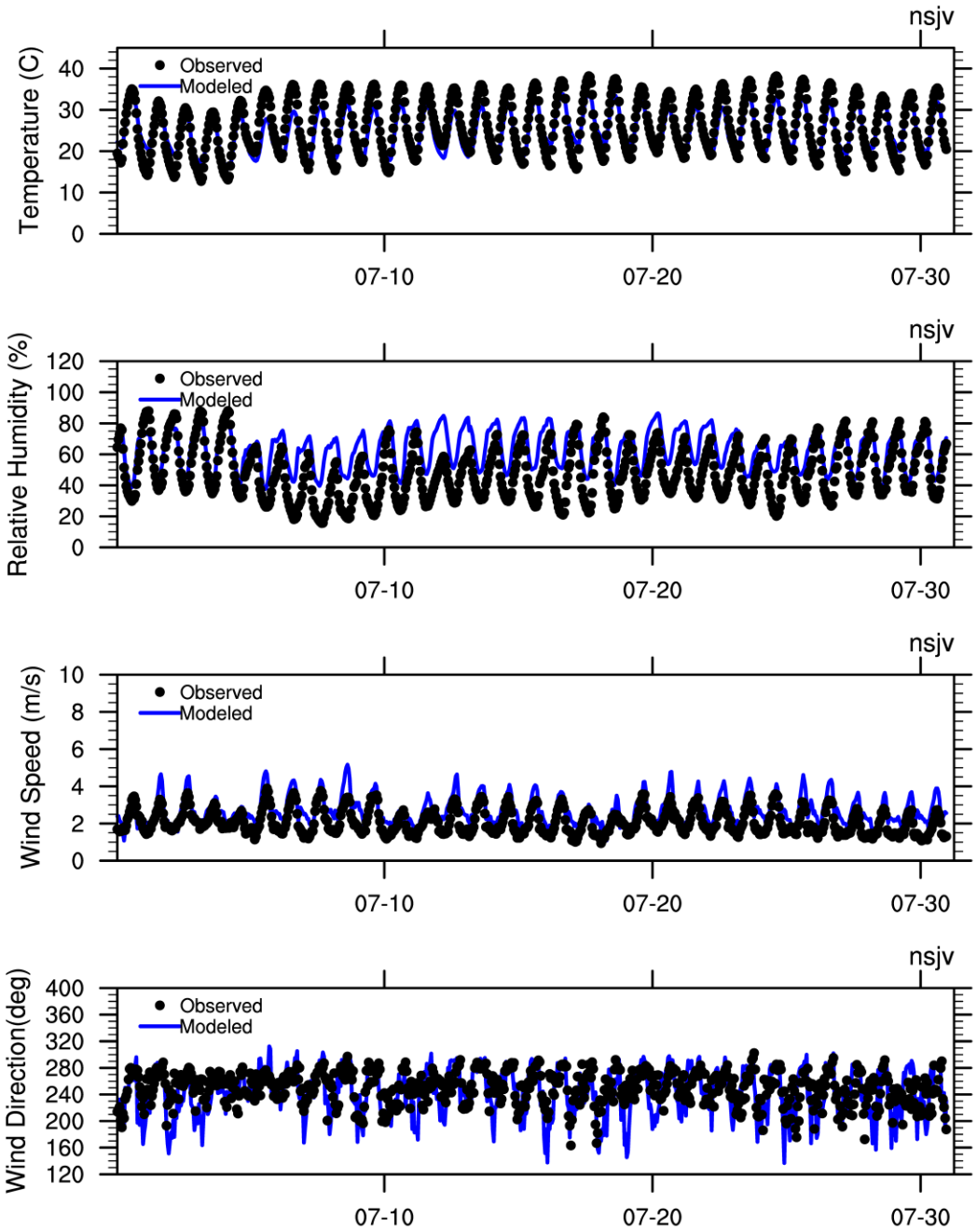

Figure S 11. Time series of temperature, relative humidity, wind speed, and direction for the Central San Joaquin Valley in July 2018.

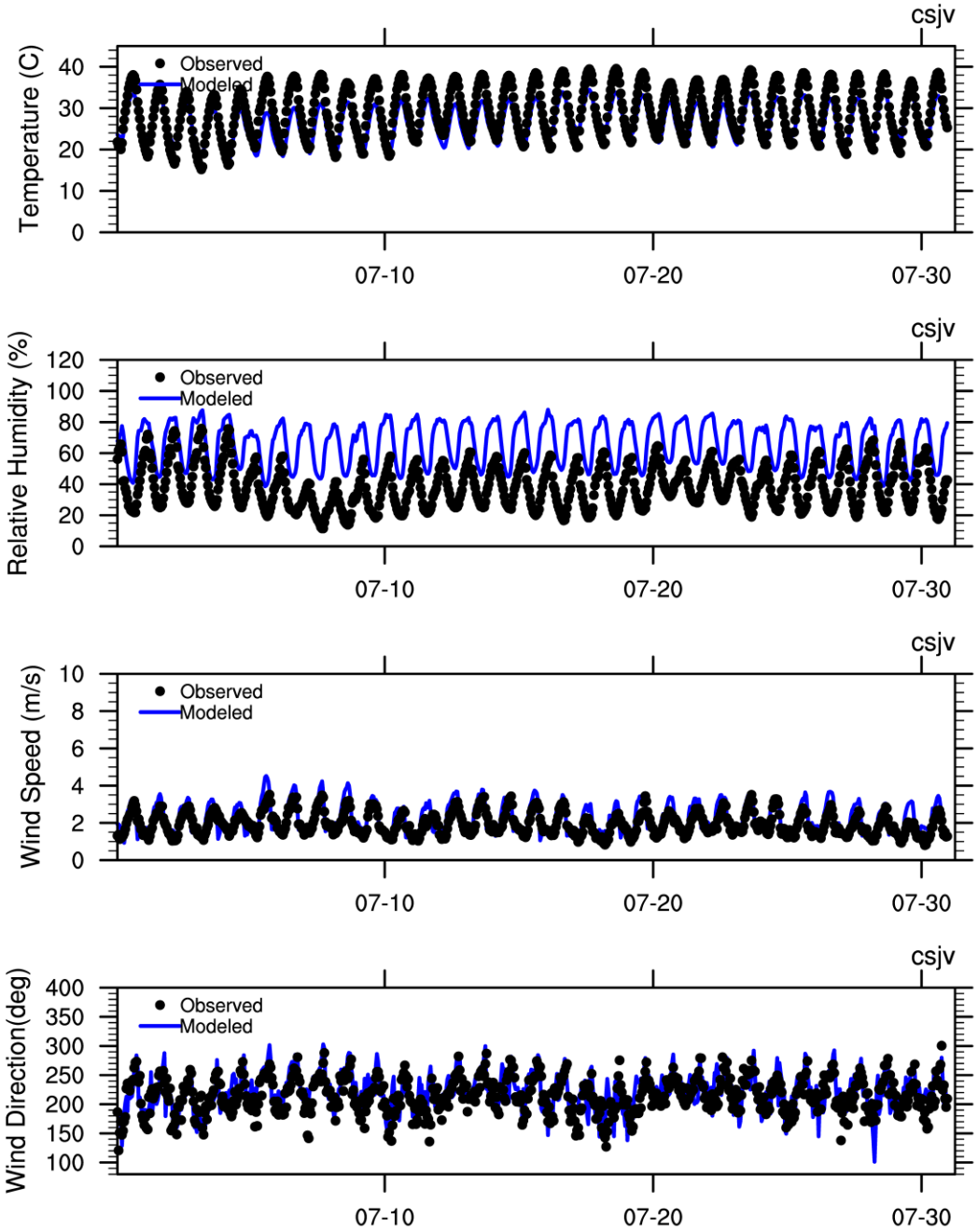

Figure S 12. Time series of temperature, relative humidity, wind speed, and direction for the Southern San Joaquin Valley in July 2018.

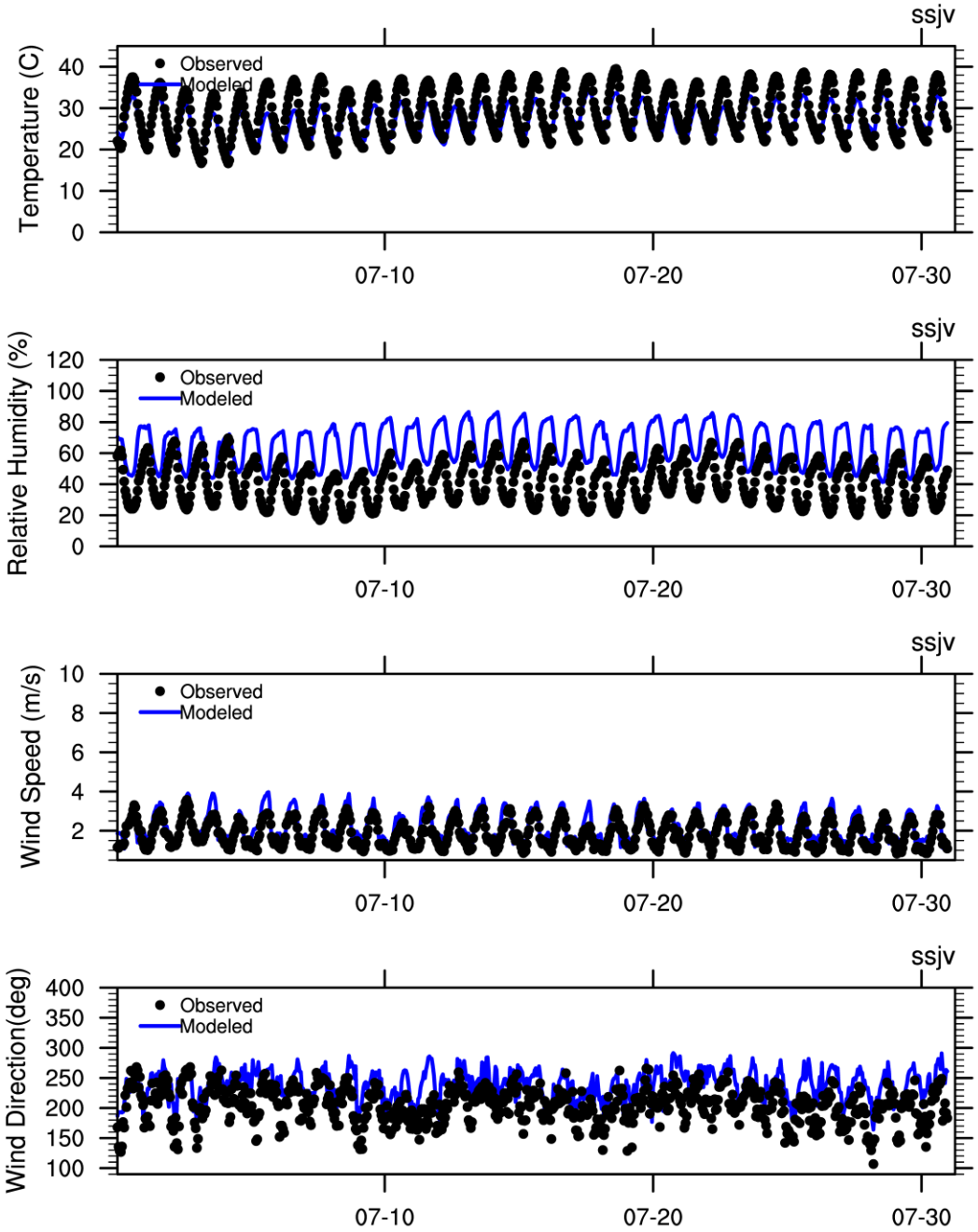

Figure S 13. Time series of temperature, relative humidity, wind speed, and direction for the Northern San Joaquin Valley in August 2018.

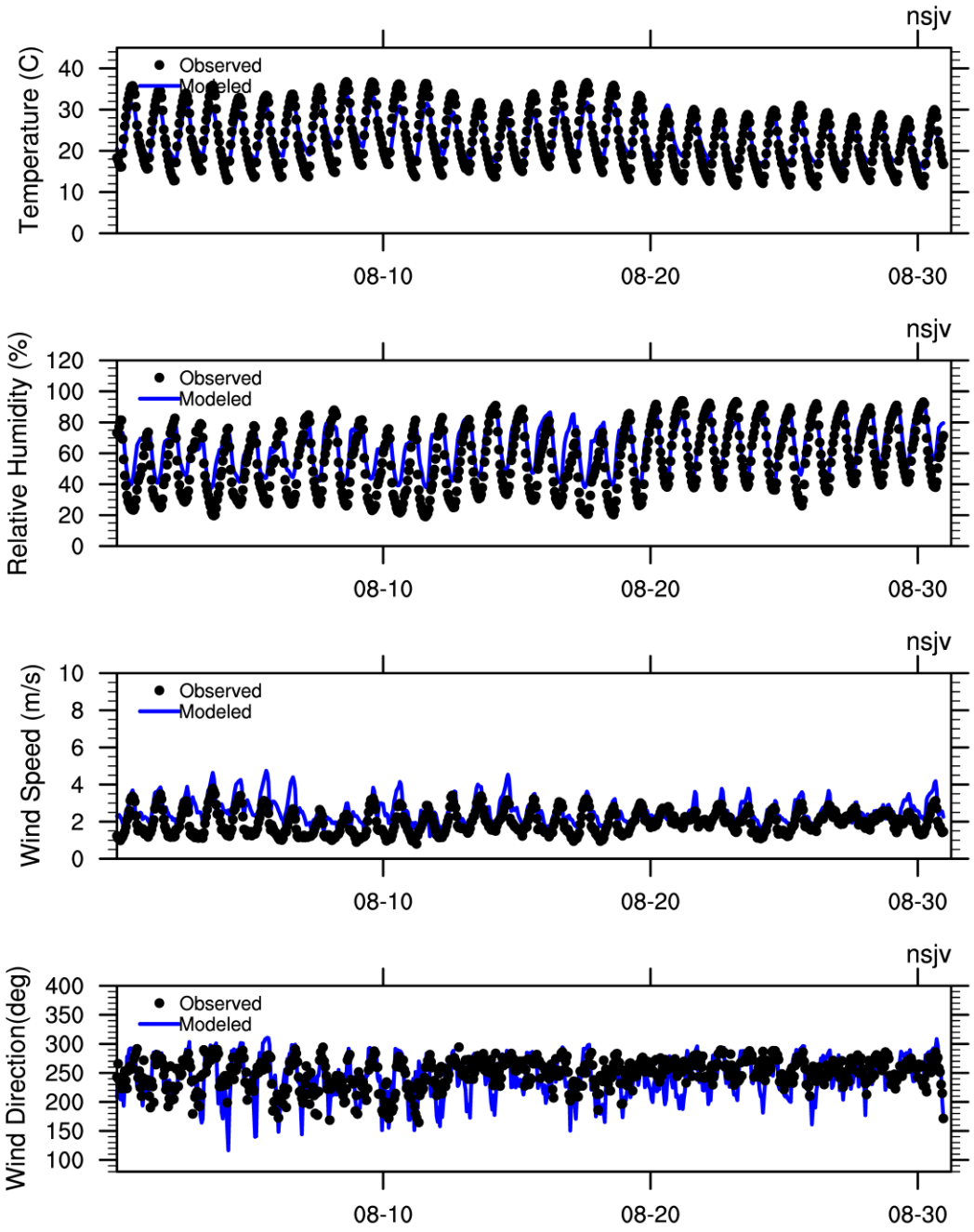

Figure S 14. Time series of temperature, relative humidity, wind speed, and direction for the Central San Joaquin Valley in August 2018.

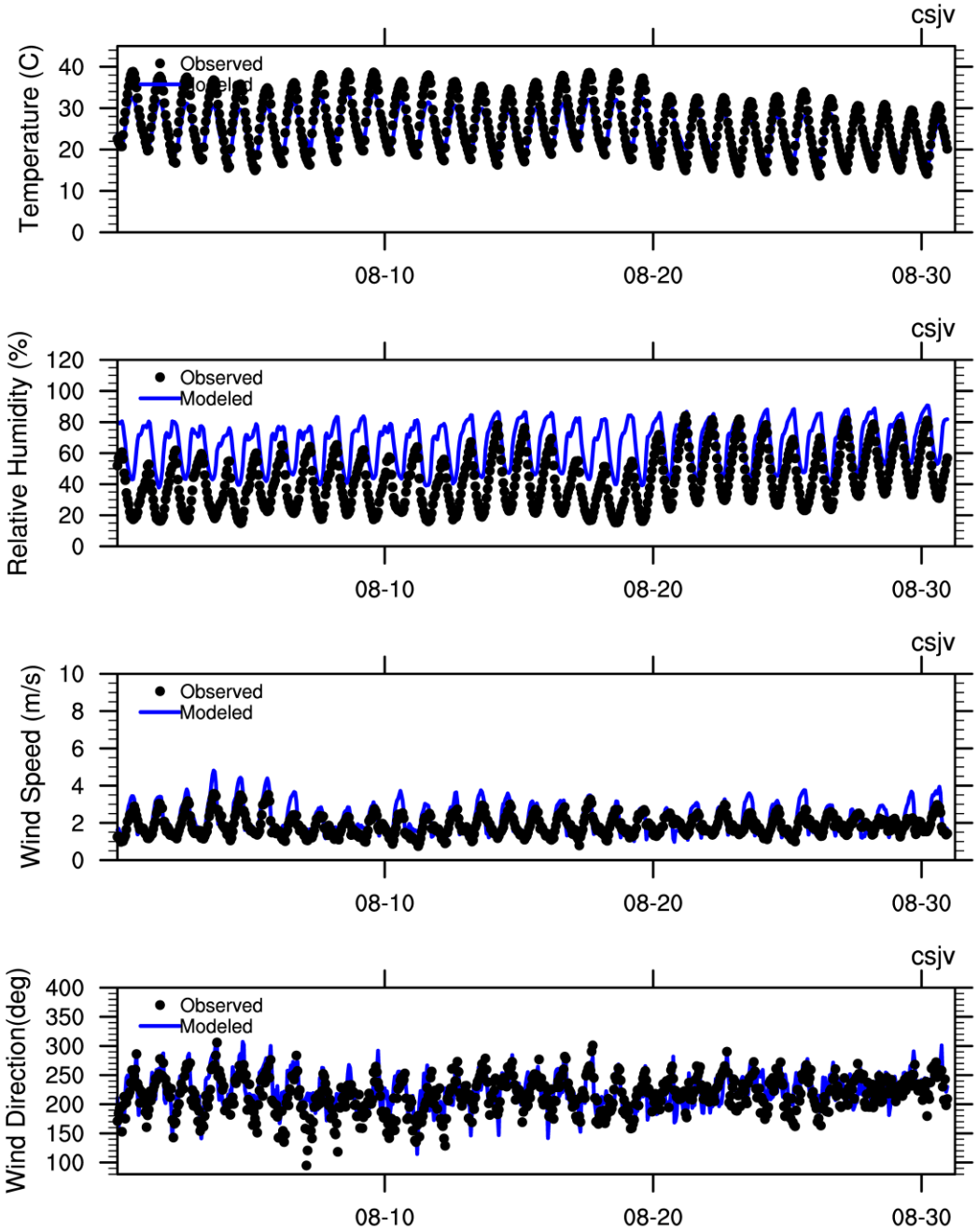

Figure S 15. Time series of temperature, relative humidity, wind speed, and direction for the Southern San Joaquin Valley in August 2018.

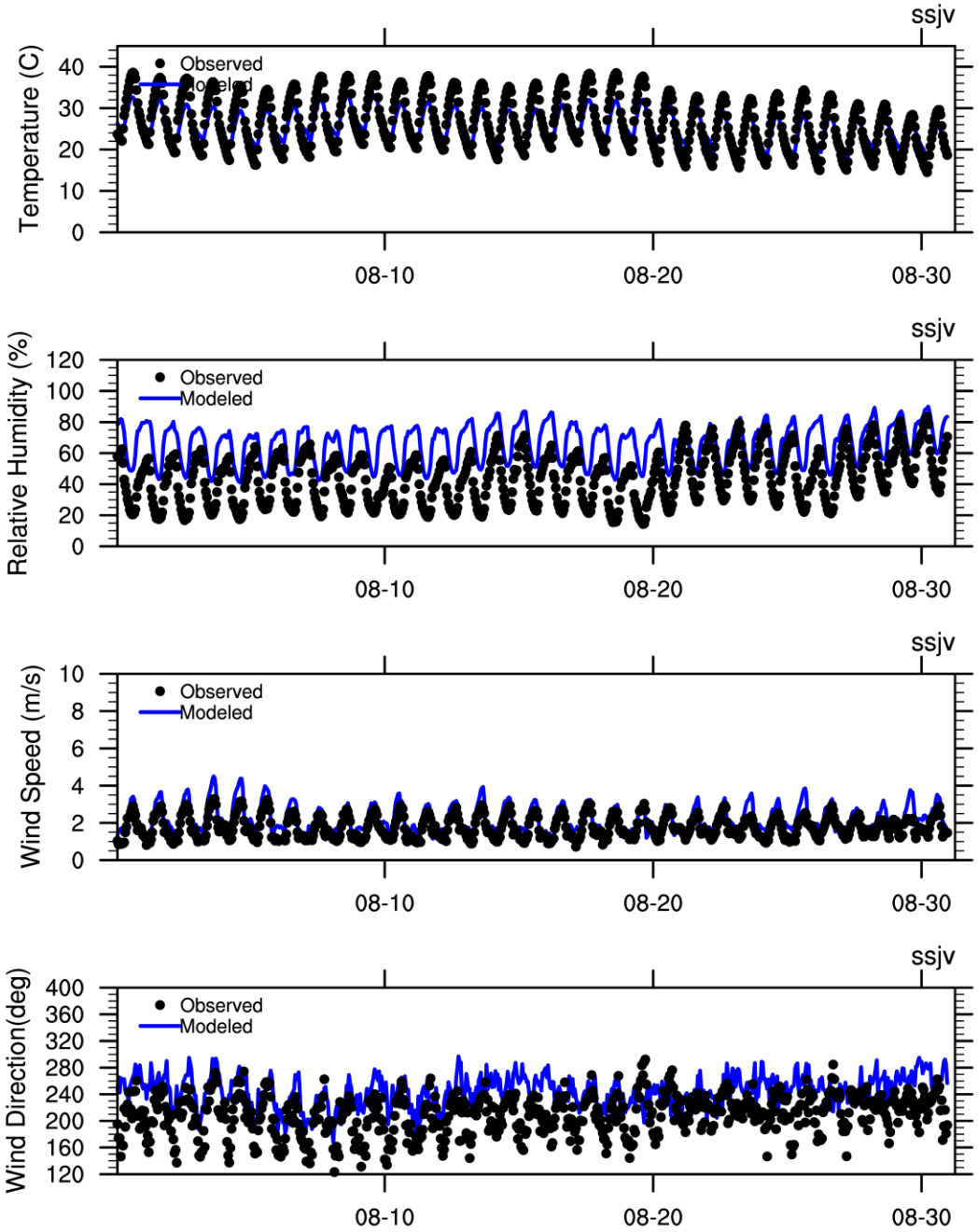

Figure S 16. Time series of temperature, relative humidity, wind speed, and direction for the Northern San Joaquin Valley in September 2018.

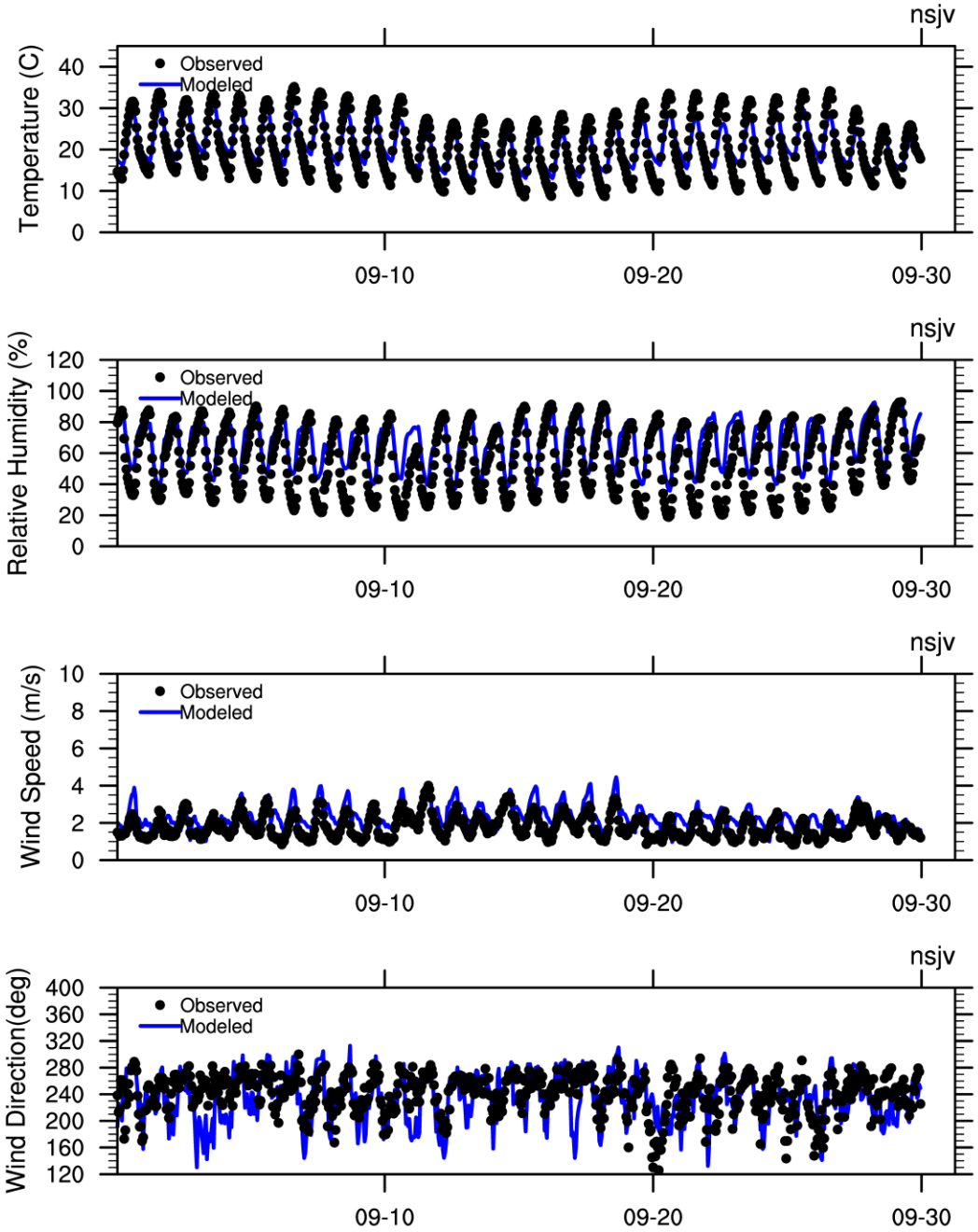

Figure S 17. Time series of temperature, relative humidity, wind speed, and direction for the Central San Joaquin Valley in September 2018.

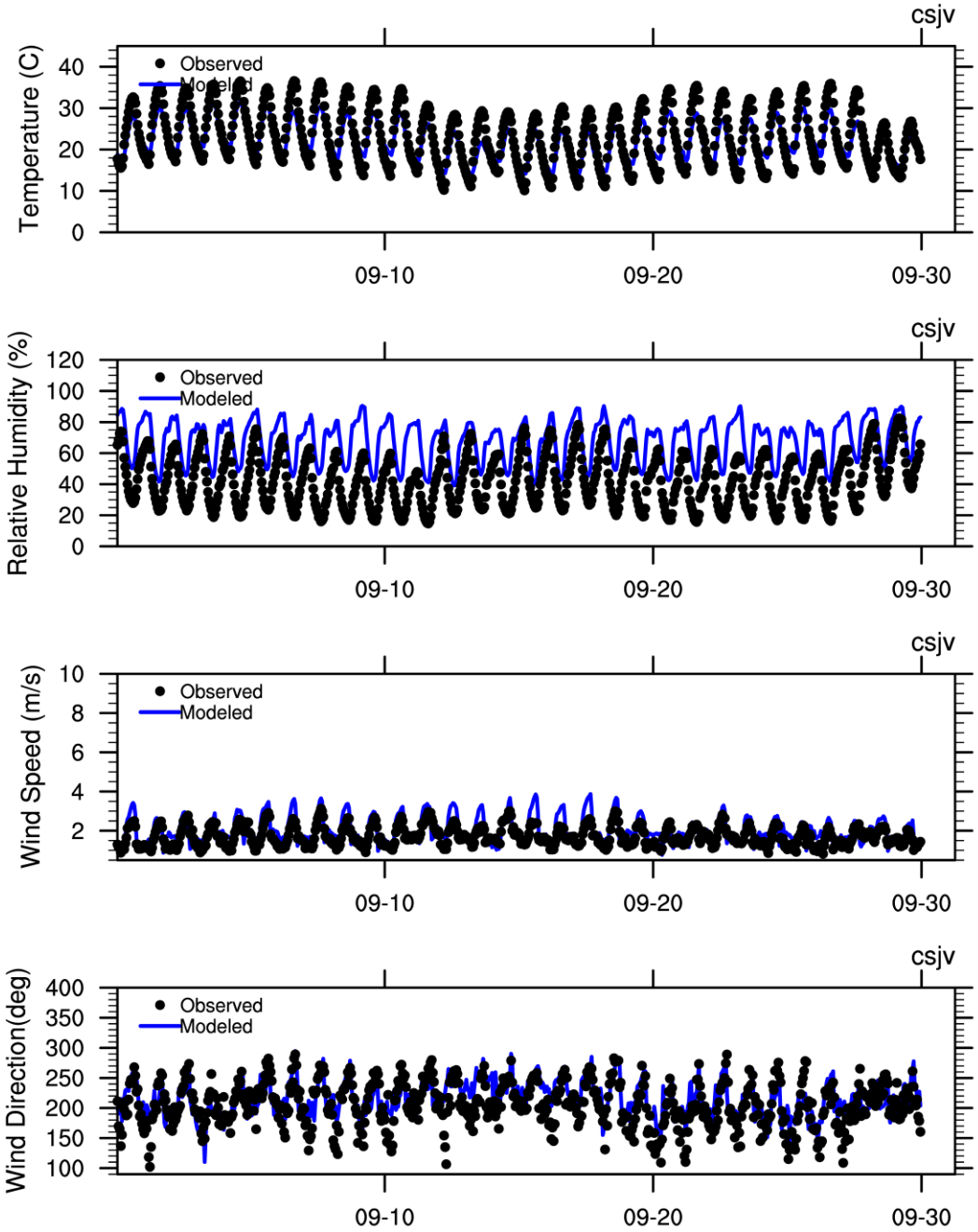

Figure S 18. Time series of temperature, relative humidity, wind speed, and direction for the Southern San Joaquin Valley in September 2018.

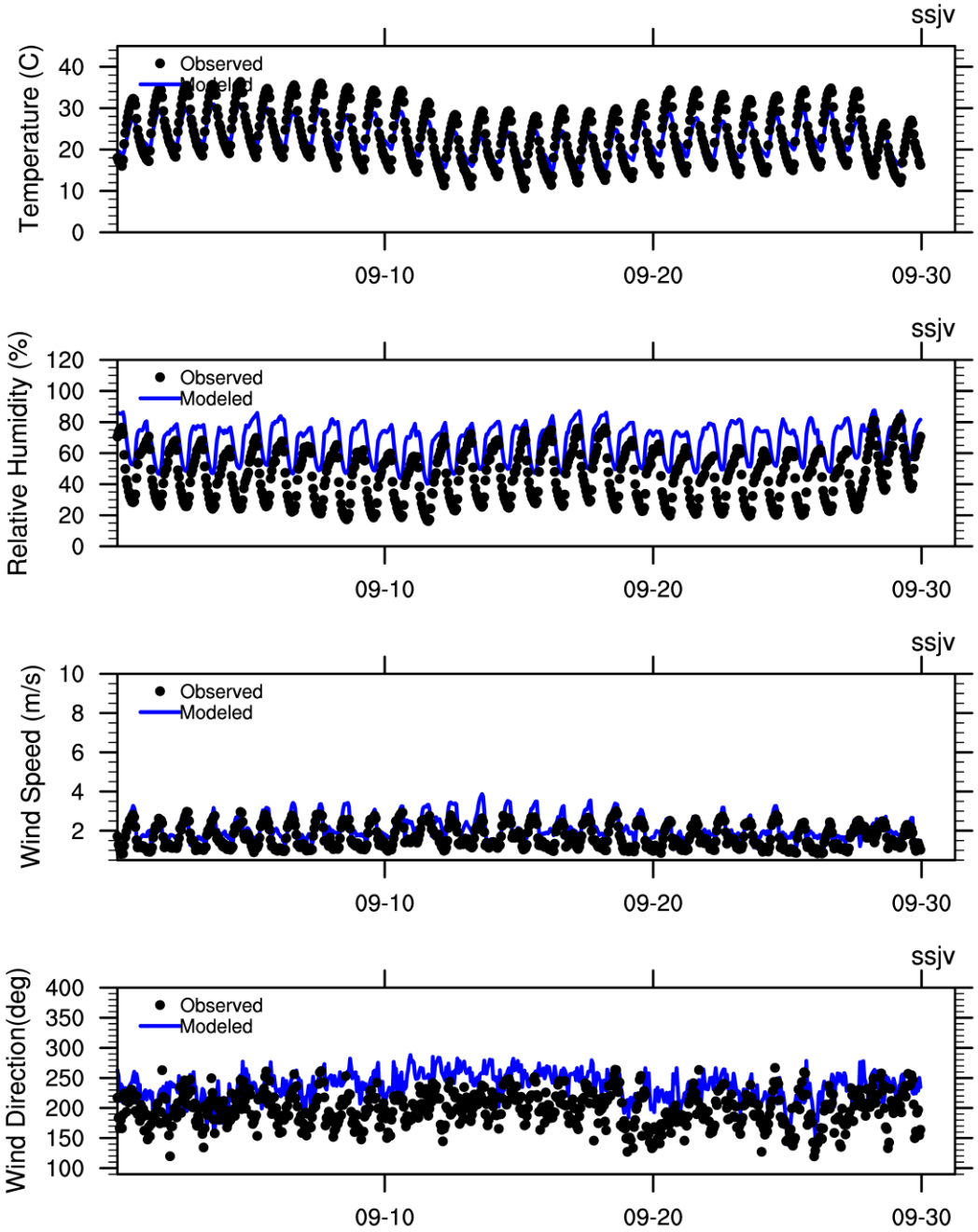

Figure S 19. Time series of temperature, relative humidity, wind speed, and direction for the Northern San Joaquin Valley in October2018.

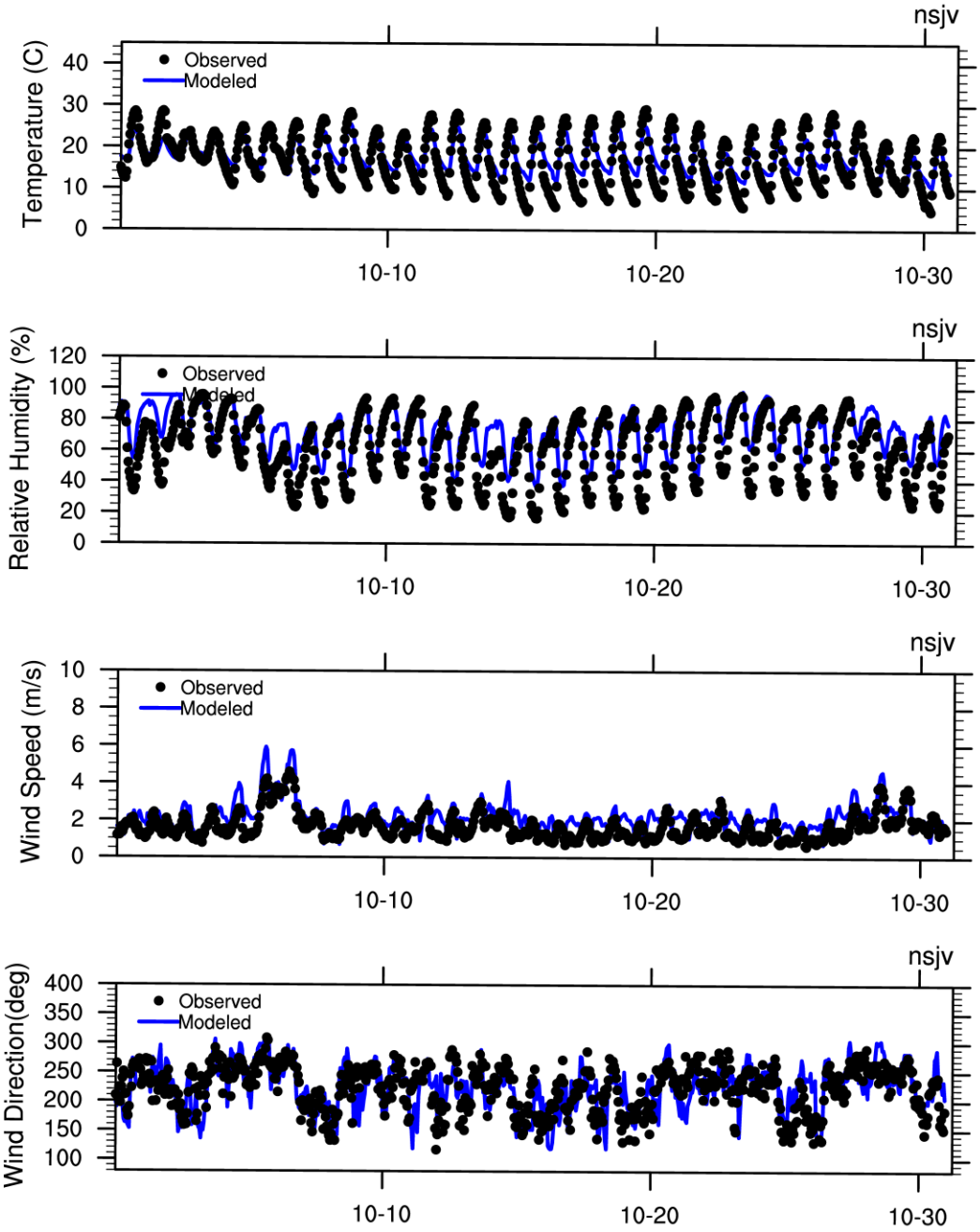

Figure S 20. Time series of temperature, relative humidity, wind speed, and direction for the Central San Joaquin Valley in October 2018.

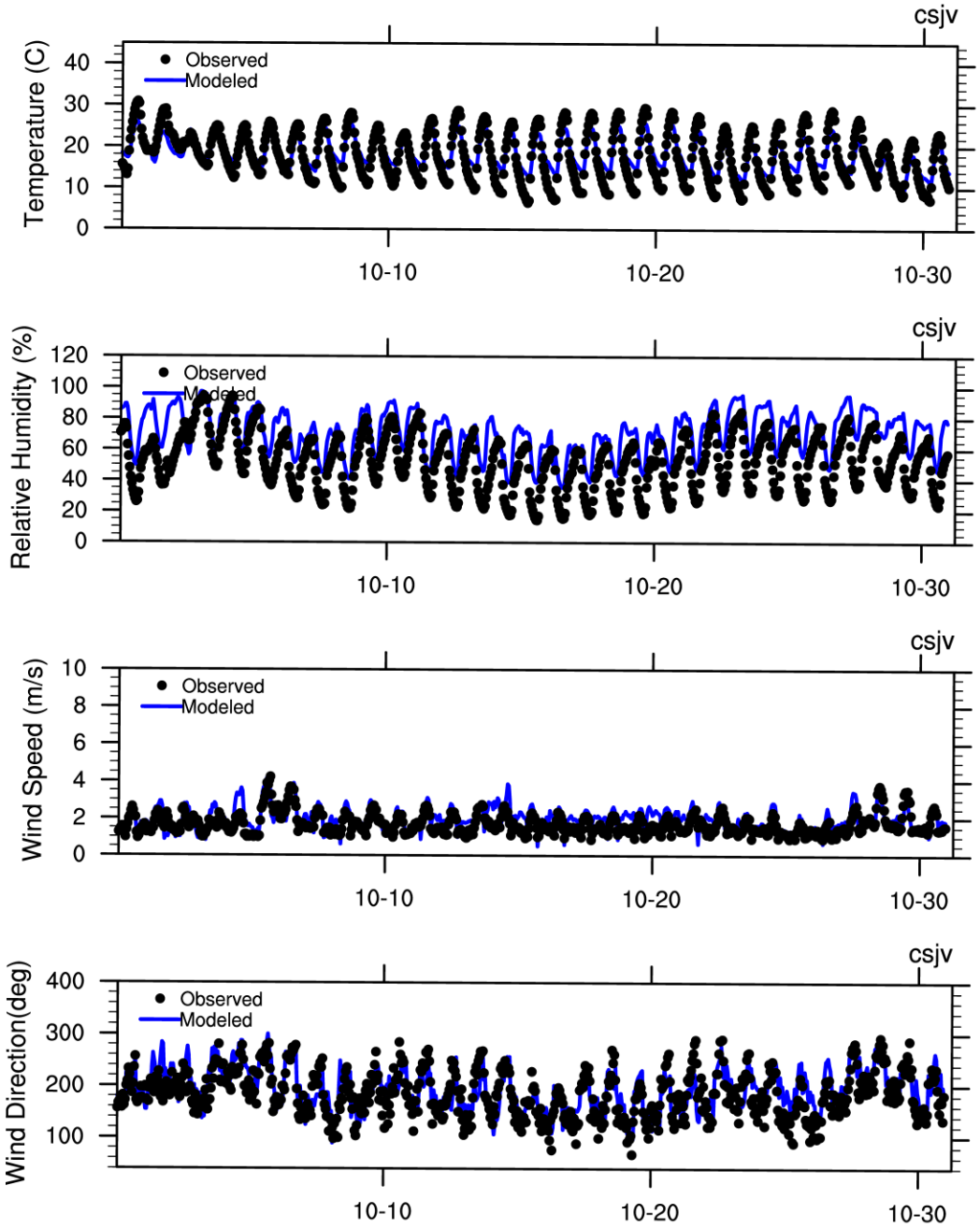

Figure S 21. Time series of temperature, relative humidity, wind speed, and direction for the Southern San Joaquin Valley in October 2018.

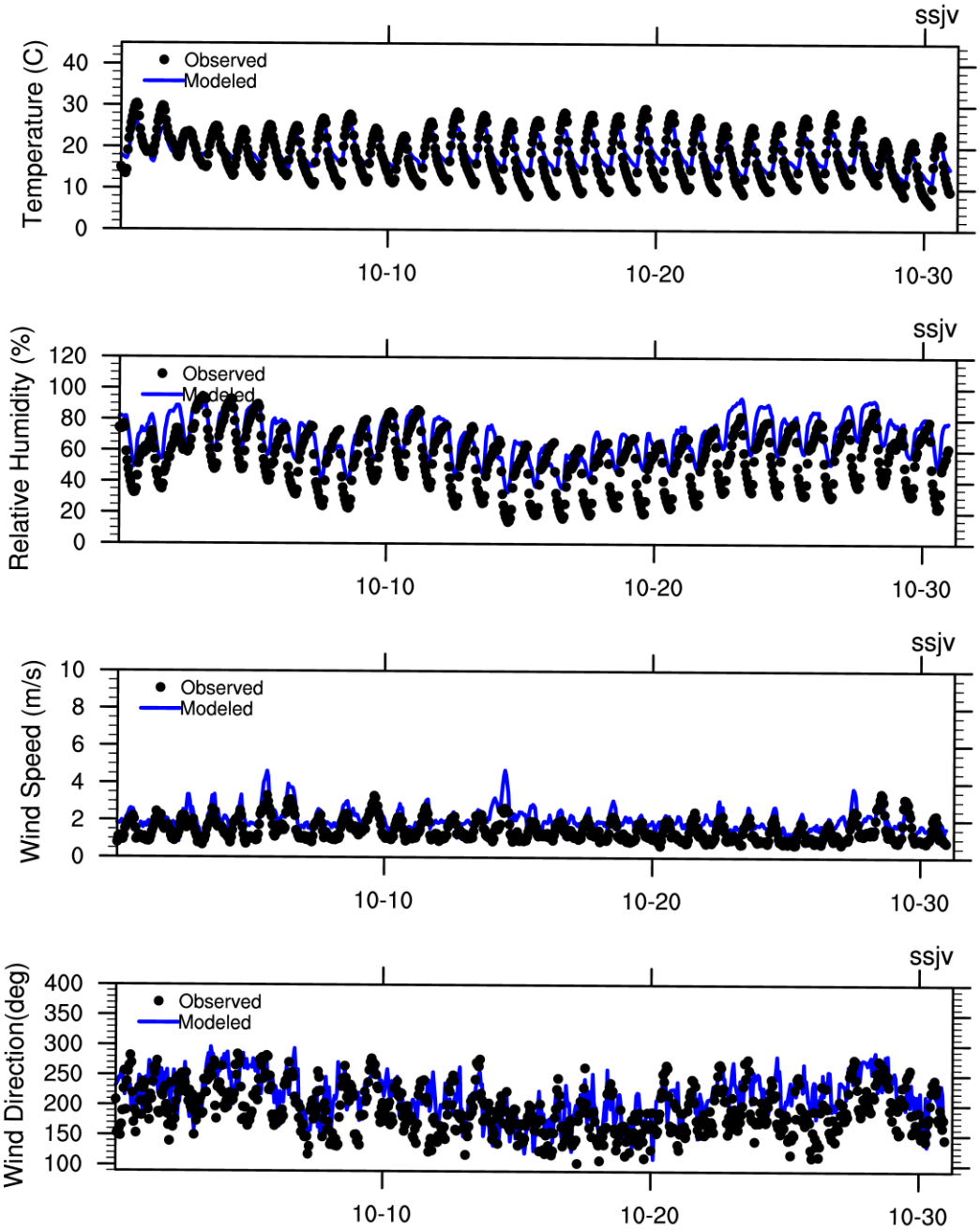

Figure S 22. Wind rose comparison between observation (Left) and WRF (Right) for surface wind at Turlock-S Minaret Street (top), Fresno State #2 (middle) and Edison (bottom).

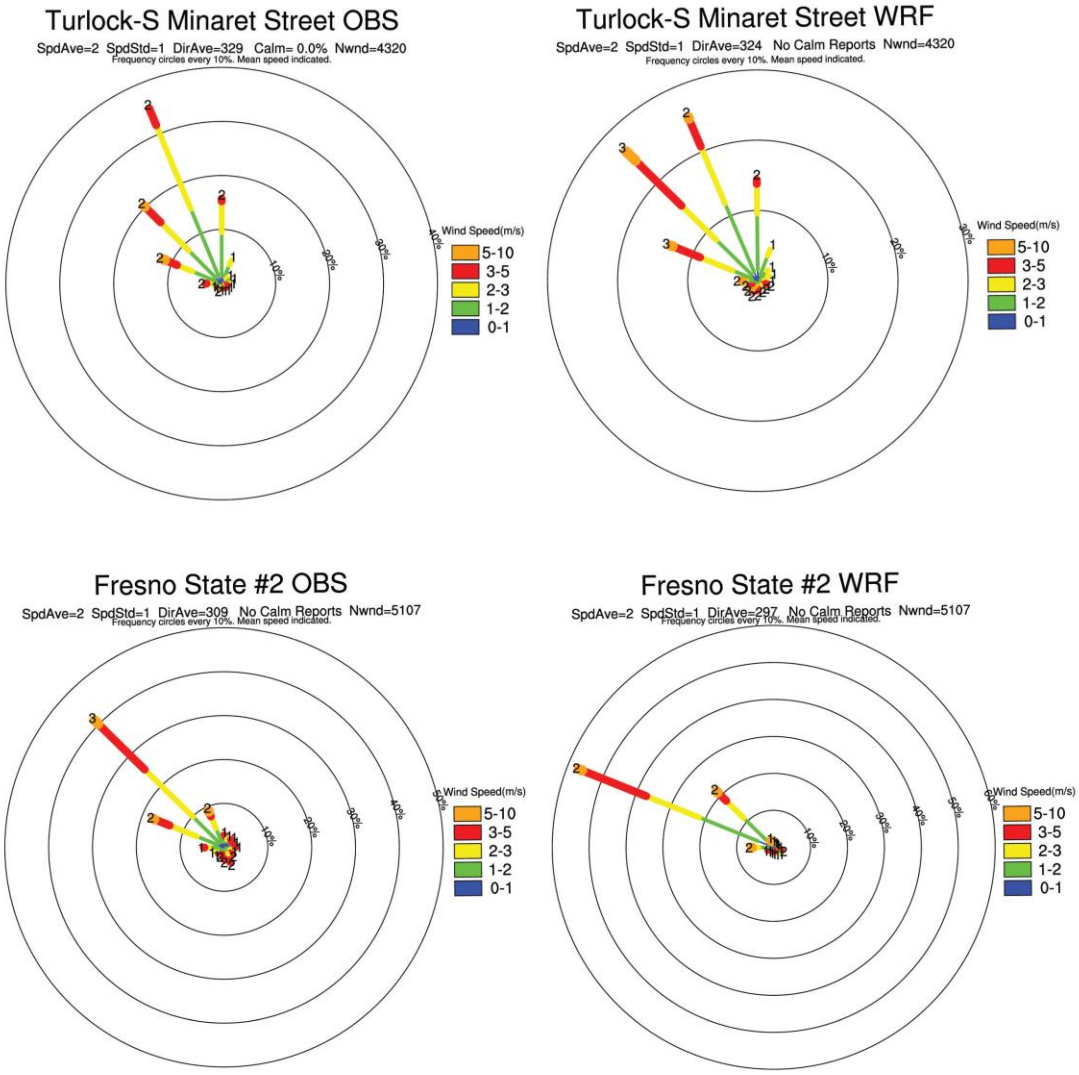

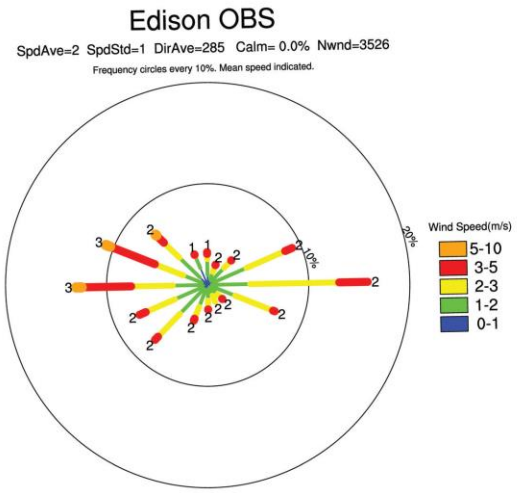
Edison OBS
SpdAve=2 SpdStd=1 DirAve=285 Calm= 0.0% Nwnd=3526
Frequency circles every 10%. Mean speed indicated.
Wind Speed(m/s)
5-10
3-5
2-3
1-2
0-1

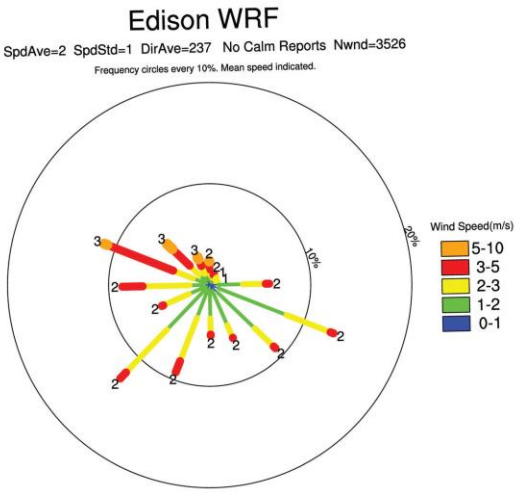
Edison WRF
SpdAve=2 SpdStd=1 DirAve=237 No Calm Reports Nwnd=3526
Frequency circles every 10%. Mean speed indicated.
Wind Speed(m/s)
5-10
3-5
2-3
1-2
0-1

Figure S 23. Observed and modeled ozone frequency distribution for the ozone season in Northern SJV (April – October 2018)

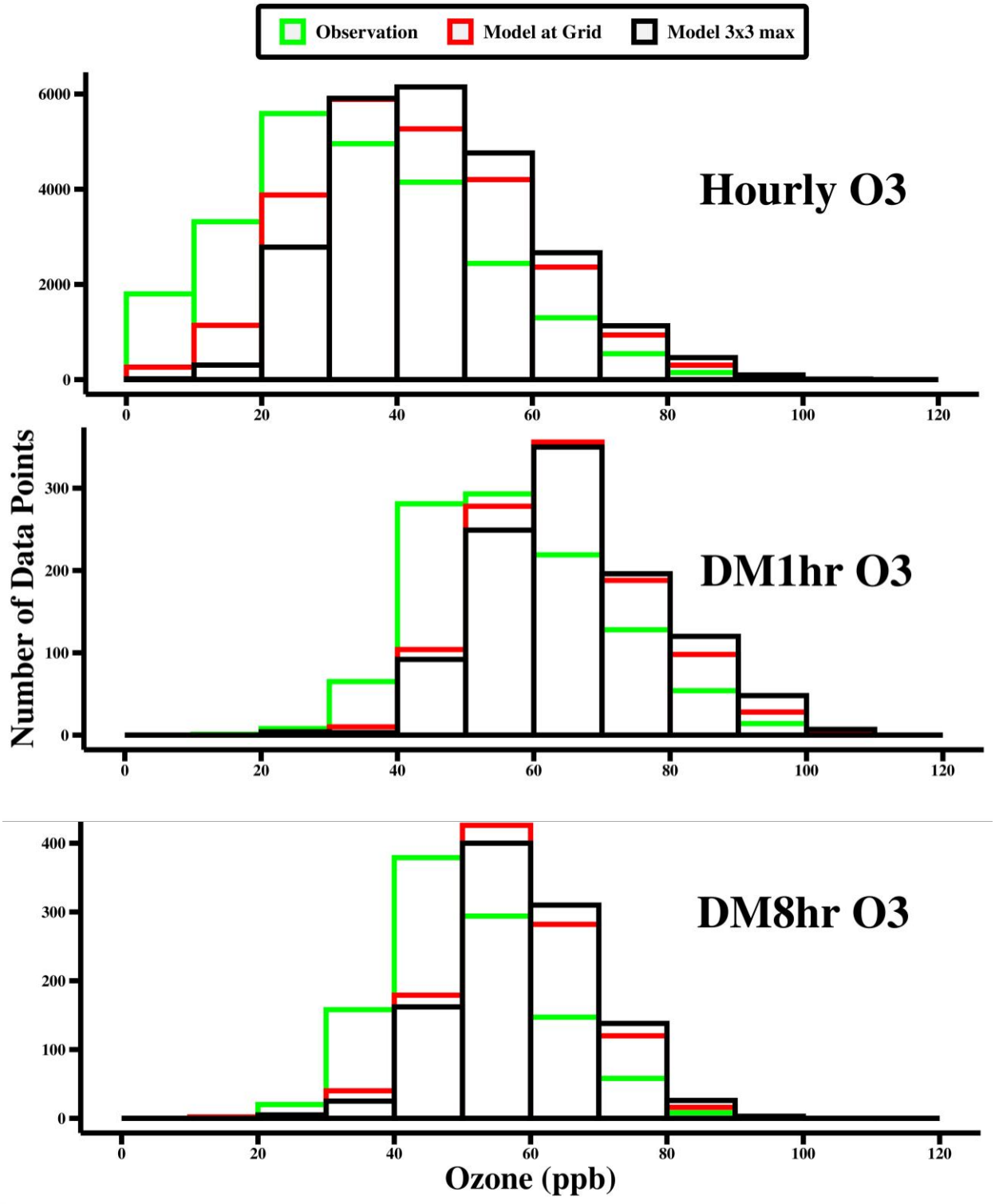

Figure S 24. Observed and modeled ozone frequency distribution for the ozone season in Central SJV (April – October 2018)

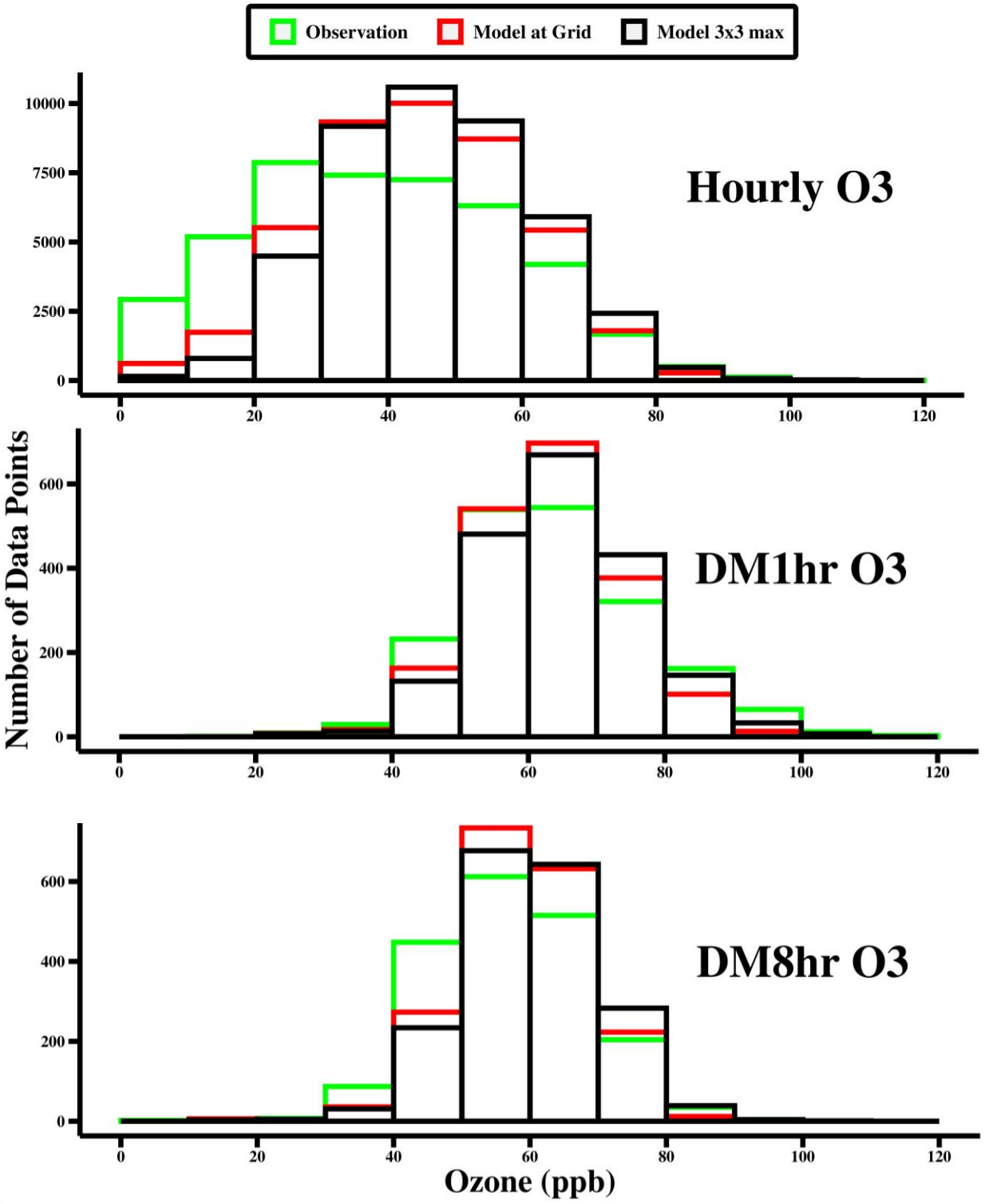

Figure S 25. Observed and modeled ozone frequency distribution for the ozone season is Southern SJV (April – October 2018)

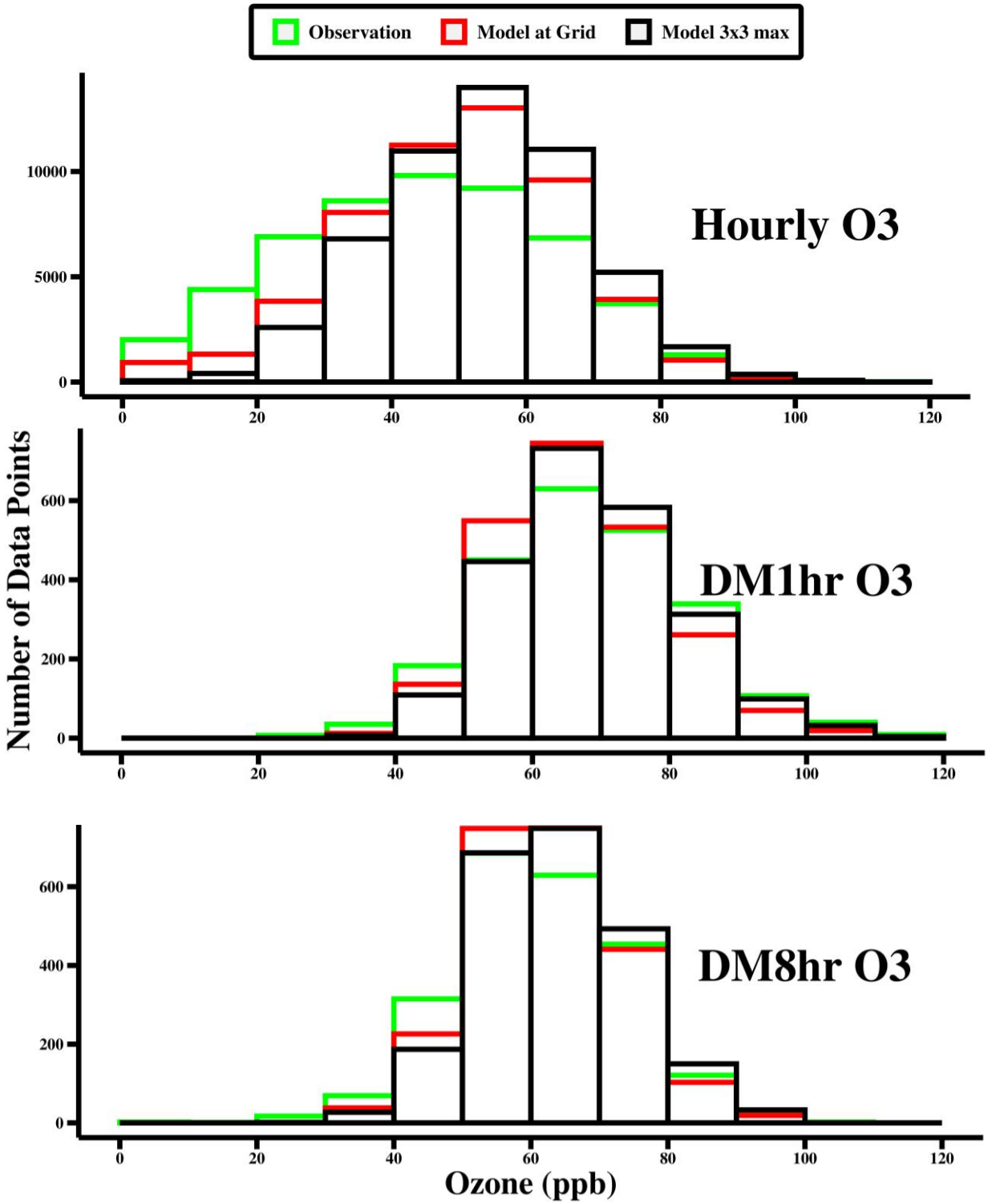

Figure S 26. Observed and modeled ozone scatter plots for the ozone season in Northern SJV (April – October 2018).

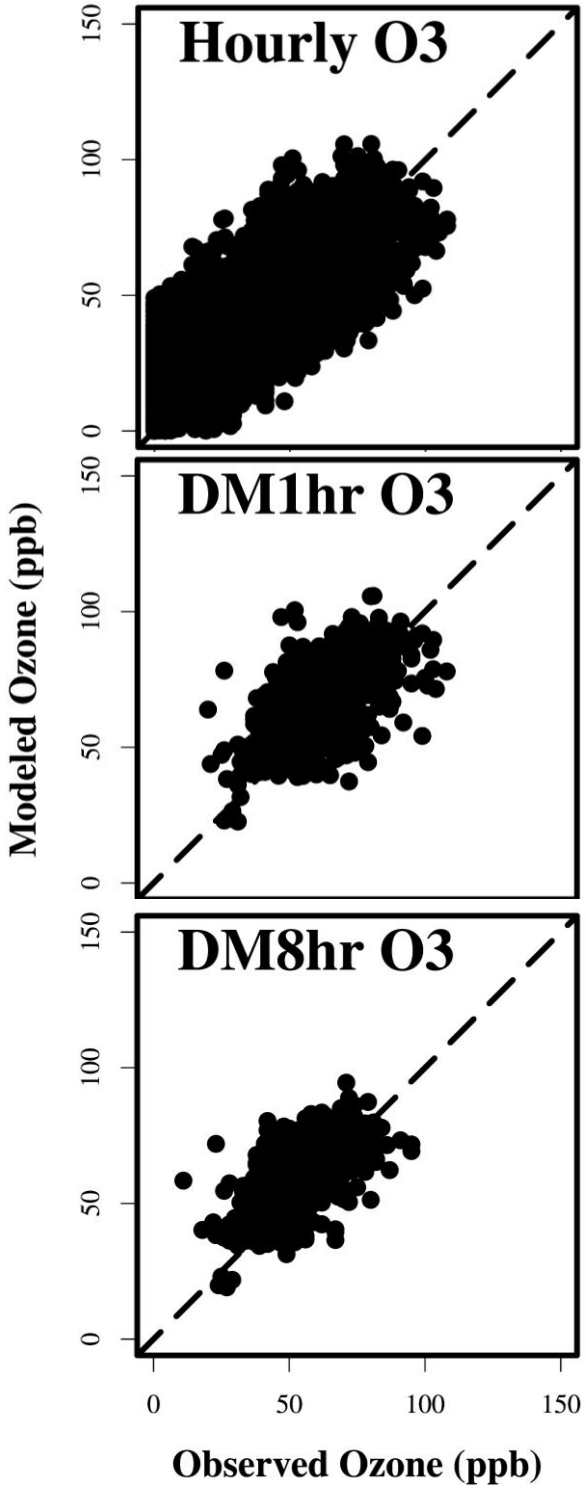

Figure S 27. Observed and modeled ozone scatter plots for the ozone season in Central SJV (April – October 2018).

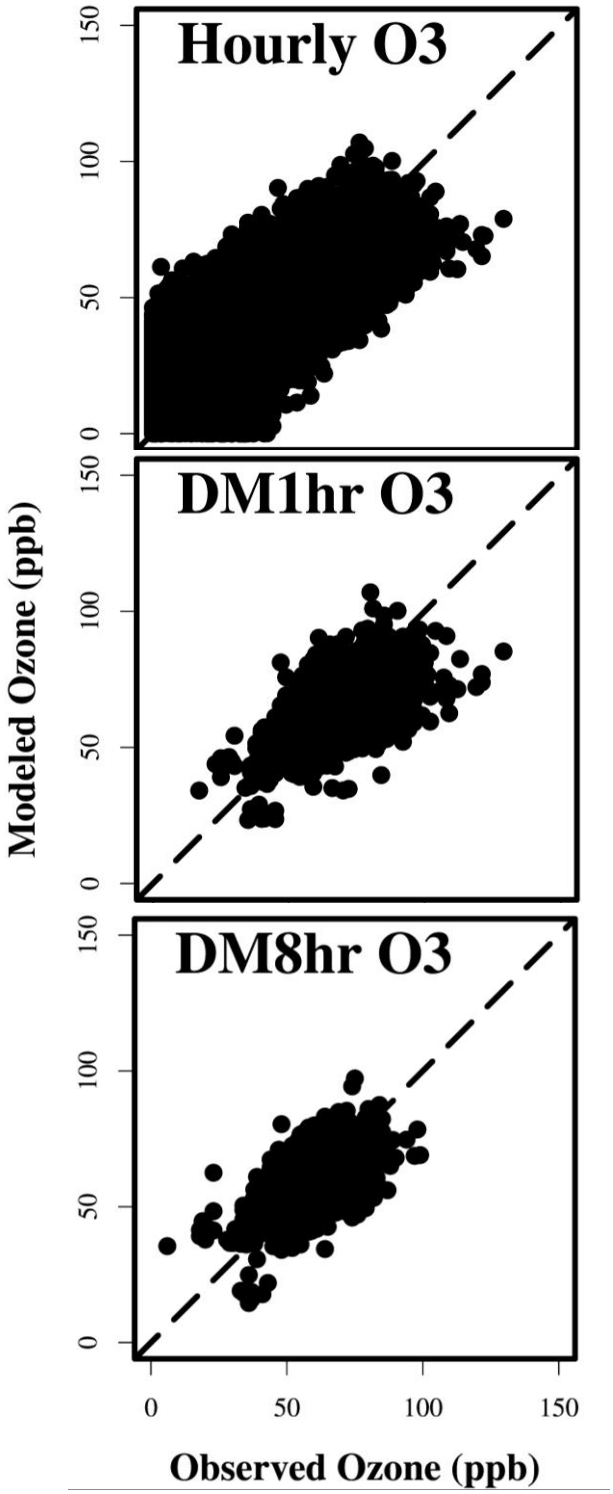

Figure S 28. Observed and modeled ozone scatter plots for the ozone season in Southern SJV (April – October 2018).

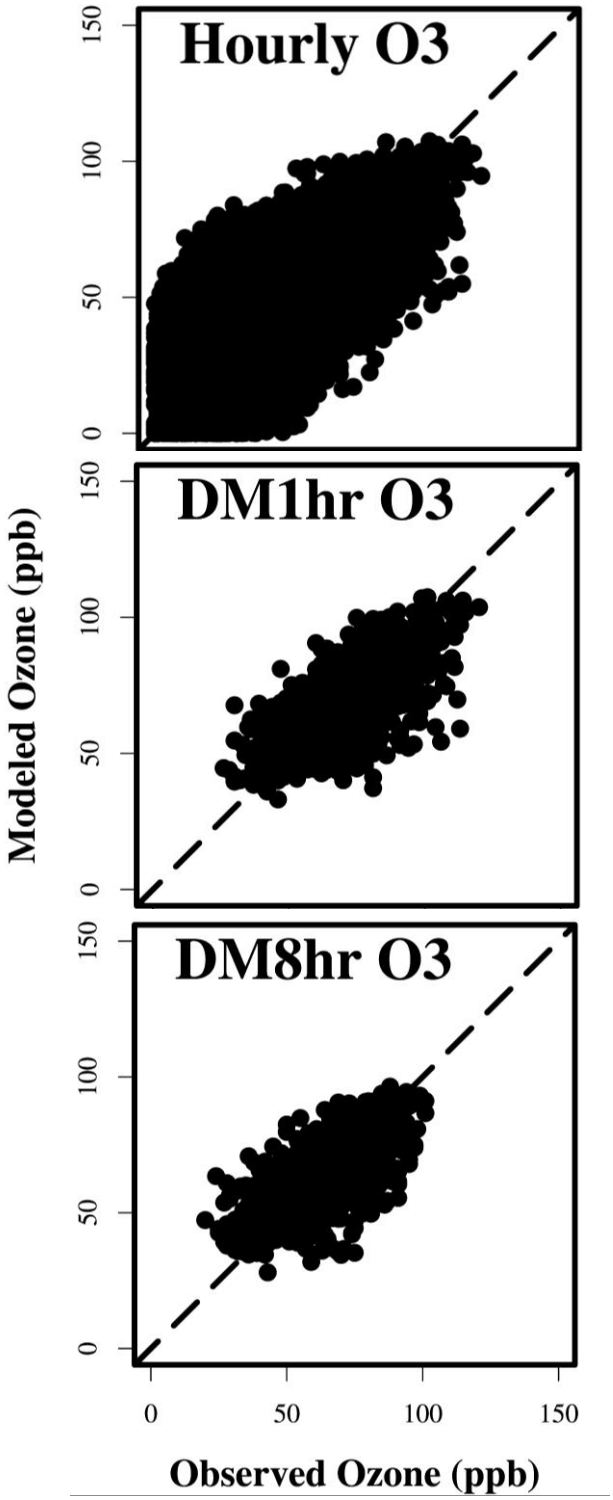

Figure S 29. Time-series of hourly ozone at the Turlock-S Minaret St. site for the ozone season (April-October 2018).

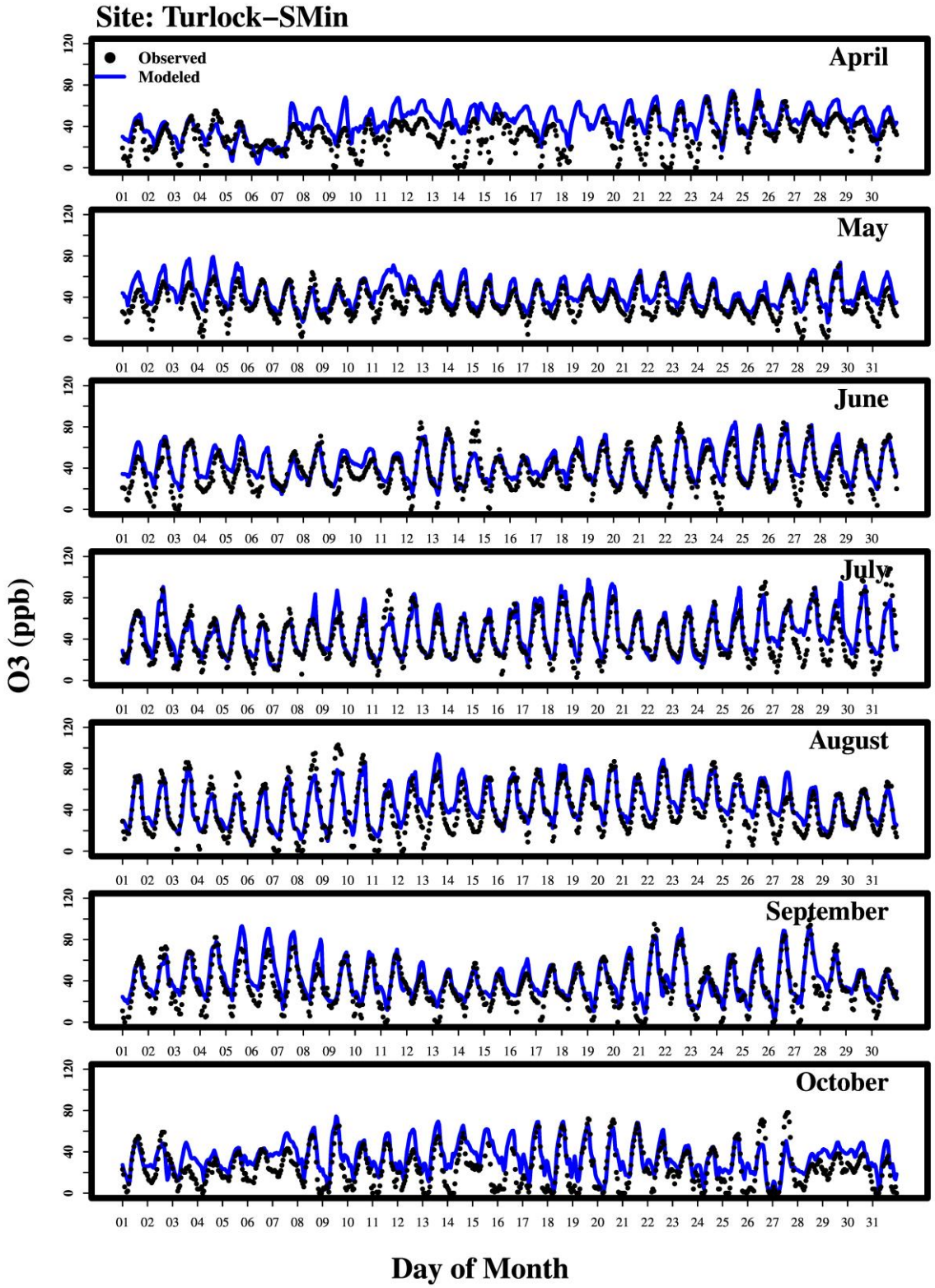

Figure S 30. Time-series of hourly ozone at the Modesto-14th St. site for the ozone season (April-October 2018).

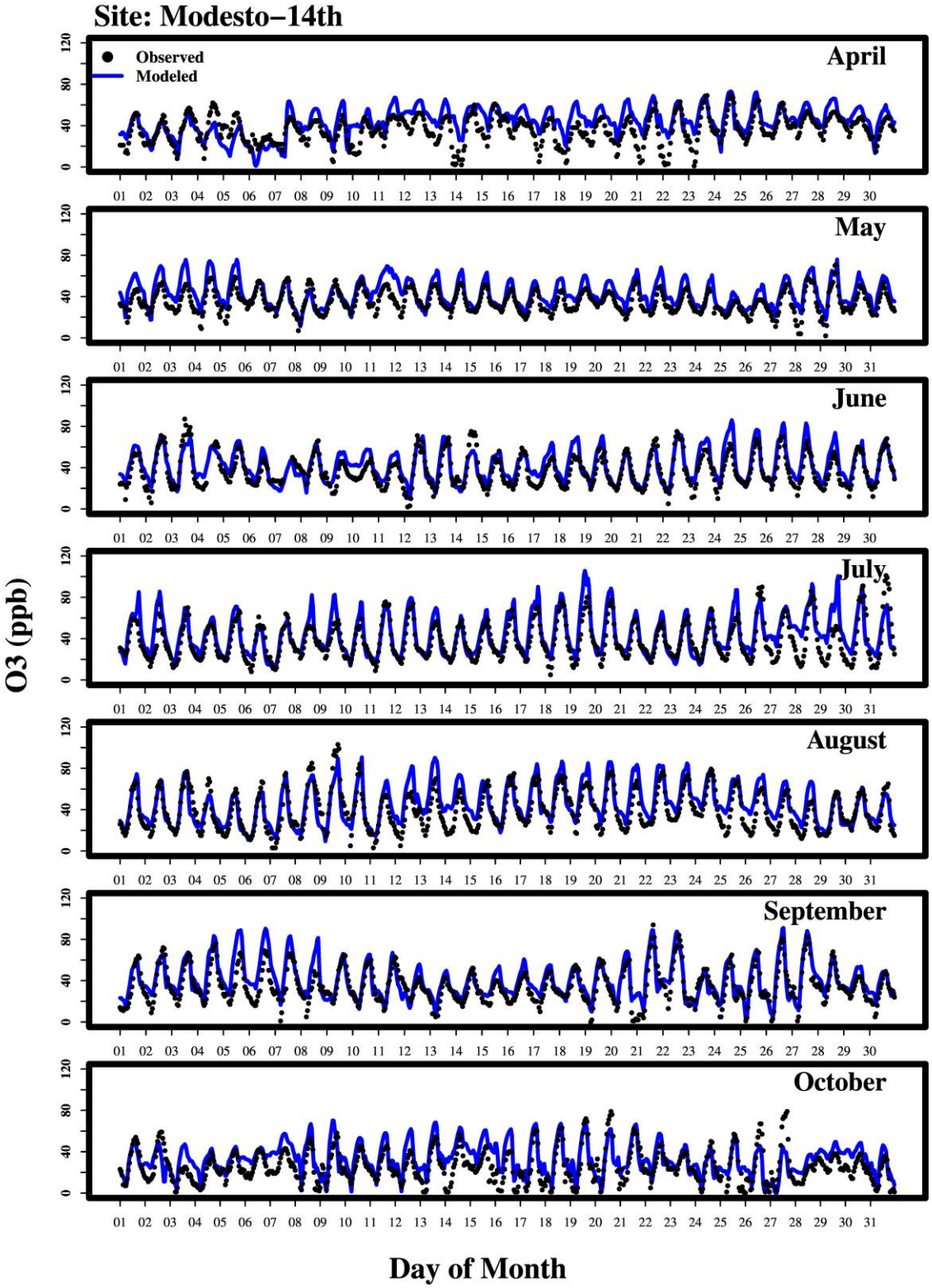

Figure S 31. Time-series of hourly ozone at the Merced-S Coffee Av. site for the ozone season (April-October 2018).

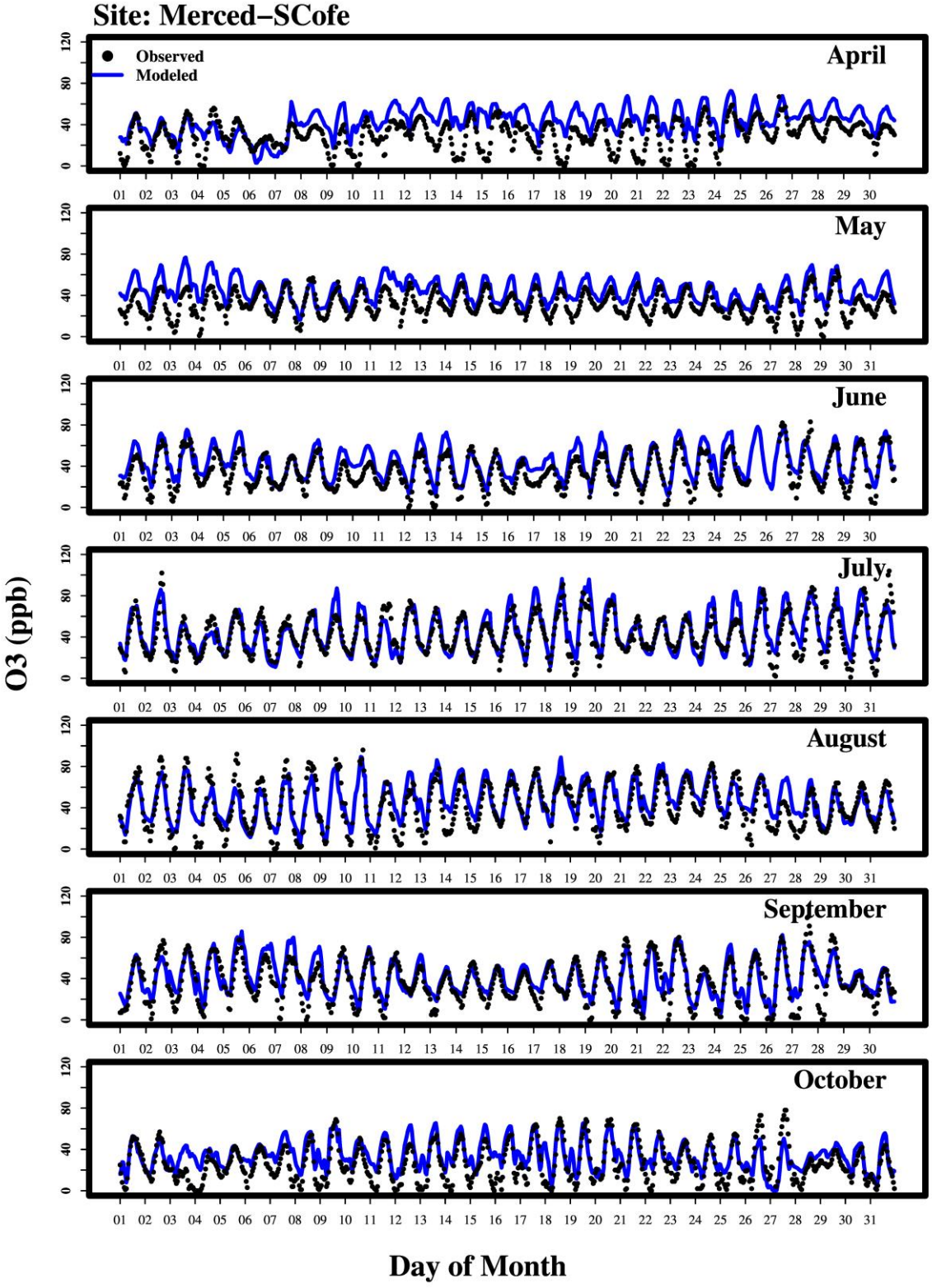

Figure S 32. Time-series of hourly ozone at the Tracy-Airport site for the ozone season (April-October 2018).

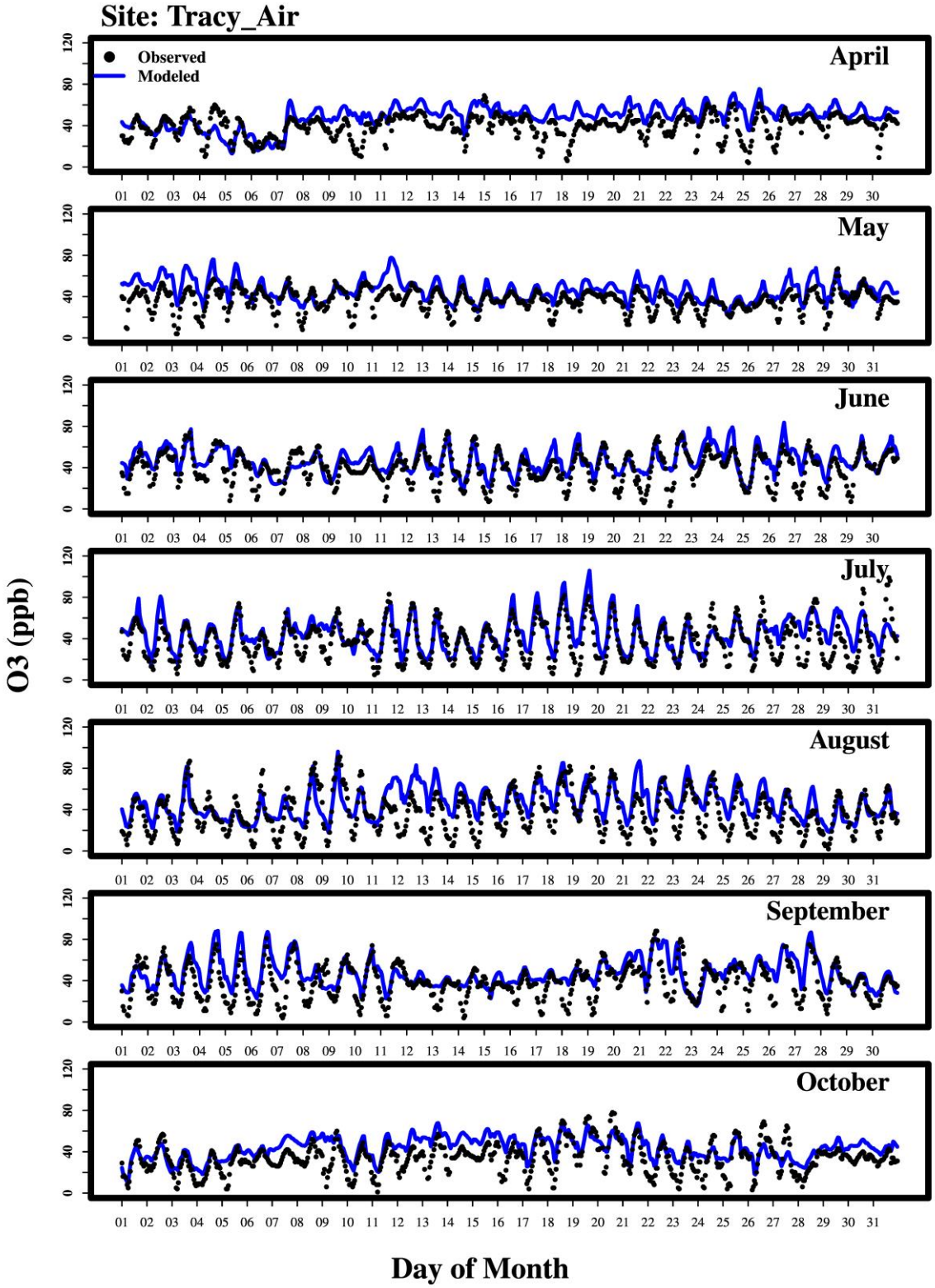

Figure S 33. Time-series of hourly ozone at the Stockton-Hazelton St. site for the ozone season (April-October 2018).

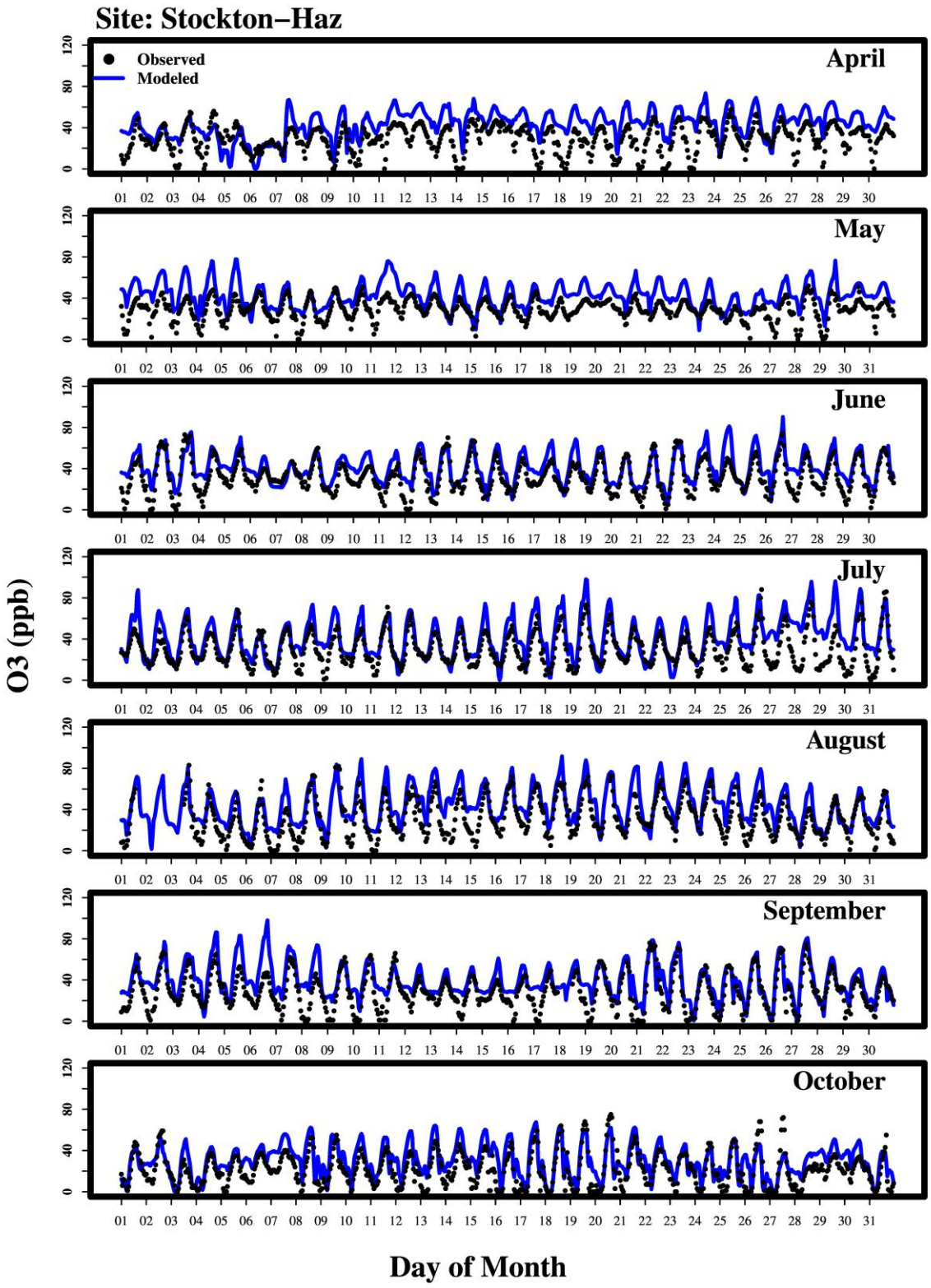

Figure S 34. Time-series of hourly ozone at the Fresno-Garland site for the ozone season (April-October 2018).

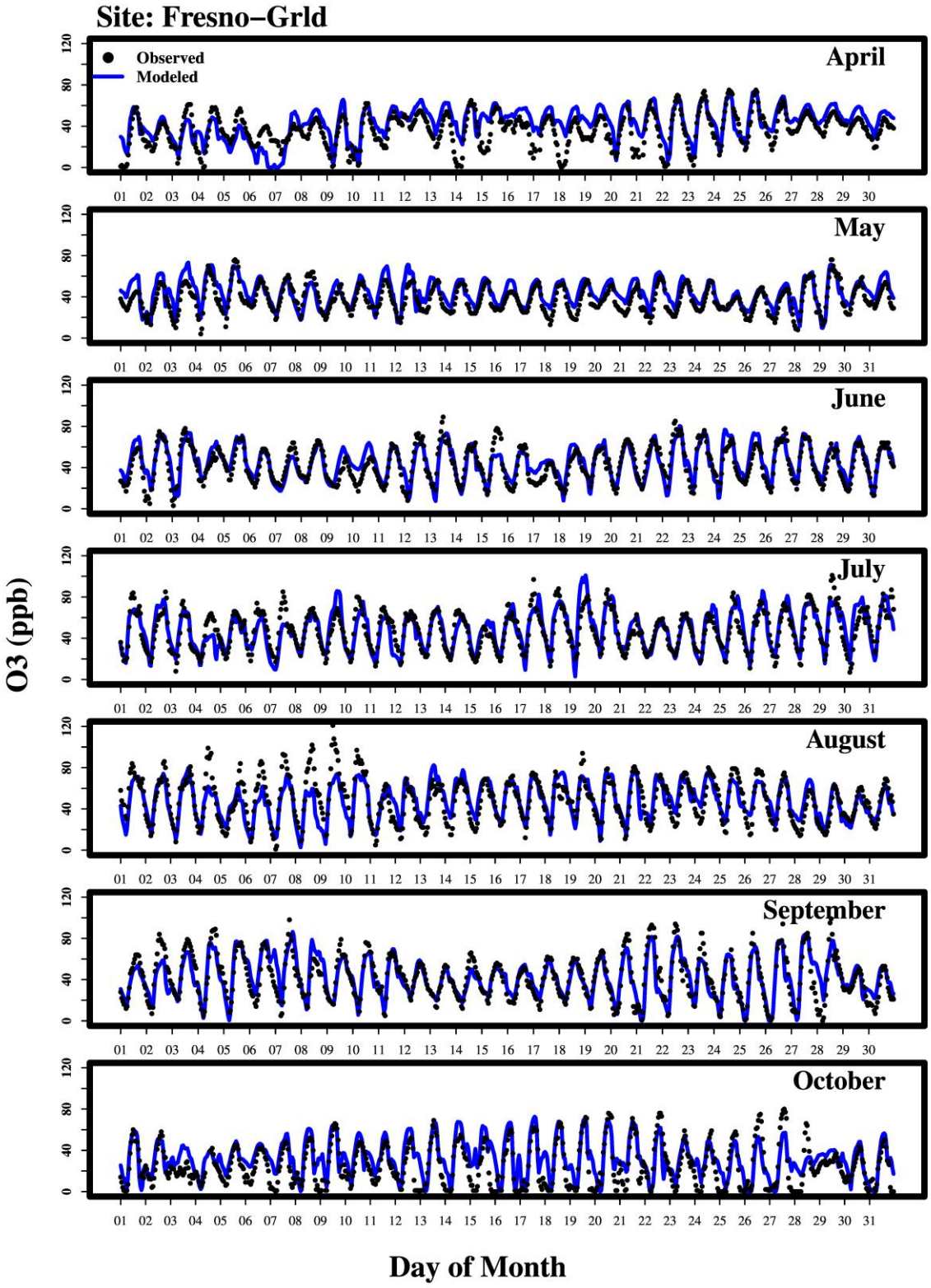

Figure S 35. Time-series of hourly ozone at the Clovis site for the ozone season (April-October 2018).

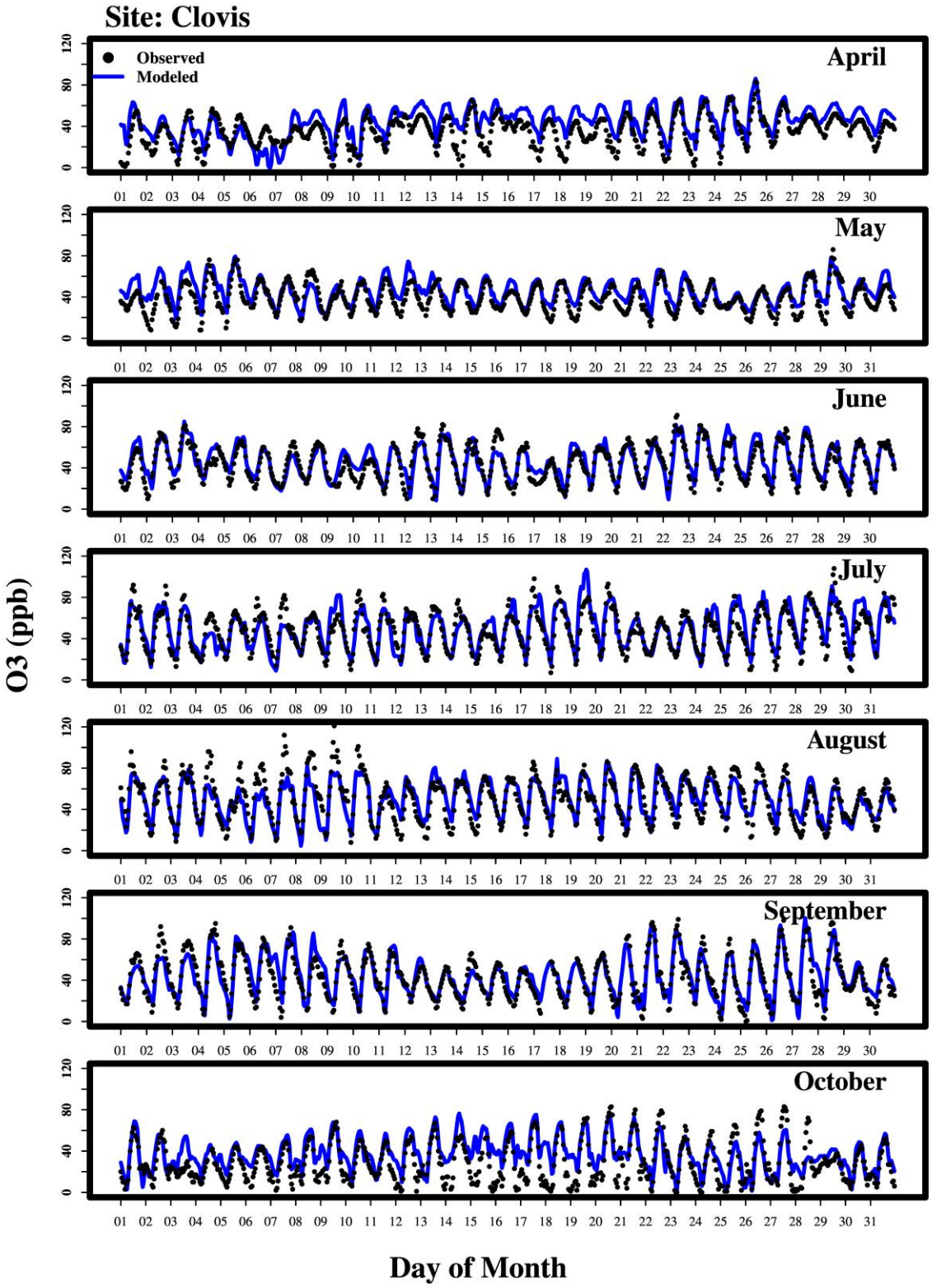

Figure S 36. Time-series of hourly ozone at the Parlier site for the ozone season (April-October 2018).

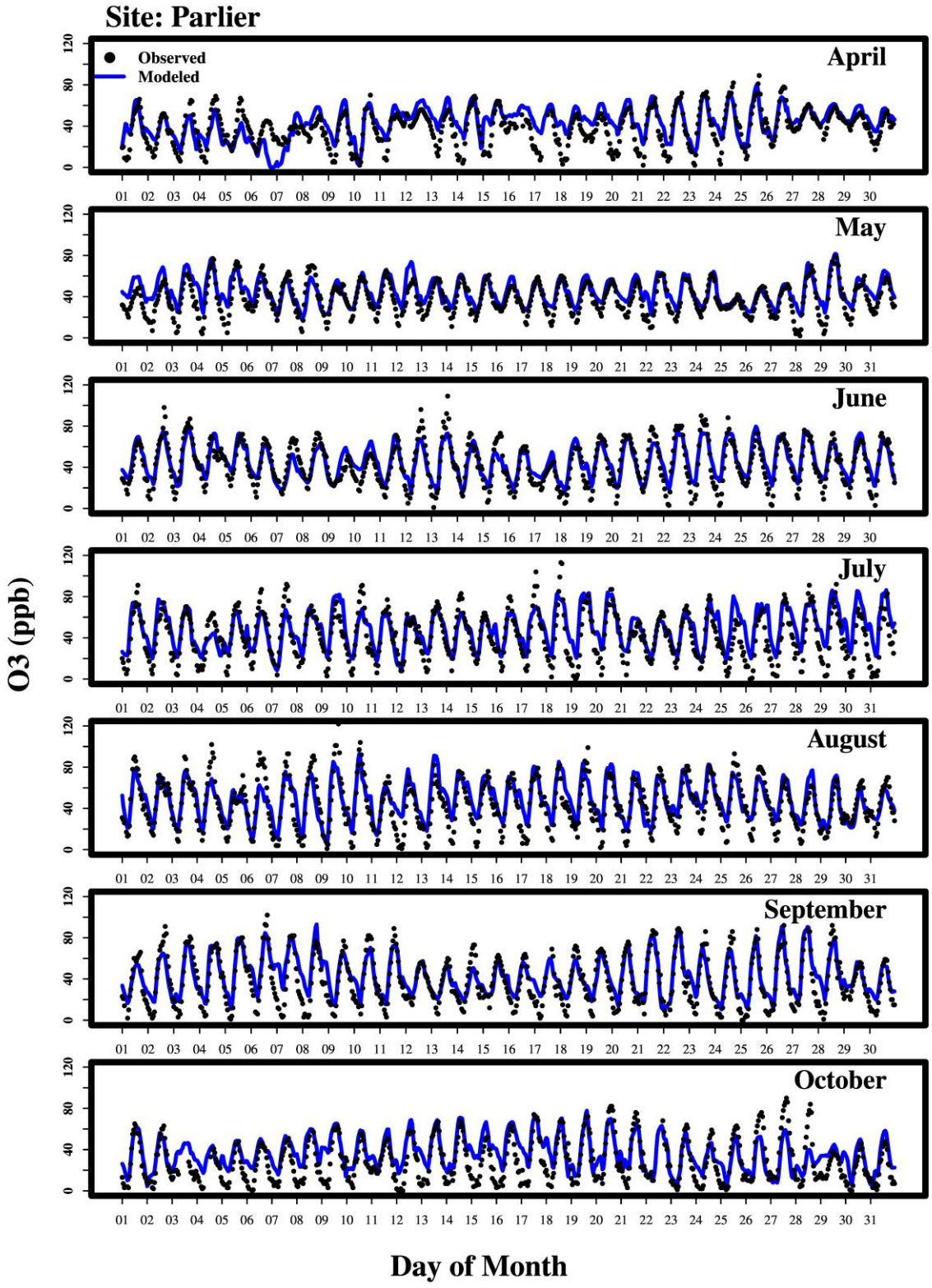

Figure S 37. Time-series of hourly ozone at the Fresno-Drummond St. site for the ozone season (April-October 2018).

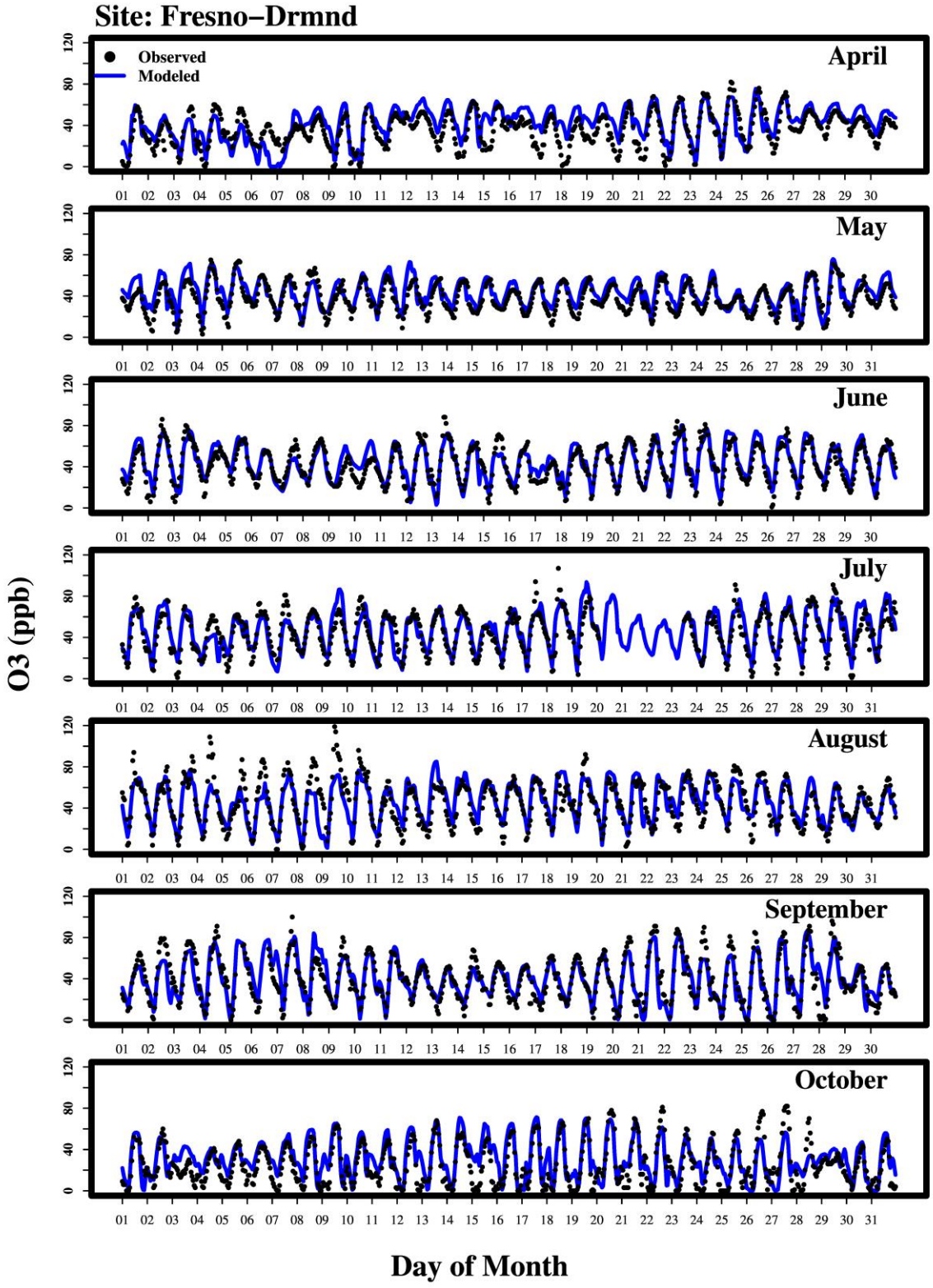

Figure S 38. Time-series of hourly ozone at the Fresno- Sierra Skypark #2 site for the ozone season (April-October 2018).

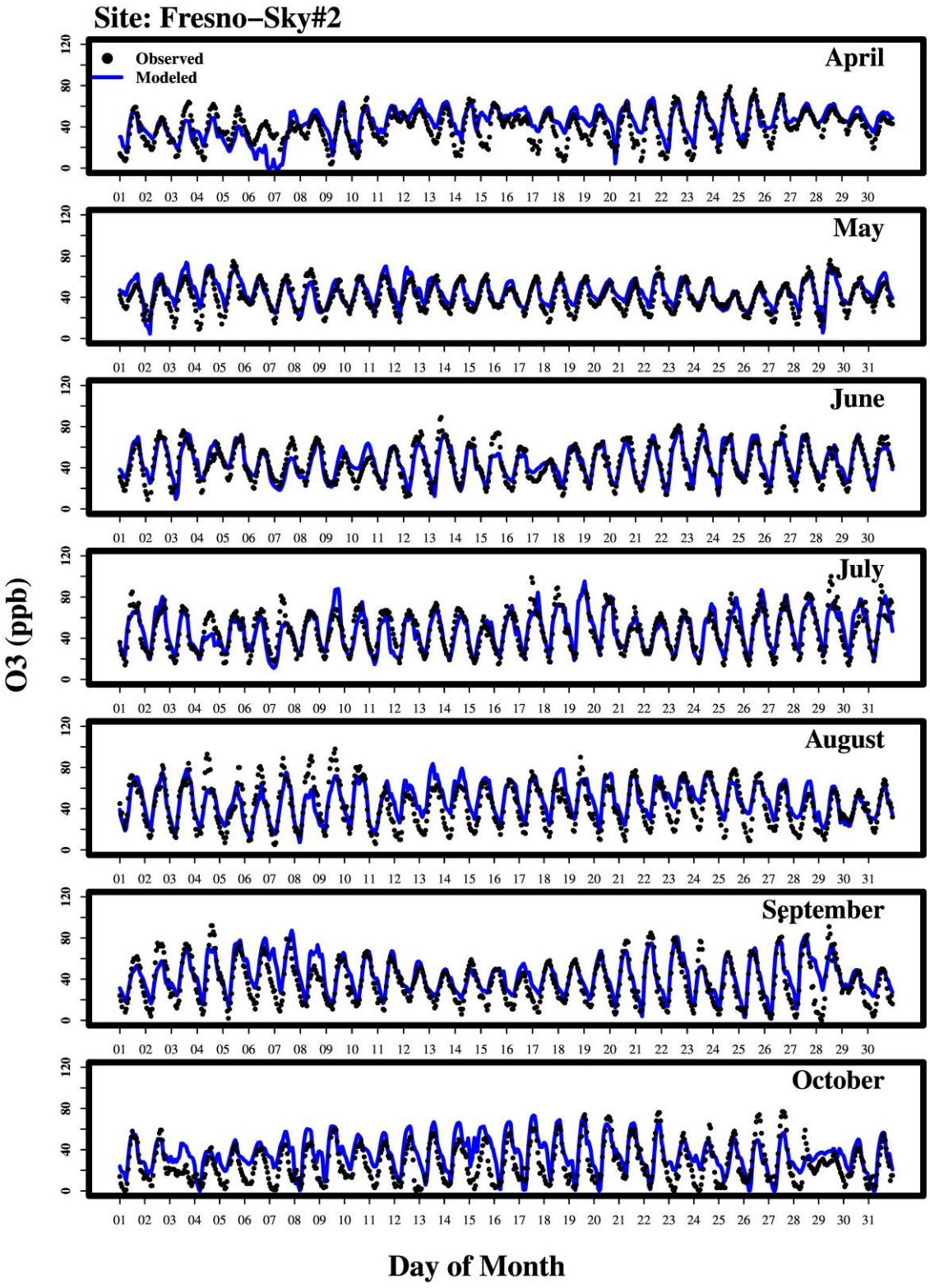

Figure S 39. Time-series of hourly ozone at the Hanford-S. Irwin St. site for the ozone season (April-October 2018).

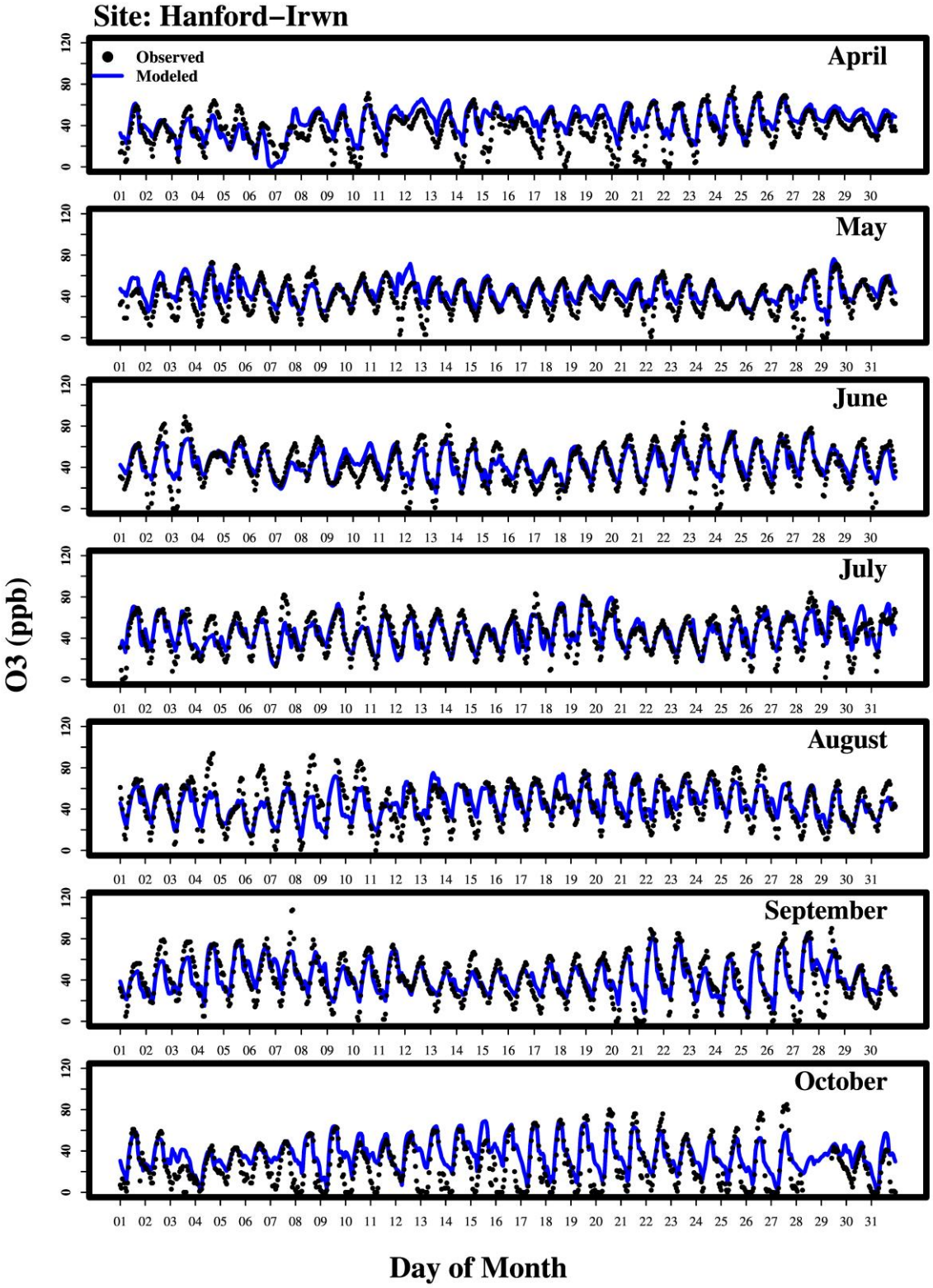

Figure S 40. Time-series of hourly ozone at the Madera-28261 Avenue 14 site for the ozone season (April-October 2018).

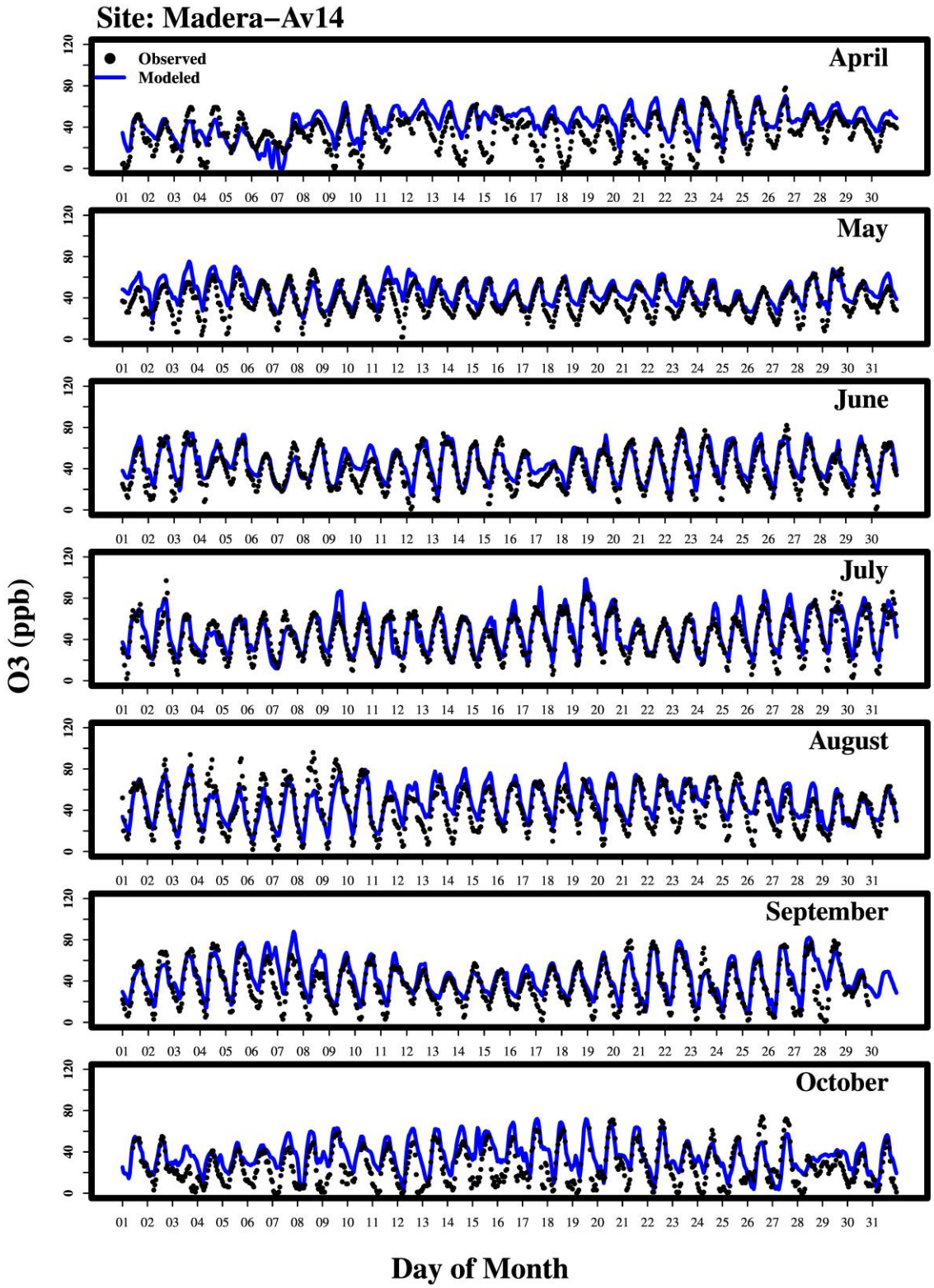

Figure S 41. Time-series of hourly ozone at the Madera-Pump Yard site for the ozone season (April-October 2018).

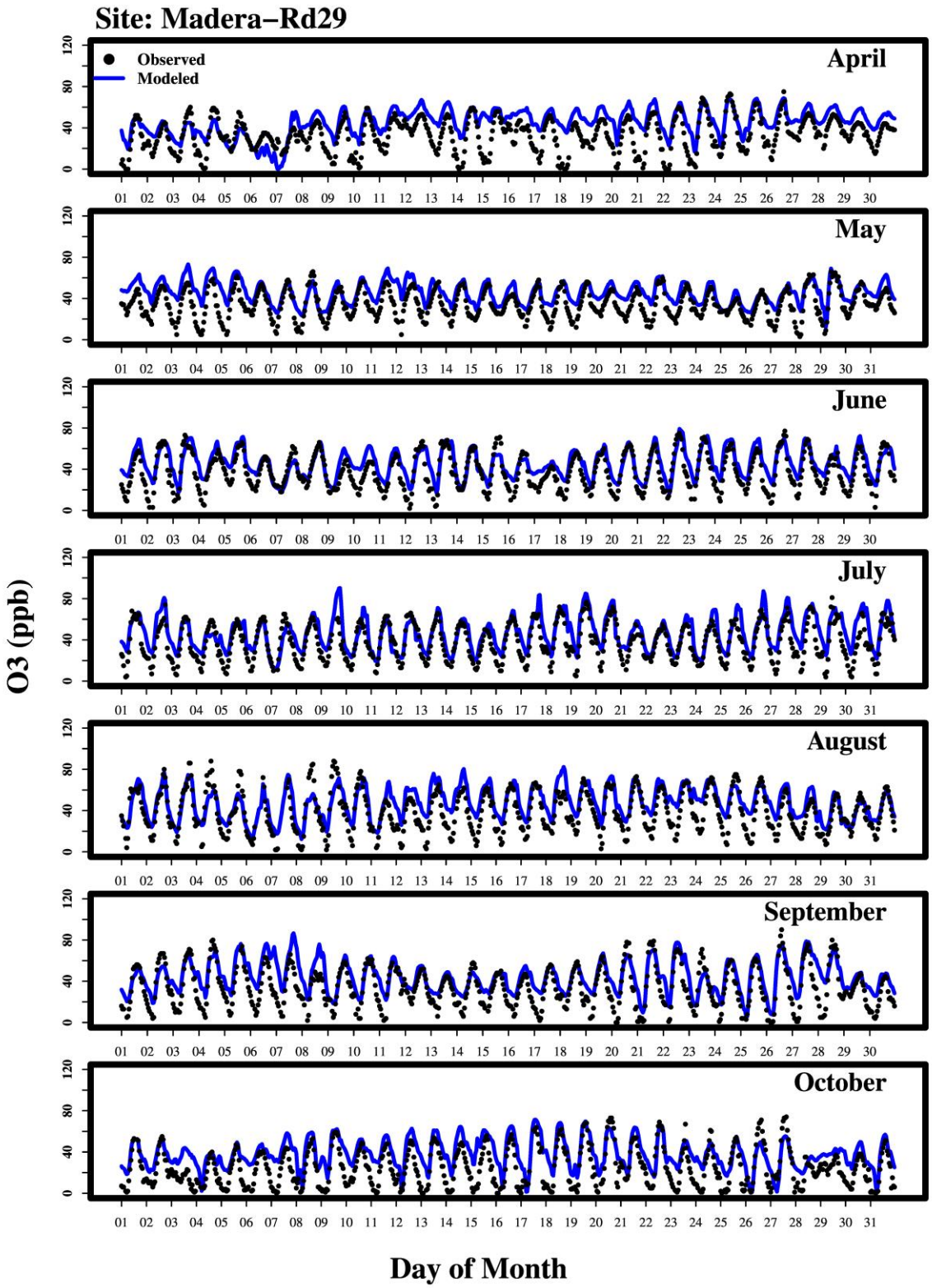

Figure S 42. Time-series of hourly ozone at the Tranquility site for the ozone season (April-October 2018).

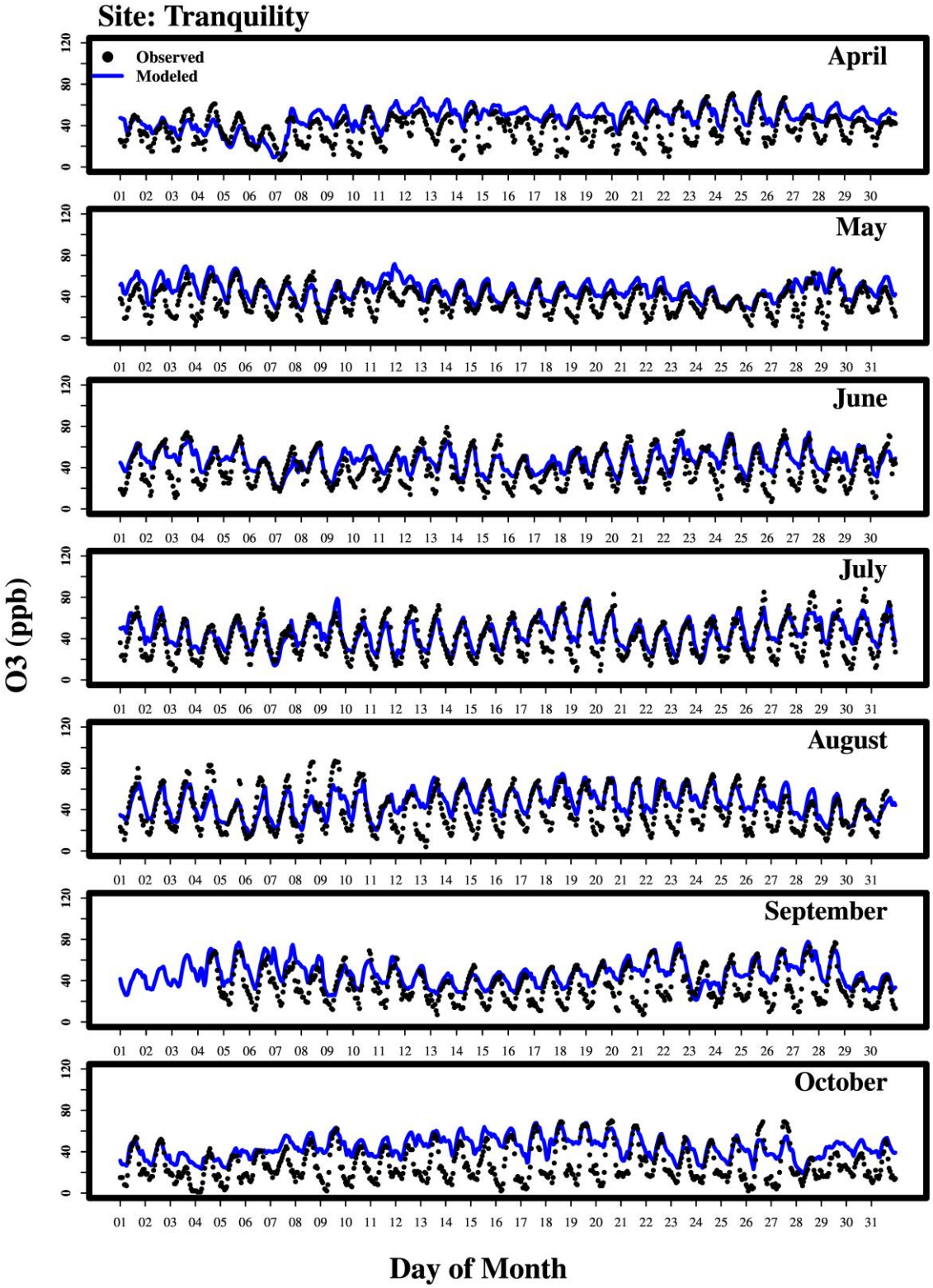

Figure S 43. Time-series of hourly ozone at the Edison site for the ozone season (April-October 2018).

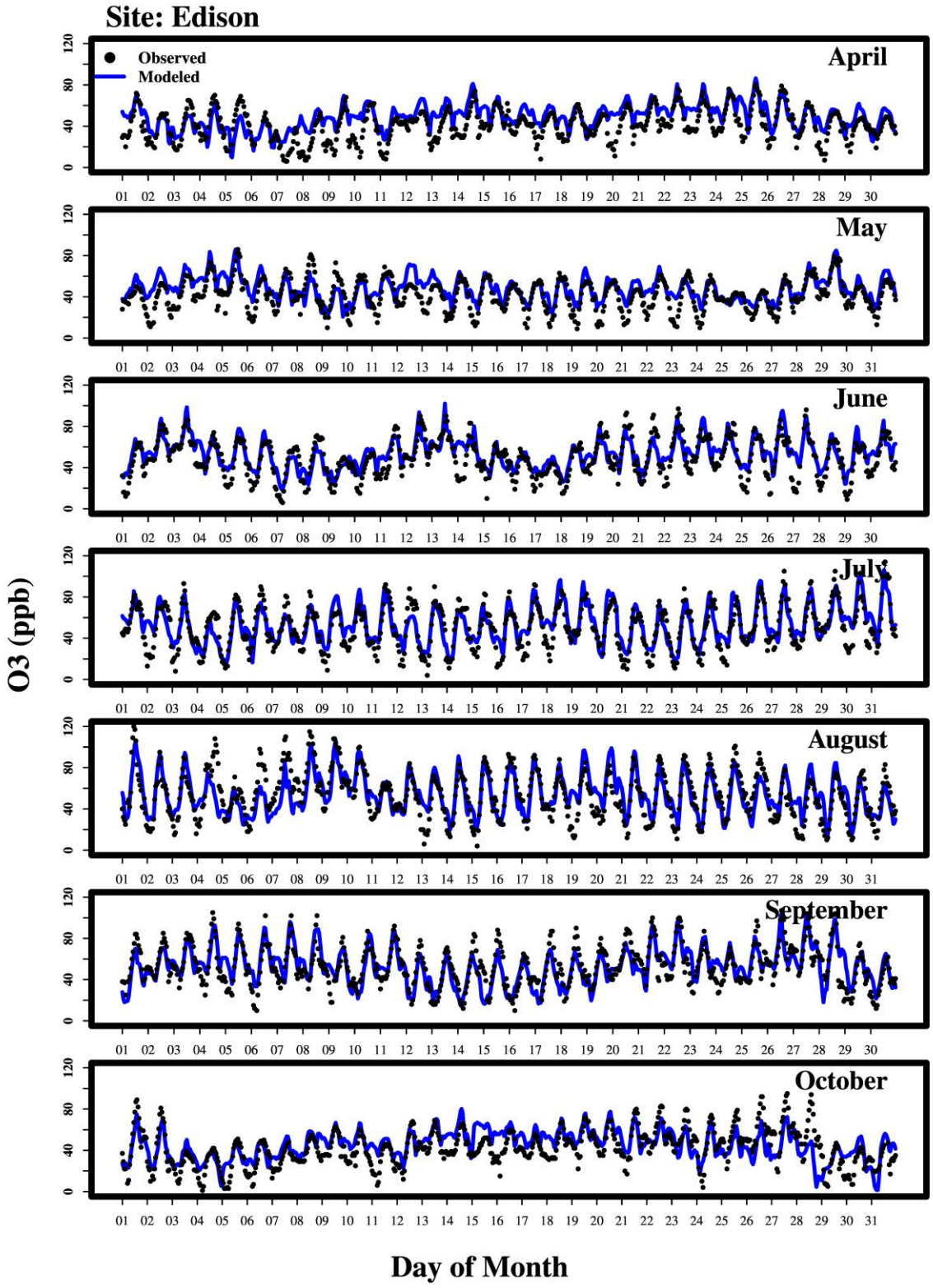

Figure S 44. Time-series of hourly ozone at the Arvin-Di Giorgio site for the ozone season (April-October 2018).

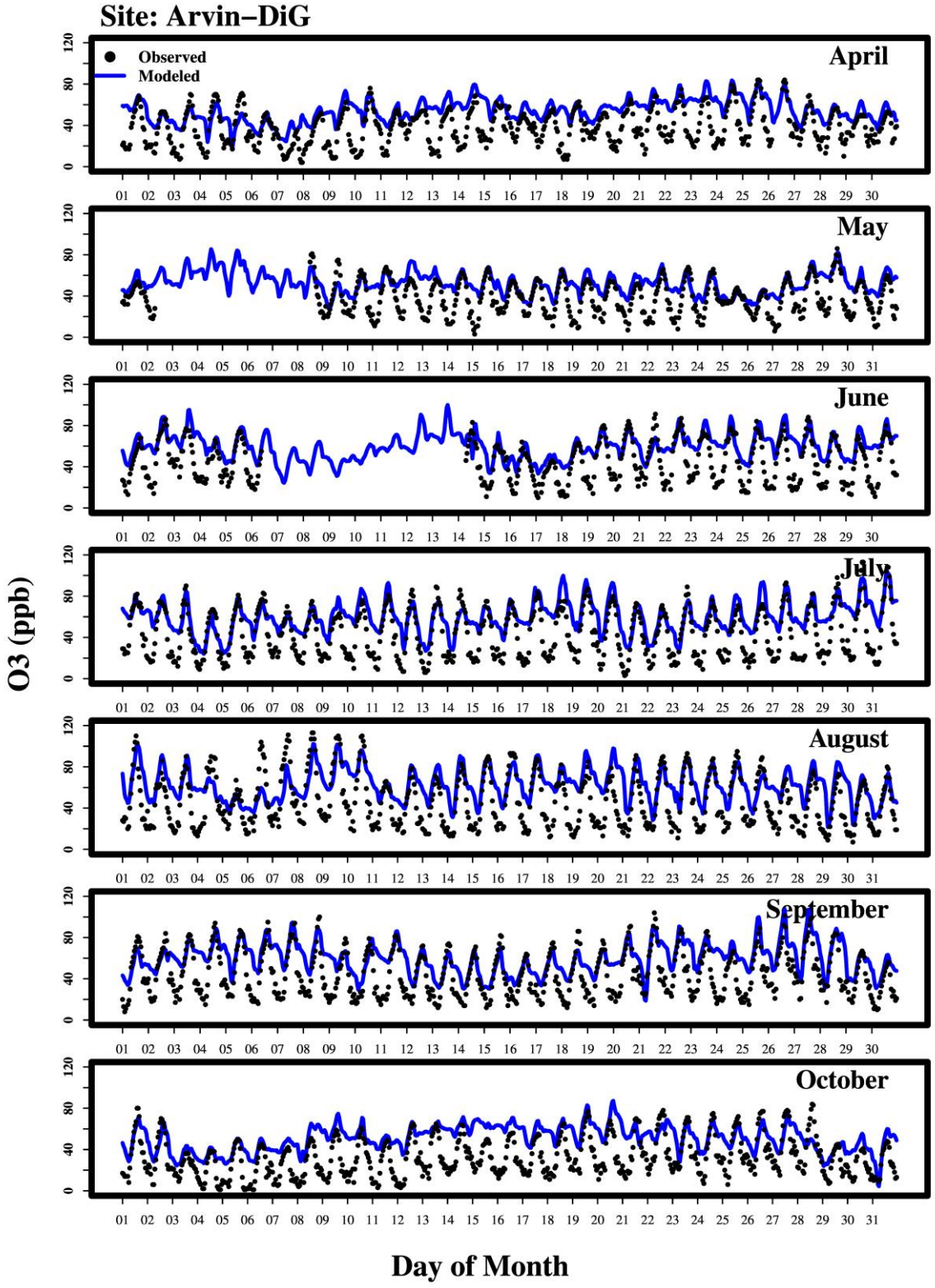

Figure S 45. Time-series of hourly ozone at the Bakersfield-5558 California Avenue site for the ozone season (April-October 2018).

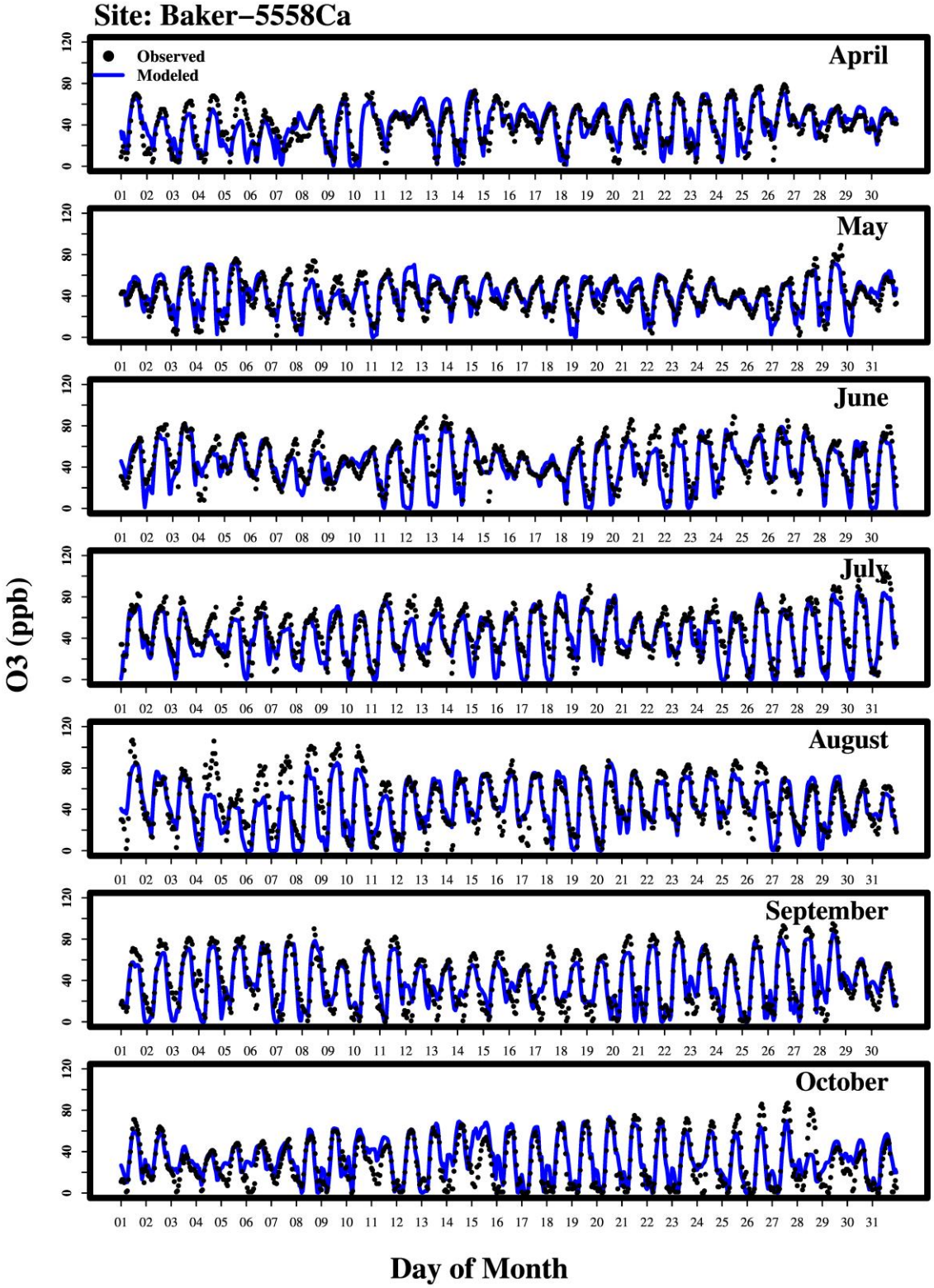

Figure S 46. Time-series of hourly ozone at the Sequoia and Kings Canyon Natl Park site for the ozone season (April-October 2018).

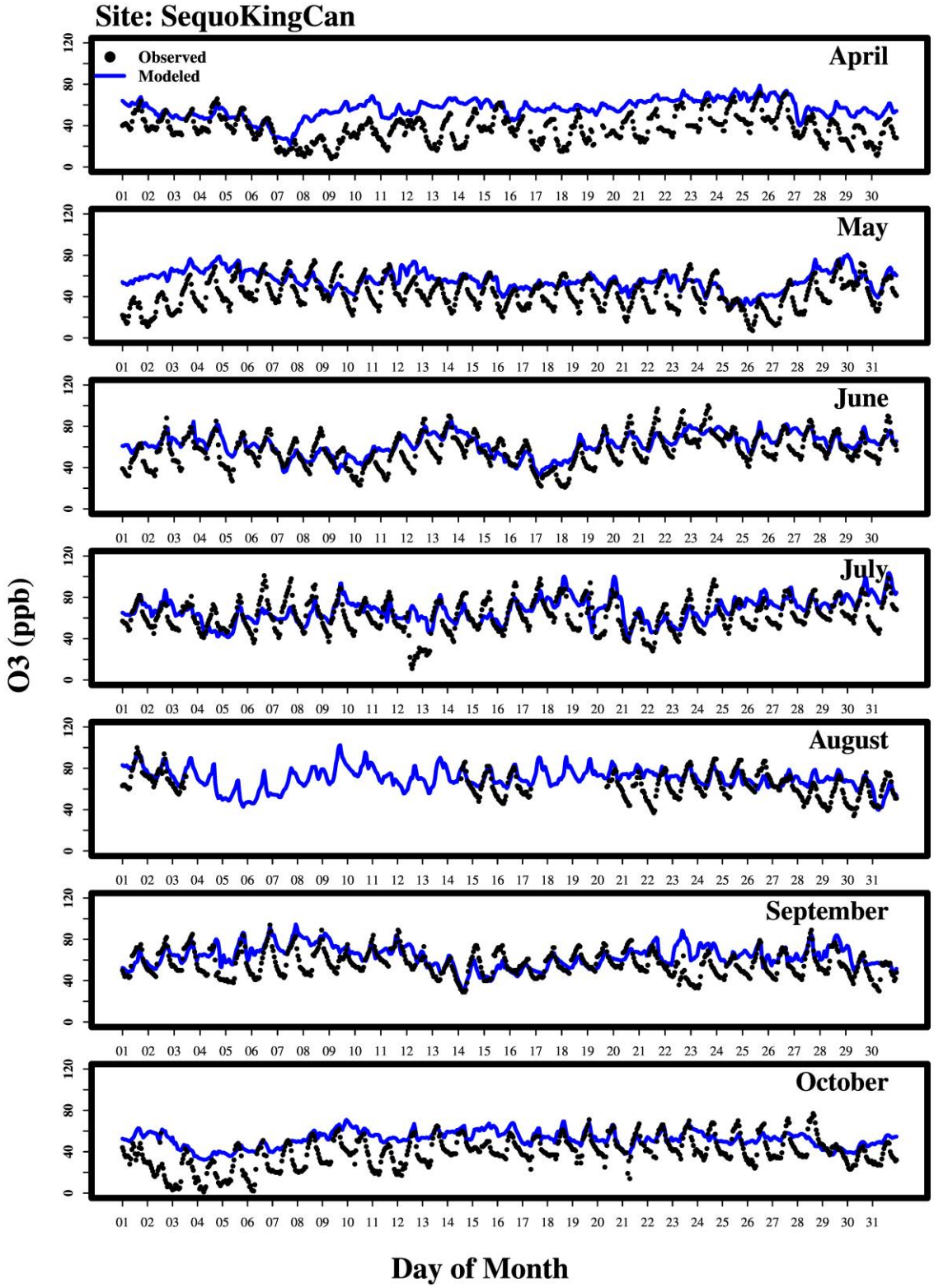

Figure S 47. Time-series of hourly ozone at the Bakersfield-Municipal Airport site for the ozone season (April-October 2018).

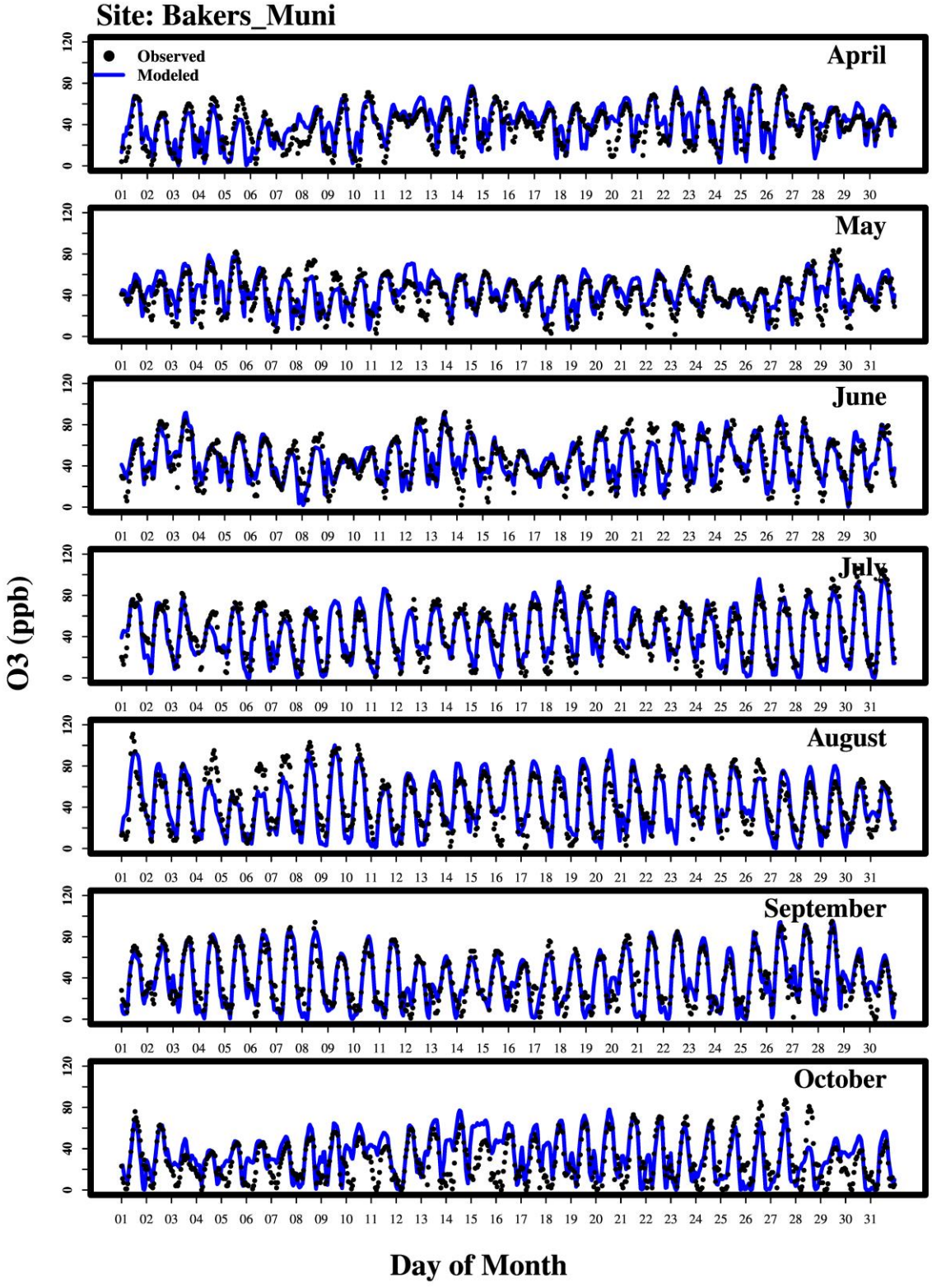

Figure S 48. Time-series of hourly ozone at the Visalia-N Church Street site for the ozone season (April-October 2018).

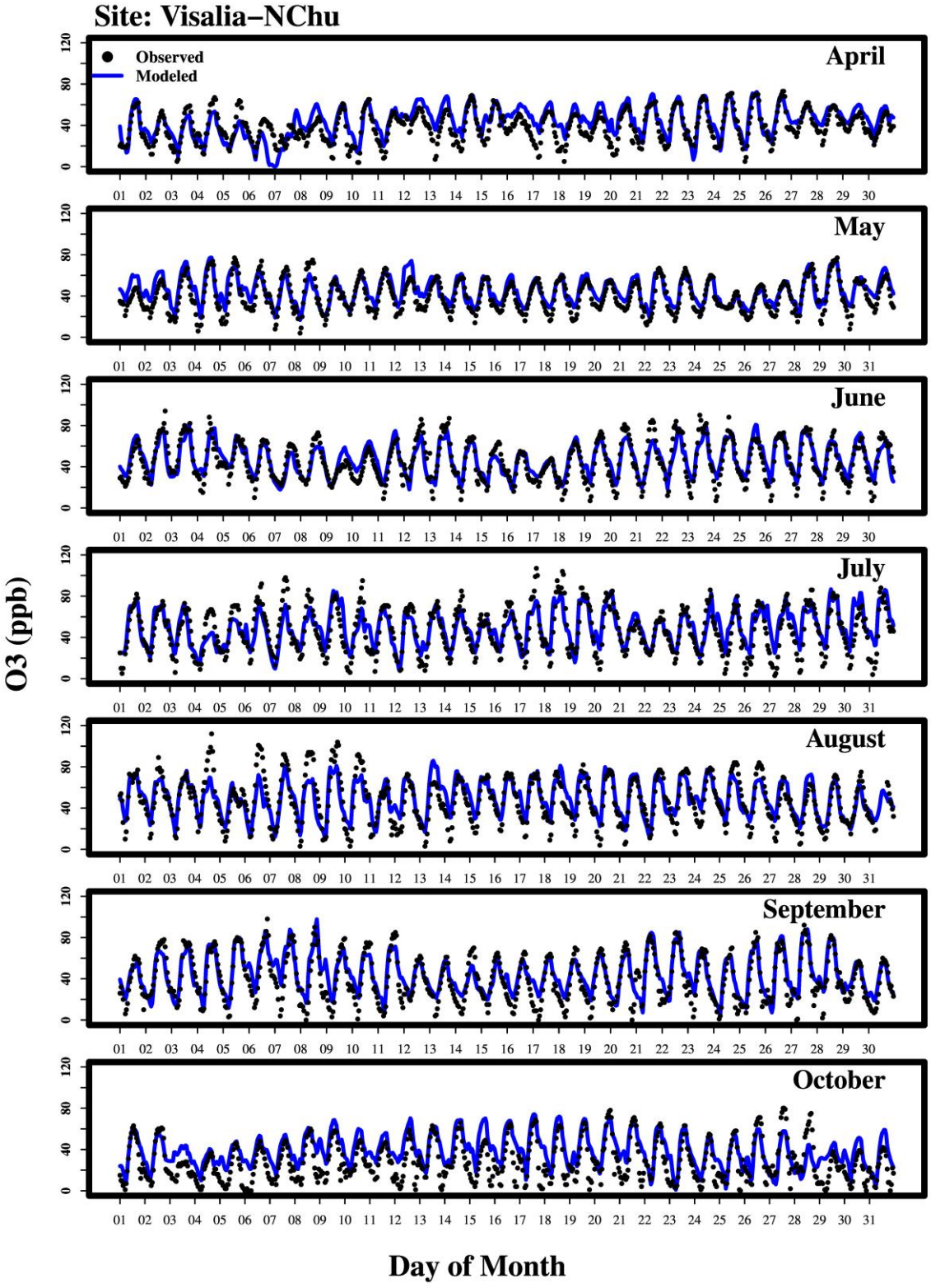

Figure S 49. Time-series of hourly ozone at the Maricopa-Stanislaus Street site for the ozone season (April-October 2018).

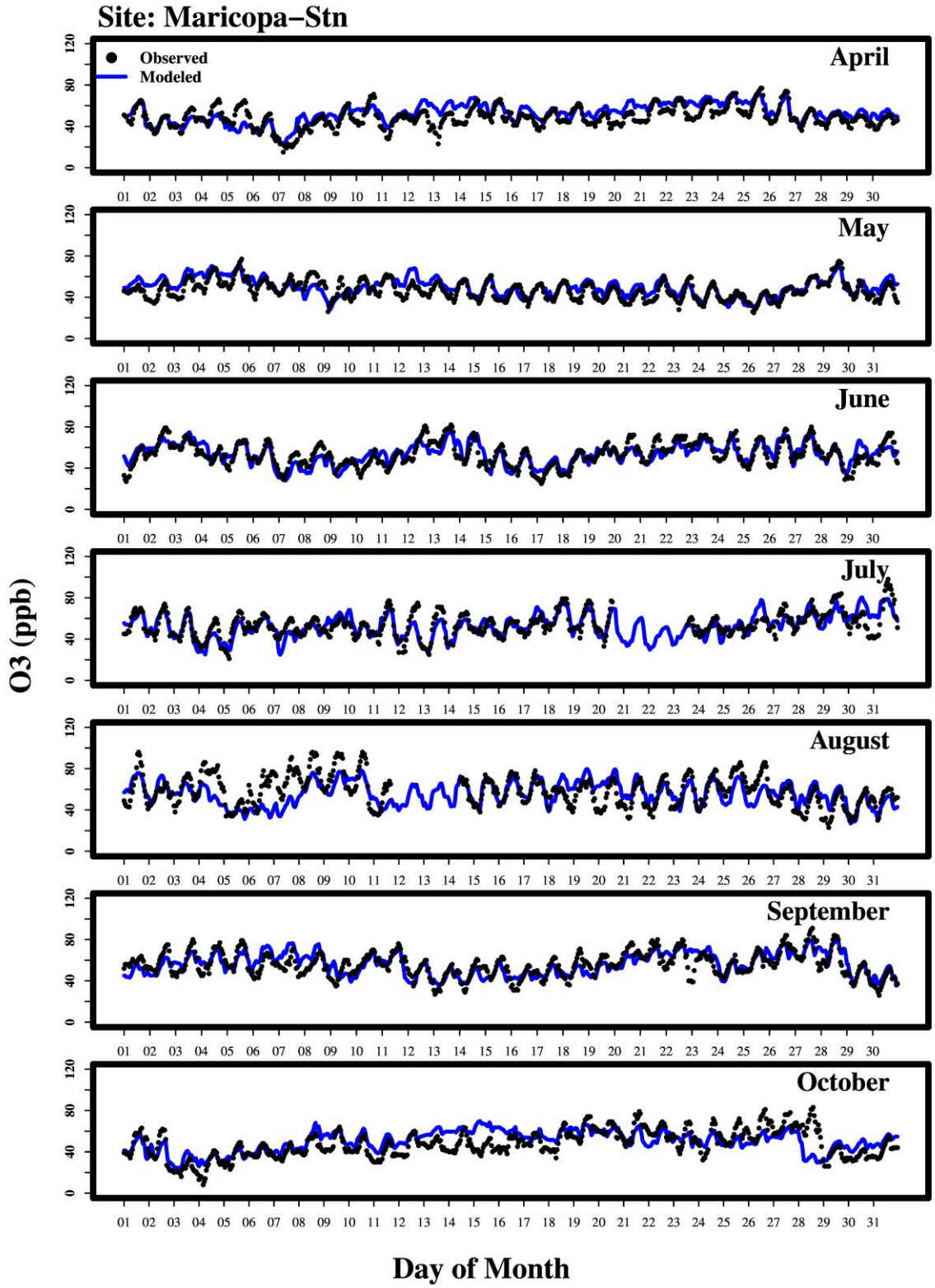

Figure S 50. Time-series of hourly ozone at the Sequoia Natl Park-Lower Kaweah site for the ozone season (April-October 2018).

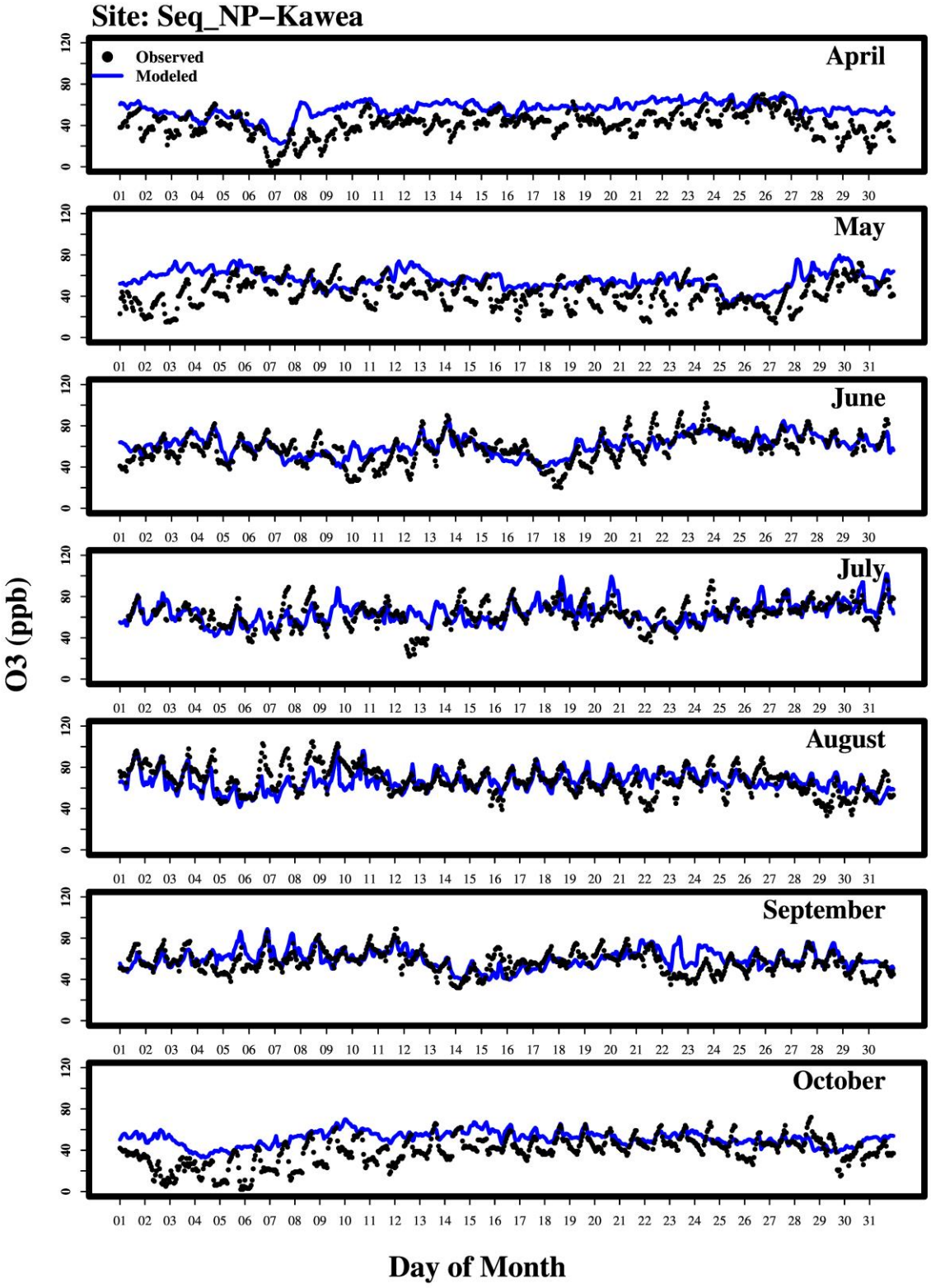

Figure S 51. Time-series of hourly ozone at the Oildale-3311 Manor Street site for the ozone season (April-October 2018).

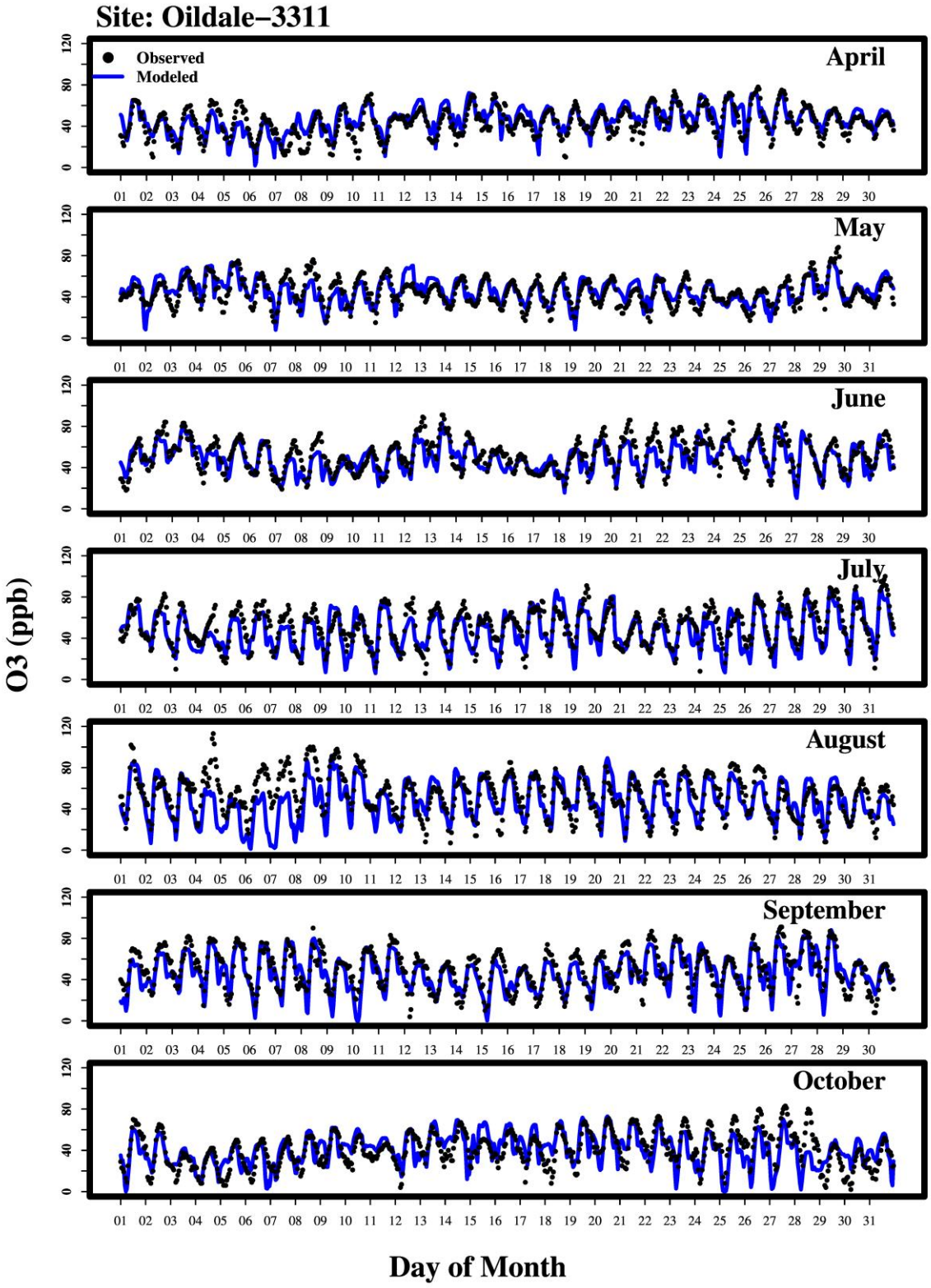

Figure S 52. Time-series of hourly ozone at the Shafter-Walker Street site for the ozone season (April-October 2018).

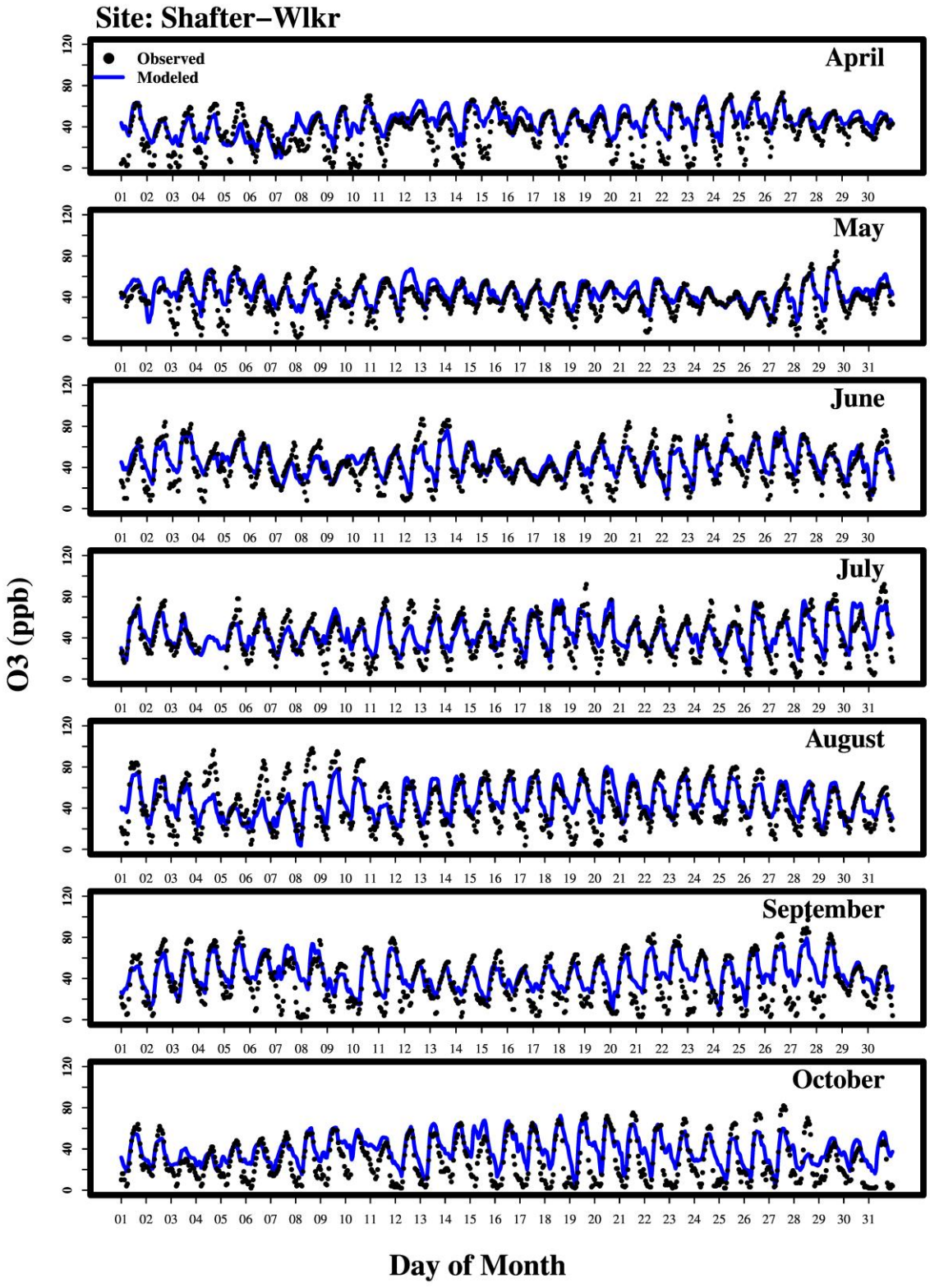

Figure S 53. Time-series of hourly ozone at the Porterville-1839 Newcomb Street site for the ozone season (April-October 2018).

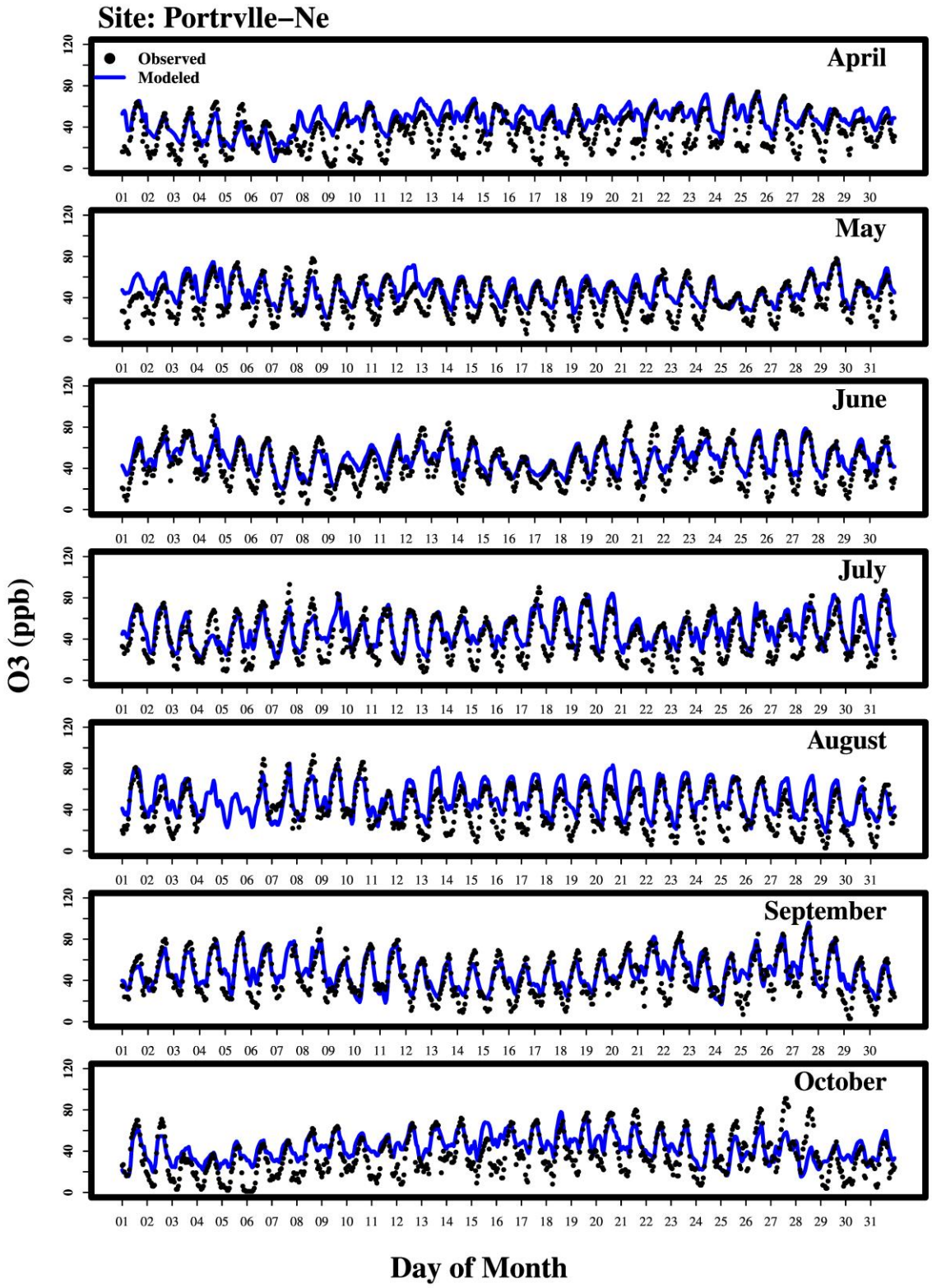

Figure S 54. Time-series of maximum daily average 1-hour ozone at the Turlock-S Minaret St. site for the ozone season (April-October 2018).

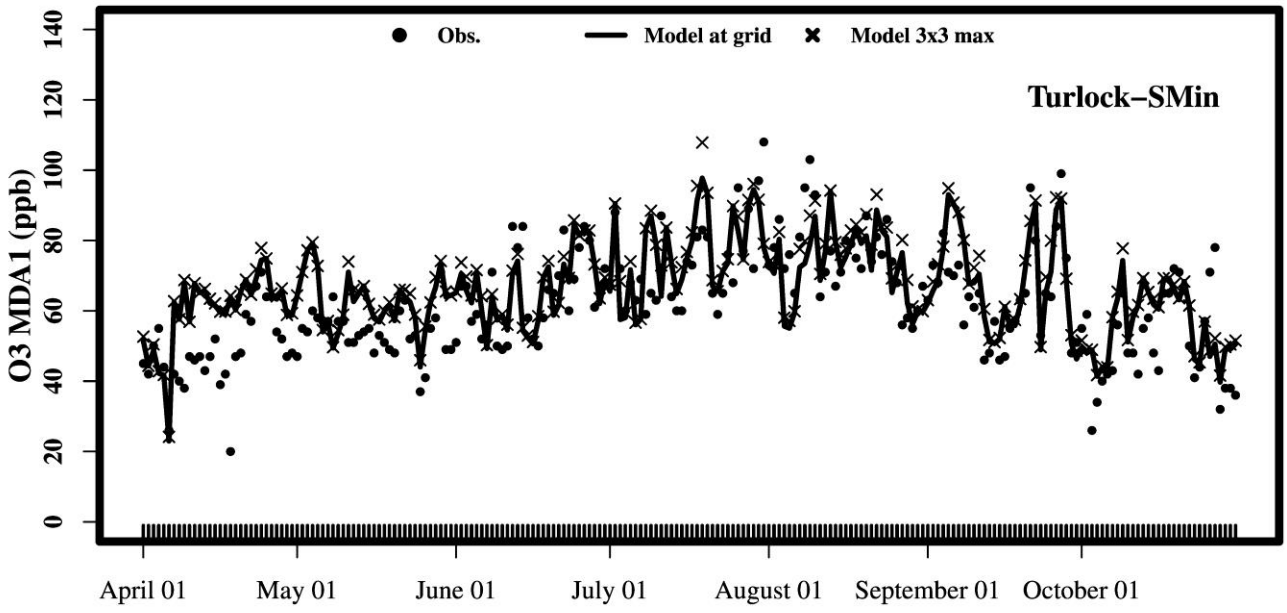

Figure S 55. Time-series of maximum daily average 1-hour ozone at the Modesto-14th St. site for the ozone season (April-October 2018).

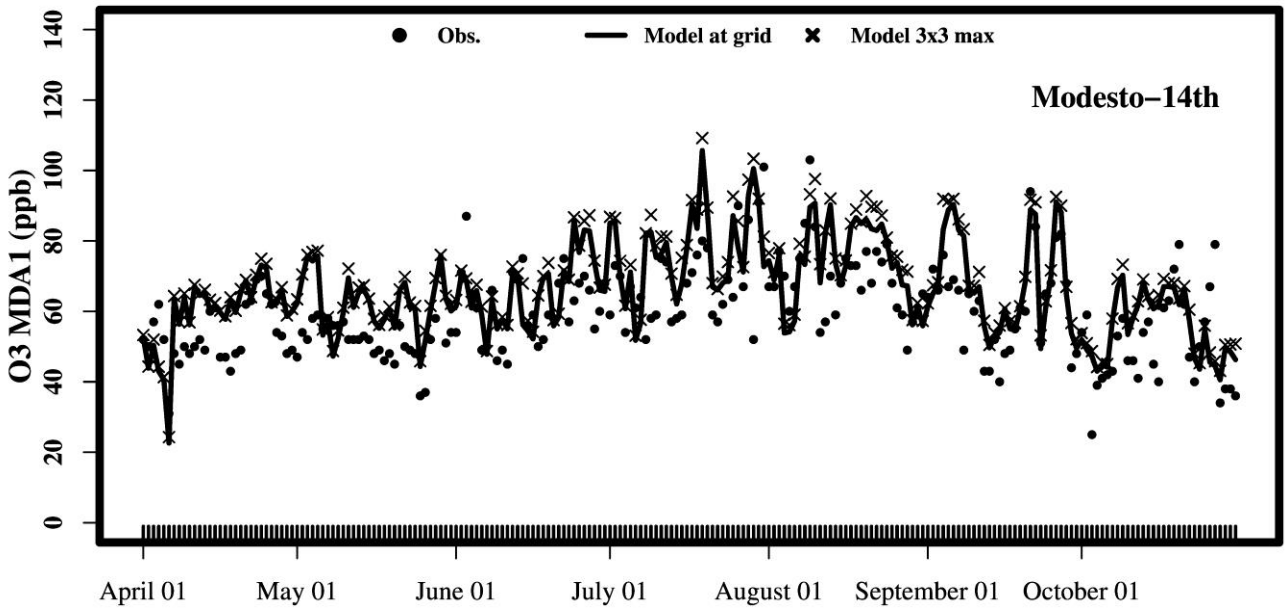

Figure S 56. Time-series of maximum daily average 1-hour ozone at the Merced-S Coffee Av. site for the ozone season (April-October 2018).

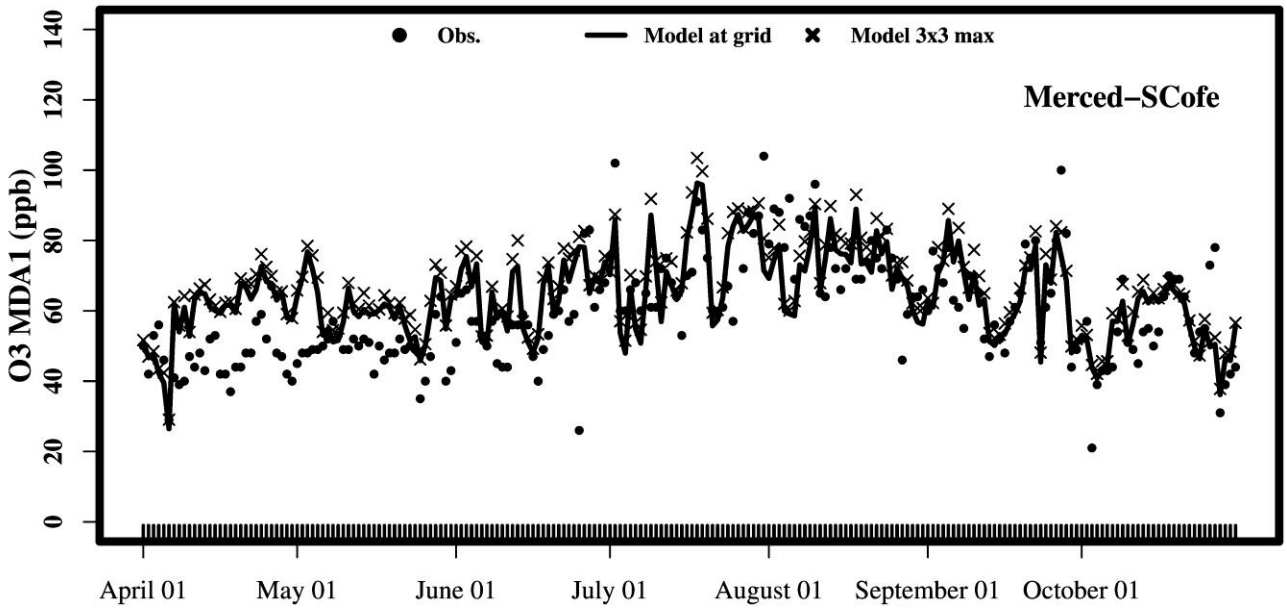

Figure S 57. Time-series of maximum daily average 1-hour ozone at the Tracy-Airport site for the ozone season (April-October 2018).

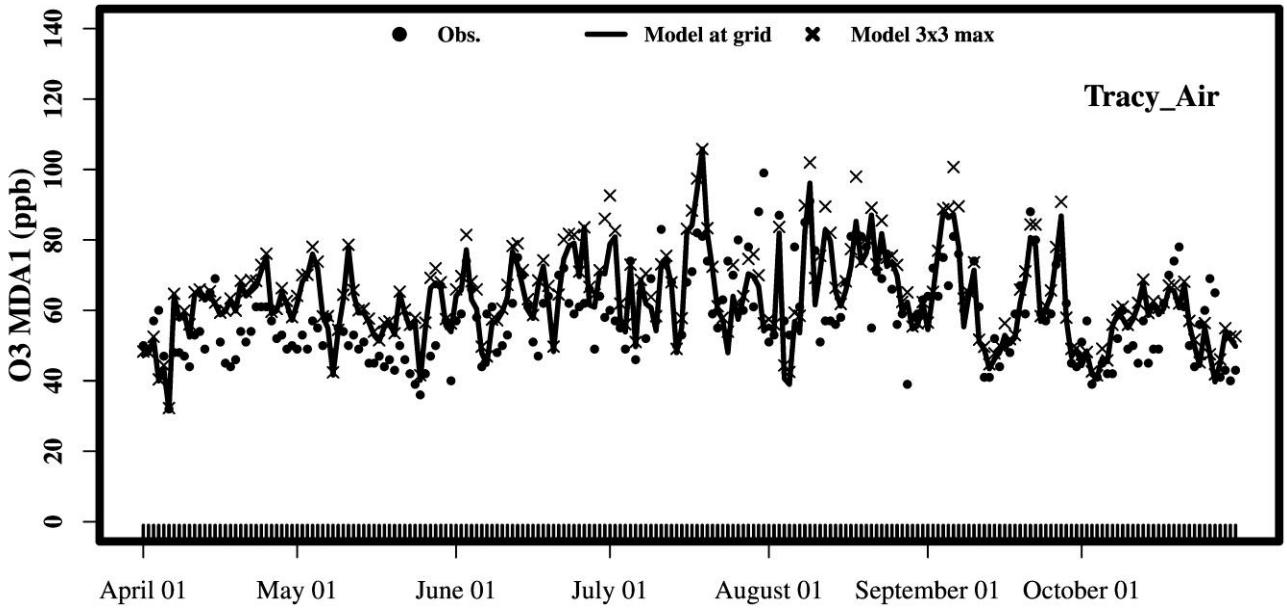

Figure S 58. Time-series of maximum daily average 1-hour ozone at the Stockton-Hazelton St. site for the ozone season (April-October 2018).

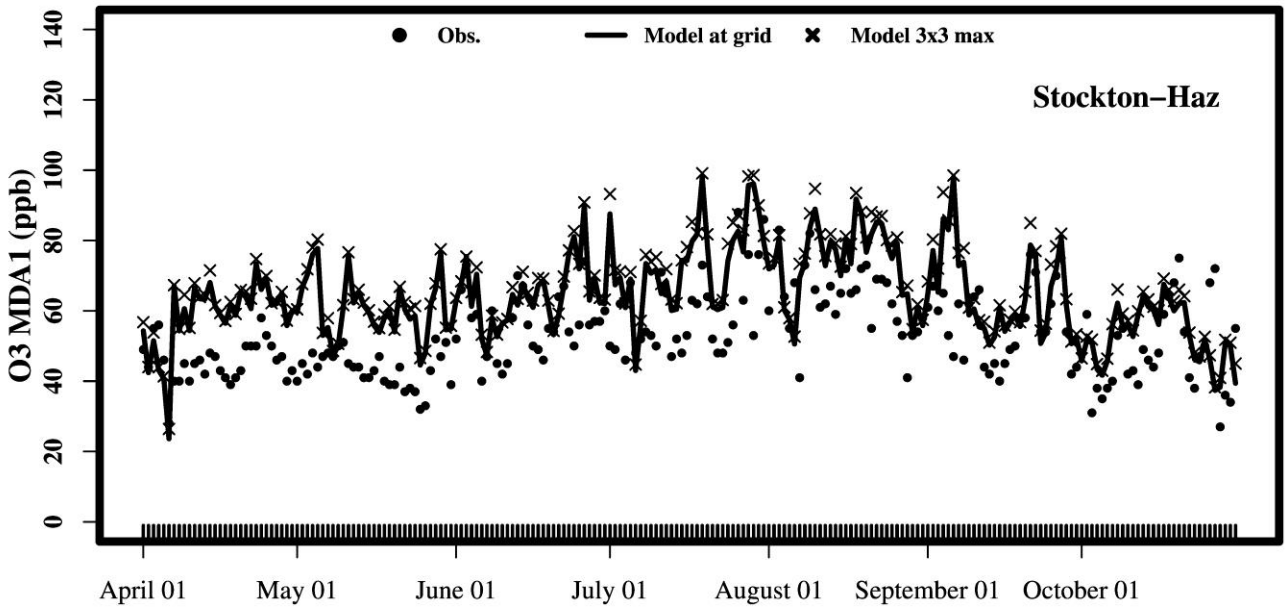

Figure S 59. Time-series of maximum daily average 1-hour ozone at the Fresno-Garland site for the ozone season (April-October 2018).

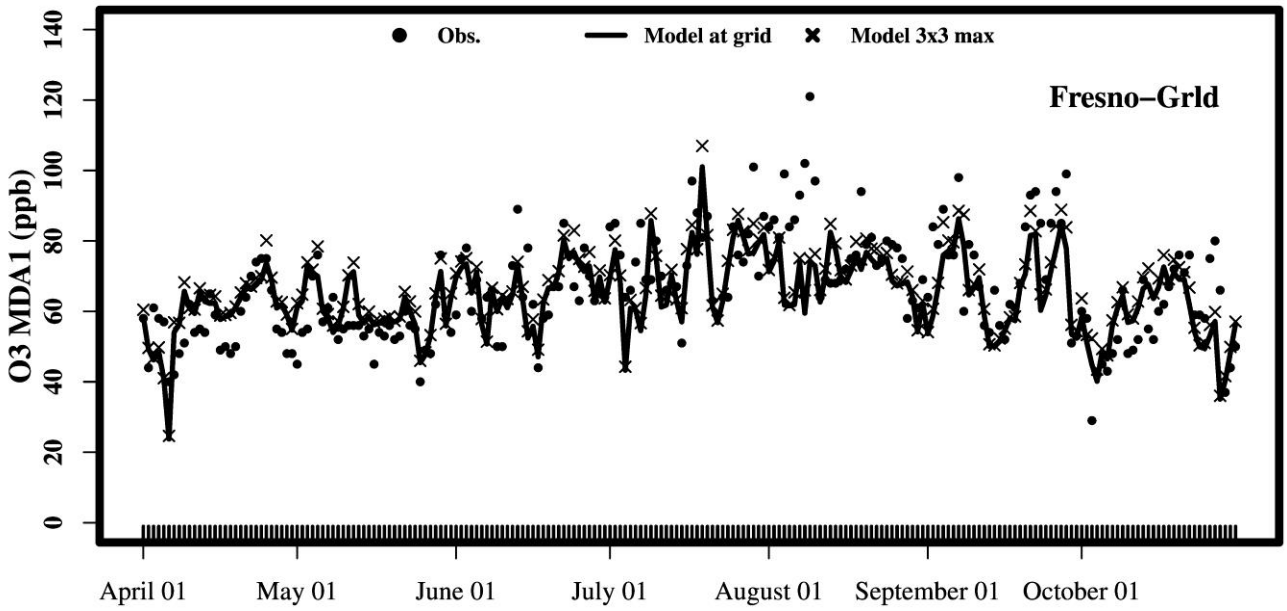

Figure S 60. Time-series of maximum daily average 1-hour ozone at the Clovis site for the ozone season (April-October 2018).

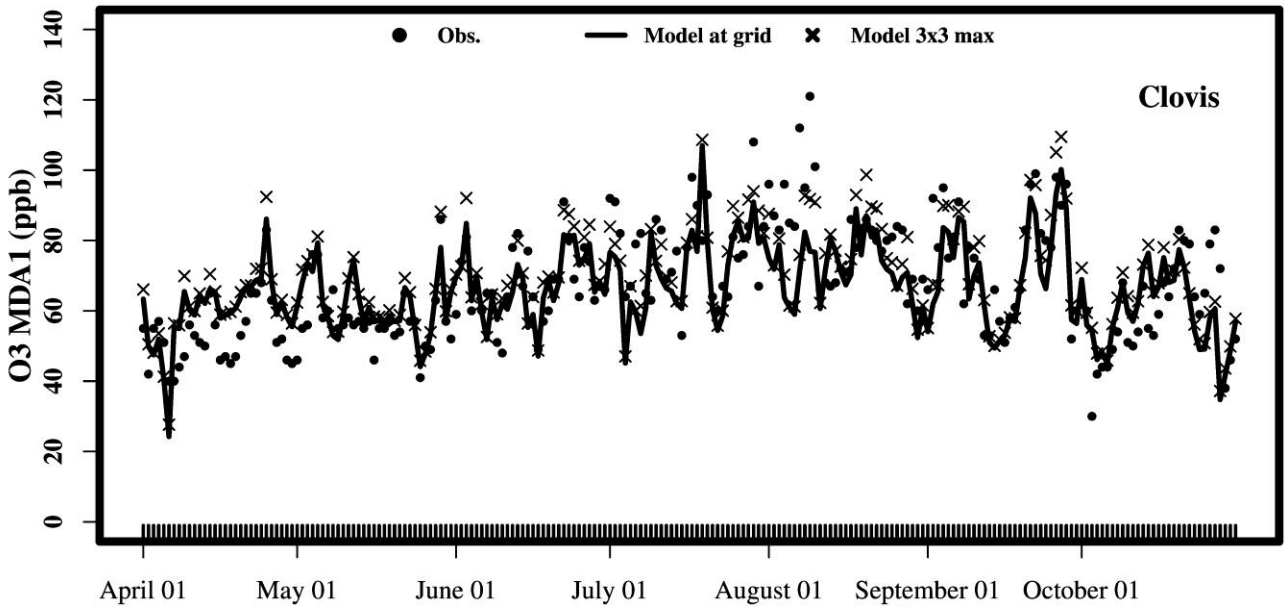

Figure S 61. Time-series of maximum daily average 1-hour ozone at the Parlier site for the ozone season (April-October 2018).

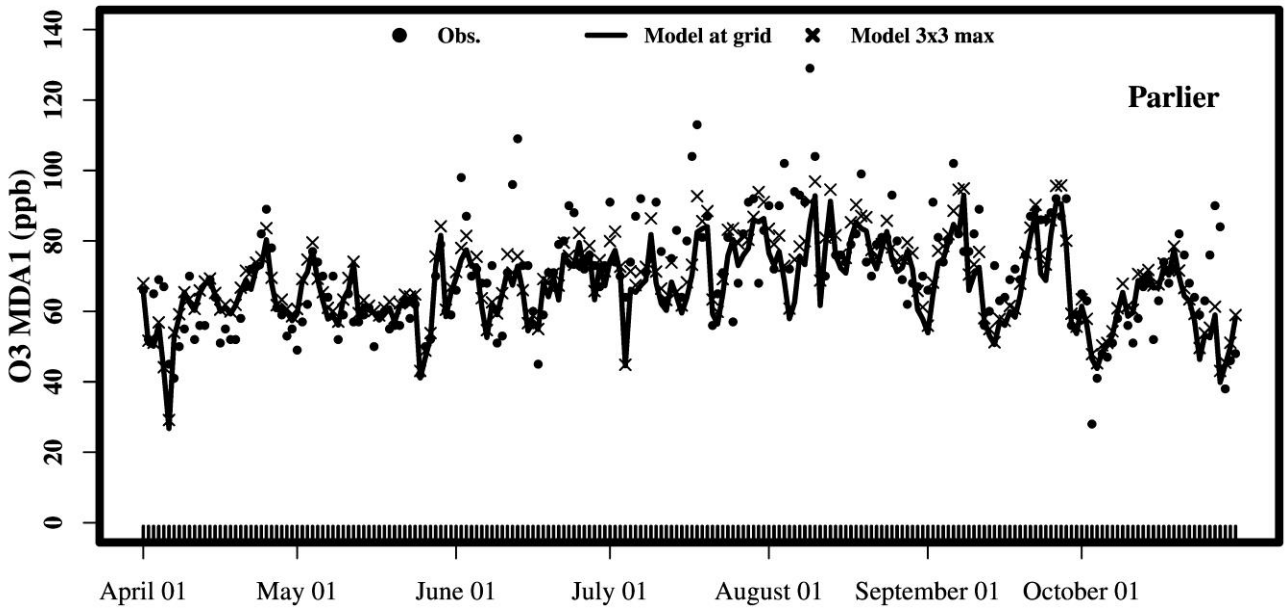

Figure S 62. Time-series of maximum daily average 1-hour ozone at the Fresno-Drummond St. site for the ozone season (April-October 2018).

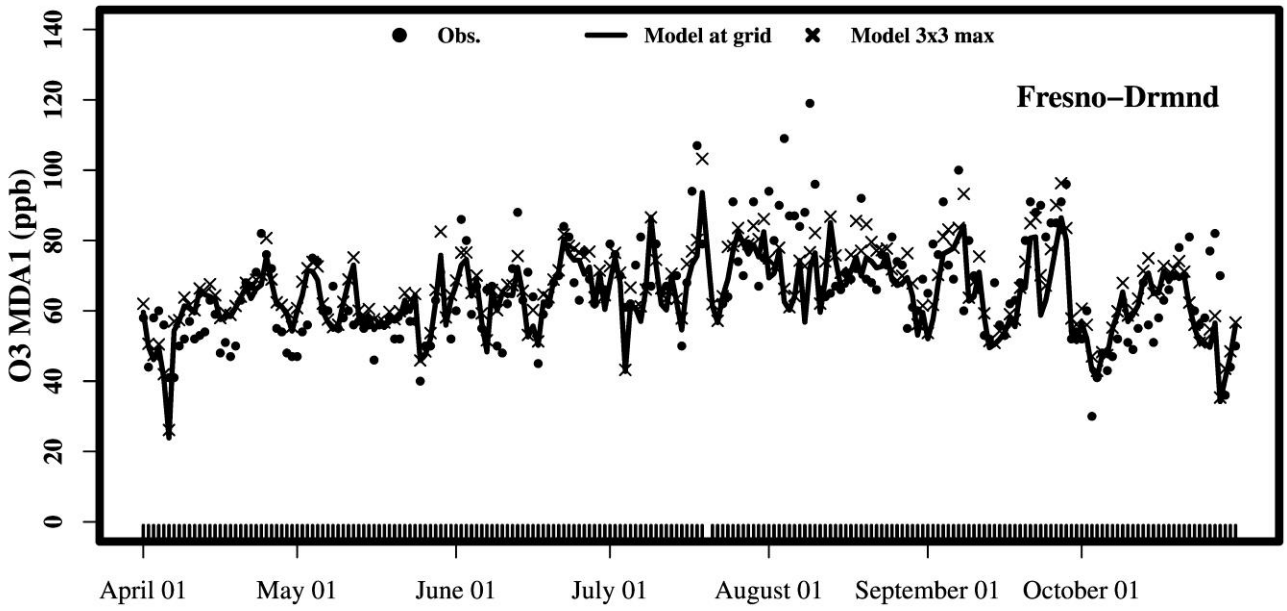

Figure S 63. Time-series of maximum daily average 1-hour ozone at the Fresno- Sierra Skypark #2 site for the ozone season (April-October 2018).

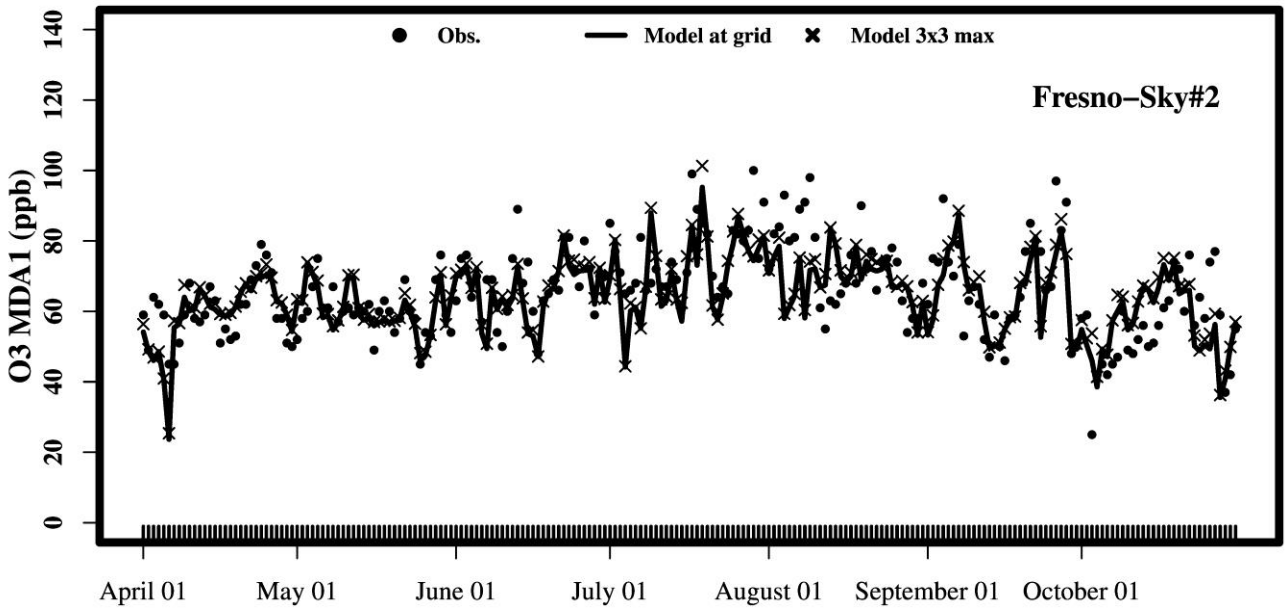

Figure S 64. Time-series of maximum daily average 1-hour ozone at the Hanford-S. Irwin St. site for the ozone season (April-October 2018).

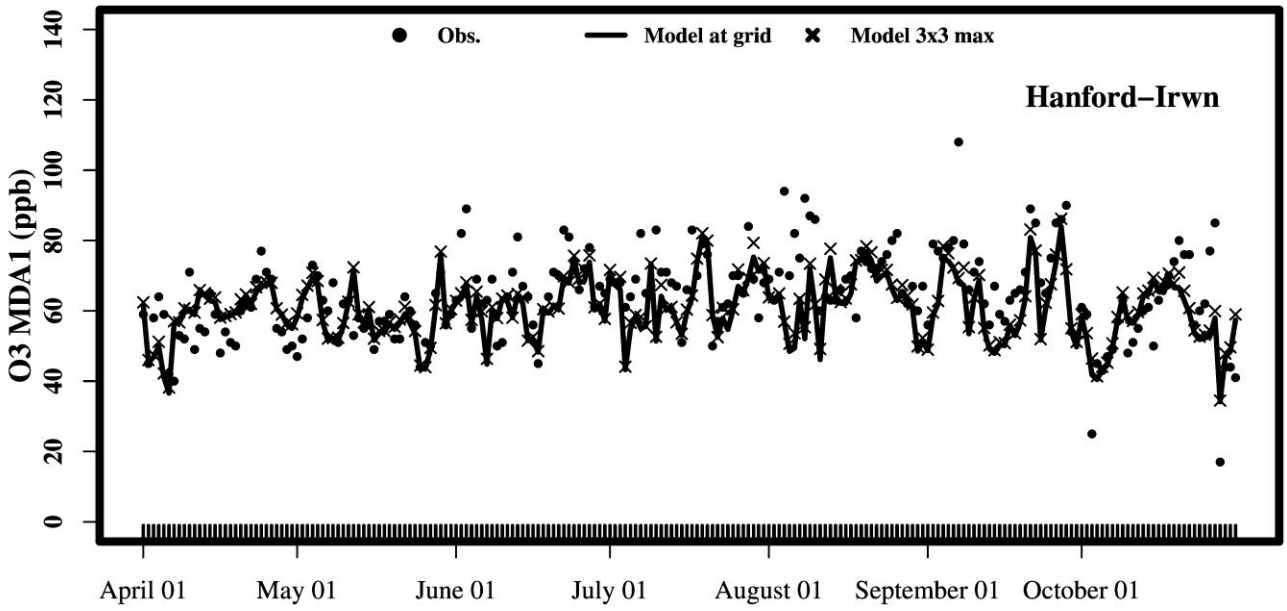

Figure S 65. Time-series of maximum daily average 1-hour ozone at the Madera-28261 Avenue 14 site for the ozone season (April-October 2018).

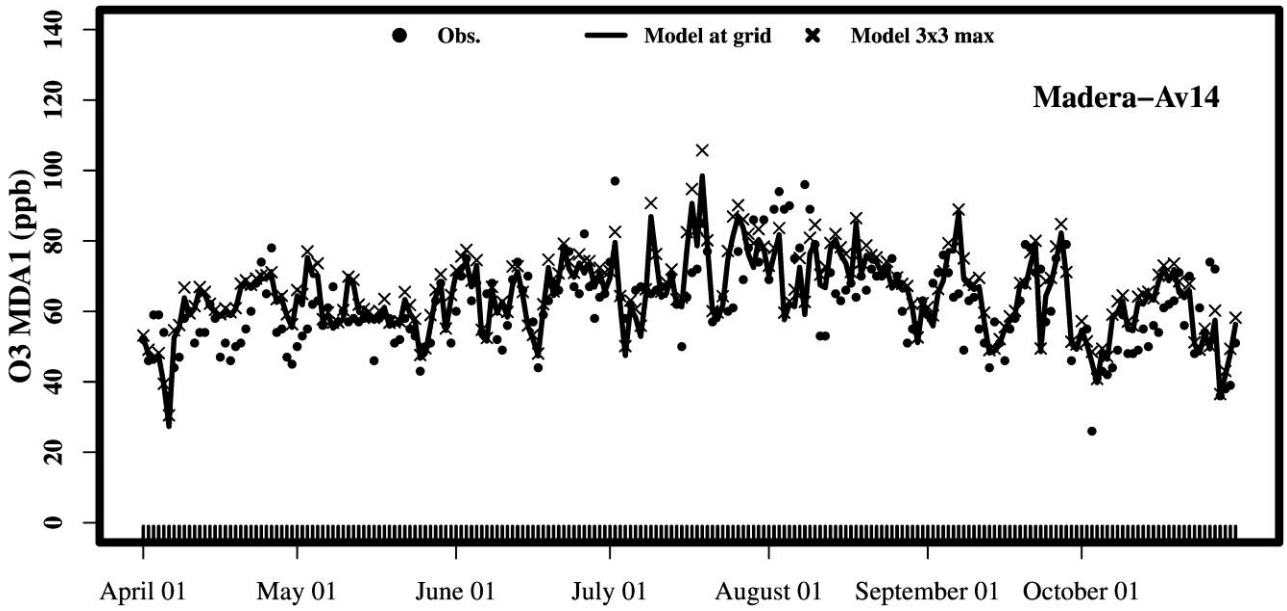

Figure S 66. Time-series of maximum daily average 1-hour ozone at the Madera-Pump Yard site for the ozone season (April-October 2018).

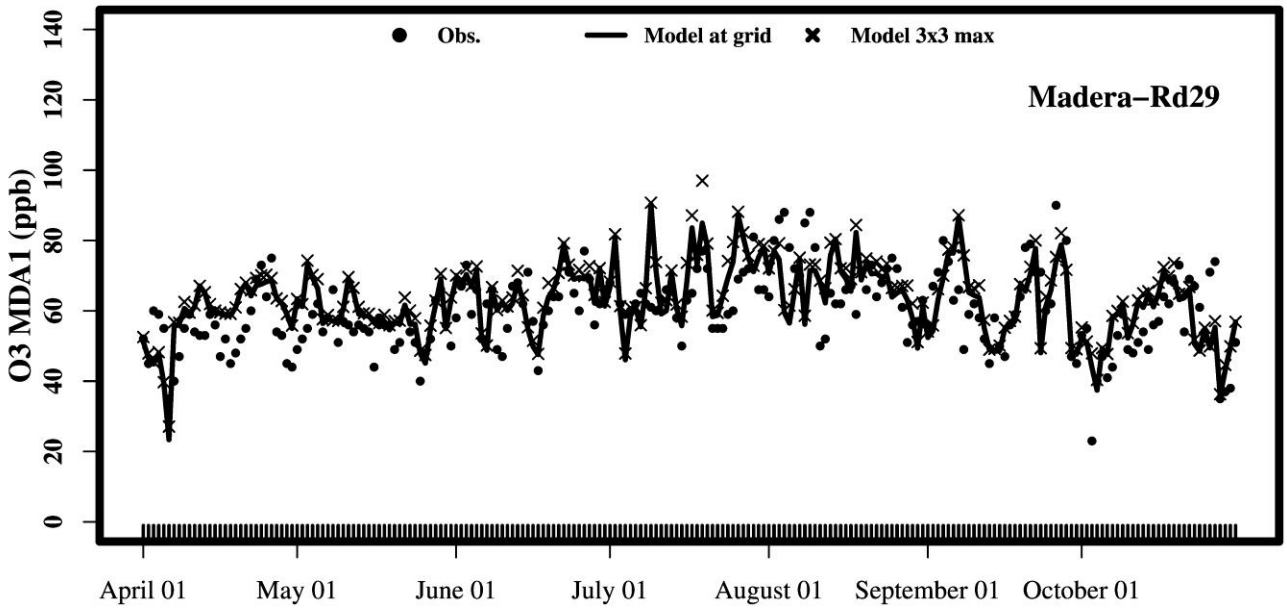

Figure S 67. Time-series of maximum daily average 1-hour ozone at the Tranquility site for the ozone season (April-October 2018).

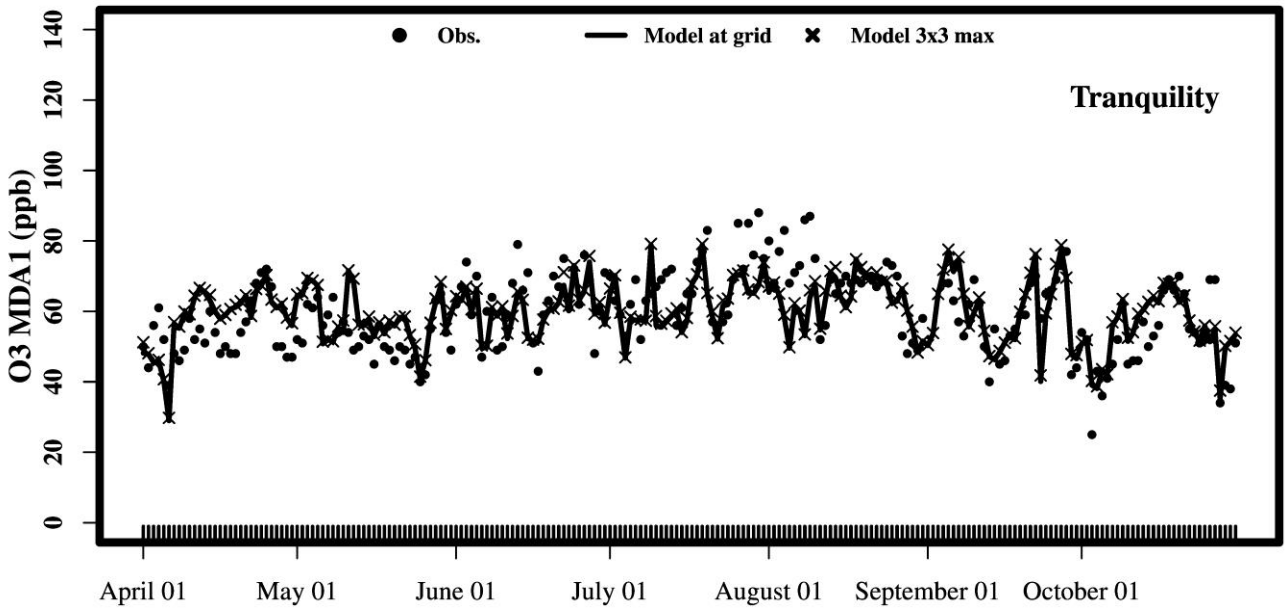

Figure S 68. Time-series of maximum daily average 1-hour ozone at the Edison site for the ozone season (April-October 2018).

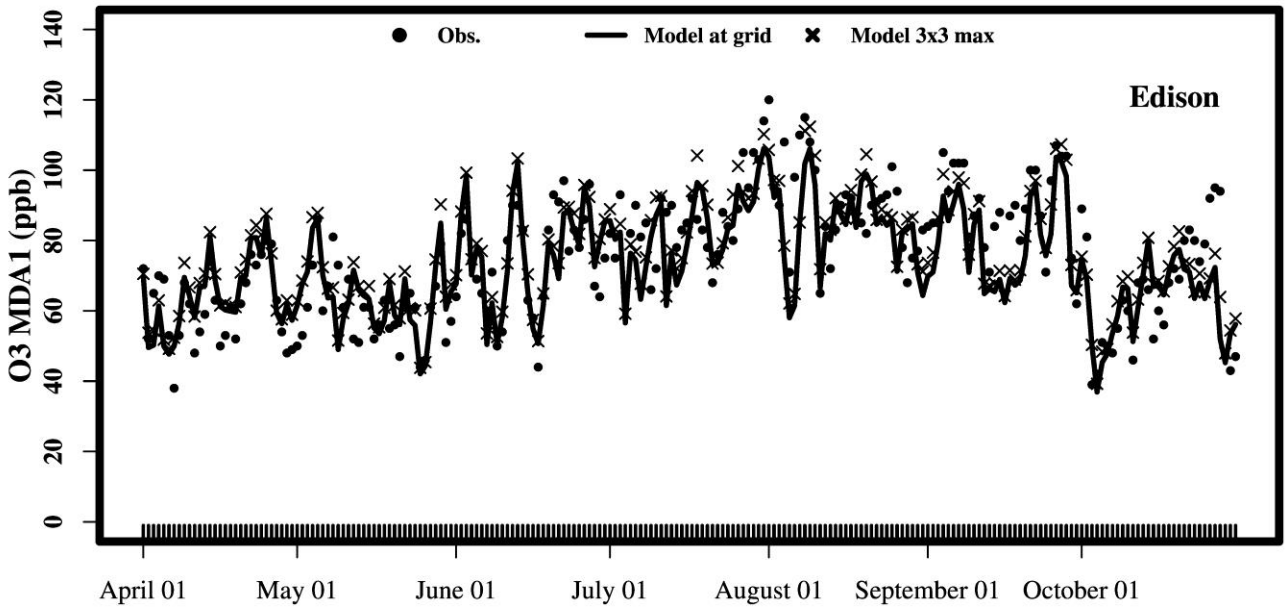

Figure S 69. Time-series of maximum daily average 1-hour ozone at the Arvin-Di Giorgio site for the ozone season (April-October 2018).

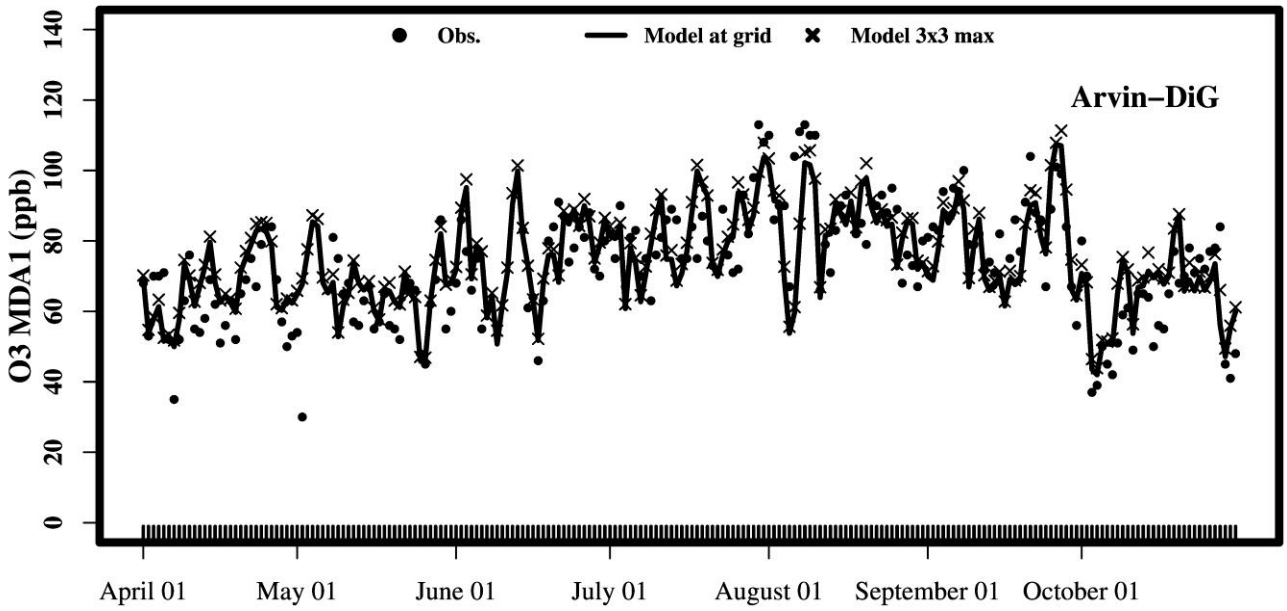

Figure S 70. Time-series of maximum daily average 1-hour ozone at the Bakersfield-5558 California Avenue site for the ozone season (April-October 2018).

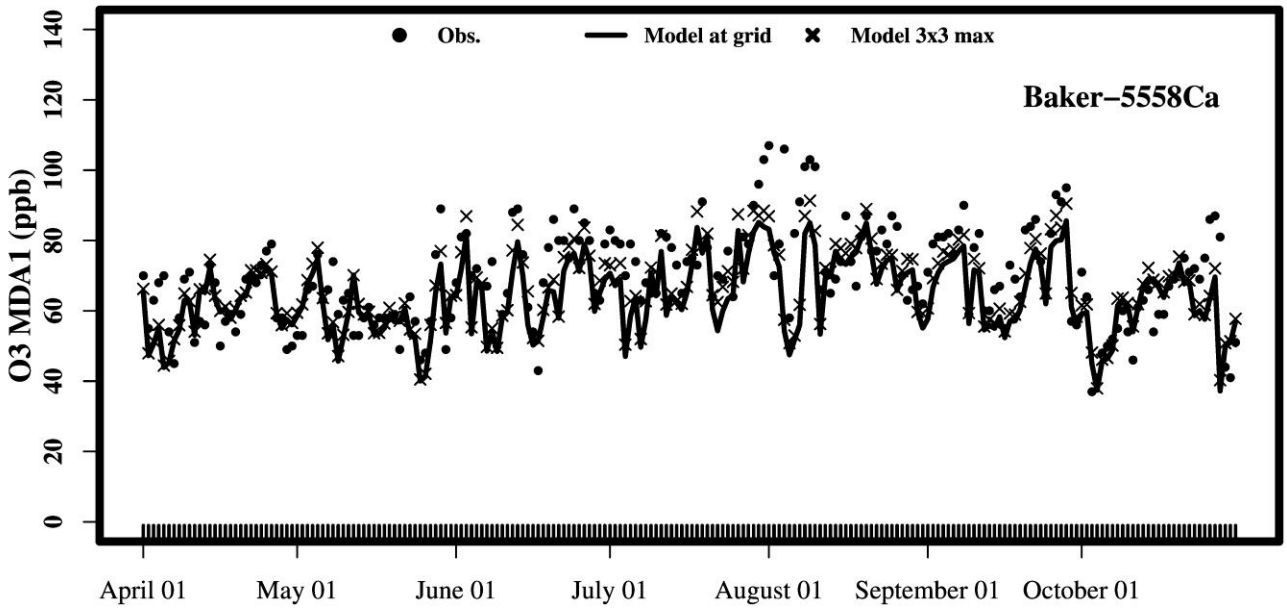

Figure S 71. Time-series of maximum daily average 1-hour ozone at the Sequoia and Kings Canyon Natl Park site for the ozone season (April-October 2018).

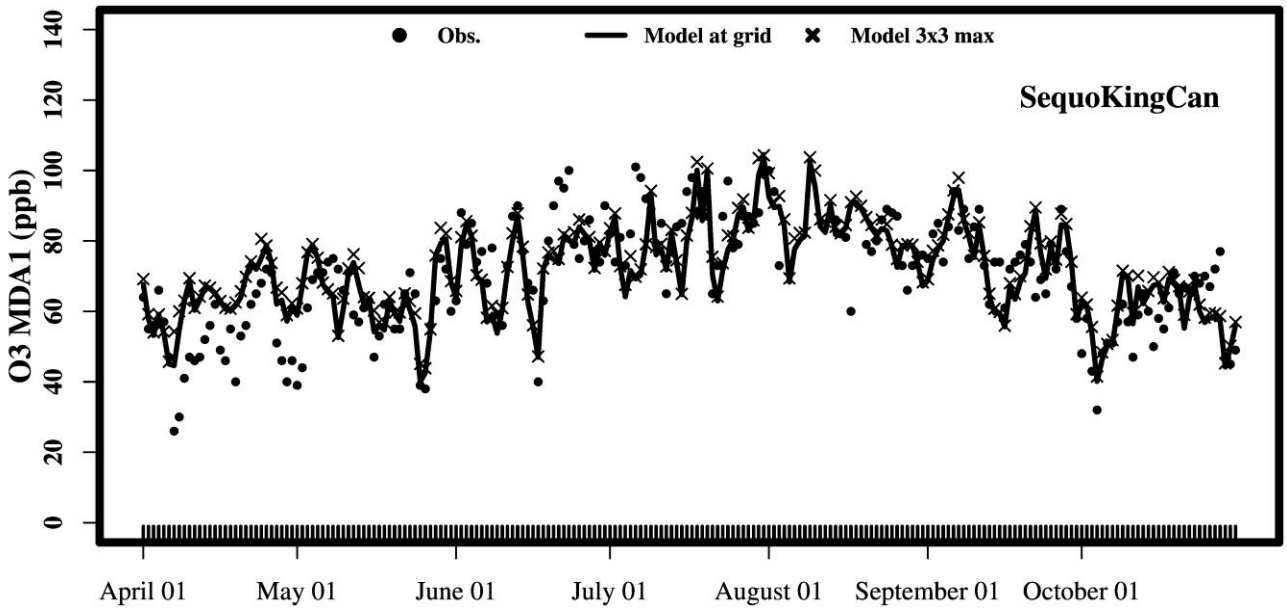

Figure S 72. Time-series of maximum daily average 1-hour ozone at the Bakersfield-Municipal Airport site for the ozone season (April-October 2018).

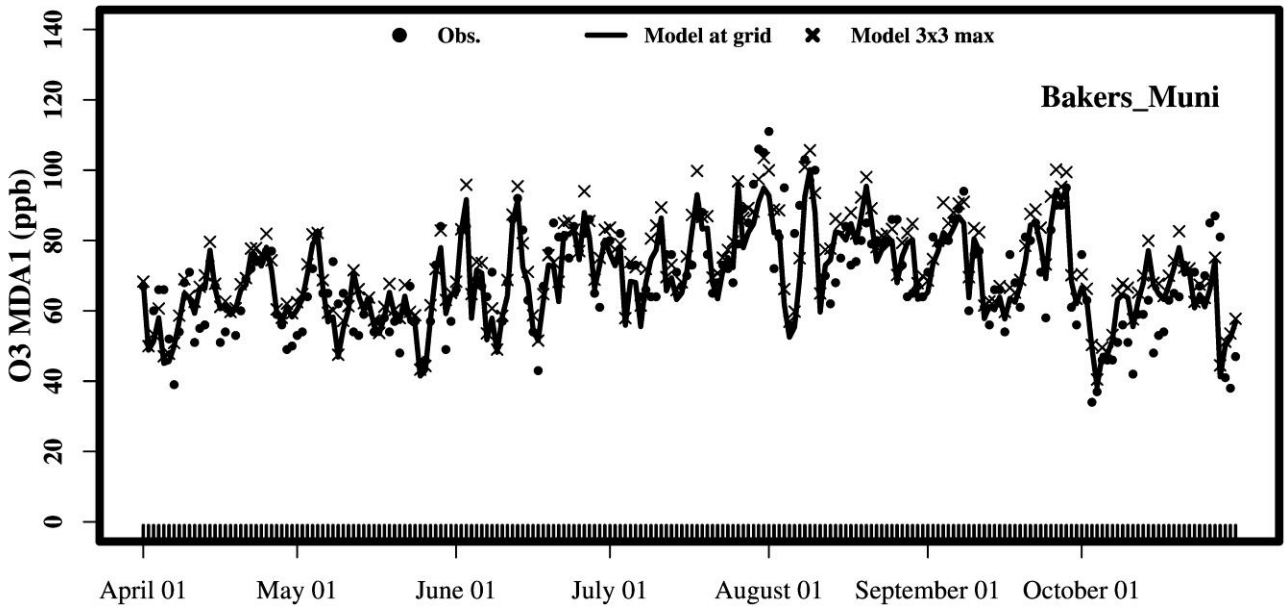

Figure S 73. Time-series of maximum daily average 1-hour ozone at the Visalia-N Church Street site for the ozone season (April-October 2018).

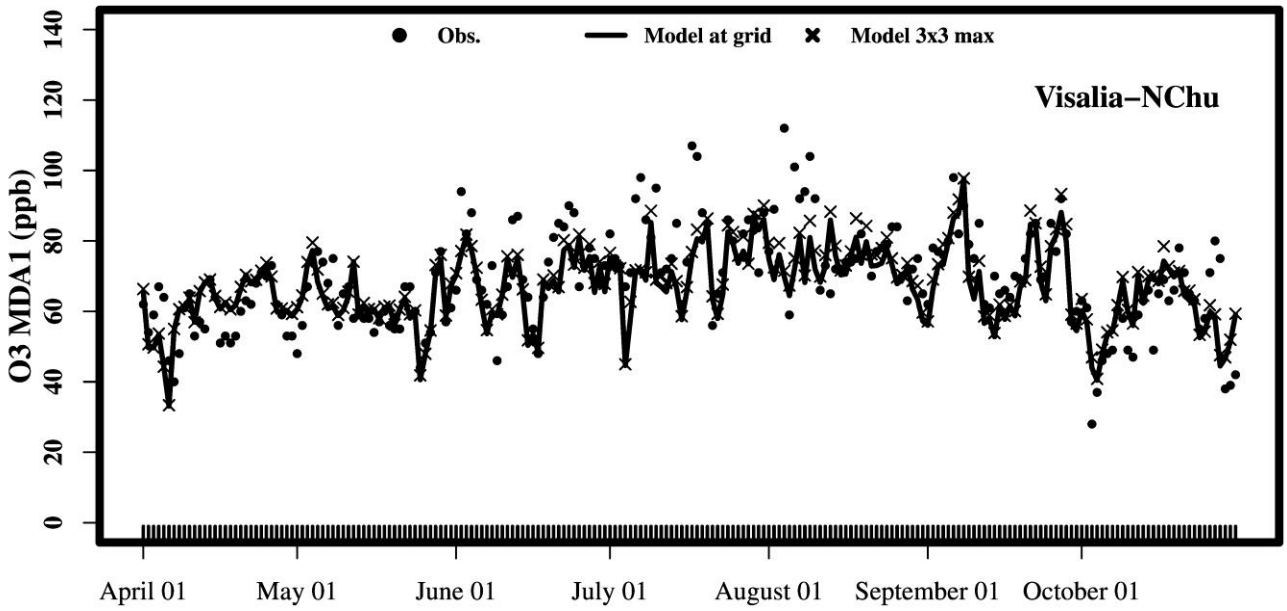

Figure S 74. Time-series of maximum daily average 1-hour ozone at the Maricopa-Stanislaus Street site for the ozone season (April-October 2018).

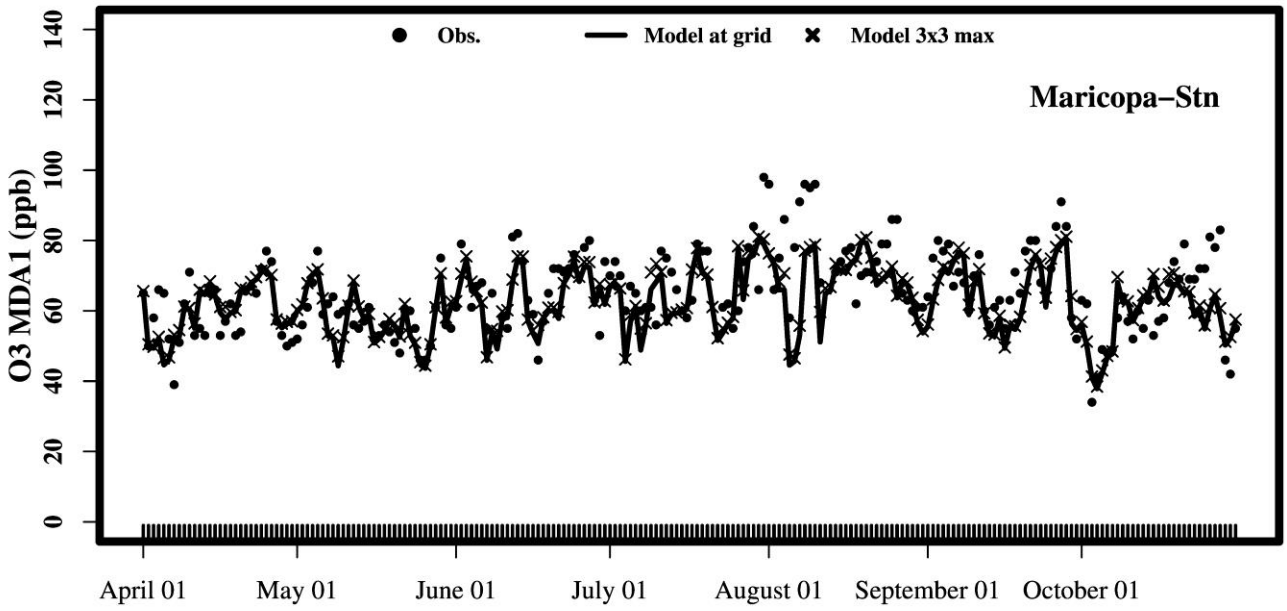

Figure S 75. Time-series of maximum daily average 1-hour ozone at the Sequoia Natl Park-Lower Kaweah site for the ozone season (April-October 2018).

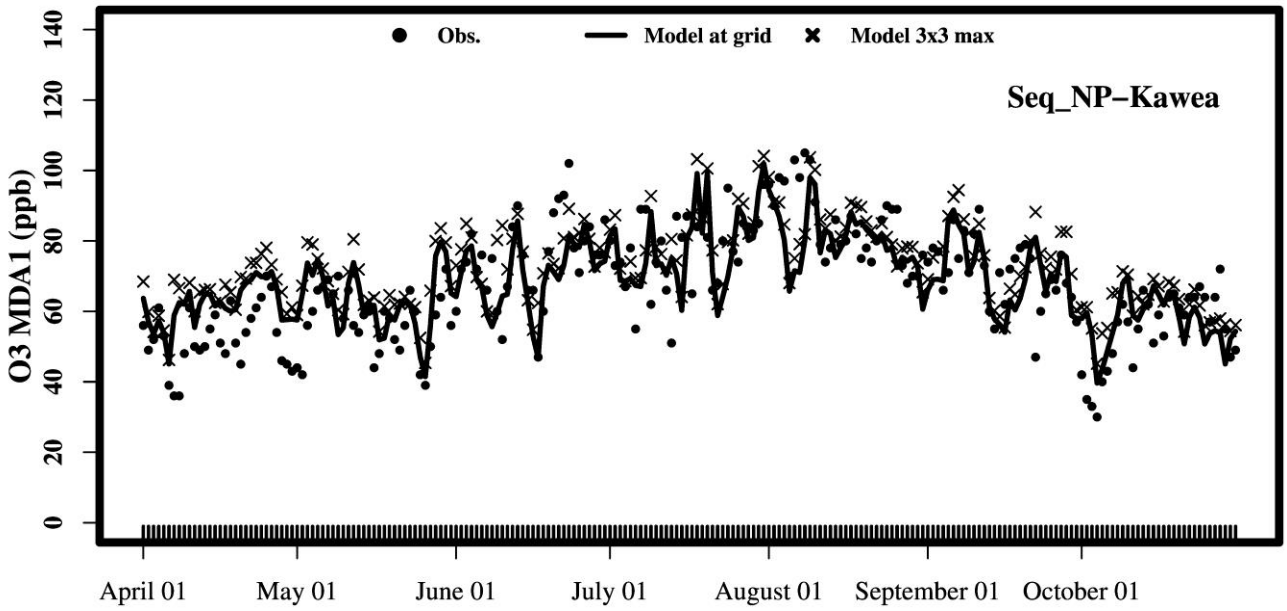

Figure S 76. Time-series of maximum daily average 1-hour ozone at the Oildale-3311 Manor Street site for the ozone season (April-October 2018).

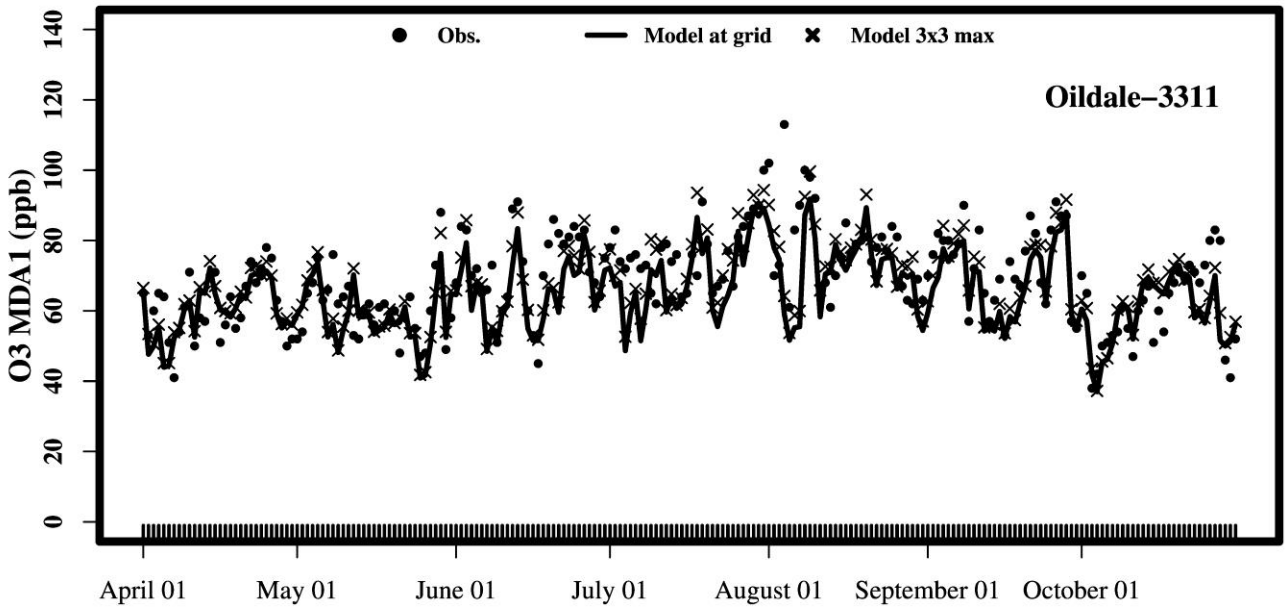

Figure S 77. Time-series of maximum daily average 1-hour ozone at the Shafter-Walker Street site for the ozone season (April-October 2018).

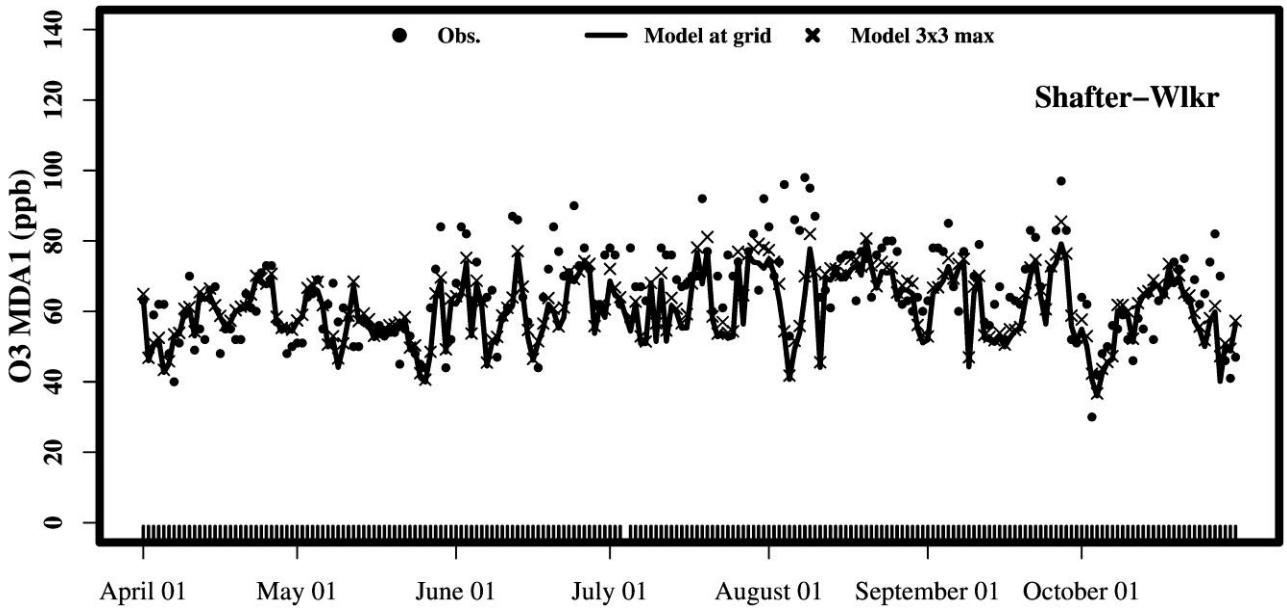

Figure S 78. Time-series of maximum daily average 1-hour ozone at the Porterville-1839 Newcomb Street site for the ozone season (April-October 2018).

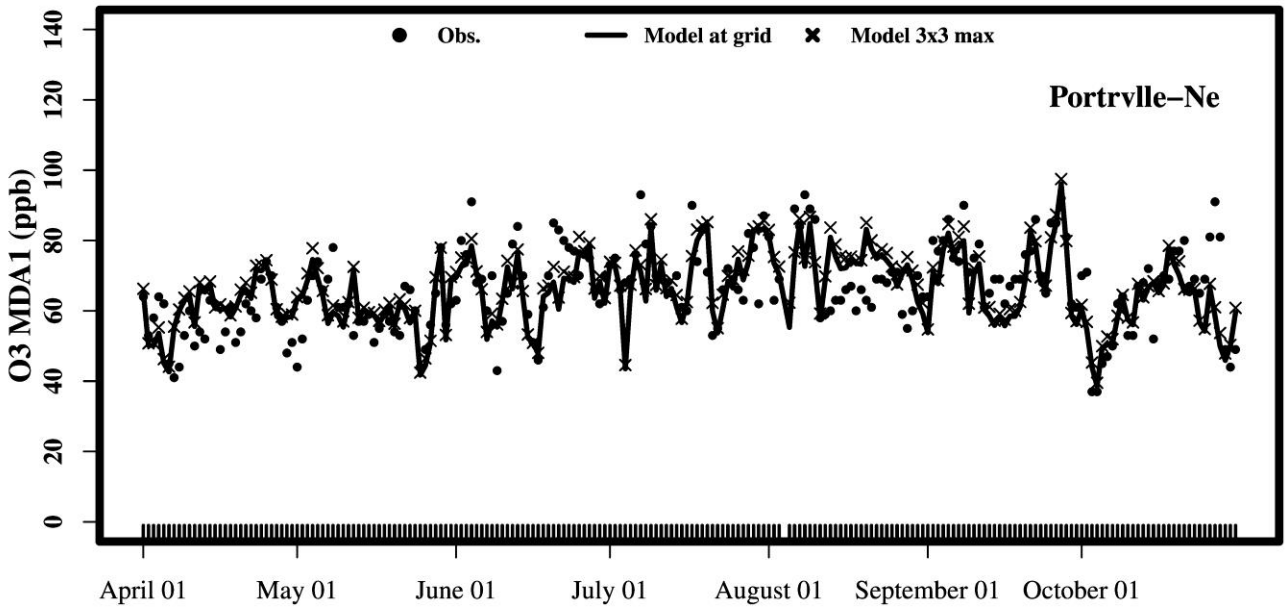

Figure S 79. Time-series of maximum daily average 8-hour ozone at the Turlock-S Minaret St. site for the ozone season (April-October 2018).

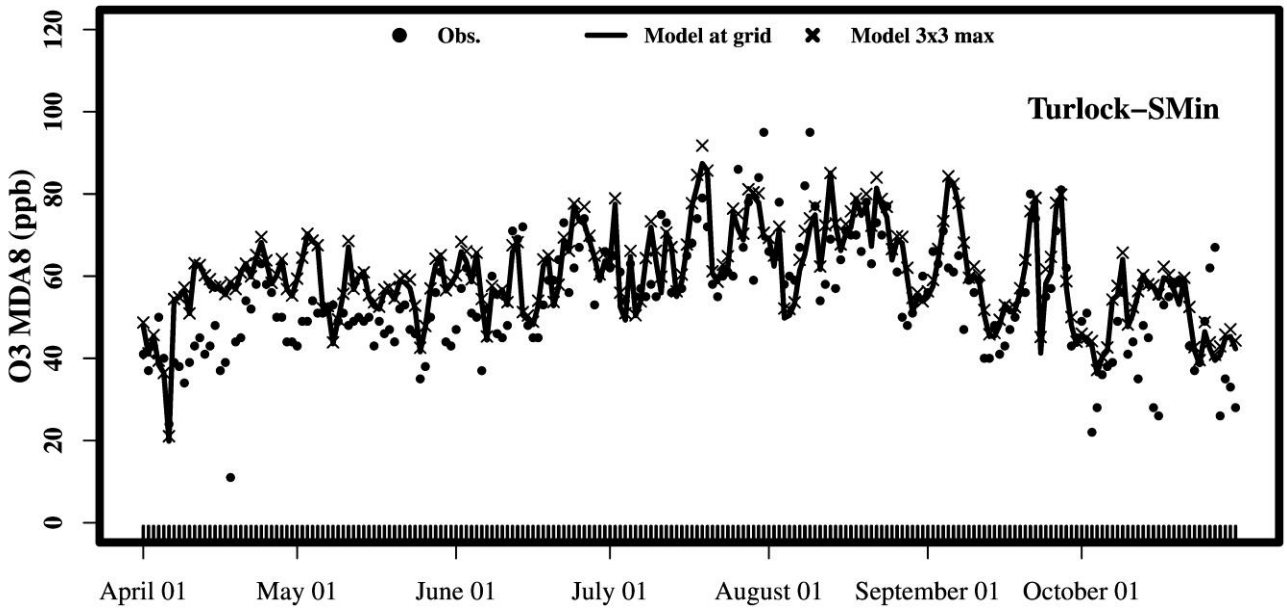

Figure S 80. Time-series of maximum daily average 8-hour ozone at the Modesto-14th St. site for the ozone season (April-October 2018).

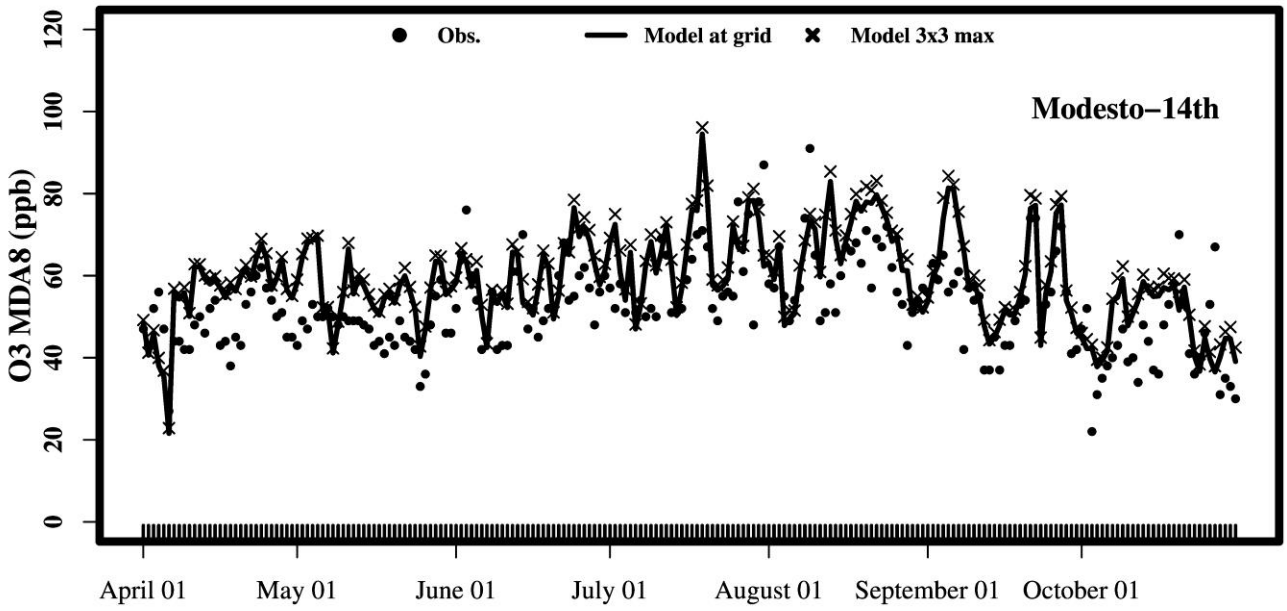

Figure S 81. Time-series of maximum daily average 8-hour ozone at the Merced-S Coffee Av. site for the ozone season (April-October 2018).

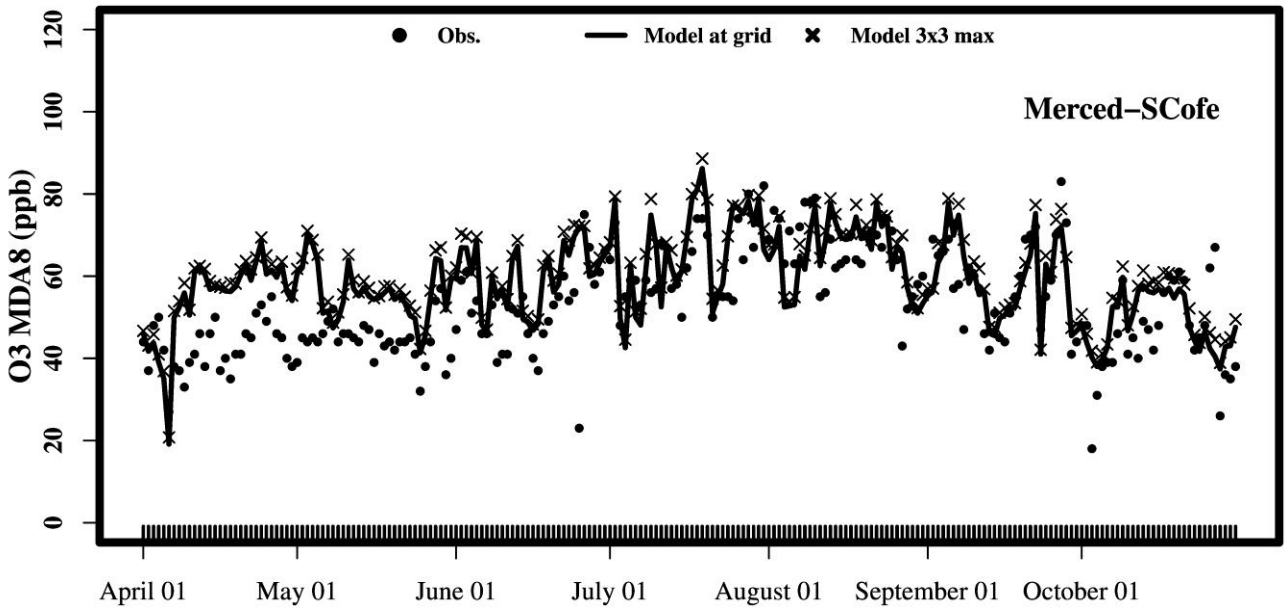

Figure S 82. Time-series of maximum daily average 8-hour ozone at the Tracy-Airport site for the ozone season (April-October 2018).

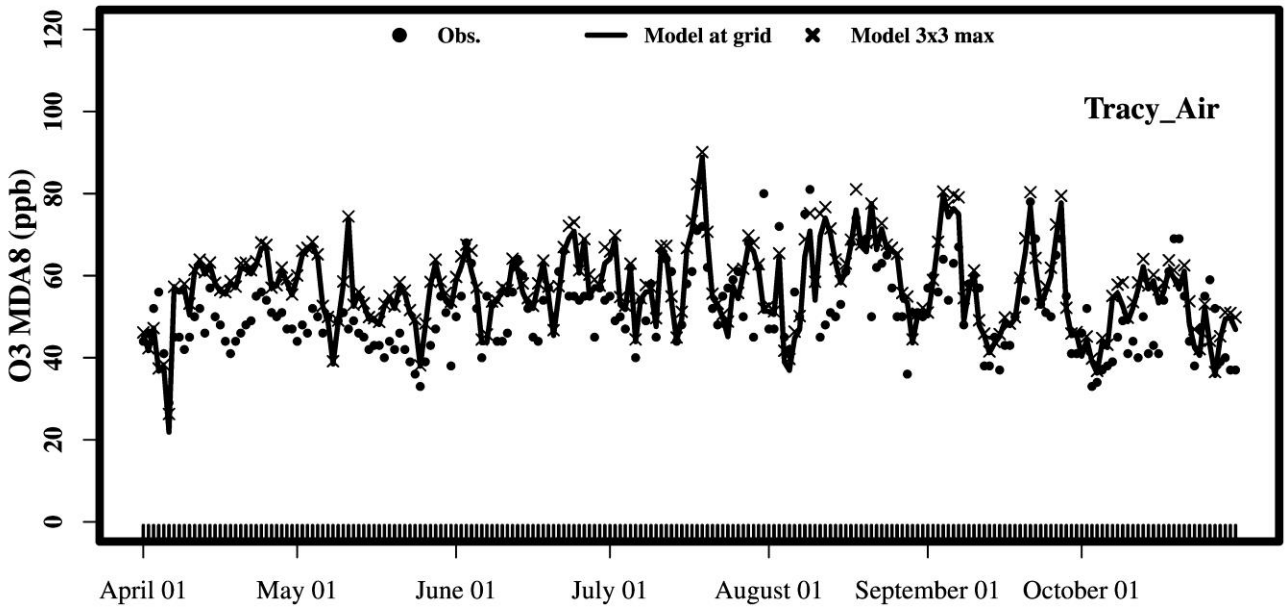

Figure S 83. Time-series of maximum daily average 8-hour ozone at the Stockton-Hazelton St site for the ozone season (April-October 2018).

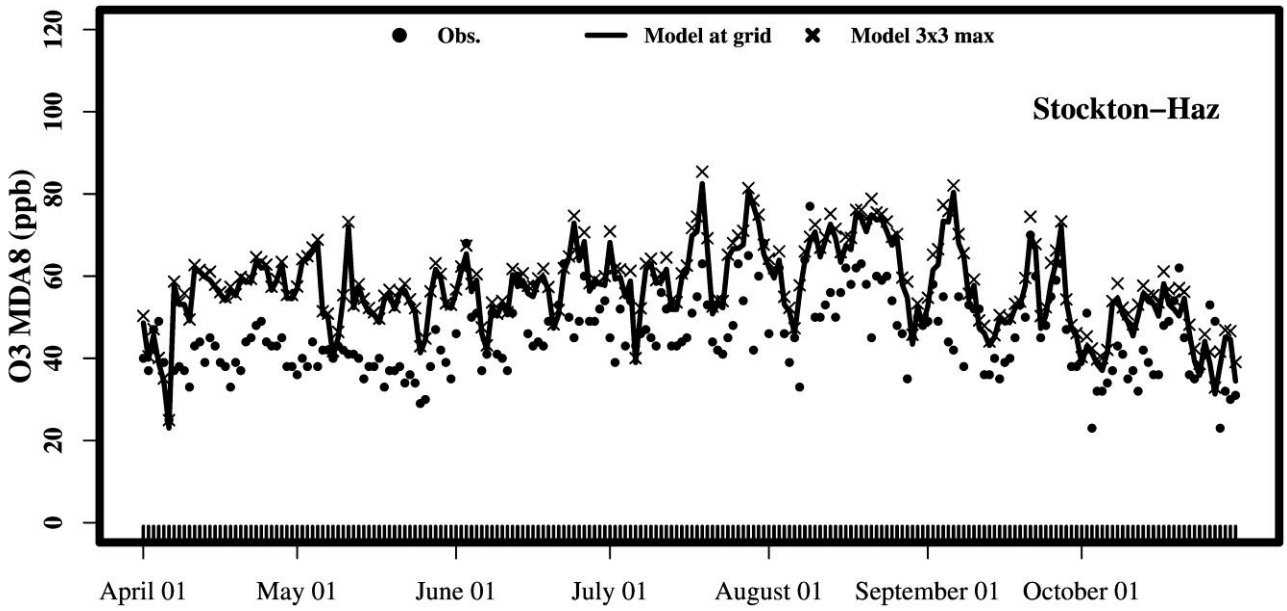

Figure S 84. Time-series of maximum daily average 8-hour ozone at the Fresno-Garland site for the ozone season (April-October 2018).

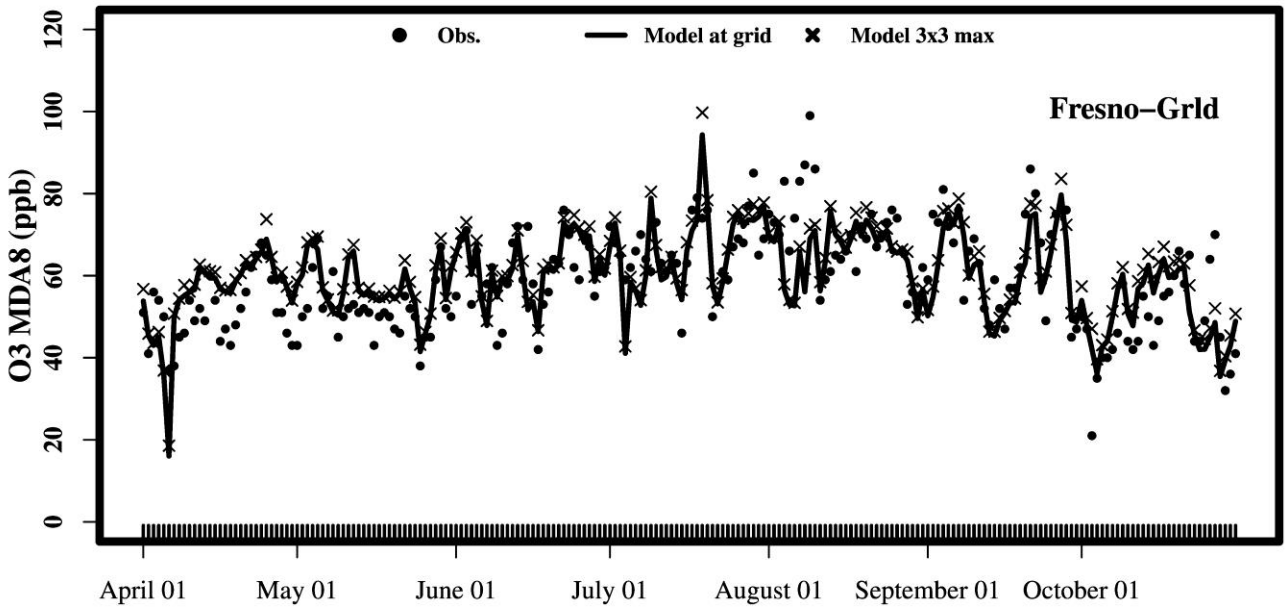

Figure S 85. Time-series of maximum daily average 8-hour ozone at the Clovis site for the ozone season (April-October 2018).

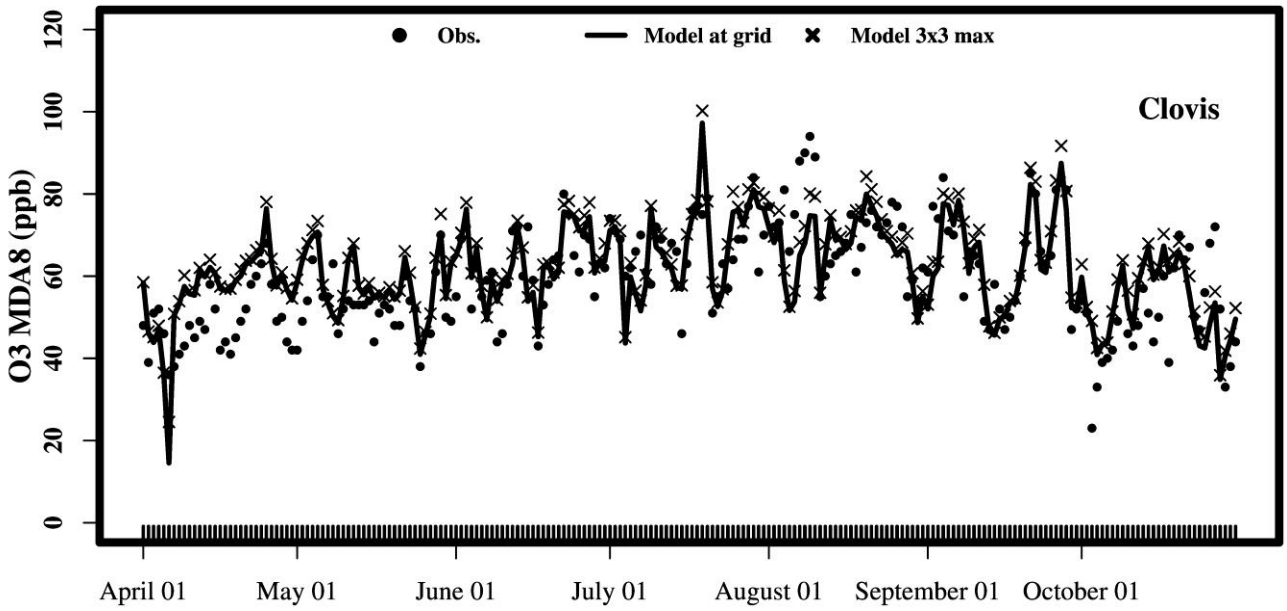

Figure S 86. Time-series of maximum daily average 8-hour ozone at the Parlier site for the ozone season (April-October 2018).

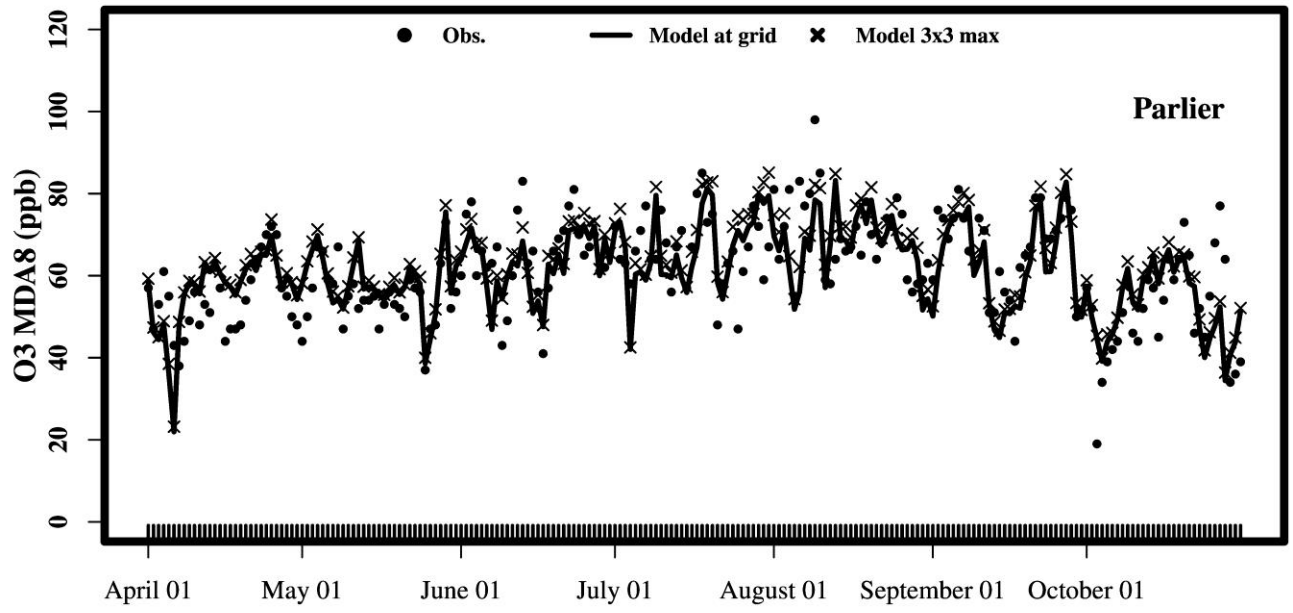

Figure S 87. Time-series of maximum daily average 8-hour ozone at the Fresno-Drummond St. site for the ozone season (April-October 2018).

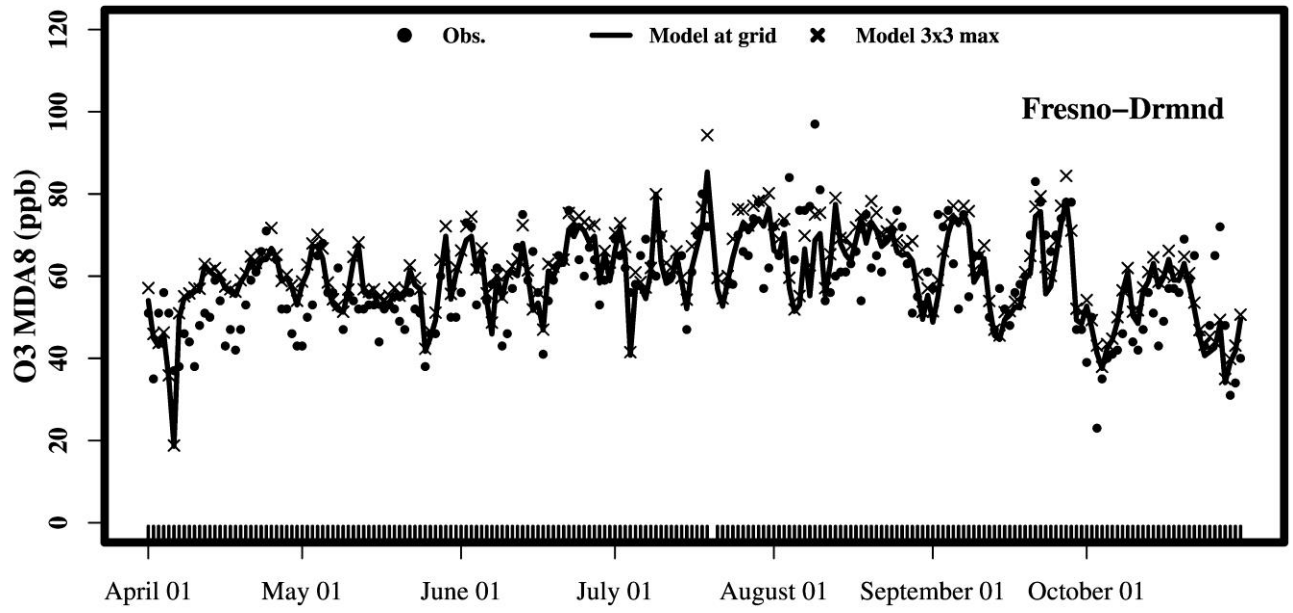

Figure S 88. Time-series of maximum daily average 8-hour ozone at the Fresno- Sierra Skypark #2 site for the ozone season (April-October 2018).

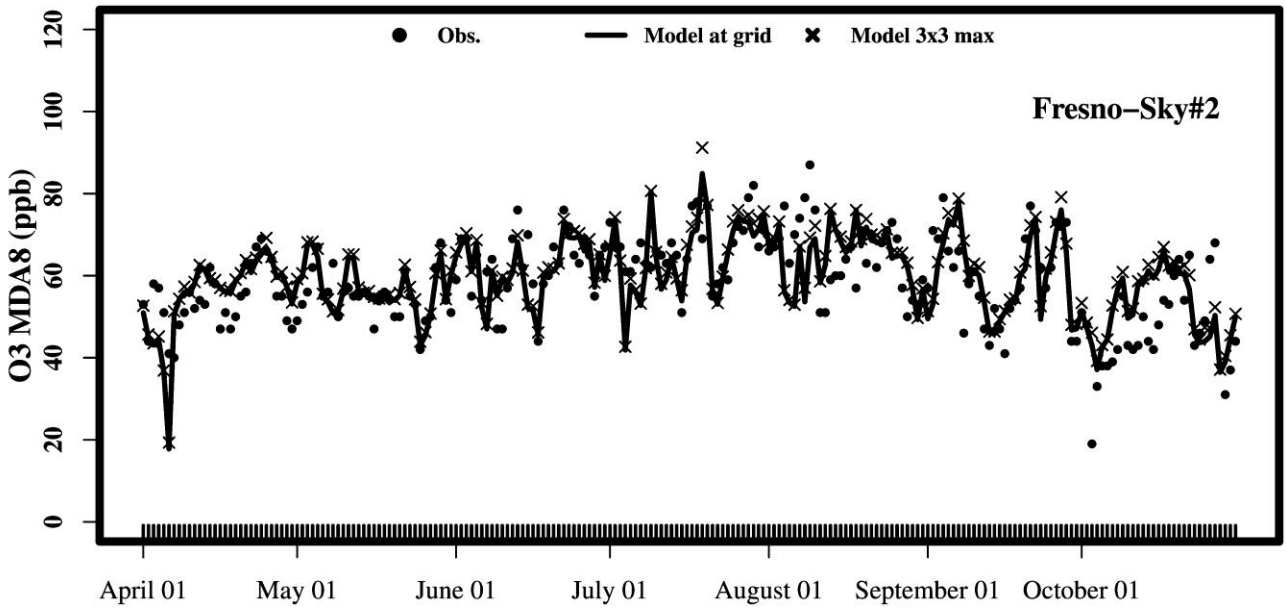

Figure S 89. Time-series of maximum daily average 8-hour ozone at the Hanford-S. Irwin St. site for the ozone season (April-October 2018).

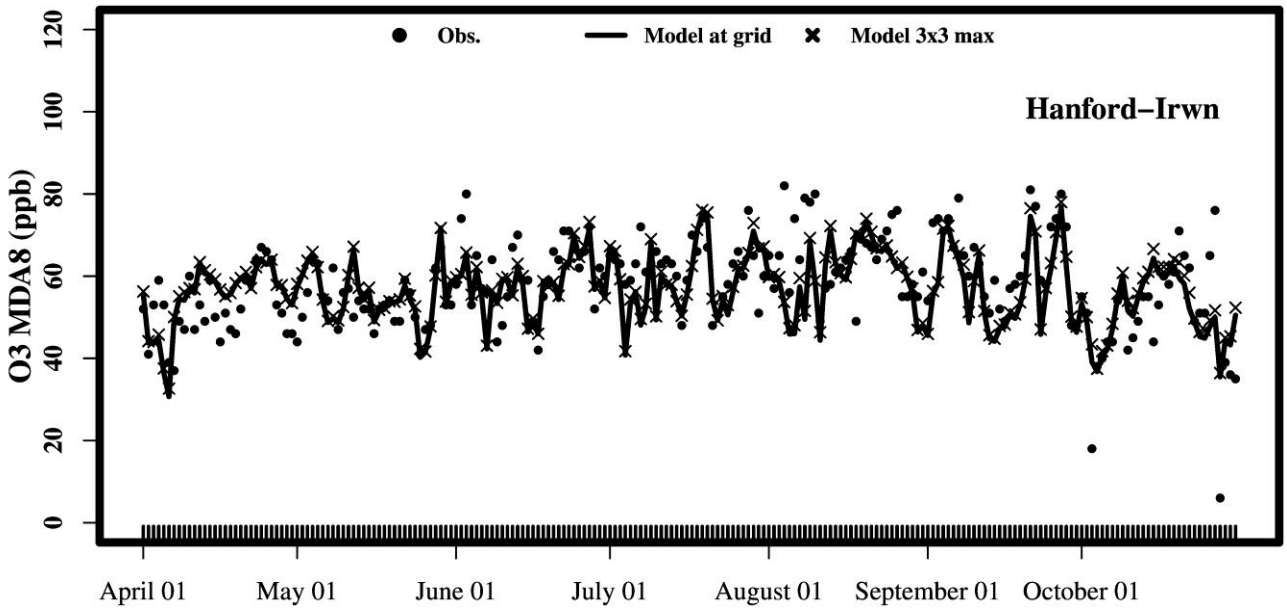

Figure S 90. Time-series of maximum daily average 8-hour ozone at the Madera-28261 Avenue 14 site for the ozone season (April-October 2018).

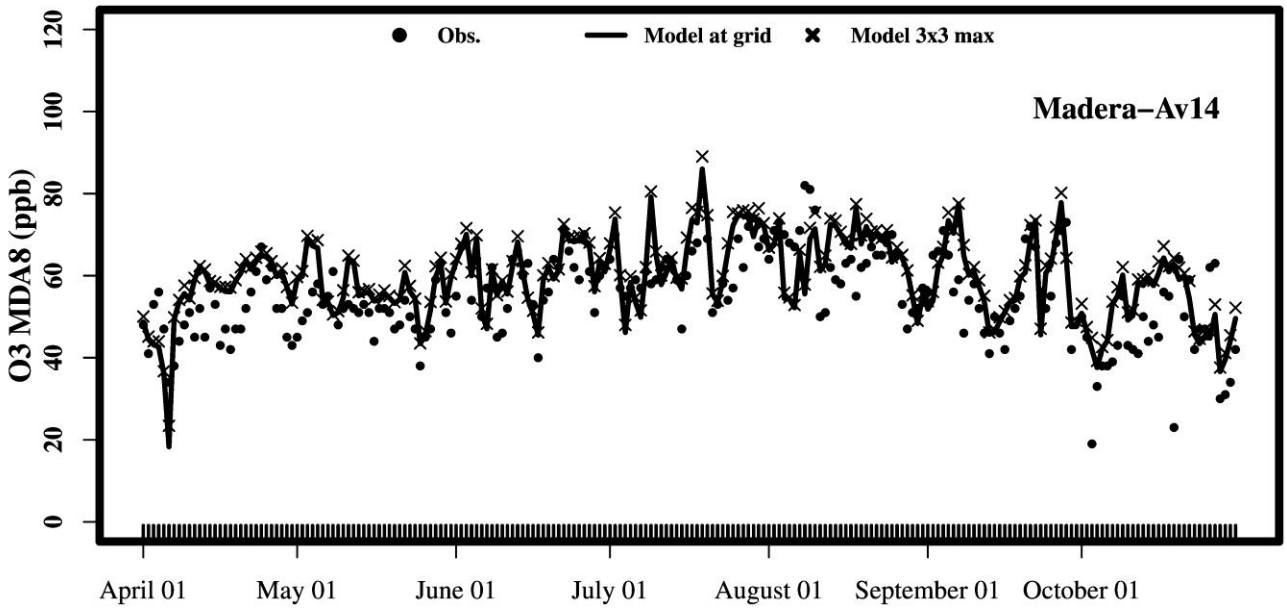

Figure S 91. Time-series of maximum daily average 8-hour ozone at the Madera-Pump Yard site for the ozone season (April-October 2018).

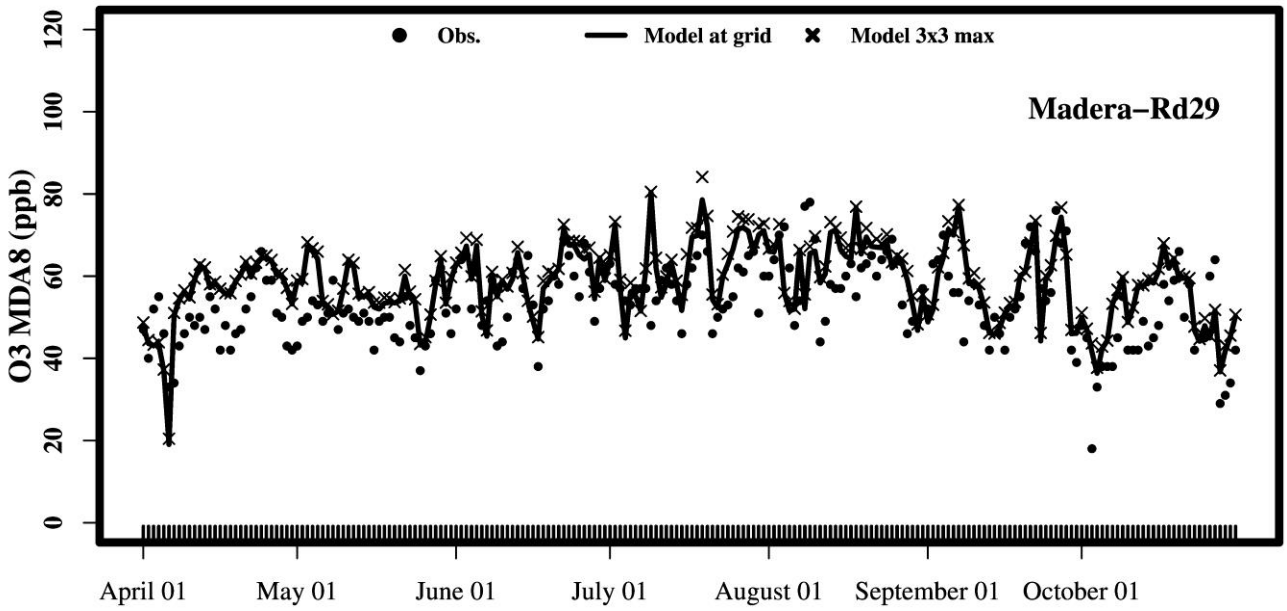

Figure S 92. Time-series of maximum daily average 8-hour ozone at the Tranquility site for the ozone season (April-October 2018).

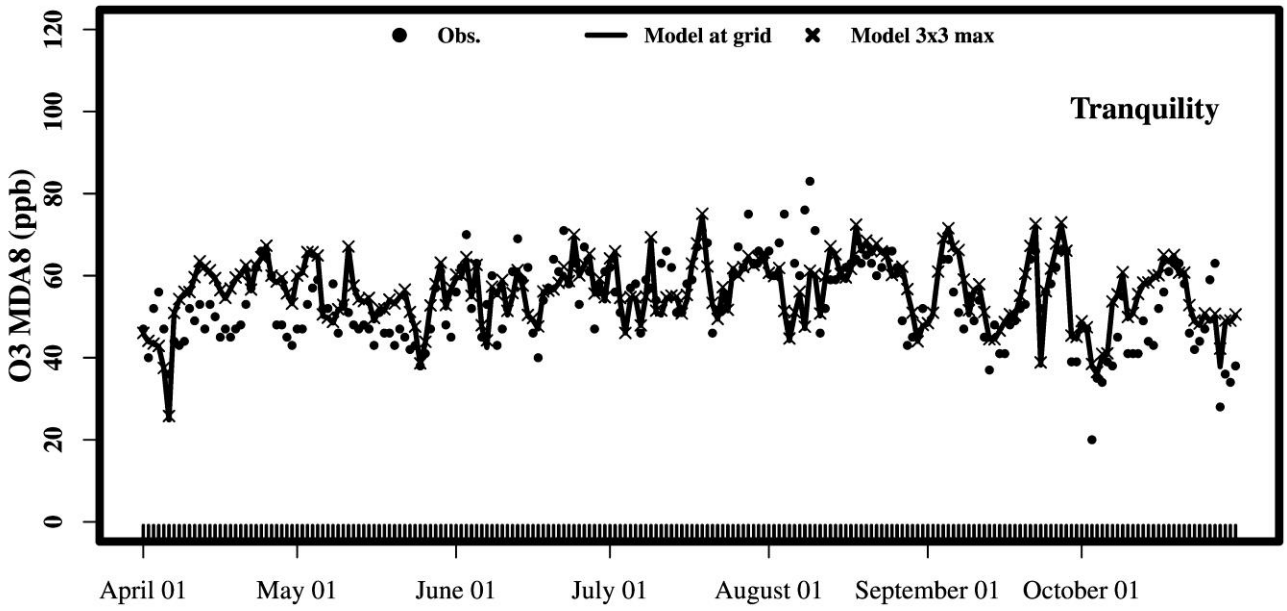

Figure S 93. Time-series of maximum daily average 8-hour ozone at the Edison site for the ozone season (April-October 2018).

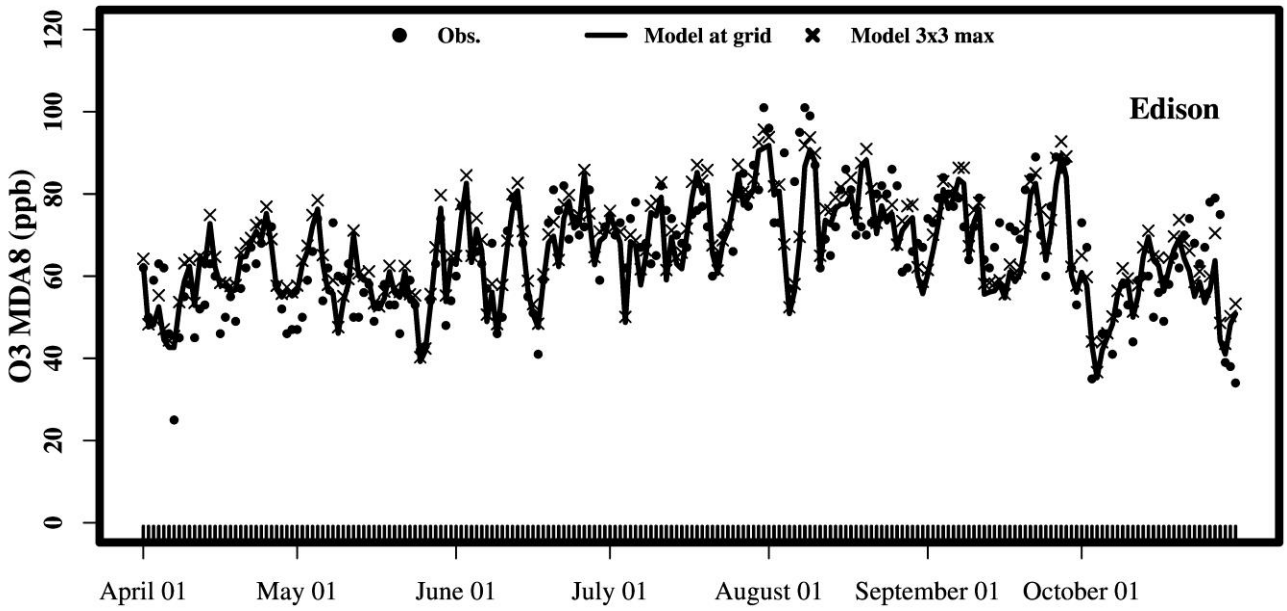

Figure S 94. Time-series of maximum daily average 8-hour ozone at the Arvin-Di Giorgio site for the ozone season (April-October 2018).

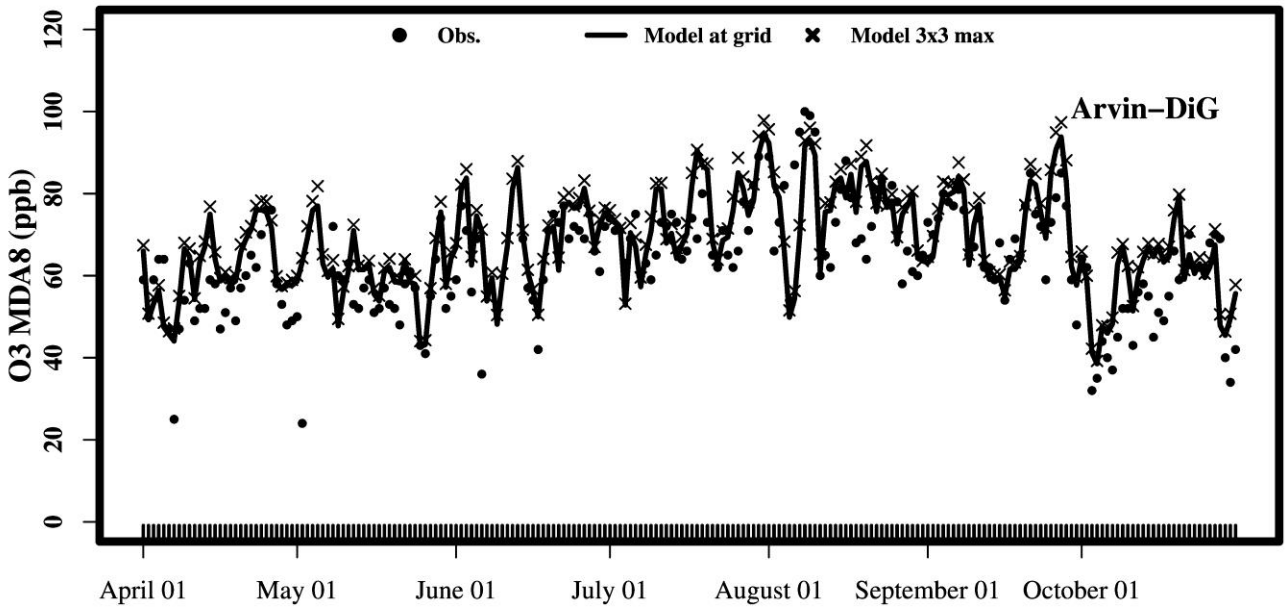

Figure S 95. Time-series of maximum daily average 8-hour ozone at the Bakersfield-5558 California Avenue site for the ozone season (April-October 2018).

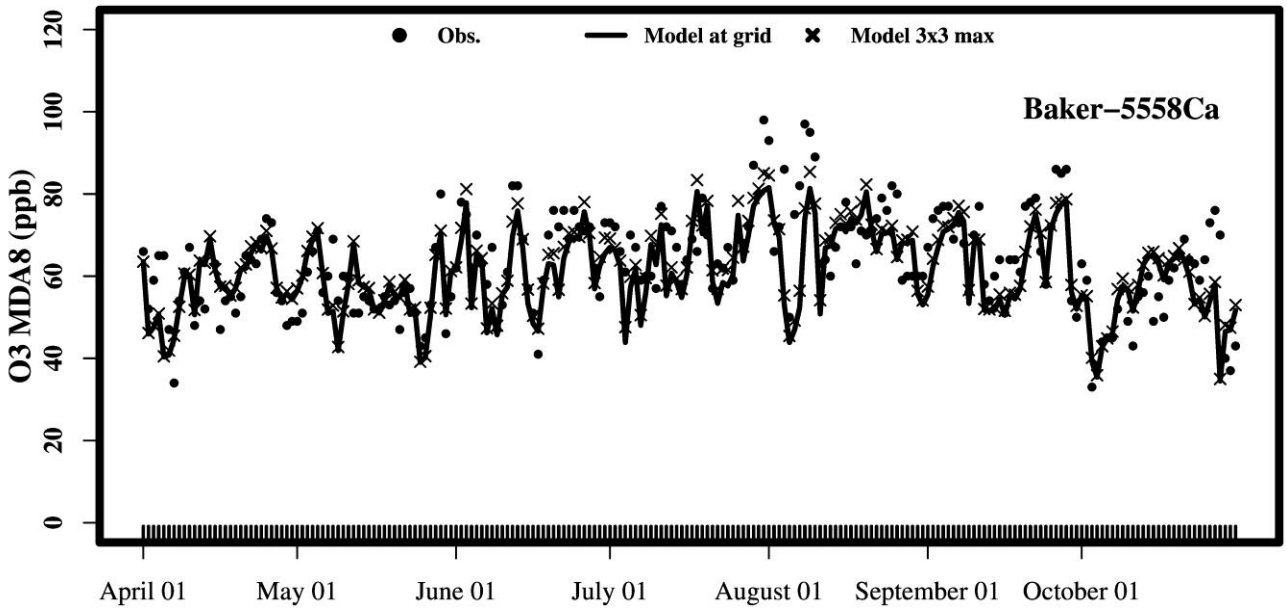

Figure S 96. Time-series of maximum daily average 8-hour ozone at the Sequoia and Kings Canyon Natl Park site for the ozone season (April-October 2018).

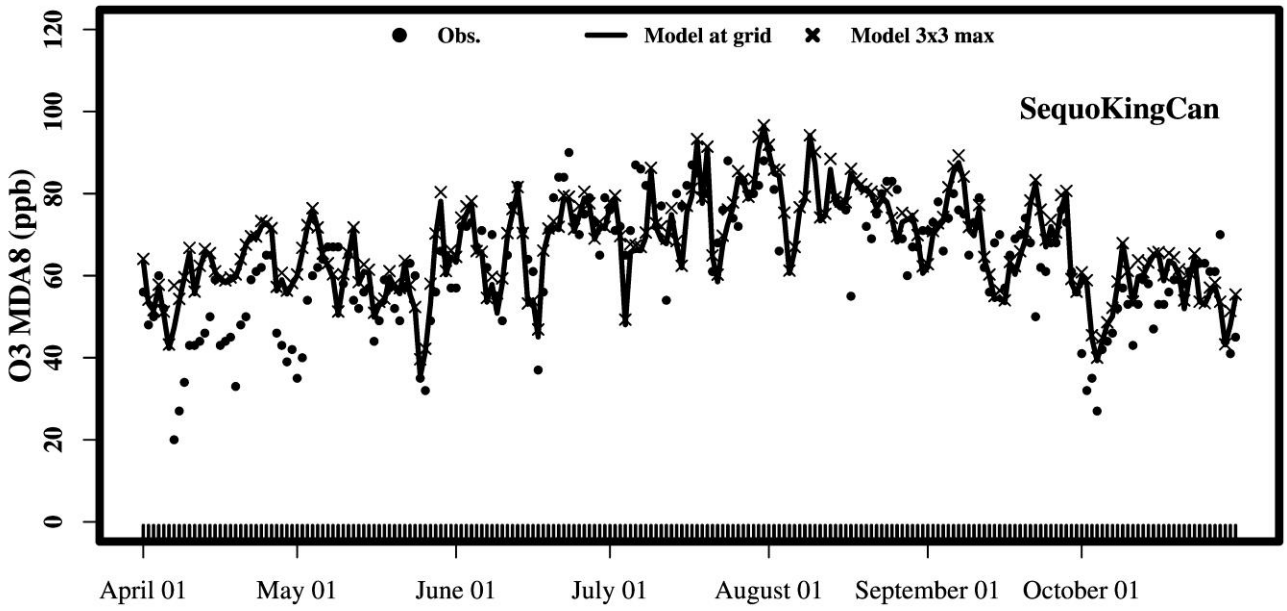

Figure S 97. Time-series of maximum daily average 8-hour ozone at the Bakersfield-Municipal Airport site for the ozone season (April-October 2018).

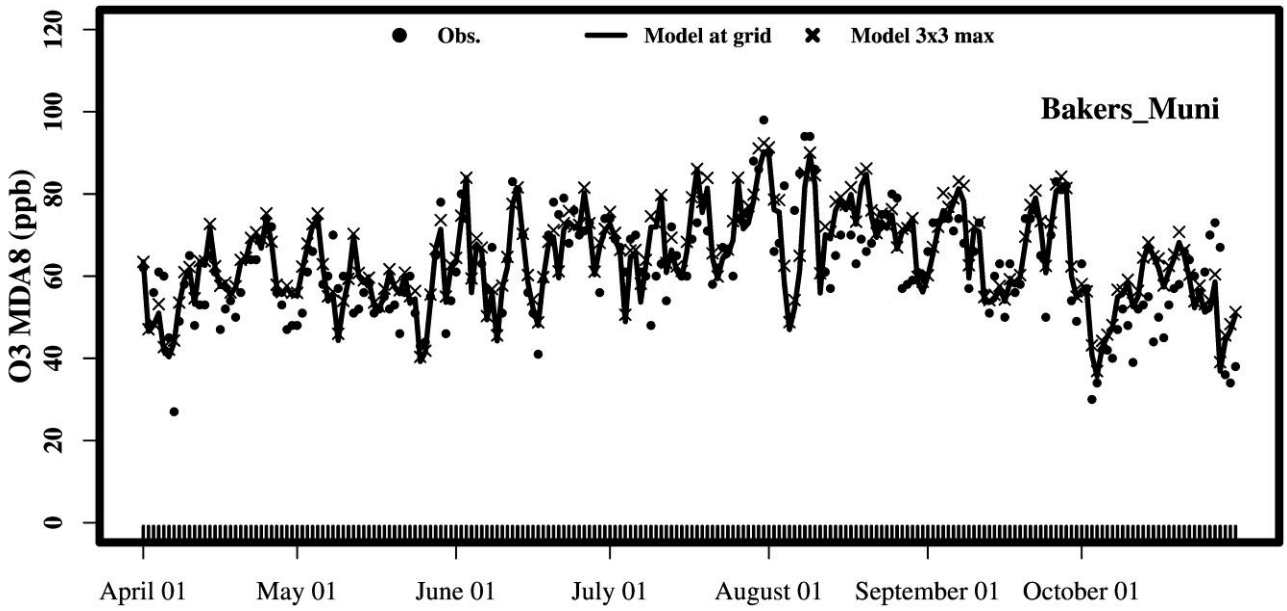

Figure S 98. Time-series of maximum daily average 8-hour ozone at the Visalia-N Church Street site for the ozone season (April-October 2018).

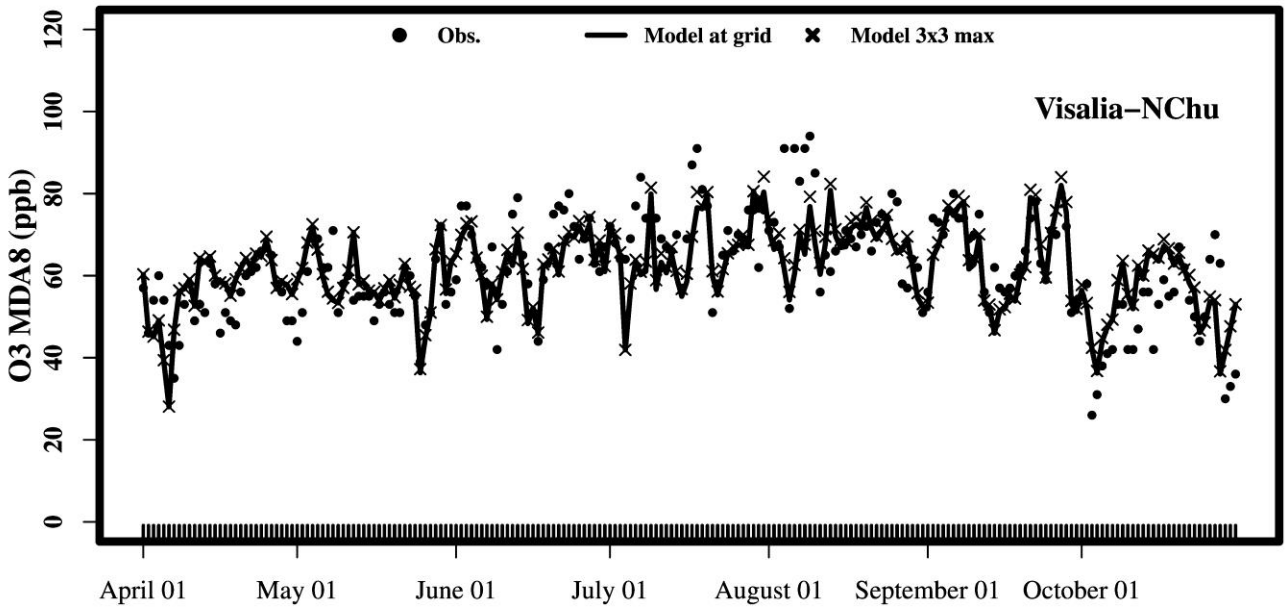

Figure S 99. Time-series of maximum daily average 8-hour ozone at the Maricopa-Stanislaus Street site for the ozone season (April-October 2018).

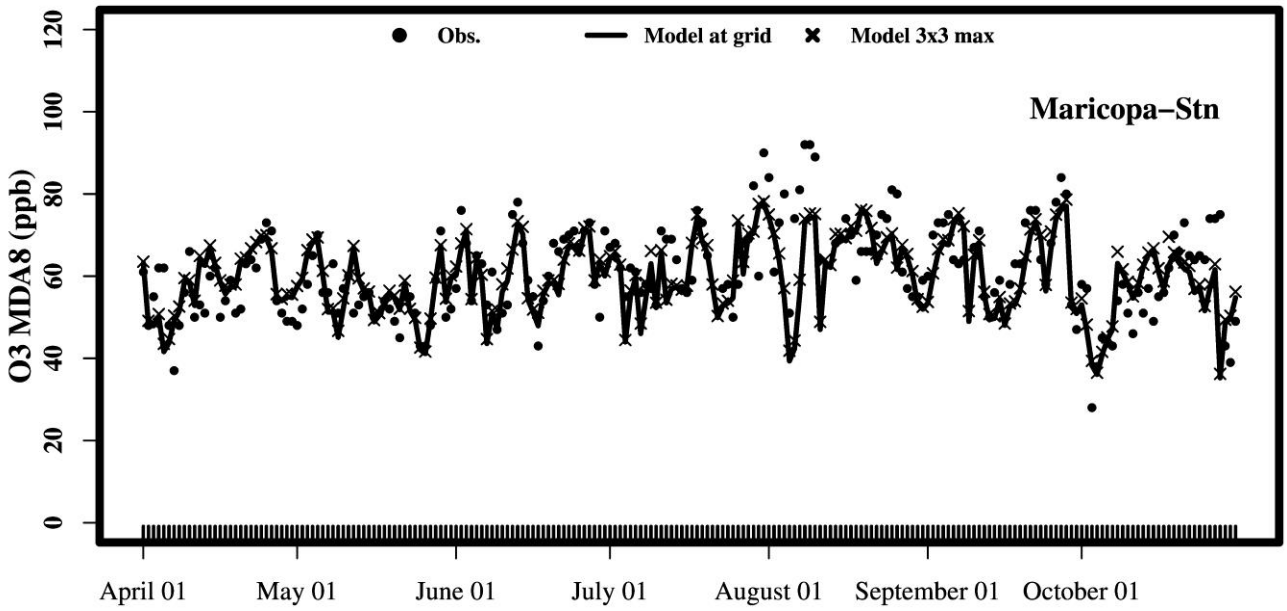

Figure S 100. Time-series of maximum daily average 8-hour ozone at the Sequoia Natl Park-Lower Kaweah site for the ozone season (April-October 2018).

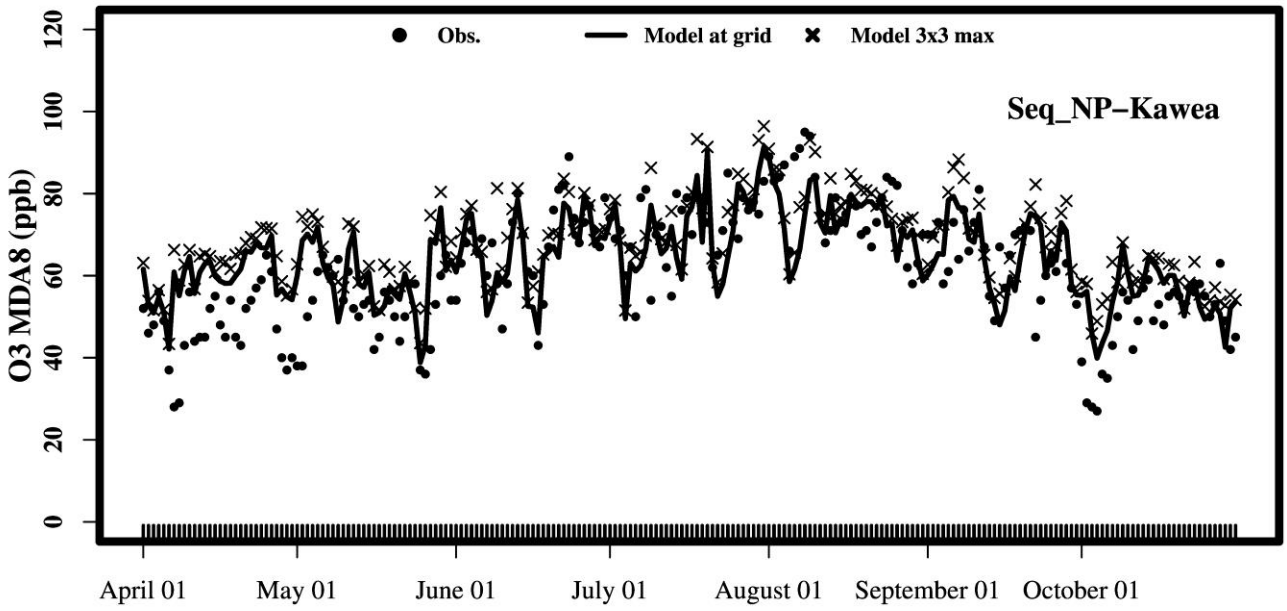

Figure S 101. Time-series of maximum daily average 8-hour ozone at the Oildale-3311 Manor Street site for the ozone season (April-October 2018).

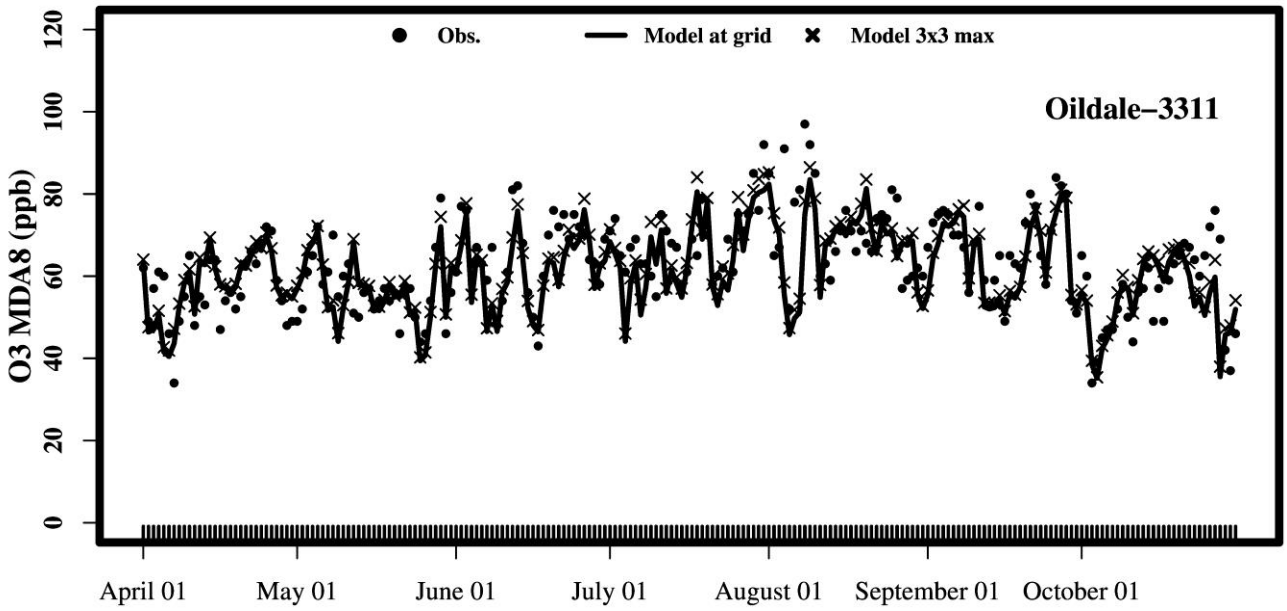

Figure S 102. Time-series of maximum daily average 8-hour ozone at the Shafter-Walker Street site for the ozone season (April-October 2018).

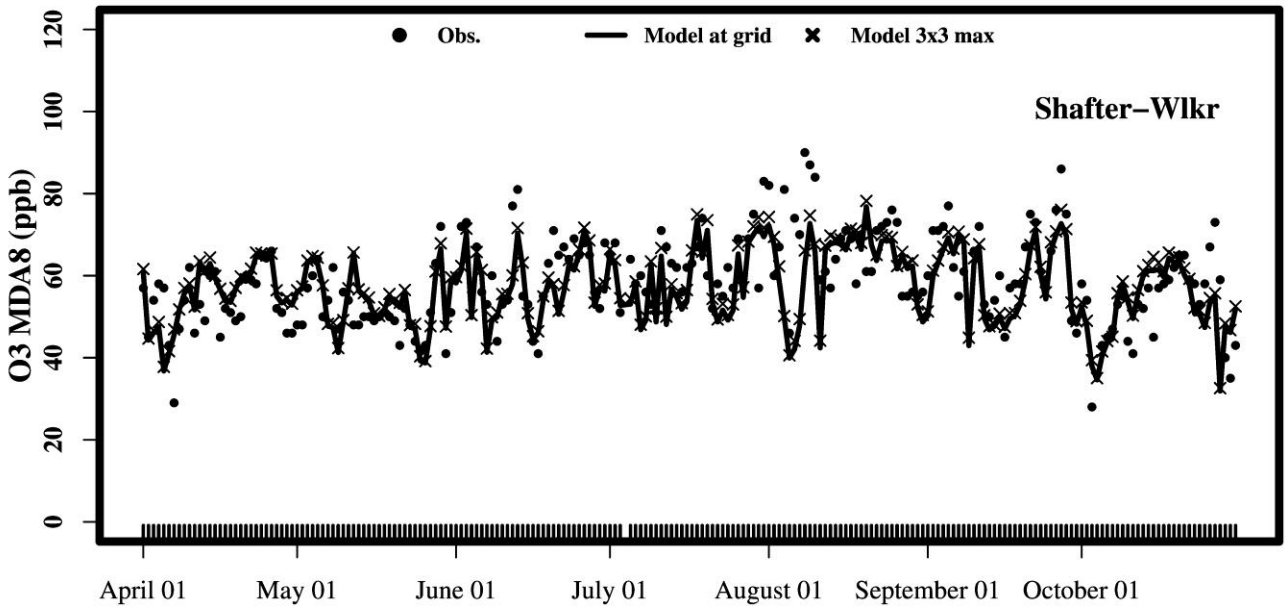

Figure S 103. Time-series of maximum daily average 8-hour ozone at the Porterville-1839 Newcomb Street site for the ozone season (April-October 2018).

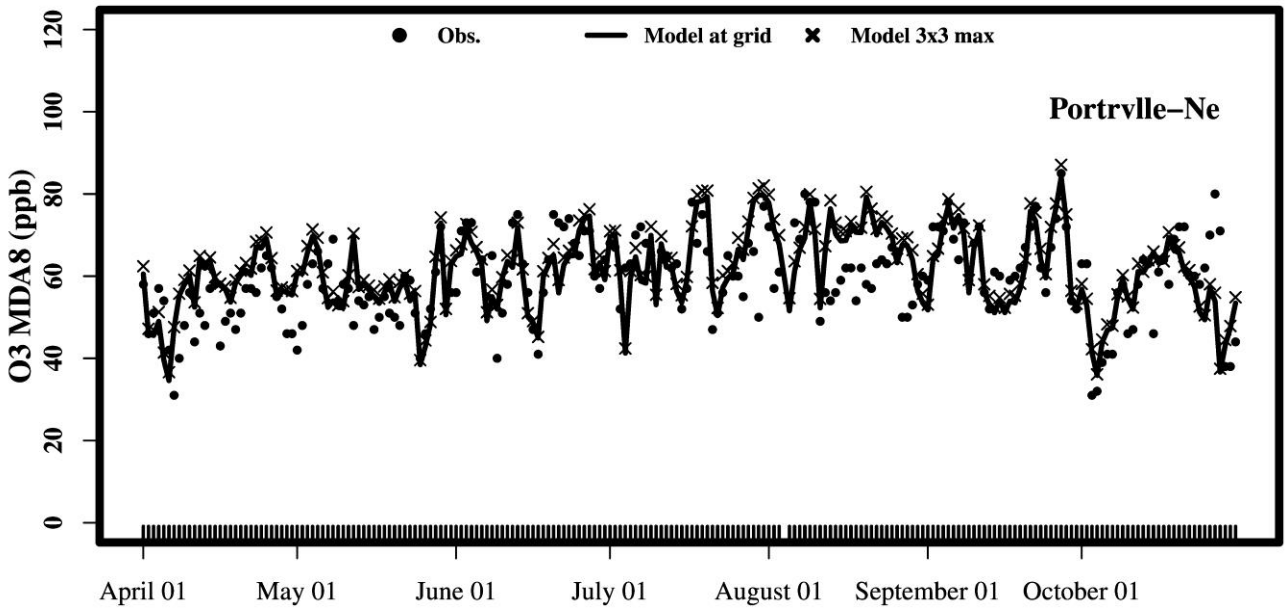

Figure S 104. Observed and modeled daily average NOx scatter plots for the ozone season in Northern SJV (nsjv), Central SJV (csjv) and Southern SJV (ssjv) (April-October 2018).

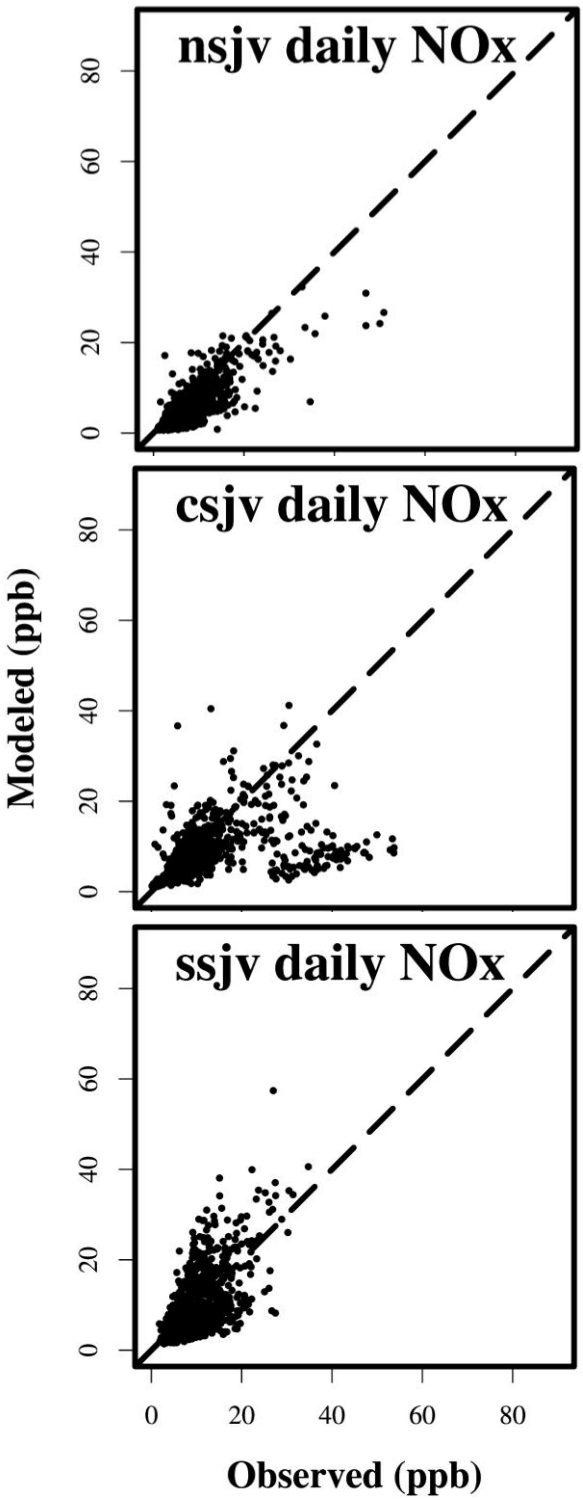

Figure S 105. Curtain plot of monthly averaged O_3 concentrations in May 2018 and 2037 along row 64 of modeling domain.

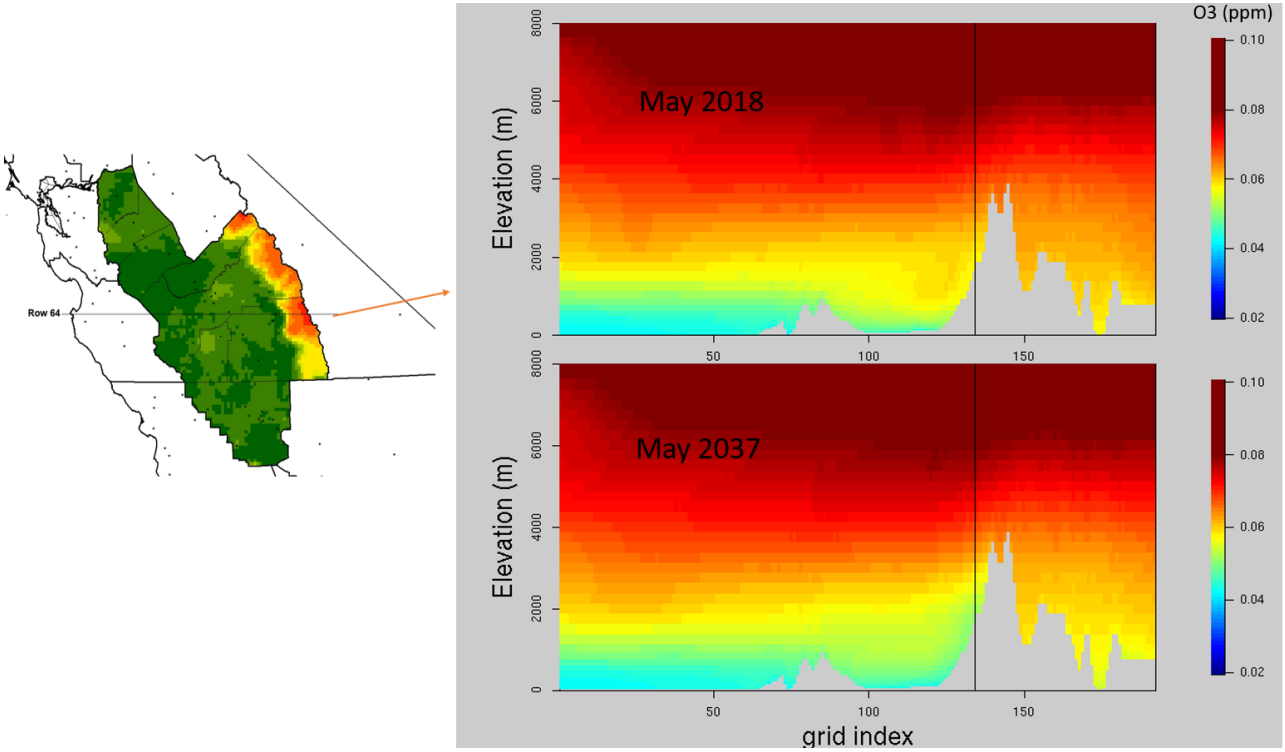

Figure S 106. Curtain plot of monthly averaged O_3 concentrations in August 2018 and 2037 along row 64 of modeling domain.